THE
PHYSICAL REVIEW
A Journal of Experimental and Theoretical Physics Established by E. L. Nichols in 1893
VOL. 59, NO. 12 JUNE 15, 1941 SECOND SERIES

Nuclear Particles in the Cosmic Radiation

S. A. KORFF
Bartol Research Foundation of the Franklin Institute, Swarthmore, Pennsylvania
(Received April 7, 1941)

A series of balloon flights employing proportional counters has been carried out. In these flights the instrument measures the number of events liberating more than an assignable minimum of ionization in the instrument. The contribution due to each of several types of such events is evaluated, the effect of large showers is considered and instrumental errors are discussed. It is found that alpha-particle counts due to slow-neutron-induced boron disintegrations may account for about one-third of the discharges observed with BF_3 counters. Counters in which other gases are used permit an estimate to be made of the flux of highly ionizing particles, mostly protons, which is found to be about 10^{-3} per sq. cm per sec. These data permit the calculation of the rate of production of protons, which is found to be of the same order as that of neutrons, namely about 5×10^{-2} per gram per sec. at the altitude corresponding to 2 meters of water equivalent below the top of the atmosphere. The energy distribution, the amount of the flux and the altitude dependence suggest that both protons and neutrons are produced about equally by a process or processes connected with the soft component of the radiation.

INTRODUCTION

VARIOUS experimenters have studied the neutrons associated with the cosmic radiation. A résumé of the experimental data has been made by Bethe, Korff and Placzek,[1] who have also discussed the interpretation of the observations and the energy distribution of the neutrons.

Other observers,[2] using cloud chambers and also the photographic plate technique, have reported evidence for the existence of slow protons (<30 Mev) and occasional heavier particles, associated with the radiation. These particles are characterized by a specific ionization greater than that of the usual fast electrons and mesotrons. Slow mesotrons, with high specific ionization, have also been reported by Herzog and Bostick, Powell and others.[3] Evidence regarding the average specific ionization of cosmic-ray particles at various elevations has been deduced from the comparison of electroscope with Geiger counter measurements.[4]

Some balloon flights to high elevations have been carried out[5] for the purpose of testing

[1] H. A. Bethe, S. A. Korff and G. Placzek, Phys. Rev. **57**, 573 (1940).

[2] C. D. Anderson and S. H. Neddermeyer, Phys. Rev. **50**, 263 (1936); W. Heitler, C. F. Powell and H. Heitler, Nature **146**, 65 (1940); M. Blau and H. Wambacher, Nature **140**, 585 (1937); E. M. Schopper and E. Schopper, Physik. Zeits. **40**, 22 (1939); E. Schopper, Naturwiss. **25**, 557 (1937); T. R. Wilkins, J. App. Phys. **11**, 35 (1940); summary and bibliography, M. M. Shapiro, Rev. Mod. Phys. **13**, 58 (1941).

[3] G. Herzog, Phys. Rev. **59**, 117 (1941); G. Herzog and W. H. Bostick, Phys. Rev. **59**, 122 (1941); W. F. Powell, Phys. Rev. **58**, 474 (1940); S. H. Neddermeyer and C. D. Anderson, Phys. Rev. **54**, 88 (1938).

[4] W. F. G. Swann and W. E. Danforth, J. Frank. Inst. **228**, 43 (1939); S. A. Korff and W. E. Danforth, J. Frank. Inst. **228**, 159 (1939).

[5] S. A. Korff, Phys. Rev. **59**, 214 (1941).

TABLE I. *Observed counts produced by proportional counters in the stratosphere, and the constants necessary for interpreting the counting rate in terms of ionizing events.*

PRESSURE INTERVAL M WATER EQUIV. BELOW TOP OF ATMOS.	FLIGHT NUMBER 21	24	25	26
	Counts per minute observed			
9			0.08	
8				0.4
7				0.8
6		0.5	0.5	1.6
5		0.4	1.6	2.4
4	1.0	1.2	2.4	3.2
3	1.5	1.7		4.8±2
2	1.5±1		8.0	12.0±4
1	7.1±1			>17.0
Counter volume, cc	240	147	390	450
Area, sq. cm	90	75	100	120
Av. path through counter, cm	3	2.5	5	5
Type of gas	BF_3	BF_3	H_2-CH_4	A
Pressure, atmos.	0.075	0.158	0.046	0.09
Lowest energy expended in ioniz. to record, E_{min}, kev	80	125	30	50
Av. neutron energy to produce observable recoil, kev	400	625	60	1000
Proton energy E_{max} to record, Mev	2	2.4	3.5	5
Range, cm, for the above protons	7	10	18	34

deductions regarding energy distribution of the neutrons made in the analysis cited.[1] In these flights, proportional counters were used. Since such counters are capable of measuring particles of an assignable specific ionization, these results have some bearing not only on the neutron problem[6] but also on that of the other particles.

APPARATUS

The apparatus used consisted of a proportional counter which was carried to high elevations by free balloons. The pulses produced by this counter, as well as the barometric pressure, were transmitted to the ground by short wave radio, using technique previously described.[7] The method of calibrating such proportional counters, to determine, by employing alpha- and beta-particles, the size of the ionizing event necessary to produce a count, has also been previously discussed.[8]

In two of the flights, counters filled with BF_3 were used; in one, a methane-hydrogen mixture (illuminating gas) and in one, argon with alcohol quenching. The purpose of using these different gases was to permit separation of the various types of ionizing events, as will be discussed below.

On flight 24, with a BF_3 counter, an arrangement was included for changing the high voltage on the counter while the flight was in progress. This consisted of a microswitch, actuated by a rotating cam, so shaped that the switch was closed for half the period of revolution of the cam, and open for the other half. This cam was driven by a small electric motor of the type used in the radiobarograph, geared to rotate the cam at one revolution per six minutes. The voltage was thus varied in cycles, each value being kept constant for three minutes. The switch caused 45 volts to be included or excluded from the counter potential. Further, the instant the switch opened, a long signal was sent out, so that it would be known what position the switch occupied and hence the voltage. A short signal was sent when it closed.

OBSERVATIONS

The counting rates observed on the several flights are presented in Table I, for the various elevations in meters of water equivalent below the top of the atmosphere. The counting rates are averaged over each meter of water, so that in the row corresponding, say, to 3 meters will be found the average counting rate produced by the counter when it was in the altitude interval between $3\frac{1}{2}$ and $2\frac{1}{2}$ meters of water. The experimental uncertainties may be judged from the standard deviations which are shown for one of the flights in the right-hand column.

The various physical properties of the counters, dimensions, nature and pressure of gas, are also given in Table I. Finally, an estimate is made, showing the smallest pulse size measured by the counter as it was adjusted in the flight, and the minimum neutron energy necessary to produce a recoil of this magnitude.

CONTROLS AND CALIBRATIONS

The counters were so adjusted that they did not respond to gamma-rays. In order to ascertain that gamma-rays did not affect the heavy particle counting rate, a radium-beryllium neutron source was placed inside a thick lead shield, 8.5 cm in radius, and located at about 40 cm

[6] H. v. Halban, L. Kowarski and M. Magat, Comptes rendus **208**, 572 (1939); E. Fünfer, Zeits. f. Physik **111**, 351 (1938).
[7] S. A. Korff, Rev. Mod. Phys. **11**, 211 (1939).
[8] S. A. Korff, Rev. Sci. Inst. **12**, 94 (1941).

from the counter. With this arrangement, a sufficient number of neutrons reached the counter, while the gamma-ray background was much reduced. The counting rate was observed. Next, a radium needle (without beryllium) was brought to such a distance that the gamma-rays passing through the counter were from 2 to 5 times as many as would be encountered in the stratosphere. No change in neutron-counting rate was observed. It was found that the radium had to be brought to such a distance that the gamma-ray intensity was 100 or more times that in the stratosphere before the counting rate was changed by an observable amount.

The effect of large showers may be considered. The maximum amount of ionization which a slow beta-ray could produce by ending its range passing along the length of the counter was about 1000 to 1500 ion pairs. A pulse of this size was not recorded, while a pulse produced by an alpha-particle liberating 4000 or more ion pairs did record. The amount of energy ($E_{\min}$) which had to be liberated as ionization to produce a count is given for each flight in Table I. In a large shower, the particles would pass through a counter with an average path which can be roughly estimated at one diameter. Most of these particles ionize like fast electrons. In these counters, therefore, each particle will liberate from 2 to 10 ions on its traversal. Hence it will require the simultaneous passage of at least 200 and often 1000 such particles to cause a count. The size of the counter is rather small compared to the physical extent of a large air shower. Further, there was little shower-producing material above or beside the counter since the batteries, etc., were located far below, and the total dense matter above the counter may be estimated at one-fourth of a unit length in radiation theory. Hence it does not seem probable that there were enough 200-ray showers passing through the counter to produce the observed counting rate.

In flight number 24, the voltage on the counter was changed during the flight by the switch described above, at 3-minute intervals. This arrangement was operated near a neutron source previous to flight, and the counting rate at each voltage for several conditions, is shown in Table II. First the neutron source was placed inside lead near the counter. The counter was surrounded by paraffin with irregular geometry. In the second test, the paraffin was removed; in the third, a cadmium shield was placed around the counter. Fourth, the neutron source was taken away, and the background determined, with and without cadmium, and finally tests were made for the effect of gamma-rays, and for disturbances produced by the switch, barograph motor, radio oscillator and other electrically connected parts.

The purpose of this test was to determine whether most of the neutrons in the upper atmosphere produced counts by boron disintegration (i.e., as slow neutrons) or by recoils (as fast neutrons). The laboratory tests showed that the change of voltage made relatively little difference to the rate of counting slow neutrons, since the neutron counter was operating on the "plateau" of its characteristic curve.[9] On the other hand, for fast neutrons, the recoil pulse size distribution even for mono-energetic neutrons will vary continuously with counter voltage. Hence, no plateau is to be expected,[10] and changing the voltage will always change the counting rate at any voltage. The interpretation of the flight data is discussed below.

TABLE II. *Tests on BF_3 counter in flight 24. It will be noted that changing the voltage changes the rate of counting recoils* (Cd *on*) *more than it changes the rate of counting slow neutrons* (*paraffin on*).

	Counts per Minute Neutron Source Near			Counts per Minute Neutron Source Removed		
Voltage	Paraffin on	Paraffin off	Cd on	Cd off	Cd on	Ra near
1260	96.0±0.2	8.14±0.4	6.25			
1305	97.1±0.2	10.44±0.3	8.45	0.165	0.07	0.17

Discussion

A proportional counter will count when an ionizing event liberating more than an assigned amount of energy, $E_{\min}$, takes place inside it. For proportional counters in the stratosphere, there will be three chief types of events liberating large amounts of ionization. The number of counts per second, (n), of the counter will be

[9] S. A. Korff and W. E. Danforth, Phys. Rev. **55**, 980 (1939).

[10] S. A. Korff, Phys. Rev. **56**, 210 (1939).

equal to the number of such events, and the total will be given by:

$$n = VN\rho\sigma_B v_B + VN\int_0^{V_{max}} i(v)\sigma(v)dv + S\int_0^{E_{max}} I(E)dE + D, \quad (1)$$

where V is the volume of the counter, N the number of atoms of the gas in the counter, S the cross-sectional area of the counter, $i(v)dv$ the current of fast neutrons per sq. cm per sec. with velocities in the interval dv, $I(E)dE$ the current per sq. cm per sec. of highly ionizing particles of any kind, with energies in the interval dE, ρ the density of neutrons per cc with velocities in the $1/v$ region, σ_B the capture cross section by boron for neutrons with velocity v_B, and σ the recoil cross section of the nuclei of the gas in the counter. The term D includes the background counting rate of the counter due to alpha-particles from natural radioactive contamination, a quantity which can easily be determined in the laboratory in the absence of neutrons, and which is subtracted from the counting rates reported in the table of observations. It also includes the number of showers large enough to produce counts, and the number of energetic recoiling copper atoms ejected from the walls of the counter by fast neutrons in the radiation.

The first term, the number of boron disintegrations, will be zero for all counter gases except BF_3, and hence will apply to flights 21 and 24 only. Flights 25 and 26 will be described by the second and third terms. The term D will be disregarded, since it includes a contribution due to large showers, which, for the reasons above cited, is assumed negligible compared to the other quantities, and wall recoils, which will be shown to be unimportant.

The contribution due to wall recoils may be estimated. Suppose the recoiling copper nucleus to have a range of $\frac{1}{2}$ cm of air equivalent in copper. Then the number of wall recoils will evidently be of the same order as the number produced in the gas, and the effect will be the equivalent of using a counter of correspondingly slightly larger volume.

TABLE III. *Values of Q, the rate of production of protons per cc per second as determined by the experiments.*

Meters of Water Equivalent	Flight Number 25	26
6	4.8×10^{-6}	6.5×10^{-6}
4	2.3×10^{-5}	1.3×10^{-5}
2	7.7×10^{-5}	4.9×10^{-5}
1		$>6.5\times10^{-5}$

The number of recoils in the gas is given by the second term in Eq. (1). Assume that σ is a constant and equal to 10^{-24} sq. cm. The observed neutron flux[6] of between 1 and 10 neutrons per sq. cm per sec. will yield about 10^{-2} to 10^{-3} per sec., between one and ten percent of the observed counting rate. Should one wish to explain the entire counting rate as due to recoils, the neutron flux must be increased by a factor of nearly 100, in which event there would be many more neutrons than all other types of cosmic-ray particles combined, and these neutrons, when slowed by collisions in the air, would produce a counting rate in the BF_3 counters some 100 times larger than is observed. Further, flight 25 used hydrogen, and flight 26 argon, with a nuclear weight ratio of about 40 : 1. Roughly the same counting rates were observed. Yet the neutron energies necessary to produce measurable recoils would be 1 Mev in flight 26 as compared to 60 kev in 25. Hence there could be very little contribution due to neutrons in this energy interval; but on the other hand, E_{max} for flight 25 is close to 4 Mev, and more energetic recoiling protons would not be counted. We may conclude that recoils can explain between one and ten percent of the observed counts.

The last term in Eq. (1) gives the contribution due to highly ionizing particles, including slow protons, passing through the counter. It is evident that we may write:

$$S\int_0^{E_{max}} I(E)dE = SQR(E_{max}),$$

where Q is the rate of production of protons per cc of air per second, and R is the range in standard air of particles whose energy is E_{max}. Here E_{max} is that proton energy which will lose an energy E_{min} in an average traversal of the counter. E_{min} is the experimentally determined

"cut-off" of the particular counter used, and at proton energies above E_{max}, the energy loss per average counter traversal is not sufficient to record. It is evident that $R(E_{max})$ is a sensitive function of the counter size and gas, and can in fact be shown to vary as the cube of the effective path length. The range R corresponding to E_{max} may be found from the tables given by Livingston and Bethe,[11] and are shown in Table I for these experiments. Inserting the observed values of S and the counting rates, and considering all the particles counted to be protons, we may compute Q for various elevations. The results are given in Table III.

These values of Q are calculated per cc of standard air per second. Dividing by the density of air we find about 5×10^{-2} per gram per second at the 2-meter level. This figure, it will be recalled, is within experimental error the same as the rate of production of neutrons[1] per gram per second at this level. The similarity of the rates of production is strongly suggestive of a possible connection, such as would arise if both protons and neutrons were produced about equally by a photonuclear disintegration process, induced by the high energy photons of the cosmic radiation. Other evidence for such a process has been discussed elsewhere.[12]

Comparing the counting rate, in flights 25 and 26, due to fast neutron recoils with that due to protons, we find that corresponding to $Q=10^{-5}$ and $R=10^{2}$ cm, the current of protons per sq. cm per sec. is about 10^{-3}, as compared to $q=10^{-5}$ and $R=10^{5}$ and i of about one for the neutrons. But the detection (recoil production) efficiencies of fast neutrons are about 10^{-4} to 10^{-5} as compared to unity for all protons losing more than E_{min} per counter traversal. Hence the fast neutrons may be expected to contribute about one to ten percent of the total number of counts. The efficiency of the BF_3 counters for the detection of neutrons in the $1/v$ region is somewhat higher than that of the recoil counters, and depends on the energy distribution of the neutrons in a manner previously discussed.[1]

Consider now the interpretation of flights 21 and 24, with BF_3 gas. To these, the first term in Eq. (1) also applies. If we suppose flights 25 and 26 determine the rate of production of protons at the 4-meter level, to be, say, 2×10^{-5} per cc per second, and calculate what counting rate we should expect in flights 21 and 24 at this level, on the basis that all the counts were due to protons, we find about 0.66 and 0.8 c.p.m. as compared to the 1.0 and 1.2 c.p.m. observed. Hence it seems reasonable to suppose that about two-thirds of the counts in the BF_3 counter are proton counts and one-third neutron counts. This estimate is necessarily inexact. Further evidence may be obtained from an additional experiment made on one of the flights.

On flight 24, the voltage on the counter was changed cyclically during the flight. This is experimentally equivalent to varying E_{min}, and hence $R(E_{max})$. It was observed that the counting rate when the voltage was low (1260 v) was about $\frac{2}{3}$ of that when it was high (1305 v). If one-third of the counts, when the voltage was high, were due to neutrons, then the rate of counting protons changed by a factor of two with the change in voltage. Taking E_{min} when the voltage was high as being 124 kev per counter traversal, we find that the counter measured all protons with energies less than 2.4 Mev, or of 10-cm range. When the voltage was lowered, E_{min} was 180 kev corresponding to 1.6-Mev protons of 5-cm range. These estimates are necessarily rough owing to the small total number of counts. However, examining the two extreme alternative interpretations, the large change in counting rate observed upon changing the voltage clearly indicates that it is not consistent with experiment to attribute all the counts of the BF_3 counter to boron disintegrations, for in this case we should expect, as shown in Table II above, a much smaller change with voltage. On the other hand, if we suppose that none of the counts were due to neutrons then the change in E_{min} corresponding to a change of 45 volts in the counter potential is too small to agree with known properties of these counters.[8] The estimate of one-third of the counts as due to neutrons is, however, consistent with the other data on protons, neutrons and counter behavior.

The proton flux is consistent with the photographic plate observations of Heitler, Powell

[11] M. S. Livingston and H. A. Bethe, Rev. Mod. Phys. 9, 268 (1937).
[12] S. A. Korff, Proc. Am. Phil. Soc., to be published.

and Fertel,[13] in which they find about 6 tracks per sq. mm per 230 days at 7 meters of water. This corresponds to a flux of 3.2×10^{-5} per sq. cm per sec. This may be compared to 6×10^{-5} observed in the present experiments at 6 meters. With an altitude dependence of two per meter of water, exact agreement is obtained, a circumstance which must be regarded as fortuitous.

The altitude dependence of the counting rate is, roughly, two per meter of water. This is the same as that of neutrons, as determined by neutron counters with boron and cadmium shields,[6,1] and also with plates.[2] The proton plates used at the Jungfraujoch were observed[13] to have ten times the number of tracks that were found at sea level in the same area and time. This corresponds to about two per meter of water. This is also the rate of increase with altitude of the soft component, a circumstance suggesting a possible connection, which has been discussed.[12]

We may also inquire whether many of the counts result from primary protons at the ends of their ranges. If we suppose the total flux of primary protons (I_{pri}) to be 0.16 per sq. cm per sec., and assume that all are stopped in the first 4 meters of water equivalent of air (4×10^5 cm), then, since they are sufficiently ionizing to be detected in these experiments only during the last 40 cm or less of their range in air, we would expect at any level to find $i=I_{pri}\times40/4\times10^5$, or 1.6×10^{-5} per sq. cm per sec., which is about one-sixtieth of the observed intensity.

Thus it appears probable that most of the discharges of the proportional counter in the stratosphere can be attributed to slow protons produced by the radiation. The majority of the slow protons (energies <10 Mev) appear to have been produced by some process connected with the soft component of the radiation, possibly nuclear photo-disintegration. Cross sections for various processes of this type have been calculated by Heitler,[14] and are found to be in sufficient agreement with experiment, considering the necessarily rough experimental data available. The neutrons, observed both by recoils and by boron disintegrations, are presumably liberated in the same process.

[13] W. Heitler, C. F. Powell and G. E. F. Fertel, Nature **144**, 283 (1939).

ACKNOWLEDGMENTS

The author wishes to acknowledge support received from the Carnegie Institution of Washington. Thanks are also due the American Philosophical Society for a neutron source used in testing the apparatus. The author wishes to thank Eric T. Clarke for assisting with the flights, and H. A. Bethe and colleagues at the Bartol Research Foundation for helpful discussions.

[14] W. Heitler, Proc. Roy. Soc. **A166**, 529 (1938).

JUNE 15, 1941 PHYSICAL REVIEW VOLUME 59

Beta-Ray Energy of H^3

SANBORN C. BROWN
Massachusetts Institute of Technology, Cambridge, Massachusetts

(Received April 12, 1941)

The maximum energy of the H^3 beta-ray spectrum has been measured by its absorption in helium. The detector was a screen-wall Geiger-Müller counter with helium at atmospheric pressure flowing through it at all times. The maximum range of the H^3 beta-rays in helium was determined as 13 ± 1 mm, corresponding to a maximum energy of 9.5 ± 2.0 kev.

A NUMBER of attempts have been made to determine the energy of the H^3 beta-rays.[1] Measurements on this spectrum are made difficult by its extremely low energy, but if we use a screen-wall Geiger-Müller counter working at atmospheric pressure and filled with

[1] L. Alvarez and R. Cornog, Phys. Rev. **57**, 248A (1940); G. U. Perlow, Phys. Rev. **58**, 218 (1940); R. D. O'Neal, M. Goldhaber, Phys. Rev. **58**, 574 (1940).

helium,[2] we have a convenient method for dealing with the problem. Although the method possesses the inherent inaccuracies of absorption methods, including the lack of a good range-energy relation in this low energy range, it allows constant counter characteristics throughout the experiment, and we can evaluate and make the corrections due both to changes in solid angle and to the failure of the sensitive volume of the counter to coincide with the physical limits of the cathode screen.

The source of H^3, which was generously supplied by the Radiation Laboratory at Berkeley, was in the form of water. No simple method of preparing the source could be found to keep the counter from becoming contaminated. Therefore a more complicated method was used. P_2O_5 was sublimed onto the source plate in a vacuum. The source plate was then suspended, without coming in contact with the air, in the radioactive water vapor in an atmosphere of helium at room temperature for twenty-four hours. With sources prepared in this manner, the background of the counter remains constant over long periods of time, and the source strength remains constant as long as a dry-ice trap is provided between the counter and the helium tank. The trap eliminates moisture which would otherwise enter the counter and be absorbed by the source, whose activity would thus be decreased.

The apparatus used to measure the range of the beta-rays is shown in Fig. 1. It consists of a 14-mesh screen-cathode Geiger-Müller counter with a plunger, which holds the source, sliding in the side arm on the counter envelope. Helium from a commercial tank flows into the counter through a dry-ice trap, down over the source, and out into the air through a bubbling bottle which serves to show the rate of flow of the helium and acts as an air lock in case the helium flow is shut off. Helium at approximately atmospheric pressure, flowing through the counter in this manner, is used for three reasons. At atmospheric pressure it is not necessary to have any window between the source and counter, so that very low energy beta-rays can be measured. If the helium is kept flowing gently through the apparatus at all times the apparatus does not have to be made vacuum tight and therefore has advantages of simplicity in construction and operation. Helium is used so that at atmospheric pressure the counter will operate at voltages which are easily obtainable by ordinary Geiger-Müller counter amplifiers. The threshold of the counter used was 1200 volts.

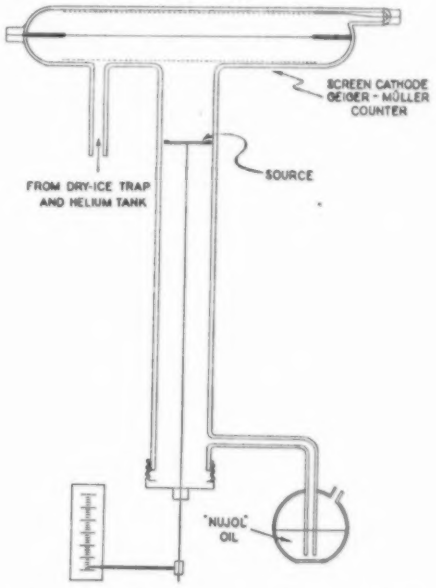

FIG. 1. Sketch of the atmospheric pressure helium flow counter used. The counter cathode is 10 centimeters long and 2 centimeters in diameter.

The counter was fed through a counting rate meter,[3] the output of which went to a galvanometer. The deflection of the galvanometer was proportional to the counting rate and was recorded photographically. The counting rate was determined as a function of the distance between the source and the outer edge of the screen. The result of this is plotted in Fig. 2.

As the source is moved away from the counter, the beta-rays are more and more strongly absorbed, and also the solid angle changes. Both these changes would affect the counting

[2] It was thought that the use of these counters was original (S. C. Brown, Phys. Rev. **58**, 1121A (1940)). It has been pointed out, however, that J. A. Bearden and C. L. Haines, Phys. Rev. **40**, 1048A (1932); and J. S. Allen and L. W. Alvarez, Rev. Sci. Inst. **6**, 329L (1935) showed that helium-filled counters could be operated at atmospheric pressure. It is unfortunate that this useful method of detecting low energy beta-rays should have been overlooked.

[3] R. D. Evans and R. L. Alder, Rev. Sci. Inst. **10**, 332 (1939).

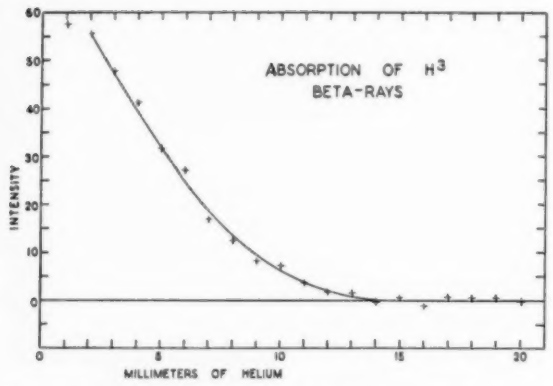

FIG. 2. Absorption curve of the H^3 beta-rays in helium at atmospheric pressure.

rate. The amount of the change due to changes in solid angle was determined by using an alpha-ray source and operating the counter as a *proportional* counter so that only alpha-rays would be recorded. When the counter is kept within the range of the alpha-particles, the counting rate as a function of distance gives the correction to be applied for changes due to solid angle. This, of course, does not change the end point, but merely the shape of the curve.

Figure 2 would give the maximum range directly if the sensitive volume of the counter coincided with the physical limits of the cathode screen. Since this is not necessarily true, the following experiment was done to determine where the electrical edge of the counter was in comparison with the physical edge. A polonium source was substituted for the H^3 source. Two sets of observations of the range were made with the counter operating in its Geiger-Müller region, one with a 0.5-mil aluminum foil wrapped around the cathode so that the field of the counter extended no farther than the edge of the screen, and another when the same aluminum foil was placed directly over the source. The measured difference in the range showed that the sensitive volume of the counter extended one millimeter beyond the physical limits of the screen, the width of the holes of which was approximately two millimeters. Applying this correction to the measured range of the H^3 beta-ray, we get for the maximum range 13 ± 1 mm of helium at atmospheric pressure.

Difficulty is encountered when one tries to convert this range into energy, because of the lack of a good range-energy relation in this low energy domain. The best that can be done at present is to compile the available data for the range of homogeneous cathode rays and put the best curve through the values obtained by a number of different authors. This curve is shown in Fig. 3. If we use this range-energy relation and the fact that 13 mm of helium correspond to 2.3×10^{-4} grams per square centimeter, the maximum energy of the H^3 beta-ray is found to be equal to 9.5 ± 2.0 kev.

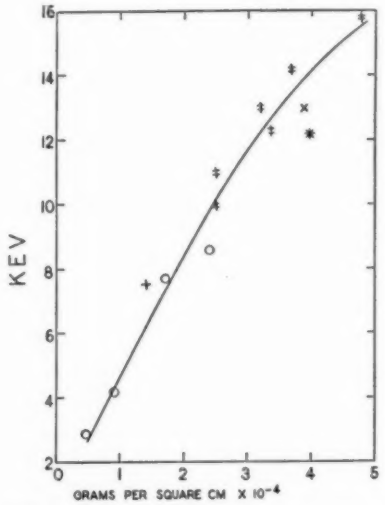

FIG. 3. Range-energy relation of homogeneous cathode rays. Data from the following authors: ○ T. Alper, Zeits. f. Physik **76**, 172 (1932); + J. M. Nuttal, E. J. Williams, Proc. Roy. Soc. **130**, 310 (1930); ‡ * B. F. J. Schonland, Proc. Roy. Soc. **108**, 187 (1925).

In conclusion I wish to acknowledge the help of Professor Robley D. Evans, under whose direction this work was carried out.

The Production of Characteristic X-Rays by Deuteron Bombardment

J. M. CORK
University of Michigan, Ann Arbor, Michigan
(Received April 12, 1941)

It is shown by a photographic method that for deuterons of 10 Mev, characteristic K radiation is emitted from targets of atomic number 38 or less. Because of absorption, the intensity appears to have a maximum for elements of atomic number about 28. Similarly, L radiation is observed for the heavier elements with a maximum in the neighborhood of atomic number 64. For a copper target the yield of x-rays is observed as a function of the exciting energy. The results are compared with the theoretical calculations of Henneberg.

THE possibility of producing x-rays by the bombardment of targets with heavy particles was demonstrated as early as 1913 by Chadwick[1] and by Rutherford and Richardson.[2] They employed the alpha-particles from radium emanation. Several later investigations have been made with alpha-particles[3] from natural radioactive sources and with protons[4] whose energies were as high as 1.76 Mev. In these investigations the x-rays have been detected by sensitive ionization chambers or Geiger counters, and the nature of the x-rays revealed by studying their absorption in aluminum. A theoretical treatment of the problem, leading to an expression for the distribution of the x-ray energy with changing atomic number of the target and with the incident energy of the particle has been presented by Henneberg.[5]

EXPERIMENTAL

In observing photographically in a magnetic field the disintegration particles resulting from deuteron bombardment in the cyclotron, a prolific yield of undeflected radiation is found for certain elements. The radiation from the target is collimated by a slit and then dispersed by the strong magnetic field of the cyclotron provided with an auxiliary magnetic shunt. The target is usually a thin strip of material about one-half mm wide and 0.025 mm thick and is mounted at an angle of 45 degrees with the deuteron beam. The radiation is observed at an angle of 90 degrees with the beam, whose dimensions are such that the source of x-rays is a vertical line about five mm long parallel to the vertical slit. The photographic plate was mounted in a carriage at any desired distance from the slit. The x-rays together with any gamma-radiation thus appear in the undeflected position on the photographic plate as shown in Fig. 1.

The energy of the bombarding deuterons was usually about 10 Mev, having a range in air of about 66 cm. For the lighter elements the thin targets had a stopping power of not over 10 cm of air so that the energy of the deuterons was only slightly reduced and the shorter wavelength x-rays were not absorbed appreciably.

Observations were made of the yield of x-rays from about 35 elements distributed throughout the whole periodic table. For those elements not available in thin foils, a finely powdered form of the material was made to adhere to a supporting fiber of one-half-mil aluminum foil. Reproductions of certain of the plates at a distance of six cm from the slit, for a bombarding beam of one microampere for one minute, are shown in Fig. 1. The relative production of x-rays is estimated from the comparative blackening of the photographic plates for identical exposures.

For a particular element such as copper, an attempt was made to determine the yield of x-rays as a function of the bombarding energy. The deuterons were allowed to pass through aluminum foils of various thicknesses before impinging on the target. Experiments were also made to show the quality of the x-rays, that is, that they are the characteristic radiation of the target element.

[1] J. Chadwick, Phil. Mag. **25**, 193 (1913).
[2] E. Rutherford and H. Richardson, Phil. Mag. **25**, 722 (1913).
[3] W. Bothe and H. Franz, Zeits. f. Physik 52, 466 (1928); C. Gersten and W. Reuse, Physik. Zeits. **34**, 478 (1933).
[4] M. Livingston, F. Genevese and E. Konopinski, Phys. Rev. **51**, 835 (1937).
[5] W. Henneberg, Zeits. f. Physik **86**, 592 (1933).

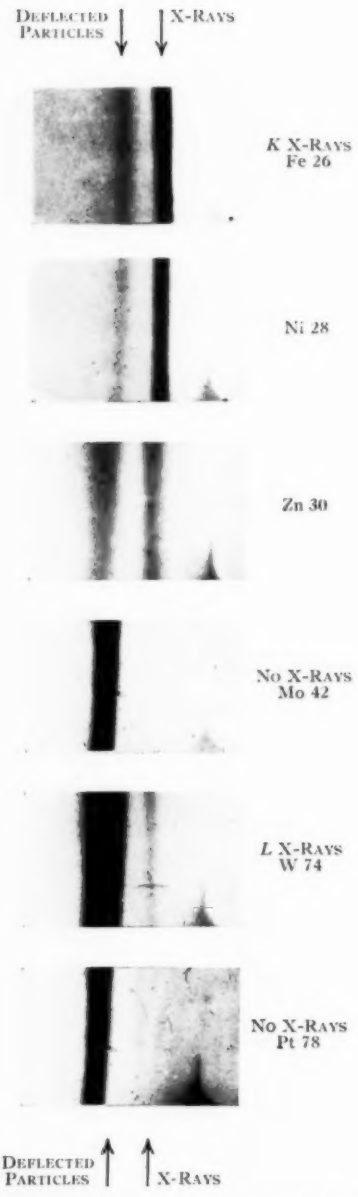

FIG. 1. Photograph showing the characteristic x-rays and deflected particles for certain elements.

RESULTS

For the incident energy of 10 Mev, characteristic K radiation is found for elements of atomic number 38 or less. The estimated relative yields are shown in Fig. 2. Between atomic numbers 52 and 78 the L series x-rays are found but much less abundant than the K radiation for the lighter elements. The maximum for the K radiation occurs for elements of atomic number around 28 and for the L radiation

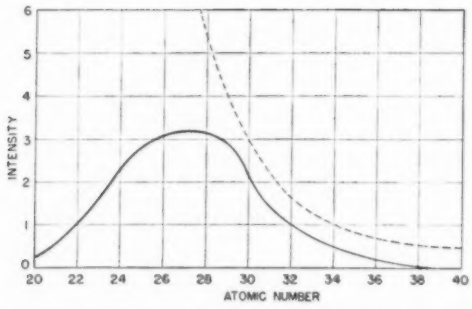

FIG. 2. Relative yield of K radiation from various elements for 10-Mev deuterons (heavy line); theoretical values adjusted at $Z=34$ (dotted line).

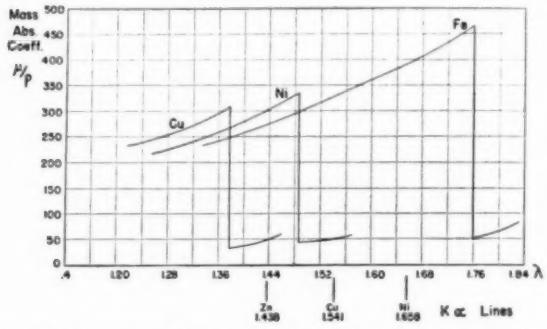

FIG. 3. Wave-lengths of K-emission lines and absorption edges for certain elements.

around atomic number 64. As the energy of the incident deuterons is decreased it is found that the x-rays from a copper target are still observable until the energy approaches 4.5 Mev, or about 17 cm air range.

To make sure that the radiations from a particular element such as copper consist solely of the K x-rays of that element, and are neither continuous nor x-rays emitted subsequent to such a process as K-electron capture by the nucleus, the following experiment was performed for both copper and zinc. The wave-length of

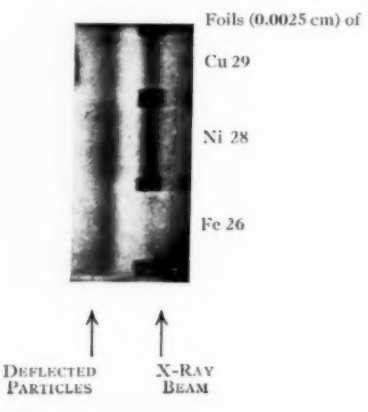

FIG. 4. Photograph showing absorption of x-rays from copper in one-mil foils of copper, nickel and iron.

the copper K alpha radiation is 1.541A. If K-electron capture had occurred in the nucleus then the subsequent x-ray emission would be the K series of zinc whose alpha-lines have a wave-length of 1.438A. The critical K-absorption edges of the elements in this part of the periodic table are shown in Fig. 3. Thus copper K alpha radiation would be strongly absorbed in iron and only slightly absorbed in nickel and copper, while zinc K radiation would be largely absorbed in nickel and iron and scarcely absorbed in copper. By covering the photographic plate with equi-thick strips (0.025 mm) of the three metals a result as shown in Fig. 4 was observed. It is apparent that the iron foil almost completely absorbs the radiation while the copper and nickel only reduce it slightly, as would be the case for copper radiation. Continuous radiation would be absorbed almost equally by the three foils. The radiation from a zinc target was almost completely absorbed by both nickel and iron and only slightly reduced by copper as would be the case for zinc K radiation.

Discussion

If one assumes an elastic impact between the deuteron and the electron, the conservation of momenta and energy expressions indicate an expected excitation energy for each element. For an incident velocity V of the heavy particle of mass M against an electron of mass m at rest, the electron would recoil with a velocity v equal to V plus V' where V' is the final velocity of the heavy particle. Since the mass of the deuteron is relatively so large, V' differs but slightly from V hence v is approximately $2V$. The energy given to the electron is therefore $4m/M$ times the incident energy of the deuteron. Conversely, the critical incident energy expected to excite the K radiation would be $M/4m$ times the well-known critical electron potentials from x-ray spectroscopy. For copper, electrons of 8.86 kev or greater excite the K radiation. The above factor indicates that deuterons of 8.2 Mev should behave similarly. Actually, deuterons with much less energy, even down to 4.5 Mev, are able to produce this effect. From the above relationship the incident energy of 10 Mev should be scarcely sufficient to excite the K radiation of gallium ($Z=31$), whereas in fact such deuterons will excite atoms as heavy as $Z=38$. This ability of the heavy particle to communicate more energy to the electron indicates the inadequacy of the simple treatment.

A more realistic treatment of the emission process based upon the Born approximation principle, as carried out by Henneberg, yields results that are not greatly in disagreement with those observed in this investigation. The theoretical expression shows the number of K electrons ejected by a constant excitation to increase progressively as the atomic number of the target decreases. Thus if in Fig. 2 the theoretical expression is adjusted at atomic number 34 to agree with the experimental after allowance for absorption is made, then its course is indicated by the dotted curve. To obtain the expected experimental curve the derived values must be multiplied by a reduction factor due to the absorption of the x-rays in an air path of 6 cm, an aluminum foil 0.0025 cm and a small effective absorption in the target. These total factors are of the order 0.6, 0.1 and 10^{-6} for atomic numbers 30, 24 and 16, respectively, thus yielding a maximum as observed. The principal disagreement is that the theory would predict a considerable yield of K x-rays for elements of atomic number greater than 38, which are not observed.

An approximate value can be ascribed to the cross section for the process of x-ray emission by the heavy particle. For the iron target under the conditions of the experiment, the theory of Henneberg would predict a cross section of about 3×10^{-21} cm^2. Experimentally 10^{14} incident particles passing through a small volume of iron containing 10^{18} particles was sufficient to blacken the photographic plate at a distance of 6 cm. By estimating the number of photons required to blacken unit area of the plate, a guess could be made of the total number of photons emitted, and hence the cross section. Such considerations lead to a value 10 to 100 times greater than the theoretical, but the difference cannot be regarded as outside the limit of error in the calculation.

This investigation was made possible by a grant from the Horace H. Rackham fund. For discussions of the theory I am especially indebted to Professors D. M. Dennison and G. E. Uhlenbeck.

On the Passage of Neutrons Through Ferromagnets

O. HALPERN AND T. HOLSTEIN
New York University, University Heights, New York, New York

(Received April 19, 1941)

The paper contains a treatment of various phenomena occurring in the passage of neutrons through domains which are regularly or irregularly magnetized. After setting up general equations for the behavior of the neutron spin in different types of magnetic fields which correspond approximately to various stages of magnetization in ferromagnets we obtain very general results for the depolarization of an originally polarized beam. These results can be easily extended to arbitrarily constituted beams. We report next, briefly, on current views concerning the domain structure of ferromagnets and discuss in detail the possibilities of investigating this structure by means of experiments with partially polarized neutron beams. The discussion divides itself naturally into the treatment of single crystals, macroscopically unmagnetized polycrystals and of polycrystals near magnetic saturation. Revising previous unsatisfactory treatments we derive in a very general manner formulae for the change of intensity and polarization of a neutron beam traversing a saturated or quasi-saturated ferromagnetic medium. The formulae obtained constitute the basis for a modified theory of the well-known neutron polarization experiments. A closing paragraph contains a brief comparison between theory and experiment as far as it can be carried out without evaluating certain phenomenological constants, a task reserved for the following paper.

I. INTRODUCTION

THE study of the passage of neutrons through ferromagnets promises to lead to results which will be interesting from two points of view. On the one hand experiments with polarized neutron beams should reveal important information about the magnetic structure of the ferromagnets dependent upon the state of saturation, the mechanical, and the crystallographic condition of the material. On the other hand it will be seen that the magnetic condition of the ferromagnet is of decisive importance for all experiments which aim to produce polarization phenomena with the aid of permanent magnets.

The underlying concept is essentially very simple. Interaction will always be set up between the neutron spin, or more precisely its magnetic moment, and the magnetic field of the ferromagnet. The effects of the interaction will depend obviously on the variation of the magnetic field along the neutron's path in magnitude and direction. One has therefore to examine how the spin of a neutron will behave in magnetic fields the variation of which may follow several different sufficiently simple and general assumptions.

In the same way that magnetic fields influence the state of polarization of a polarized beam they will also affect and in general retard the production of a polarized beam inside of a ferromagnet. The theoretical prediction of the result of a polarization experiment can therefore only be made when these retarding factors are fully taken into account. The revised theory of polarization experiment shows that the effect of depolarization is much greater than previously expected so that, for example, the deviation from magnetic saturation must lie in the neighborhood of 0.1 percent if the experiments are not to be affected appreciably.

II. GENERAL THEORY OF THE SPIN MOTION OF A NEUTRON IN MAGNETIC DOMAINS

The variation of the spin axis of a neutron passing through a magnetic domain is determined by the "classical" equation of motion:

$$d\mathbf{s}/dt=[\boldsymbol{\mu}\times\mathbf{H}(\mathbf{r})]/h=g\mathbf{s}\times\mathbf{H}(\mathbf{r}), \qquad (2.1)$$

where $\mathbf{s}$ is the operator for the spin of the neutron in units of h, $\boldsymbol{\mu}$ the magnetic moment of the neutron, $\mathbf{H}$ the magnetic field of the domain, $g=(\boldsymbol{\mu}/h)\mathbf{s}$ the gyromagnetic ratio of the neutron, and $\mathbf{r}$ its location.

From the quantum-mechanical point of view $\mathbf{s}$, $\boldsymbol{\mu}$ and $\mathbf{r}$ are operators. To see that the passage to the classical interpretation will give correct answers, one observes the following: (1) The size of the regions over which the magnetic field of the domains suffers appreciable variation ($>10^{-4}$ cm) is much larger than the wave-length of the neutron ($\sim 10^{-8}$ cm). This circumstance allows one to treat the positional motion classically. (2) As will be shown later, the quantity de-

termining the neutron polarization as measured in the transmission experiments is the *expectation* value of the spin, i.e., the classical observable. (3) Since the equation is linear in the operators (all the other quantities being ordinary numbers), no error is incurred by replacing each by its expectation value. (If there occurred terms of the form $s_x s_y$, this replacement would be incorrect, since $s_x s_y \neq s_y s_x$.) The classical interpretation of (1) will, hence, be used exclusively.

In applying Eq. (2.1) to determine the rotation of the spin axis of a neutron in traversing a magnetic medium one assumes the medium to be made up of a series of regions $(1 \cdots i \cdots n)$ in each of which the magnetic field $\mathbf{H}_i$ is constant in direction. From Eq. (2.1) and the above considerations it is readily seen that in passing through the ith region the change of spin is such that (1) the component parallel to $\mathbf{H}_i$ is unchanged ($\mathbf{s}_{\|i} = \mathbf{s}_{\|(i-1)}$) and (2) the component lying in a plane perpendicular to $\mathbf{H}_i$ precesses about H_i with angular velocity $\omega_i = gH_i$, i.e.

$$\mathbf{s}_{\perp i} = \mathbf{s}_{\perp(i-1)} \cos\left(\int_0^{\tau_i} gH_i dt\right) + \mathbf{s}_{\perp(i-1)} \times \mathbf{H}_i / H_i \sin\left(\int_0^{\tau_i} gH_i dt\right), \tag{2.2}$$

where H_i is the *algebraic* magnitude of $\mathbf{H}_i$ with reference to an arbitrarily defined sense. If we write

$$\mathbf{s}_{\|(i-1)} = (\mathbf{s}_{i-1} \cdot \mathbf{H}_i) \cdot \mathbf{H}_i / H_i^2 \quad \text{and} \quad \mathbf{s}_{\perp(i-1)} = \mathbf{s}_{i-1} - (\mathbf{s}_{i-1} \cdot \mathbf{H}_i)\mathbf{H}_i / H_i^2,$$

$\mathbf{s}_i$ is given by $\mathbf{s}_i = A_i \mathbf{s}_{(i-1)}$ where A_i is the dyadic[1]

$$A_i = \frac{\mathbf{H}_i \mathbf{H}_i}{H_i^2} + \left(1 - \frac{\mathbf{H}_i \mathbf{H}_i}{H_i^2}\right) \cos\left(\int_0^{\tau_i} gH_i dt\right) - \sin\left(\int_0^{\tau_i} gH_i dt\right) \frac{\mathbf{H}_i \times}{H_i}. \tag{2.3}$$

By successive application of this procedure the final value of the spin $\mathbf{s}_f$ is given by $\mathbf{s}_f = A_n \cdots A_i \cdots A_1 \mathbf{s}_0$. This gives the rotation of the spin axis of a neutron traversing a *given path*. The magnitude of the spin is, of course, constant. To obtain the spin of the emerging neutron beam, $\mathbf{s}_f$ must be averaged over all neutron paths. If the initial beam is polarized it is clear that the magnitude of the average spin of the emerging beam is, in general, smaller than that of the incident beam and hence the medium has a depolarizing action on the incident beam. As to the averaging process itself, it will be assumed that the fields $\mathbf{H}_i$ and the magnitude of the intervals τ_i have no statistical connection with each other; under these conditions the $\mathbf{H}_i$ can be averaged before the τ_i, a procedure which will be employed consistently in what follows.

When the averaging process is applied to ferromagnetics there arises the question: What is the magnetic field acting on the neutron? From the atomistic standpoint this field is the Lorentz $\mathbf{H}$, the strong variation of which over atomic distances gives rise to magnetic scattering. However, to find the effect of the magnetic field on the *transmitted* beam one must average over a region containing many atoms. This process, however, is precisely that which is used to establish the connection between the equations of Lorentz and Maxwell; the result is the well-known identification of the atomic $\mathbf{H}$ with the Maxwell $\mathbf{B}$.

III. Depolarization of Neutrons in Different Types of Domains[2]

Case 1

The magnetic fields of the domains are directed successively parallel and antiparallel to a fixed axis. In this case it is clear that

$$\mathbf{s}_{\|f} = \mathbf{s}_{\|0}; \quad \mathbf{s}_{\perp f} = \mathbf{s}_{\perp 0} \cos\phi + \mathbf{s} \times \mathbf{B}/B \sin\phi; \quad \phi = \int_0^{\tau} gB dt.$$

[1] In what follows, the usual dyadic notation is employed. A is always of the form $c_1 \mathbf{ab} + c_2 \mathbf{q}\times$, where c_1 and c_2 are constants, and where $\mathbf{a}$, $\mathbf{b}$ and $\mathbf{q}$ are vectors. This symbolism acquires a meaning only when the dyadic operates on a vector, *viz.* $A \cdot \mathbf{v} \equiv c_1 \mathbf{ab} \cdot \mathbf{v} + c_2 \mathbf{q} \times \mathbf{v}$.

[2] We have abstained in this section from reporting on detailed calculations dealing with fluctuations, etc.; though some of the formulae given below do not maintain their simple form in the case of a more general treatment, their content and applicability remain unaffected.

In averaging over the beam it is necessary to know the values of ϕ for the different paths. If it be assumed that this distribution is symmetrical about the value $\phi=0$, which amounts to assuming that the average value of $\mathbf{B}$ is 0, one has

$$\mathbf{s}_{\parallel f}=\mathbf{s}_{\parallel 0};\quad \mathbf{s}_{\perp f}=\mathbf{s}_{\perp 0}\langle\cos\phi\rangle_{Av}. \tag{3.1}$$

Case 2

The magnetic field B_i of the ith domain (corresponding to the ith time interval τ_i) is random in direction, but constant both in magnitude and direction throughout τ_i. I.e.,

$$\langle B_{xi}\rangle_{Av}=\langle B_{yi}\rangle_{Av}=\langle B_{zi}\rangle_{Av}=0, \tag{3.2a}$$

$$\langle B_{xi}B_{yi}\rangle_{Av}=0 \quad \text{for all } x,\ y,\ z \text{ and } i\neq j, \tag{3.2b}$$

$$\langle B_{xi}B_{yi}\rangle_{Av}=0 \quad \text{for } x\neq y, \tag{3.2c}$$

$$\langle B_x{}^2\rangle_{Av}=\langle B_y{}^2\rangle_{Av}=\langle B_z{}^2\rangle_{Av}=\tfrac{1}{3}\langle B^2\rangle_{Av}, \tag{3.2d}$$

$$\partial\mathbf{B}_i/\partial t=0. \tag{3.2e}$$

From Eq. (3.2a)

$$A_i=\frac{\mathbf{B}_i\mathbf{B}_i}{B_i{}^2}+\left(1-\frac{\mathbf{B}_i\mathbf{B}_i}{B_i{}^2}\right)\cos gB\tau_i-(\sin gB_i\tau_i)\frac{\mathbf{B}_i\times}{B_i}$$

and from Eq. (3.2b) it can be seen that $\langle A_n\cdots A_1\rangle_{Av}=\langle A_n\rangle_{Av}\cdots\langle A_1\rangle_{Av}$. To find $\langle A_i\rangle_{Av}$ one observes from (3.2c) and (3.2d) that

$$\begin{aligned}\langle\mathbf{B}_i\mathbf{B}_i\rangle_{Av}&=\langle(\mathbf{i}B_{xi}+\mathbf{j}B_{yi}+\mathbf{k}B_{zi})(\mathbf{i}B_{xi}+\mathbf{j}B_{yi}+\mathbf{k}B_{zi})\rangle_{Av}\\&=\tfrac{1}{3}\langle B^2\rangle_{Av}(\mathbf{ii}+\mathbf{jj}+\mathbf{kk})=\tfrac{1}{3}\langle B^2\rangle_{Av}\end{aligned}$$

and from (3.2a) that $\langle\mathbf{B}_i\times\rangle_{Av}=0$. Hence

$$\langle A_i\rangle_{Av}=\tfrac{1}{3}+\tfrac{2}{3}\cos gB_i\tau_i=1-(4/3)\sin^2\tfrac{1}{2}gB_i\tau_i$$

or

$$\mathbf{s}_f=\pi_i[1-(4/3)\sin^2\tfrac{1}{2}gB_i\tau_i]\mathbf{s}_0. \tag{3.3}$$

The further development of (3.3) depends upon the size of the domains, as expressed by the magnitude of the τ_i. We distinguish two cases.

a. $\tfrac{1}{2}gB_i\tau_i\ll 1$: $\pi_i[1-(4/3)\sin^2\tfrac{1}{2}gB_i\tau_i]\leqq\pi_i(1-\tfrac{1}{3}g^2B_i{}^2\tau_i{}^2)$

$$\leqq\exp[-\tfrac{1}{3}g^2\textstyle\sum_i B_i{}^2\tau_i{}^2]=\exp[-\tfrac{1}{3}g^2\langle B_{Av}{}^2\rangle\textstyle\sum_i\tau_i{}^2].$$

Hence

$$s_f=s_0\exp[-\tfrac{1}{3}g^2\langle B^2\rangle_{Av}\langle\tau^2\rangle_{Av}T/\tau_{Av}].$$

Since in the applications of this formula only the order of magnitude of the exponent is of importance, one may write

$$s_f=s_0\exp[-\tfrac{1}{3}g^2\langle B^2\rangle_{Av}T\tau],$$

which, in terms of the thickness of the material traversed d, the average linear dimension of the domain δ, and the velocity of the neutrons v, becomes:

$$s_f=s_0\exp[-\tfrac{1}{3}g^2\langle B^2\rangle_{Av}d\delta/v^2]. \tag{3.4a}$$

b. $\tfrac{1}{2}gB_i\tau_i\geqq 1$: Using, again, a procedure which gives the order of magnitude of the exponential without regard for numerical factors of order unity, one obtains

$$\pi_i[1-(4/3)\sin^2\tfrac{1}{2}gB_i\tau_i]\leqq[1-(4/3)\sin^2\tfrac{1}{2}gB_i\tau_i]^{T/\tau_{Av}}\leqq(\tfrac{1}{3})^{T/\tau}\leqq e^{-d/\delta}. \tag{3.4b}$$

The physical distinction between the two cases arises from the fact that, when $\frac{1}{2}gB_i\tau_i \ll 1$, the depolarization is produced by a succession of small rotations the magnitude of which is given by the quantity $gB_i\tau_i$, whereas, when $\frac{1}{2}gB_i\tau_i > 1$, the rotation in each domain is so large that the component of the initial spin perpendicular to $\mathbf{B}_i$, $\mathbf{s}_{\perp(i-1)}$, averages out to zero, leaving only the parallel component $\mathbf{s}_{\parallel i}$, the magnitude of which is independent of $gB_i\tau_i$. Since the average of $\mathbf{s}_{\parallel(i-1)}$ over all directions of the field is $\frac{1}{3}\mathbf{s}_{i-1}$ the depolarization factor is $\frac{1}{3}$ per domain or $3^{-n}=3^{-d/\delta}$ for the whole specimen.

Case 3

The total field $\mathbf{B}$ of each domain is the sum of two fields $\mathbf{B}_0$ and $\mathbf{B}_i$ of which the first, $\mathbf{B}_0$, is constant throughout the time interval T; the second, $\mathbf{B}_i$, is constant within the subinterval τ_i, its direction being perpendicular to that of $\mathbf{B}_0$ but otherwise random. As regards the relative magnitudes, $B_i \ll B_0$. Furthermore, it will be assumed that the initial direction of the spin $\mathbf{s}$ is parallel or anti-parallel to that of B_0. Expressed mathematically these conditions read:

$$B_{zi}=0 \quad (z\text{-axis parallel to } \mathbf{B}_0), \tag{3.5a}$$

$$\langle B_{xi}B_{yi}\rangle_{Av}=0 \quad \text{unless } x=y,\ i=j, \tag{3.5b}$$

$$\langle B_{xi}^2\rangle_{Av}=\langle B_{yi}^2\rangle_{Av}=\tfrac{1}{2}\langle B_i^2\rangle_{Av}, \tag{3.5c}$$

$$B_i \ll B_0, \tag{3.5d}$$

$$s_x=s_y=0, \tag{3.5e}$$

$$\partial B_i/\partial t=0. \tag{3.5f}$$

By arguments similar to those of Case 2 it is readily seen from (2.3) that

$$\langle A_i\rangle_{Av}=\left\langle\frac{\mathbf{B}_0\mathbf{B}_0+\mathbf{B}_i\mathbf{B}_i}{B_0^2+B_i^2}\right\rangle_{Av}+\left\langle 1-\frac{\mathbf{B}_0\mathbf{B}_0+\mathbf{B}_i\mathbf{B}_i}{B_0^2+B_i^2}\right\rangle_{Av}\cos gB_0\tau_i-\frac{\sin gB_0\tau_i}{(B_0^2+B_i^2)^{\frac{1}{2}}}\langle\mathbf{B}_0\times\rangle_{Av},$$

where the brackets denote averages over the *directions* of the $\mathbf{B}_i$ (not the magnitude) and where use has been made of (3.5d) to replace $|\mathbf{B}_0+\mathbf{B}_i|$ by B_0 in the arguments of the trigonometric functions.

It is clear from the form of the dyadics that if condition (3.5e) is satisfied for $\mathbf{s}_0$ it will be satisfied for $\mathbf{s}$ at any time; i.e., the average of $\mathbf{s}$ is always parallel to $\mathbf{B}_0$ as it must be since this direction is the only preferred direction of the whole process. This circumstance permits the dropping of the dyadics $\langle\mathbf{B}_i\mathbf{B}_i\rangle_{Av}$ and $\langle B_0\times\rangle_{Av}$. Furthermore $\mathbf{s}\cdot\mathbf{B}_0\mathbf{B}_0=B_0^2\mathbf{s}$. Hence

$$\mathbf{s}_f=\pi_i\left[\frac{B_0^2}{B_0^2+B_i^2}+\left(1-\frac{B_0^2}{B_0^2+B_i^2}\right)\cos gB_i\tau_i\right]\mathbf{s}_0=\pi_i\left[1-\left(1-\frac{B_0^2}{B_0^2+B_i^2}\right)(1-\cos gB_0\tau_i)\right]\mathbf{s}_0$$

$$\leqq\pi_i[1-2(B_i^2/B_0^2)\sin^2\tfrac{1}{2}gB_0\tau_i]\mathbf{s}_0\leqq\exp[-2\textstyle\sum_i(B_i^2/B_0^2)\sin^2\frac{1}{2}gB_0\tau_i]\mathbf{s}_0$$

with use of condition (3.5d).

As in Section 2, two cases are of interest: *a*. $\frac{1}{2}gB_0\tau_i<1$. Then,

$$\mathbf{s}_f=\mathbf{s}_0\exp[-\tfrac{1}{2}\textstyle\sum_i g^2B_i^2\tau_i^2]=\mathbf{s}_0\exp[-\frac{1}{2}g^2\langle B_i^2\rangle_{Av}\langle\tau^2\rangle_{Av}T/\tau_{Av}].$$

As in 2, one replaces τ^2_{Av} by $\langle\tau\rangle^2_{Av}\equiv\tau^2$, obtaining

$$\mathbf{s}_f=\mathbf{s}_0\exp[-\tfrac{1}{2}g^2\langle B_i^2\rangle_{Av}\tau T]=\mathbf{s}_0\exp[-\tfrac{1}{2}g^2\langle B_i^2\rangle_{Av}\delta d/v^2]. \tag{3.6a}$$

b. $\frac{1}{2}gB_0\tau_i>1$.

$$\mathbf{s}_f=\mathbf{s}_0\exp[-\textstyle\sum_i(B_i^2/B_0^2)]=\mathbf{s}_0\exp[-\langle B_i^2/B_0^2\rangle_{Av}(T/\tau)]=\mathbf{s}_0\exp[-(\langle B_\perp^2\rangle_{Av}/B_0^2)(d/\delta)]. \tag{3.6b}$$

The physical distinction between the cases *a* and *b* can be described as follows: In case *a* $gB_0\tau_i/2<1$, each domain gives rise to a small rotation of the spin $\sim g\tau_i(\mathbf{B}_0+\mathbf{B}_i)\times\mathbf{s}$. Since by hypothesis $\mathbf{s}$ is parallel to $\mathbf{B}_0$, only the random field $\mathbf{B}_i$ contributes to this rotation with the amount $g\tau_iB_i\mathbf{s}$. These rotations accumulate according to formula (3.6a). If, on the other hand, $gB_0\tau_i>1$ the component of $\mathbf{s}$ which is perpendicular to $\mathbf{B}_0+\mathbf{B}_i$ undergoes a large rotation, and if we average over B_i and τ_i this component reduces to zero. There remains, therefore, only the component parallel to $\mathbf{B}_0+\mathbf{B}_i$ with a magnitude $sB_0/|\mathbf{B}_0+\mathbf{B}_i|$. Averaging this vector component over all directions of $\mathbf{B}_i$ leaves us with

a vector parallel to $\mathbf{B}_0$ which has the magnitude

$$s(B_0^2/B_0^2+B_i^2)\sim\exp(-B_i^2/B_0^2).$$

This gives semi-quantitatively a depolarization coefficient *per domain* equal to $\exp(-B_i^2/B_0^2)$ and, correspondingly, a depolarization coefficient $\exp(-nB_i^2/B_0^2)=\exp[-(d/\delta)(B_i^2/B_0^2)]$ for the total thickness of the ferromagnet.

Case 4

(a) The field of each domain is again made up of two components. The first, $\mathbf{B}_0$, is the same for all domains; the second, $\mathbf{B}_i$, constant throughout the time interval τ_i, is completely random in direction. The magnitude of $\mathbf{B}_i$ is now taken to be of the same order as that of $\mathbf{B}_0$.

(b) The Larmor period is large compared to the time spent in a domain: $g|\mathbf{B}_0+\mathbf{B}_i|\tau_i\ll 1$.

(c) The initial direction of the spin vector is the same as that of $\mathbf{B}_0$. The constancy of $\mathbf{B}_i$ in time τ_i and the statistical independence of the $\mathbf{B}_i$ again permit the reduction of (3) to the form

$$\langle A_i\rangle_{Av}=\left\langle\frac{(\mathbf{B}_0+\mathbf{B}_i)(\mathbf{B}_0+\mathbf{B}_i)}{(\mathbf{B}_0+\mathbf{B}_i)^2}\right\rangle_{Av}+\left\langle 1-\frac{(\mathbf{B}_0+\mathbf{B}_i)(\mathbf{B}_0+\mathbf{B}_i)}{(\mathbf{B}_0+\mathbf{B}_i)^2}\right\rangle_{Av}\cos g|\mathbf{B}_0+\mathbf{B}_i|\tau_i$$
$$-\frac{\sin g\tau_i|\mathbf{B}_0+\mathbf{B}_i|}{|\mathbf{B}_i+\mathbf{B}_i|}\langle(\mathbf{B}_0+\mathbf{B}_i)\times\rangle_{Av}.$$

The mathematics of the averaging process is complicated by the dependence of $|\mathbf{B}_0+\mathbf{B}_i|$ on $\cos(\mathbf{B}_0,\mathbf{B}_i)$ which must be taken into account in averaging over the direction of $\mathbf{B}_i$. One can get around this difficulty by employing condition (b). Expanding $\cos(g|\mathbf{B}_0+\mathbf{B}_i|\tau_i)$ and $\sin(g|\mathbf{B}_0+\mathbf{B}_i|\tau_i)$ in terms of their argument, one obtains:

$$A_i=1-\tfrac{1}{2}g^2\tau_i^2[(\mathbf{B}_0+\mathbf{B}_i)^2-(\mathbf{B}_0+\mathbf{B}_i)(\mathbf{B}_0+\mathbf{B}_i)]-g\tau_i(\mathbf{B}_0+\mathbf{B}_i)\times,$$

which, when averaged over the directions of $\mathbf{B}_i$, gives

$$\langle A_i\rangle_{Av}=1-\tfrac{1}{2}g^2\langle\tau_i^2[B_0^2+B_i^2-\mathbf{B}_0\mathbf{B}_0-\tfrac{1}{3}B_i^2]\rangle_{Av}.$$

Now, by condition (c), $\mathbf{B}_0\mathbf{B}_0\cdot\mathbf{s}=B_0^2\mathbf{s}$ hence

$$\langle A_i\rangle_{Av}=1-\tfrac{1}{3}g^2\tau_i^2\langle B_i^2\rangle_{Av}=\exp[-\tfrac{1}{3}g^2\langle\tau_i^2B_i^2\rangle_{Av}]$$

or

$$\mathbf{s}_f=\mathbf{s}_0\exp[-\tfrac{1}{3}\textstyle\sum_i\langle g^2\tau_iB_i^2\rangle_{Av}]=\mathbf{s}_0\exp[-\tfrac{1}{3}g^2\langle B_i^2\rangle_{Av}\langle\tau^2\rangle_{Av}T/\tau]$$
$$\backsimeq\mathbf{s}_0\exp[-\tfrac{1}{3}g^2\langle B_i^2\rangle_{Av}\tau T]=\mathbf{s}_0\exp[-\tfrac{1}{3}g^2\langle B_i^2\rangle_{Av}d\delta/v^2]. \quad (3.7)$$

IV. Domain Structure of Ferromagnets

According to present ideas, a ferromagnetic material consists of domains of microscopic size in each of which the atomic spins are lined up to give a *spontaneous* magnetization. In the unmagnetized state the directions of these spontaneous magnetizations are such that the macroscopic magnetization is zero. The application of an external field causes these directions to shift in such a way as to reduce the angle between the magnetization and this field. The net effect is then no longer zero; in other words the system is magnetized.

The nature of the domains is determined, as is to be expected, quite sensitively by the physical state of the material. For the purposes of this paper these states are classified according to the following scheme: (1) single crystals, (2) unmagnetized polycrystals, which will now be discussed in order.[3]

(1) Single crystals

The distinguishing feature of crystal ferromagnetism is *anisotropy* of magnetization. It is

[3] The case of magnetized polycrystals, in which the magnetic inhomogeneities are due to the slight deviations of the magnetizations of the component crystals from the direction of the external field is discussed in Section VII.

found that the increase of magnetization in an applied field is strongly dependent on the direction of this field with respect to the crystal axes. For instance, in the case of iron, a field of only a few gauss suffices to produce saturation parallel to a cubic axis, whereas saturation along a [1, 1, 1] plane requires a field of almost 400 gauss. Thus, for iron, the cubic axes are the *preferred* or "easy" axes of magnetization, whereas the [1, ±1, ±1] planes are the "difficult" axes. For a more complete discussion of the experiments the reader is referred to the standard texts,[4,5] it will suffice, here, to state the concepts which have resulted from them. The process of magnetization is, at present, regarded as proceeding in the following manner. In the unmagnetized state the domains are lined up along the preferred axes in such a way that the macroscopic magnetization is zero. When a field is applied, the domains readily shift their directions to that preferred axis which makes the smallest angle with the field, the ease with which this change is accomplished being determined by the coercive force, which is very small for single crystals. Further increase of the field causes the magnetization vector to be rotated away from the preferred axis, macroscopic saturation being attained when this vector is brought into coincidence with the direction of the field.

Up to this point, the properties of domains have been discussed solely from the standpoint of their role in macroscopic phenomena. The most important progress in recent times, however, has been achieved by the method of colloidal magnetic powders.[6] The principle upon which this method is based is identical with that behind the elementary demonstration of magnetic fields by the use of iron filings: The magnetic powder is acted on by a force which drives it to the place of strongest field strength. In practice, a suspension or colloidal solution of magnetic powder is placed on a smooth surface of the specimen. The resultant pattern, which is determined by the fields arising from the presence of surface domains, is examined with a microscope.

Unfortunately, the detailed interpretation of the results is subject to a serious limitation.[7] It has been found that the patterns formed on mechanically polished surfaces, in general, differ from those formed on naturally smooth surfaces. The question arises as to whether the observed domain structure is really characteristic of the whole crystal, or whether it is merely a surface phenomenon connected with some magneto-mechanical effect of the polishing operation.

The only experiments which seem free from this objection are those of Elmore,[8] who investigated the powder patterns of cobalt. The surfaces on which the patterns were observed were prepared by electrolytic polishing. It was found that mechanical polishing, followed by electrolytic treatment, did not change the type of pattern; hence it was reasonably certain that the surface structure is independent of the treatment and that, consequently, this structure could be identified with that existing in the interior. The observations themselves indicated the existence of plate-like or thread-like domains with magnetization alternately parallel and anti-parallel to the hexagonal axis. (Cobalt possesses a hexagonal crystal structure.) As this axis is the only preferred direction, this result coincides quite satisfactorily with those of the anisotropy experiments. It was also found that the shortest dimension of the domain always lay perpendicular to the hexagonal axis, its magnitude lying between the limits of 1 to 70μ.

(2) Unmagnetized polycrystalline media

The domain structure of polycrystalline media is obviously much more complicated than that of single crystals. The origin of these complications is twofold. First, the axes of easy magnetization vary in a more or less random fashion through the specimen with the result that at the boundary of the crystal grains discontinuities in magnetization give rise to free magnetic charges; these charges, in turn, set up a magnetic field whose reaction on the domain magnetization can be quite appreciable, even to the extent of rotating

[4] F. Bitter, *Introduction to Ferromagnetism* (McGraw-Hill Book Company, Inc., New York and London, 1937), Sections 57–62.

[5] E. C. Stoner, *Magnetism and Matter* (Methuen and Company, London, 1934), Chapter XI, Section 6.

[6] For a comprehensive review of this method, see reference 4, Sections 33, 34.

[7] W. C. Elmore, "Properties of the surface magnetization in ferromagnetic crystals," Phys. Rev. **51**, 982 (1937).

[8] W. C. Elmore, Phys. Rev. **53**, 757 (1938).

this magnetization somewhat from the preferred axes.[9] Secondly, the usual polycrystalline samples are in a more or less strained condition. Strains produce two effects: the setting up of new preferred axes[10] and the increase of the coercive force and hysteresis.

Direct information concerning the domain structure of polycrystals has been obtained almost exclusively from experiments on the Barkhausen effect. It is noticed that when a ferromagnetic material is subjected to an increasing external magnetic field, there occur sudden reversals of the magnetization of the domains; these reversals are detected by amplification of the pulse produced in a secondary coil surrounding the specimen. A systematic investigation of the size and direction of single reversals in iron, conducted by Bozorth and Dillinger[11] has revealed the following: (a) On the steep part of the magnetization curve, the direction of the reversals is mainly parallel to the applied field. The average volume of a single reversal is of the order 10^{-9} to 10^{-8} cm^3. (b) On that part of the curve above the knee ($B\sim 14{,}000$ gauss, $H\sim 5$ gauss) the direction is mainly transverse with respect to the field. The volume of the reversals is of the order of 10^{-12} cm^3. (c) With fields high enough to produce a quasi-saturated condition *no reversals* have been noticed; the approach to saturation seems to take place mainly by the process, described in the preceding section, of a rotation of the magnetization vectors of the individual crystal grains away from the preferred axis toward the direction of the external field. The Barkhausen jumps are thus linked up with the irreversible hysteresis processes occurring mainly in low fields ~ 0 to 20 gauss. (d) The above observations, including the numerical values of the volume of the reversals, hold for all types of iron, ranging from well-annealed to cold-worked specimens, as well as for nickel and Permalloy. Since the size of the crystal grains differs considerably for these various cases, the volume of a Barkhausen reversal may be larger than, equal to, or smaller than the volume of a single grain.

These results have been interpreted by some authors[12] as indicating that the size of the domains is independent of the crystalline structure. On the basis of this concept a single domain would include regions of widely different elastic and crystalline condition, a conclusion which one would accept only with extreme reluctance. If, on the other hand, the domains are of the same size, a single Barkhausen jump must involve the simultaneous reversal of the magnetization of several domains.

V. Applications of Depolarization of Neutrons to the Study of the Domain Structure of Single Crystals

The concept of the domain structure of cobalt as an alternating series of parallel and anti-parallel magnetizations, as obtained from Elmore's experiments, will be used as a starting point in the discussion of depolarization effects in single crystals. The results for this case can be written down immediately from Section III (1), provided it can be shown that the magnetic field $\mathbf{B}$ is also either parallel or anti-parallel to a fixed direction. Since

$$\mathbf{B}=\mathbf{H}+4\pi\mathbf{M}$$

and

$$\mathbf{H}=\nabla\int \mathrm{div}\mathbf{M}(\mathbf{r}')/|\mathbf{r}-\mathbf{r}'|\,dx'dy'dz',$$

the only deviation from the conditions of III (1), can arise from the existence of a "free charge" on the surface of the crystal; in the interior, the direction of magnetization is always parallel to the domain boundaries, i.e., perpendicular to the direction of variation of $\mathbf{M}$, with the result that $\mathrm{div}\mathbf{M}=0$. It can also be shown that, by suitable experimental arrangement, the surface effects can be avoided. Therefore, one has $\mathbf{B}=4\pi\mathbf{M}$ which, when substituted into (3.1) gives

$$\mathbf{s}_{\perp f}=\mathbf{s}_{\perp 0}\langle\cos 4\pi Mg\theta\rangle, \tag{5.1a}$$
$$\mathbf{s}_{\parallel f}=\mathbf{s}_{\parallel 0}, \tag{5.1b}$$

where θ is the excess time spent in the positively oriented domains. The consequences of these formulae will now be treated in the order enumerated:

[9] When there is no free charge a field $\mathbf{B}=4\pi\mathbf{M}$ is still present; the torque per unit volume exerted by this field, $4\pi\mathbf{M}\times\mathbf{M}$ is, however, zero.

[10] Reference 4, Section 54–58, Chapter VII.

[11] R. M. Bozorth, Phys. Rev. **39**, 353 (1932); R. M. Bozorth and J. F. Dillinger, *ibid.* **34**, 772 (1929); **35**, 733 (1930).

[12] R. M. Bozorth, Phys. Rev. **39**, 353, 375 (1932); E. C. Stoner, reference 5, page 413; W. F. Brown, Phys. Rev. **53**, 482 (1938).

(1) Depolarization of the perpendicular component

As stated in III (1), the magnitude of this effect depends upon the distribution of θ, which, in turn, depends upon the domain structure. Now, whether the domains have the form of layers or threads, it seems highly unlikely that the parallel regions would be exactly compensated by the antiparallel; one would, in general, expect that the excess of one over the other would be of the order $n\delta$ where δ is the average linear dimension of the domain and n a numerical factor of the order of magnitude unity. If the beam is directed perpendicular to the hexagonal axes, a tentative estimate of the uncompensated path can be attained by taking $n=1$ and δ of the order of magnitude of the sizes observed by Elmore 1 to 70μ. Taking the corresponding value of $\theta=\delta/v$ to be the width of the distribution function, $f(\theta)$, of the neutron paths over the possible values of θ, one finds that the argument of the cosine of (5.1a) varies over the interval $|\phi|<4\pi Mg\delta/v$ which, with $M=1400$ gauss (for cobalt), $g=2e/M_nc$ (M_n = mass of neutron), is of the order of magnitude $3\times10^3\delta$. It is thus apparent that any amount of depolarization can be secured depending on the value of δ. In the case of one extreme, $\delta=1\mu$, $\langle|\phi|\rangle_{Av}\sim0.3$ radian, and $\langle\cos\phi\rangle_{Av}\sim1$. For the other extreme $\delta=70\mu$, $\langle|\phi|\rangle_{Av}=20$ radians; tentatively assuming the distribution function for ϕ to be constant up to $\phi=20$ and zero for ϕ greater than this value, one obtains $\langle\cos\phi\rangle_{Av}\sim1/20$ or residual polarization 5 percent of the initial value.

In order to obtain a suitable variation of δ and, hence, of ϕ it is not necessary to employ different samples. If the beam is sent through the crystal with an inclination of χ with respect to the hexagonal axis, all the domain lengths are increased by a factor

$$\csc\chi, \quad \text{i.e.} \quad \phi_x=\phi_0\csc\chi,$$

where ϕ_0 represents the value of ϕ for $\chi=90°$. The depolarization effect for any angle χ is, then,

$$\langle\cos\phi_x\rangle_{Av}=\int\cos(\phi_0\csc\chi)g(\phi_0)d\phi_0,$$

where $g(\phi)$ is the distribution function for ϕ corresponding to $f(\theta)$. By studying the depolarization as a function of χ one can obtain the Fourier components of $g(\phi)$ over a large range and hence obtain some idea of the shape of this function, itself. The width of the distribution, in particular, is determined by the angle χ at which the residual polarization drops off appreciably from unity, i.e., when $\langle\phi_0\rangle_{Av}\csc\chi\sim1$, from which, in turn, one can obtain an estimate of the domain size to be compared with the results of Elmore.

(2) Constancy of the parallel component

The preceding discussion has shown that appreciable depolarization effects are to be expected whenever the magnetizations of the domains are not parallel to the spin of the incident neutrons. Depolarization experiments should therefore provide information concerning the directional properties of single crystal domains. Examples of such experiments are as follows:

(*a*) *Unmagnetized cobalt crystals.*—In this case the magnetizations are parallel to the hexagonal axis—hence no effect on the polarization (cf. (5.1b)). However, heat treatment or the application of stress may cause deviations which could then be detected by depolarization.

(*b*) *Magnetized cobalt crystals.*—One can test for nonparallel domains at all stages of the magnetization curve. One would have to take into account the depolarizing effects arising from the external field; this should not be difficult in view of the extremely small value of this field.

(*c*) *Unmagnetized iron crystals.*—In an ordinary single crystal of iron the preferred directions of magnetization are the three cubic axes. A neutron beam should suffer depolarization on passing through such a medium regardless of the direction of its original polarization. However, it may be possible, by the application of stress along one of the preferred directions, to align the magnetization of all domains parallel and antiparallel to this direction. In that case, one could, as before, arrange an experiment in which no depolarization took place.

(*d*) *Demagnetization of iron.*—Although a crystal without previous magnetic treatment may have domains whose magnetizations are oriented along all of the three preferred axes, the demagnetization of a sample, magnetically saturated parallel to any one of them, might occur unidirectionally, i.e. the total magnetic moment would be

cut down by the formation of domains whose magnetizations point in the opposite direction. This hypothesis could be tested by a depolarization experiment. If such an arrangement of the domains actually exists, one could investigate its stability towards heat treatment and the application of small stresses.

VI. Applications of Depolarization of Neutrons to the Study of Domain Structure of Polycrystalline Media

Formulae describing the depolarization of neutrons in polycrystals are contained in III (2); one has only to investigate how far the assumptions underlying that treatment are fulfilled in this case.

(1) Randomness of domains

The first theory, discussed at the end of IV (2), states that the domain size is independent of the crystalline structure; the direction of magnetization of these domains must then be assumed to be random.[13] As far as the second theory is concerned, the domains in different crystals certainly have no correlation with each other, because of the arbitrariness of orientation of crystal axes in a polycrystal. For domains contained in the same crystal, the discussion of V has shown that there exist domain arrangements of magnetizations parallel and anti-parallel to a fixed axis in the case of cobalt, which has only one easy axis, but not in the case of iron, which has three. The general effect of such arrangements is to cut down the depolarization. The correction to the formulae arising from these considerations will be presented at the end of this section; for the present, it will be assumed that the magnetizations are randomly oriented.

(2) Constancy of the field B_i over the ith domain

This assumption is open to two objections:

(a) The magnetization of the domains in polycrystalline media may not be constant throughout the domain, but may vary gradually so as to give a continuous transition between different domains. In single crystals the domains are lined up parallel to the easy axes; the transition region between any two domains, in which the magnetization rotates from one preferred direction to another, has been estimated theoretically[14] to be $\sim 10^{-6}$ cm, which is compatible with the observations of Elmore. The application of these ideas to polycrystalline media is, however, not advisable, due to the presence of elastic inhomogeneities and internal magnetic fields, both of which may appreciably alter the direction of magnetization so as to result in a broader transition region.

(b) Even if the magnetization were constant over a domain, the same could not be said for the induction since this quantity is not proportional to the magnetization; one must add to the $4\pi\mathbf{M}$ term the field arising from the existence of magnetic poles at the boundaries of domains. In general, this field is not parallel to the magnetization; in fact, the well-known boundary conditions for the fields—normal component of $\mathbf{B}$ tangential component of $\mathbf{H}$ continuous—preclude this relationship except under most artificial conditions.

These objections indicate that a treatment more suitable than III(2), would be one which provided for a continuous variation of the field along a neutron path. However, the authors are of the opinion that this refinement is unnecessary, for the following reasons:

(a) The main characteristic of the motions considered in III is that the time in which the magnetic field changes appreciably is not larger than the Larmor period of the neutron spin, i.e., from the quantum-mechanical point of view, the motion is non-adiabatic. Now, in the present case, even though the transitions between the different magnetic fields may be continuous, i.e., they may require times of the order τ_i, the variation is sufficiently rapid for the motion to be classed as non-adiabatic. This feature is immediately apparent when one recalls that the spin of a thermal neutron precesses, on the average, about 1 to 2 radians in a region of 10^{-3} cm. Since the linear dimensions of the largest domains do not exceed this quantity, the transition from one field to the other will *a fortiori* take place in a small fraction of a complete precession. Thus, the non-adiabatic character of the motion is preserved.

(b) In view of these considerations, the treatment of III (2), should give results of the correct order of magnitude, the only effect of the variation of $\mathbf{B}_i$ in the time interval being a change in the numerical factors of the exponents of the depolarization formulae (8.1a) (8.1b) of the order of magnitude. However, one would not want any greater accuracy since the size of the domains may be expected to vary over a correspondingly wide range.[15]

The assumptions underlying III (2), can then be taken as essentially valid; the existence of magnetic charge will be approximated by

[13] One might think that the domains would tend to line themselves up in such a way as to avoid as much as possible the creation of magnetization charge; this can, however, be produced merely by having the normal component vary continuously across a boundary, the tangential component being free to change by any value. Such an arrangement would not be random in the sense of III (2), but its effect on the depolarization would be the same to within a numerical factor of the order unity, of III (3), case (1).

[14] L. Landau and E. Lifshitz, Physik. Zeits. d. Sowjetunion **8**, 153 (1935).

[15] A more accurate treatment would be necessary if one were to investigate, say, the distribution of domain sizes; such problems are not contemplated in the present paper.

the insertion of a demagnetizing factor, i.e., $B_i \cong (4\pi-\gamma)M$ where $\gamma \sim (4/3)\pi$. Inserting this relation into (3.4a) and (3.4b), one obtains:

(*a*) For $(4\pi-\gamma)Mg\tau/2 \ll 1$,

$$s_f/s_0 = \exp[-\tfrac{1}{3}(4\pi-\gamma)^2(gM/v)^2 d\delta]. \quad (6.1a)$$

(*b*) For $(4\pi-\gamma)Mg\tau/2 \gtrsim 1$,

$$s_f/s_0 = e^{-d/\delta}. \quad (6.1b)$$

These formulae will now be applied to distinguish between the two theories discussed in IV (2).

(*1*) *Domain size* $\sim 10^{-9}-10^{-8}$ *cm³ independent of crystal structure.*—$(4\pi-\gamma)Mg\tau/2$ has an upper limit of 2. The depolarization is then given by (6.1b) for all materials investigated by Bozorth and Dillinger,[10] in particular for all types of iron. With $\delta \sim 10^{-3}$ cm a sample of thickness 5×10^{-3} cm suffices to depolarize the beam completely.

(*2*) *Domain size of the order or smaller than the size of the crystal grains.*—In this case the depolarization should depend quite strongly on the previous treatment of the specimen. If the crystal grains have linear dimensions $<3\times10^{-4}$ cm, $(4\pi-\gamma)Mg\tau/2$ has an upper limit of 0.25 and the depolarization is then given by (6.1a). It can then be seen that, even if the domains are assumed to be identical with the crystal, a sample the linear size of whose grains is $\sim 10^{-4}$ cm would give a depolarization effect of an altogether smaller order of magnitude from that of (1). In fact:

$$\tfrac{1}{3}[g(4\pi-\gamma)M/v]^2 d\delta \gtrsim \tfrac{1}{3}(1.7\times10^3)^2\times10^{-4}d = 10^2 d,$$

and, hence, the polarization of a beam passing through a sample 5×10^{-3} cm should be cut down by a factor not smaller than $e^{-1} \sim 60$ percent.

The difference in depolarization predicted by the two theories should be especially noticeable for thin films whose thickness is of the order of 6μ. The first theory then predicts that the linear dimensions of the domains should be of the same order of magnitude as the thickness of the film. One can then obtain results of the correct order of magnitude by employing (6.1a) for both theories. The first, predicting domain sizes of the order of magnitude of the film thicknesses, gives a depolarization effect $s_f/s_0 = e^{-1} = 70$ percent. According to the second theory, for which the domains are not larger than the crystals (in this case $<10^{-5}$ cm), no effect should be observed.

Before (6.1a) and (6.1b) can be employed to establish the application of depolarization experiments to more general problems of polycrystalline domain structure, the possibility of ordered arrangements of the domains within one crystal grain must be investigated in some detail. This will now be done for the cases of iron, nickel, and cobalt.

(1) Iron and nickel: In crystal grains composed of these substances, the magnetization may be oriented along any one of several directions ((1, 0, 0) directions for iron, (1, 1, 1) for nickel). The only arrangement which can cut down the depolarization effect is one of alternately parallel and antiparallel domains (see next paragraph). From the energetic standpoint, however, there is no reason why this arrangement is to be preferred. Hence magnetizations along all "easy axes" may be present. The passage of a polarized neutron beam in a region where the directions of the domain magnetizations change by 90° (iron) or by 63° (nickel) gives rise to strong depolarization effects which are, if anything, somewhat underestimated by the assumption of randomness of direction, and thus tend to compensate the reduction due to the presence of parallel-antiparallel arrangements. As far as order of magnitude estimates are concerned, therefore, the existence of ordered domain structures within crystal grains should not affect the validity of (6.1a), (6.1b) for iron and nickel.

(2) Cobalt: Here, the existence of only one preferred axis should cause appreciable cancellation of the rotation of the neutron spin in separate domains. The problem has been treated for two types of arrangements: plate-like and cylindrical domains, (case of $g(4\pi-\gamma)M\delta/(2v) \ll 1$). The results are:

(a) For domains in the form of plates

$$s_f/s_0 = \exp(-\tfrac{3}{4}(4\pi Mg)^2 d\delta/v^2), \quad (6.2a)$$

where δ now represents the average thickness of the plates.

(b) For domains in the form of cylinders:

$$s_f/s_0 = \exp(-\tfrac{1}{2}(4\pi Mg/v)^2 \delta d[(\delta/\delta_0)\log 2\delta_0/\delta]), \quad (6.2b)$$

where δ is the average thickness of the cylinders and δ_0 the average linear dimension of the crystal grains.

The resemblance of (6.2a) to (6.1a) is quite satisfactory, the only difference apart from numerical factors being that the δ of (6.1b) is the domain length averaged over its shape, whereas for (6.2a) it is its shortest length. The form of (6.2b) does differ somewhat from these two except in the case $\delta \sim \delta_0$; it may be mentioned in passing, however, that the theoretical treatment of single crystal domains by Landau and Lifshitz[12] indicates that the cylindrical arrangements require more energy than the plate-like and hence should not occur.

Equations (6.1a, b) (6.2a, b) establish the connection between depolarization experiments and domain size. Such experiments, then, should yield important information on the general problem of domain structure in polycrystals, e.g., its dependence on grain size, internal strain, chemical composition (presence of impurities) and previous magnetic history.

VII. Depolarization of Neutrons in Polycrystalline Media Near Saturation

The magnetic domains whose nature has been discussed in the three preceding sections are characteristic of ferromagnets in small external fields $\lesssim 10$ gauss. When this field is increased to a value $\gtrsim 200$ gauss, these domains are wiped out. As was stated at the beginning of VI (1), the anisotropy experiments show that, under such conditions, the main, if not the sole, process governing the variation of magnetization in single crystals is the rotation of the magnetic vector (towards the direction of the external field). The angle between the two is determined by equating the torque exerted by the crystalline field to that arising from the action of the magnetic field; this equation has the form: $\mathbf{T}(\theta, \phi)=\mathbf{M}\times\mathbf{H}$, where $\mathbf{T}(\theta, \phi)$ is a vector function of the polar coordinates, θ and ϕ of the magnetic vector with respect to the crystal axes.[16]

The application of these ideas to the behavior of polycrystalline samples in high fields leads to the following picture. Each crystal grain possesses a magnetization whose magnitude is equal to the saturation value; the direction of this magnetization deviates somewhat from that of the external field. If the specimen has not been subjected to special mechanical treatment, e.g., plastic deformation, the axes of the microcrystals will be oriented at random; it then follows that the deviations of the magnetizations of the separate crystals are also random. The macroscopic magnetization is given by the average of the component of the magnetization parallel to the external field.

This model is readily seen to correspond to that of III (3), as in VI, the assumption that the random field $\mathbf{B}_i$ is constant in time τ_i is not true in the actual physical case; however, again, the variation of the size of crystals in a single specimen and the consequent uncertainty in the depolarization formulae renders any attempts to obtain better accuracy quite purposeless. The field will hence be considered constant, its relationship to the magnetization will be described, as in VI, by a demagnetizing factor. Thus

$$\mathbf{B}_i=(4\pi-\gamma)\delta\mathbf{M}_i\leqq(8/3)\pi\delta\mathbf{M}_i,$$

where $\delta\mathbf{M}_i$ is the vector deviation of the magnetic vector of the ith crystal from the macroscopic magnetization. The dependence of the depolarization formulae (3.6a) and (3.6b) on $\mathbf{B}_i$ is given in terms of its average square,

$$\langle B_i^2\rangle_{Av}\leqq(8\pi/3)^2\langle(\delta\mathbf{M}_i)^2\rangle_{Av}.$$

Now $(\delta\mathbf{M}_i)^2=M_s^2-M_{\parallel i}^2$ where M_s is the saturation value of the magnetization and $M_{\parallel i}$ the component parallel to the macroscopic magnetization, $\mathbf{M}_0$. Then

$$\langle(\delta\mathbf{M}_i)^2\rangle_{Av}=M_s^2-M_0^2\leqq 2M_0\Delta M,$$

where $\Delta M\equiv M_s-M_0$ is the *deviation* of the macroscopic magnetization from its saturation value. $\mathbf{B}_0$ of course, is given by the familiar relation $\mathbf{B}_0=4\pi\mathbf{M}_0+\mathbf{H}$. Thus, from (3.6a, b)

$$s_f/s_0=\exp[-(8\pi/3)^2M_0\Delta M\delta d/v^2],$$

$$\text{if } 2\pi gM_0\delta/v<1; \quad (7.1a)$$

$$s_f/s_0=\exp[-(4/3)(\Delta M/M_0)d/\delta],$$

$$\text{if } 2\pi gM_0\delta/v>1, \quad (7.1b)$$

where δ is the average linear dimension of the crystal grains. The value of δ at which (7.1a) goes into (7.1b) is given by

$$\delta=v/(2\pi gM_0)\leqq 1.5\times10^5/2\times10^{-8}$$

$$\sim 7\times10^{-4}\text{ cm}. \quad (7.2)$$

The applicability of these formulae rests on the assumption that the magnetic inhomogeneities arise solely from the angular deviation of the crystal magnetizations from the macroscopic magnetization. Now it is conceivable, although highly unlikely, that even at high fields there persist regions whose magnetizations are oriented at random, i.e., Barkhausen domains which have not yet flipped over. The contribution of such regions to the observed difference between the macroscopic and saturation magnetization has been shown to be negligible. The presence of these domains, therefore, cannot change the depolarization unless they exert an effect disproportionately large compared to their influence on the magnetization.

[16] When strains are present, the energy is dependent upon the direction of the magnetization with respect to axes defined by the strain. The net effect is merely to set up new crystal axes with new anisotropy constants.

The disproof of the existence of such an effect follows readily from Eq. (3.7) of III (4). This equation represents the depolarization due to a medium consisting of randomly oriented domains in the presence of an external field. In the present case these random domains occupy only a fraction of the total volume of the specimen; this fraction is given by $\eta=\Delta M_1/M_s$ where ΔM_1 is the deviation from saturation due to the presence of these domains. Thus the quantity d in the exponent of (3.7) must be replaced by

$$\eta d=(\Delta M_1/M_s)d\leqq(\Delta M_1/M_0)d_0.$$

Furthermore,

$$\mathbf{B}_i\leqq(4\pi-\gamma)\mathbf{M}_i\sim(8/3)\pi\mathbf{M}_i;\quad|\mathbf{M}_i|\sim M_s\leqq M_0.$$

Therefore:

$$s_f/s_0\leqq\exp[-\tfrac{1}{3}g^2(8\pi/3)^2M_0\Delta Md\delta/v^2].$$

The exponent of this equation, apart from numerical constants of the order unity, has the same functional form as that of (7.1a). Hence, for a given ΔM the two cases can differ only in the values of δ the domain, or crystal, size. Now, in most of the practical cases, the crystal sizes are not far from the borderline between (7.1a) and (7.1b) as given by (7.2). Therefore, whatever the size of the domains, their effect per unit ΔM is, at most, of the same order as that of the crystal grains. The depolarization due to unoriented domains is, hence, important only if the corresponding ΔM is an appreciable fraction of the total ΔM, a hypothesis which cannot be admitted.

Finally, it should be mentioned that, in materials possessing an average magnetic moment different from zero, there will be a *polarization* effect which will either add to, or subtract from, the depolarization. The polarization will be discussed fully in the next section; at this point it is sufficient to point out that, both from theoretical estimates, and from the experiments, no appreciable modification of (7.1a), (7.1b) need be feared.

The order of magnitude of the depolarization effect in high fields will now be estimated. If the crystals have linear dimensions not less than 10^{-3} cm, $gB_0\tau/2>1$ and (7.1b) is to be employed. For the usual samples of soft iron, δ ranges from 10^{-3} to 10^{-2} cm. In order, then, for a reduction of the polarization to $1/e$ of the initial value in 1 cm of material to take place, the relative deviation from saturation, $\Delta M/M_0$, need only be 0.1 percent to 1 percent.

In conclusion, (7.1a) and (7.1b) can be used to investigate the properties of ferromagnets near saturation. One determines the depolarization as a function of the macroscopic magnetization. The ratio of $\log(s_f/s_0)$ to ΔM should be a constant $\leqq(4/3)(d/\delta)(1/M_0)$ or $\frac{1}{3}g^2(8\pi/3)^2M_0d\delta$ from which one can obtain an estimate of δ to be compared to the observed grain size. If these predictions are not fulfilled, it will be necessary to revise the concepts which have been advanced to explain the magnetic behavior of ferromagnets in saturation fields.

VIII. Transmission of Neutrons in Saturated Polycrystalline Media

The transmission of neutrons has been treated heretofore as a purely atomic problem. One first calculated the atomic scattering cross section for beams in the different spin states. To find the effect of a differential layer of material on the transmitted beam, one multiplied this quantity by the number of atoms in the layer and subtracted the resultant total scattering intensity from the incident intensity. The results of these calculations expressed in differential form are:

$$d/dx(I/v)=-\lambda I/v+w\sigma, \tag{8.1a}$$

$$d\sigma/dx=-\lambda\sigma+wI/v, \tag{8.1b}$$

where I is the current density, σ the spin density, v the velocity of the neutrons, λ the sum of the absorptions due to capture and total scattering, both magnetic and nuclear, and w a constant depending on the details of the atomic scattering process and the direction of the beam with respect to the magnetic field.[17]

Now, it has been shown in the previous section that depolarization effects can be avoided only in the case of extreme saturation; if this situation does not obtain, the polarization resulting from the scattering process will be cut down. From the standpoint of the treatments heretofore given, this feature can be taken into account by the insertion into the second equation of a term proportional to the polarization, the coefficient

[17] J. S. Schwinger, Phys. Rev. **51**, 544 (1937).

of proportionality being determined by the rate of depolarization as given by (7.1). It is the opinion of the present authors, however, that the transmission formulae are inadequate in other respects, and that it is necessary to reinvestigate the whole problem in detail.

When one is dealing with a case of coherent scattering the fundamental unit is not the atom but the microcrystal. The procedure of multiplying the atomic cross section by the density of atoms to obtain the absorption of the transmitted beam is correct for gases, liquids, and amorphous solids; for crystalline substances the method is applicable only in the case of wave-length small compared to the separation of the atoms. Now, in order to obtain appreciable magnetic scattering, it is necessary that the wave-length of the neutron be *large* compared to atomic radii; otherwise, the interference of the scattered waves arising from different parts of the atom cuts down the amplitude of the magnetic scattering. Since the separation of the atoms is of the same order as their linear dimensions, it is clear that crystal structure plays an important role in the polarization process. *The method of adding over atomic cross sections must therefore be renounced.*[18] The remainder of this section is devoted to a derivation of the transmission formulae from the standpoint of scattering in crystalline media. An important result of the calculations will be the confirmation of (21); the numerical values of λ and w, however, will obviously be different from those given in previous treatments.

Before any calculations are performed, the meaning of the term *microcrystal* must be clarified. From x-ray studies it is known that crystals which are macroscopically perfect are usually composites of much smaller units, whose linear dimensions are of the order 10^{-5} cm. These sub-units have significance only with respect to wave-mechanical properties; in all other respects the crystal acts as a single entity. Indeed, such a system can conceivably be formed of units whose crystal axes are all oriented in the same direction but whose relative positions are variable over a distance of the order of the lattice spacing. The medium is then homogeneous from the standpoint of elastic and magnetic properties, but waves (x-rays, neutrons, electrons, etc.) emanating from the different sub-units do not superpose coherently. In order to obtain the intensity of scattering due to the whole crystal, one must square the amplitude of each of these waves, and sum the resultant intensities. In the calculations which follow, the term *single crystal* denotes a unit of polycrystalline material which is elastically homogeneous, whereas its sub-units, each of which scatter as a coherent whole, will be designated as *microcrystals*.

The Schrödinger equation for the system, microcrystal plus neutron, is

$$-(\hbar^2/2M_n)\nabla^2\psi+V\psi=E\psi,$$

where M_n denotes the mass of the neutron and V the interaction between the neutron and macrocrystal; this interaction is the sum of the potentials of the constituent atoms. Now, the unit cell of an iron crystal, which has a body-centered structure, can be regarded as a superposition of two simple cubic cells. The potential of one of these is

$$V_I=\sum_{\mathbf{g}} V_{\mathbf{g}I}\exp(i\mathbf{g}\cdot\mathbf{r});\quad \mathbf{g}=\mathbf{g}_1n_1+\mathbf{g}_2n_2+\mathbf{g}_3n_3;\quad n_i \text{ integral},$$

where the $\mathbf{g}$'s are reciprocal lattice wave vectors. The potential of the two cells is then

$$V=\sum_{\mathbf{g}}\left(V_{\mathbf{g}I}\exp(i\mathbf{g}\cdot\mathbf{r})+V_{\mathbf{g}I}\exp(i\mathbf{g}\cdot\{\mathbf{r}+\tfrac{1}{2}\mathbf{a}_1+\tfrac{1}{2}\mathbf{a}_2+\tfrac{1}{2}\mathbf{a}_3\})\right),$$

$\frac{1}{2}\mathbf{a}_1+\frac{1}{2}\mathbf{a}_2+\frac{1}{2}\mathbf{a}_3$ being the coordinate of the origin of one of the cubic systems with respect to the origin of the other, expressed in terms of the lattice vectors $\mathbf{a}_i$. It is convenient to define a new quantity $V_{\mathbf{g}}$ such that $V=\sum_{\mathbf{g}} V_{\mathbf{g}}\exp(i\mathbf{g}\cdot\mathbf{r})$; $V_{\mathbf{g}}=V_{\mathbf{g}I}(1+\exp[\frac{1}{2}i\mathbf{g}\cdot(\mathbf{a}_1+\mathbf{a}_2+\mathbf{a}_3)])$. Now $\mathbf{g}_1\cdot\mathbf{a}_1=2\pi n_1$. Therefore $V_{\mathbf{g}}=2V_{\mathbf{g}I}$ if $n_1+n_2+n_3$ is even, zero if this sum is odd. $V_{\mathbf{g}I}$ of course, is calculated from $V(\mathbf{r})$ by means of the inverse Fourier integral

[18] Halpern, Hamermesh and Johnson, Phys. Rev. **55**, 1125A (1939).

$$V_{\mathbf{g}'}=(1/a^3)\int_{\tau_0} V(\mathbf{r})\exp(-i\mathbf{g}\cdot\mathbf{r})d\tau_0$$

where τ_0 is the volume of the unit cell.

$V(\mathbf{r})$, itself, is the sum of the nuclear and magnetic potentials arising from the atoms of a constituent simple cubic cell:

$$V=V_{\text{nuc}}+V_{\text{mag}}.$$

For V_{nuc} one takes a fictitious form which gives the same scattering for an individual nucleus and which is suitable for the application of the Born approximation. V_{mag} represents the interaction of the neutron magnetic moment with the field set up by the electronic currents, i.e., $V_{\text{mag}}=\mu_n\boldsymbol{\sigma}\cdot\mathbf{B}$, where μ_n is the magnetic moment of the neutron, $\boldsymbol{\sigma}$ the Pauli spin operator[19] and $\mathbf{B}$ the magnetic field of the electrons.

One can now proceed to calculate the scattering of a microcrystal by the well-known Born method. Let

$$\psi=\exp(i\mathbf{K}_0\cdot\mathbf{r})\chi+\psi_1,$$

where χ is a two-component column matrix on which the neutron spin operator acts.[20] Then

$$(\nabla^2+K^2)\psi_1=(2M_n/h^2)V\psi_0;\quad K^2=2M_nE/h^2,$$

the solution of which is:

$$\psi_1(\mathbf{R})=(M_n/2\pi h^2)\int_\tau[\exp(iK|\mathbf{R}-\mathbf{r}|)/|\mathbf{R}-\mathbf{r}|]V(\mathbf{r})\psi_0(\mathbf{r})d\tau,$$

which, for R large compared to the linear dimensions of the microcrystal, becomes:

$$\psi_1(\mathbf{R})=(M_n/2\pi h^2)\sum_{\mathbf{g}}V_{\mathbf{g}}\chi(e^{iKR}/R)\int\exp[i(\mathbf{K}_0+\mathbf{g}-\mathbf{K})\cdot\mathbf{r}]d\tau,$$

where $\mathbf{K}_0$ and $\mathbf{K}$ are the propagation vectors of the incident and scattered waves, respectively. The integration gives:

$$\psi_1(\mathbf{R})=\frac{M_n}{2\pi h^2}\sum_{\mathbf{g}}V_{\mathbf{g}}\chi\frac{e^{iKR}}{R}\left(\frac{1-\exp[i(K_{0x}+g_x-K_x)l]}{i(K_{0x}+g_x-K_x)}\right)\left(\frac{1-\exp[i(K_{0y}+g_y-K_y)l]}{i(K_{0y}+g_y-K_y)}\right)\times\left(\frac{1-\exp[i(K_{0z}+g_z-K_z)l]}{i(K_{0z}+g_z-K_z)}\right),$$

where l^3 is the volume of a microcrystal, assumed, for the sake of simplicity, to be a cube.

The corresponding scattered current per unit area of a sphere of radius R is:[21]

$$s=v\psi_1^*\psi_1$$

$$=\frac{2M_n^2}{\pi^2h^4}\sum_{\mathbf{g}}\frac{\chi^*|V_{\mathbf{g}}|\chi}{R^2}\left(\frac{1-\cos l(K_{0x}+g_x-K_x)}{(K_{0x}+g_x-K_x)^2}\right)\left(\frac{1-\cos l(K_{0y}+g_y-K_y)}{(K_{0x}+g_x-K_x)^2}\right)\left(\frac{1-\cos l(K_{0z}+g_z-K_z)}{(K_{0z}+g_z-K_z)^2}\right).$$

---

[19] It is assumed that the spin of the neutron is $\frac{1}{2}$.

[20] In the calculation of the scattered intensity the zeroth Fourier coefficient of the potential is neglected. Ordinarily this feature is trivial since the resultant change in zeroth-order energy is negligible compared to the kinetic energy of the neutron. In this case, however, a certain complication arises due to the fact that the coefficient has opposite signs for the two spin states, i.e., the "indices of refraction" of waves in these states are different. A numerical calculation indicates that the phase difference between the waves becomes appreciable when a distance of the order 10^{-3} cm has been traversed. If the single crystal were composed of one microcrystal, this difference would actually have to be taken into account; since it is assumed that the scattering units have linear dimensions of the order 10^{-5} cm, the zero Fourier coefficient can forthwith be neglected.

[21] The different Laue spots are assumed not to overlap, in which case the cross terms ($\mathbf{g}\neq\mathbf{g}'$) drop out of the expression for the scattered current.

For variations of K_{0x} and K_x of the order of g_x the quantity $(1-\cos Kl)/K^2$ resembles a δ function in that it has appreciable values only for $K=0$. Since

$$\int_{-\infty}^{+\infty} dK(1-\cos Kl)/K^2=\pi l,$$

the scattered current becomes

$$s=(2\pi M_n{}^2l^3/h^4)\sum_g[(\chi^*|V_g|{}^2\chi)/R^2]\delta(\mathbf{K}_0+\mathbf{g}-\mathbf{K}),$$

where the δ function is three dimensional.

To find the total scattered current, one integrates over a sphere of radius R:

$$S=v\int\psi_1{}^*\psi_1 d\Sigma=(2\pi M_n{}^2l^3v/h^4)\sum_g(\chi^*|V_g|{}^2\chi)\int\int[\delta(\mathbf{K}_0+\mathbf{g}-\mathbf{K})/R^2](R/z)dxdy,$$

where $(R/z)dxdy$ gives the expression for a surface element in Cartesian coordinates. Taking the z axis along the direction of $\mathbf{K}_0+\mathbf{g}$ one obtains

$$S=(2\pi M_n{}^2l^3v/h^4)\sum_g(\chi^*|V_g|\chi)\int\int(1/R^2)\delta(Kx/R)\delta(Ky/R)\delta(Kz/R-|\mathbf{K}_0+\mathbf{g}|)(R/z)dxdy,$$

where $K_x=Kx/R$, etc.; since $\delta(ax)=\delta(x)/a$ the result of the integration is:

$$S=(2\pi M_n{}^2l^3v/h^4K^2)\sum_g(\chi^*|V_g|{}^2\chi)\delta(|\mathbf{K}_0+\mathbf{g}|-K).$$

One now takes cognizance of the mosaic structure of the crystal by adding the integrated intensities originating from the component microcrystals. Since the crystal axes of these smaller units are assumed to cluster around the value indicated by the macroscopic properties of the system, all of the contributions have the same form. Thus

$$s=\sum S=SL^3/l^3=(2\pi M_n{}^2L^3v/h^4K^2)\sum_g(\chi^*|V_g|{}^2\chi)\delta(|\mathbf{K}_0+\mathbf{g}|-K),$$

L^3 being the volume of a single crystal. Apparently the same formula is obtained if the single crystal is treated as perfect instead of mosaic; the difference, however, is contained in the δ function, whose value and width are still proportional to l and $1/l$, respectively.

One has now to average over all orientations of the single crystal, i.e., over the direction of the vector $\mathbf{g}$. For this purpose the explicit dependence of V_g on $\mathbf{g}$ must be determined. The potential $V(\mathbf{r})$ of one of the two component simple cubic structures of the system is given by the relation

$$\sum_i \alpha a^3\delta(\mathbf{r}-\mathbf{r}_i)-\mu_n\boldsymbol{\sigma}\cdot\mathbf{B}, \tag{8.2}$$

where a is the lattice spacing, α a constant given in terms of the nuclear cross section, and where the summation runs over all atoms contained in a simple cubic lattice. Here, as pointed out at the beginning of this treatment, use has been made of the trick of replacing the actual nuclear potential by a fictitious potential suitable for the application of the Born perturbation method. $\mathbf{B}$ is the magnetic field due to the atomic magnets; it is determined by the equations

$$\mathrm{div}\mathbf{B}=0;\quad \mathrm{curl}\mathbf{B}=4\pi\,\mathrm{curl}\mathbf{M}.$$

Expressed in terms of Fourier components, these equations read[22]

$$\mathbf{g}\cdot\mathbf{B}_g=0;\quad \mathbf{g}\times\mathbf{B}_g=4\pi\mathbf{g}\times\mathbf{M}_g.$$

Taking the cross product of the second equation with $\mathbf{g}/\mathbf{g}^2$ one obtains:

$$\mathbf{B}_g=-(4\pi/g^2)\mathbf{g}\times(\mathbf{g}\times\mathbf{M}_g).$$

[22] The Fourier coefficients of V and $\mathbf{B}$ due to a simple cubic structure are written as V_g and $\mathbf{B}_g$ instead of V_{gl} and $\mathbf{B}_{gl}$ as at the beginning of the section.

A superposition of the Fourier components of two cubic systems as described at the beginning of this section gives:

$$V_{\mathbf{g}\ \text{total}}=2(\alpha-\mu_n\boldsymbol{\sigma}\cdot B_{\mathbf{g}});\quad \text{or}\quad V_{\mathbf{g}\ \text{total}}=0$$

depending on whether the sum of the components of $\mathbf{g}$ in the reciprocal lattice system, $n_1+n_2+n_3$, is even or odd. One then has:

$$s=(8\pi M_n{}^2L^3v/h^4K^2)\sum_{\mathbf{g}}\delta(|\mathbf{K}_0+\mathbf{g}|-K)\chi^*[|\alpha|^2+\mu_n{}^2\boldsymbol{\sigma}\cdot\mathbf{B}_{\mathbf{g}}{}^*\boldsymbol{\sigma}\cdot\mathbf{B}_{\mathbf{g}}-\mu_n\boldsymbol{\sigma}\cdot\mathbf{B}_{\mathbf{g}}{}^*\alpha-\mu_n\alpha^*\boldsymbol{\sigma}\cdot\mathbf{B}_{\mathbf{g}}]\chi.$$

If each atom is taken to be the center of a unit cubic cell, the quantity

$$\mathbf{M}_{\mathbf{g}}=(1/a^3)\int_{-a/2}^{+a/2}\int_{-a/2}^{+a/2}\int_{-a/2}^{+a/2}\mathbf{M}(\mathbf{r})\exp(-i\mathbf{K}\cdot\mathbf{r})dx_0dy_0dz_0\ [\text{with } dx_0dy_0dz_0=d\tau_0]$$

is real by asymmetry; hence $\mathbf{B}_{\mathbf{g}}$ is real. Thus

$$s=(8\pi M_n{}^2L^3v/h^4K^2)\sum_{\mathbf{g}}\delta(|\mathbf{K}_0+\mathbf{g}|-K)\chi^*[|\alpha|^2+\mu_n{}^2\boldsymbol{\sigma}\cdot\mathbf{B}_{\mathbf{g}}\boldsymbol{\sigma}\cdot\mathbf{B}_{\mathbf{g}}-2\mu_n\boldsymbol{\sigma}\cdot\mathbf{B}_{\mathbf{g}}\alpha_R]\chi,$$

where α_R is the real part of α. The second term can be simplified further by use of the property of the Pauli matrices:

$$(\boldsymbol{\sigma}\cdot\mathbf{A})(\boldsymbol{\sigma}\cdot\mathbf{c})=\mathbf{A}\cdot\mathbf{c}+i\boldsymbol{\sigma}\cdot\mathbf{A}\times\mathbf{c},$$

where $\mathbf{A}$ and $\mathbf{c}$ are any two vectors.[23] Substituting, also, for $\mathbf{B}_{\mathbf{g}}$ in terms of $\mathbf{M}_{\mathbf{g}}$ one has:

$$s=(8\pi M_n{}^2L^3v/h^4K^2)\sum_{\mathbf{g}}\delta(|\mathbf{K}_0+\mathbf{g}|-K)\chi^*[|\alpha|^2+(8\pi/g^2)\mu_n\boldsymbol{\sigma}\cdot\{\mathbf{g}\times(\mathbf{g}\times\mathbf{M}_{\mathbf{g}})\}\alpha_R$$
$$-(16\pi^2/g^2)\mu_n{}^2\mathbf{M}_{\mathbf{g}}\cdot\{\mathbf{g}\times(\mathbf{g}\times\mathbf{M}_g)\}]\chi. \quad (8.3)$$

From this equation it is apparent that the average of s over the direction of $\mathbf{g}$ is given in terms of averages of the quantities

$$\delta(|\mathbf{K}_0+\mathbf{g}|-K)\quad\text{and}\quad(1/g^2)[\mathbf{g}\times(\mathbf{g}\times)]\delta(|\mathbf{K}_0+\mathbf{g}|-K)\equiv-(1-\mathbf{gg}/g^2)\delta(|\mathbf{K}_0+\mathbf{g}|-K),$$

now

(a) $$\langle\delta(|\mathbf{K}_0+\mathbf{g}|-\mathbf{K})\rangle_{Av}=2K\langle\delta(K^2-(\mathbf{K}_0+\mathbf{g})^2)\rangle_{Av}=2K\langle\delta(g^2+2\mathbf{K}\cdot\mathbf{g})\rangle_{Av}$$
$$=K\int_0^{\pi}\delta(g^2+2Kg\cos\theta)\sin\theta d\theta=1/2g\quad\text{if } g<2K=K_0;\ 0\text{ if } g>2K,$$

(b) $$\langle(\mathbf{gg}/g^2)\delta(|\mathbf{K}_0+\mathbf{g}|-K)\rangle_{Av}=(2K/4\pi)\int_0^{\pi}\int_0^{2\pi}[(\mathbf{i}\cos\phi\sin\theta+\mathbf{j}\sin\phi\sin\theta+\mathbf{k}\cos\theta)(\mathbf{i}\cos\phi\sin\theta$$
$$+\mathbf{j}\sin\phi\sin\theta+\mathbf{k}\cos\theta)\delta(g^2+2K_0g\cos\theta)\sin\theta d\theta d\varphi,$$

where θ and ϕ are the polar coordinates of $\mathbf{g}$ with respect to a Cartesian system whose z axis is parallel to $\mathbf{K}_0$ and where $\mathbf{i}$, $\mathbf{j}$, and $\mathbf{k}$ are orthogonal unit vectors, such that $\mathbf{k}=\mathbf{K}_0/K$;

$$\langle(\mathbf{gg}/g^2)\delta(|\mathbf{K}_0+\mathbf{g}|-K)\rangle_{Av}=(1/2g)\int_0^{\pi}[\tfrac{1}{2}(\mathbf{ii}+\mathbf{jj})\sin^2\theta+\mathbf{kk}\cos^2\theta]\delta(g/2K_0+\cos\theta)\sin\theta d\theta$$
$$=(1/2g)\{\tfrac{1}{2}(\mathbf{ii}+\mathbf{jj})(1-g^2/4K^2)+\mathbf{kk}g^2/4K^2\}=(1/4g)[(1-g^2/4K^2)+\mathbf{kk}((3g^2/4K^2)-1)],$$

(c) $$\langle[g\times(g\times)]\delta(|\mathbf{K}_0+\mathbf{g}|-K)/g^2\rangle_{Av}=-\langle(1-\mathbf{gg}/g^2)\delta(|\mathbf{K}_0+\mathbf{g}|-K)\rangle_{Av}$$
$$=-(1/4g)[(1+g^2/4K^2)+\mathbf{kk}(1-3g^2/4K^2)=-(1/4g)[(1+g^2/4K^2)+(\mathbf{K}_0\mathbf{K}_0/K^2)(1-3g^2/4K^2)].$$

---

[23] P. A. M. Dirac, *Quantum Mechanics* (Oxford University Press, 1930) first edition, page 248, Eq. (25).

The average of s is, hence,

$$s=(4\pi M_n^2L^3v/h^4K^2)\sum_{\varrho<2K}(1/g)\chi^*[|\alpha|^2-2\pi\mu_n\boldsymbol{\sigma}\cdot\{(1+g^2/4K^2)+(\mathbf{K}_0\mathbf{K}_0/K^2)(1-3g^2/4K^2)\}$$
$$\cdot\mathbf{M}_g\alpha_R+4\pi^2\mu_n^2\mathbf{M}_g\cdot\{(1+g^2/4K^2)+(\mathbf{K}_0\mathbf{K}_0/K^2)(1-3g^2/4K^2)\}\cdot\mathbf{M}_g]\chi. \quad (8.4)$$

Here the first term in the square brackets represents the nuclear scattering, the third the magnetic scattering, and the second the interference resulting from the superposition of nuclear and magnetic scattered *amplitudes*. It is this interference which leads to a polarization of neutrons; one can see that the sign of the second term and, consequently, the magnitude of the total scattering is different for the different spin states.

The average weakening of the beam is given by the ratio of the scattered current s, given by (8.4), to the incident current $I=vL^2$. Thus

$$A=s/I=L\chi^*[\kappa_n+\kappa_m+\kappa_i\sigma_z]\chi,$$

where

$$\kappa_n=(4\pi M_n^2/h^4K^2)\sum_{\varrho<2K}|\alpha|^2/g, \quad (8.5a)$$

$$\kappa_m=(4\pi M_n^2/h^4K^2)\sum_{\varrho<2K}(4\pi\mu_n^2/g)\mathbf{M}_g^2\{1+g^2/4K^2+(K_{0z}K_{0z}/K^2)(1-3g^2/4K^2)\}, \quad (8.5b)$$

$$\kappa_i=-(4\pi M_n^2/h^4K^2)\sum_{\varrho<2K}(2\pi\mu_n/g)|\mathbf{M}_g|\alpha_R\{1+g^2/4K^2+(K_{0z}K_{0z}/K^2)(1-3g^2/4K^2)\}, \quad (8.5c)$$

the magnetic vector being directed along the z axis. It will be noticed that terms in A proportional to σ_x, σ_y have been dropped; the lack of influence of such terms is due to the precession of the spin about the direction of the magnetic field; the rapidity of this precession obliterates any possible effect of polarization in directions other than that defined by the field.

For the state $\chi_{\frac{1}{2}}$

$$A=L[\kappa_n+\kappa_m+\kappa_i];$$

for the state $\chi_{-\frac{1}{2}}$

$$A=L[\kappa_n+\kappa_m-\kappa_i].$$

Let it now be supposed that, at a depth x, the intensities of $\chi_{\frac{1}{2}}$ and $\chi_{-\frac{1}{2}}$ are, respectively, $I_{\frac{1}{2}}$ and $I_{-\frac{1}{2}}$. Then

$$\Delta I=\Delta(I_{\frac{1}{2}}+I_{-\frac{1}{2}})=[I_{\frac{1}{2}}(X+L)-I_{\frac{1}{2}}(X)]+[I_{-\frac{1}{2}}(X+L)-I_{-\frac{1}{2}}(X)]$$
$$=-L[(\kappa_n+\kappa_m)(I_{\frac{1}{2}}+I_{-\frac{1}{2}})-\kappa_i(I_{\frac{1}{2}}-I_{-\frac{1}{2}})]$$
$$=LI(\kappa_n+\kappa_m)-L\kappa_i\zeta,$$

where $\zeta=I\sigma_z$. For ζ itself, one obtains the difference equation

$$\Delta\zeta=[I_{\frac{1}{2}}(X+L)-I_{\frac{1}{2}}(X)]-[I_{-\frac{1}{2}}(X+L)-I_{-\frac{1}{2}}(X)]$$
$$=L\zeta(\kappa_n+\kappa_m)-LI\kappa_i.$$

At this point the effects due to true absorption (capture) and incoherent scattering processes should be included. This is readily done by adding to the quantity $(\kappa_m+\kappa_n)$ the absorption coefficients for these processes, κ_c and κ_s, respectively. Denoting the sum $\kappa_m+\kappa_n+\kappa_c+\kappa_s$ by the single letter κ, and replacing κ_i by the notation $-w$ one has, finally

$$\Delta I/L=I\kappa+w\zeta, \quad \Delta\zeta/L=-\zeta\kappa+wI,$$

which, in differential form, read:

$$dI/dx=-\kappa I+w\zeta, \quad (8.6a)$$

$$d\zeta/dx=-\kappa\zeta+wI \quad (8.6b)$$

to be compared with (8.1a), (8.1b).

In conclusion, the relations (8.5a, b) for the absorption and polarization coefficients will be expressed in terms of the nuclear cross section and the macroscopic magnetization. (a) The quantity α which symbolized the amplitude of nuclear scattering, can immediately be related to the nuclear cross section, σ; one need only calculate this cross section with the potential $V=\alpha a^3\delta(\mathbf{r})$.[24] Using the Born perturbation method, one obtains:

$$\alpha^2=\pi\sigma\hbar^4/M_n^2a^6;\quad \alpha_R=[(\pi\sigma)^{\frac{1}{2}}\hbar^2/M_na^3]\cos\delta,$$

where δ is the phase difference between the incident and scattered nuclear wave. Due to the non-existence of a resonance level of iron for thermal neutrons, $|\cos\delta|$ is expected to be quite close to unity. (b) The quantity, which represents the magnetic scattering, is defined by the integral $(1/a^3)\int\mathbf{M}\exp(-i\mathbf{g}\cdot\mathbf{r})d\tau_0$ where $\mathbf{M}$ is the density of atomic magnetization. Remembering that this integral goes over only one atom, located in the center of the volume of integration, one obtains

$$\mathbf{M}_g=(1/a^3)\boldsymbol{\mu}_aF(\mathbf{g}).$$

Here, $\boldsymbol{\mu}_a$ is the atomic magnetic moment and $F(\mathbf{g})=\int\exp(i\mathbf{g}\cdot\mathbf{r})\rho_md\tau_0$ where ρ_m is the distribution, normalized to unity, of the atomic magnetization. $\boldsymbol{\mu}_a$ itself can be expressed in terms of the macroscopic magnetization $\mathbf{M}_0=N\boldsymbol{\mu}_a$ where $N=2/a^3$ is the number of atoms per cubic centimeter.[25] Hence $\mathbf{M}_g=\mathbf{M}_0F(\mathbf{g})/2$. (c) Inserting these values for α and $\mathbf{M}_g$ into (8.5) one obtains

$$\kappa_n=(N\sigma/4\pi)(\lambda^2/a^2)\sum_{l<2a/\lambda}1/l, \tag{8.7a}$$

$$\kappa_m=(M_n^2\lambda^2a\mu_n^2M_0^2/2\hbar^4)\sum_{l<2a/\lambda}(1/l)[F(1/a)]^2\{1+\lambda^2l^2/4a^2+(\cos^2\theta)(1-3\lambda^2/4a^2)\}, \tag{8.7b}$$

$$w=(M_n\lambda^2M_0\cos\delta(\pi\sigma)^{\frac{1}{2}}/(2\pi\hbar^2a^2))\sum_{l<2a/\lambda}(1/l)F(1/a)\{1+\lambda^2l^2/4a^2+(\cos^2\theta)(1-3\lambda^2l^2/4a^2)\}, \tag{8.7c}$$

where θ is the angle between the magnetization and the direction of the beam, $\lambda=2\pi/K$ is the wave-length of the neutrons, and the summation over $\mathbf{l}=\mathbf{g}a/2\pi$, whose components are integers, goes over values of $\mathbf{l}$ for which $l_1+l_2+l_3$ is even.

IX. Transmission of Neutrons in Incompletely Saturated Polycrystalline Ferromagnetic Media

Equations (8.6a) (8.6b) describe the transmission and polarization of neutrons in a medium in which the magnetic induction $\mathbf{B}$ of Maxwell's equations, i.e., the average over atomic distances of the Lorentzian magnetic field $\mathbf{H}$ always points in one direction. For polycrystals, as has been seen in Section VII, this condition obtains only when the medium is completely saturated; in all other cases, the deviations of the fields of the constituent crystals give rise to depolarization effects as given by (7.1a) and (7.1b). These equations have the general form:

$$s_{fz}=s_{0z}e^{-pz}$$

from which one obtains, for the differential change of the polarization:

$$ds_z/dx=-ps_z$$

or, in terms of the variable $\zeta\equiv\sigma_zI=2s_zI$

$$d\zeta/dx=-p\zeta.$$

To obtain the effect of this depolarization on the transmission of neutrons, one merely inserts the

[24] Cf. (8.2).
[25] The factor 2 comes in because of the body-centered structure.

term $-p\zeta$ into (8.6b). The complete transmission equations now read:[26]

$$dI/dx = -\kappa I + w\zeta, \tag{9.1a}$$

$$d\zeta/dx = -\kappa\zeta - p\zeta + wI. \tag{9.1b}$$

These equations can be simplified by the substitution

$$I = je^{-\kappa x}; \quad \zeta = \eta e^{-\kappa x}$$

to give:

$$dj/dx = w\eta, \tag{9.2a}$$

$$d\eta/dx = -p\eta + wj. \tag{9.2b}$$

Since the quantity of interest in the experiments is the relative change in transmitted intensity $\Delta I/I = \Delta j/j$, one need not refer back to this substitution, but merely treat j and η as the particle and spin current, respectively.

Equations (9.2) will first be solved for the important case $wx \ll 1$, i.e., transmission effect small. In this case, one can replace j in (9.2b) by j_0, the initial current. Thus

$$d\eta/dx = -p\eta + wj_0,$$

which has the solution

$$\eta = \eta_0 e^{-px} + (wj_0/p)(1 - e^{-px}), \tag{9.3a}$$

where η_0 is the initial polarization. Substituting in (9.2a), one obtains:

$$j = j_0(1 + (w^2/p^2)(px - 1 + e^{-px})) + (\eta_0 w/p)(1 - e^{-px}). \tag{9.3b}$$

Equations (9.2) can also be solved exactly; the result is

$$j = j_0 e^{-px}\left\{\frac{\sinh[x((p/2)^2+w^2)^{\frac{1}{2}}]}{((2w/p)^2+1)^{\frac{1}{2}}} + \cosh[x((p/2)^2+w^2)^{\frac{1}{2}}]\right\} + \frac{\eta_0 e^{-px}\sinh[x((p/2)^2+w^2)^{\frac{1}{2}}]}{((p/2w)^2+1)^{\frac{1}{2}}}, \tag{9.4a}$$

$$\eta = \eta_0 e^{-px}\left\{\cosh[x((p/2)^2+w^2)^{\frac{1}{2}}] - \frac{\sinh[x((p/2)^2+w^2)^{\frac{1}{2}}]}{((2w/p)^2+1)^{\frac{1}{2}}}\right\} + j_0 e^{-px}\frac{\sinh[x((p/2)^2+w^2)^{\frac{1}{2}}]}{((p/2w)^2+1)^{\frac{1}{2}}}. \tag{9.4b}$$

Two cases are of practical importance:

(1) $$wx \ll 1, \quad px \sim 1, \quad \text{i.e.} \quad p \gg w.$$

Here (9.4) reduces directly to (9.3).

(2) $$wx \ll 1, \quad p \sim w, \quad \text{i.e.} \quad px \ll 1.$$

In this case (9.4) reduces to

$$j = j_0\{1 + w^2x^2/2\} + \eta_0 wx,$$
$$\eta = \eta_0 + j_0 wx,$$

which can also be obtained from (9.3) for $px \ll 1$ by expansion of the exponentials in these equations. Thus (9.4) reduces to (9.3) for $wx \ll 1$ and *all* values of p.

The applications of (9.3) to the different types of transmission experiments will now be discussed.

(1) Single transmission

This experiment consists of the measurement of neutron transmission through a ferromagnetic magnetized and unmagnetized; the relative difference is called the *single transmission effect*. The

[26] In what follows, the constant κ and w will be treated phenomenologically; their numerical evaluation will appear in the following paper by O. Halpern, M. Hamermesh, and M. H. Johnson.

theoretical estimate of this effect is obtained directly from (31) with the initial condition $\eta=0$. Thus

$$\Delta j/j_0 \equiv (j-j_0)/j_0 = (w^2/p^2)\{px-1+e^{-px}\} = (w^2x^2/2)f(px), \tag{9.5}$$

where

$$f(\xi) = 2(\xi-1+e^{-\xi})/\xi^2. \tag{9.6}$$

When there is no depolarization $f(px)=1$ and $(\Delta j/j_0)=w^2x^2/2$ in conformance with previous results. In all other cases the maximum transmission effect is reduced by the factor $f(px)$. For small px, $f(px)\cong 1-px/3$; for large px, $f(px)\cong 2/px$.

To illustrate the sensitivity of the single transmission effect to the degree of magnetic saturation, let it be supposed that the average crystal size is 10^{-8} cm[3],[27] i.e., $\delta=2\times10^{-3}$ cm. The corresponding value of p is, by (7.1b), $(\frac{2}{3})\times10^3\Delta M/M_0$. If $\Delta M/M_0=1$ percent and the thickness of the sample $d=1$ cm, $pd=20/3$ and the transmission effect drops to 30 percent of its maximum value.

The presence of depolarization is most easily detected experimentally by observations on the dependence of the transmission effect upon the thickness of the ferromagnet. In the absence of depolarization, this dependence is quadratic ($\Delta j=j_0w^2x^2/2$); the depolarization has the effect of cutting down the increase with thickness; in the limit $px\gg1$ the dependence is linear.

(2) Double transmission

In this experiment one compares the transmission through two ferromagnetic plates magnetized in the same direction to that obtained with the magnetizations oppositely directed. Let d_1 and d_2 be the thickness of the two plates, w_1 and w_2 their polarization coefficients, which are equal in magnitude but may differ in sign depending on whether the magnetizations are parallel or antiparallel, and p_1, p_2 their depolarization coefficients. From (9.2) the current and polarization of the beam emerging from the first plate are

$$j_1 = j_0\{1+(w_1^2d_1^2/2)f(p_1d_1)\}, \tag{9.7a}$$

$$\eta_1 = (w_1j_0/p_1)\{1-\exp[-p_1d_1]\}. \tag{9.7b}$$

Using these values as initial conditions for the second transmission, one obtains:

$$j_2 = j_1\{1+(w_2^2d_2^2/2)f(p_2d_2)\}+(\eta_1w_2/p_2)\{1-\exp[-p_1d_2]\}$$

or

$$j_2 = j_0\{1+(w_2^2d_2^2/2)f(p_2d_2)\}\left\{1+\frac{w_1^2d_1^2}{2}f(p_1d_1)\right\}+j_0(w_1w_2/p_1p_2)\{1-\exp[-p_1d_1]\}\{1-\exp[-p_2d_2]\}. \tag{9.8}$$

The double transmission effect is the relative difference in j_2 for the two cases $w_1=w_2$ and $w_1=-w_2$. Thus:

$$\Delta j/j_0 = (2w^2/p_1p_2)\{1-\exp[-p_1d_1]\}\{1-\exp[-p_2d_2]\}$$

$$= 2w^2d_1d_2g(p_1d_1)g(p_2d_2), \tag{9.9}$$

where $g(\xi)=(1-e^{-\xi})/\xi$. It should be noticed that only when $p=0$ does one obtain the maximum effect $\Delta j/j_0=2w^2d_1d_2$, in conformance with previous estimates; in all other cases the effect is cut down by a factor $g(p_1d_1)g(p_2d_2)$, which, for large pd becomes $1/(p_1d_1p_2d_2)$.

It can be seen that the depolarization is much more destructive in double transmission, as compared to single transmission. Using the previous illustration of $\Delta M/M_0=1$ percent, $\delta=2\times10^{-3}$ cm, one obtains, with $d_1=d_2=1$ cm, a reduction by a factor $(3/20)^2=0.025$. One thus sees that very small deviations from magnetic saturation suffice to wipe out any double transmission effects which are due to the magnetic scattering in ferromagnets.

---

[27] This estimate is appropriate to the case of Armco iron, as communicated to the authors by Dr. T. D. Yensen of Westinghouse Research Laboratories.

X. Comparison with Experiments

The application of the formulae developed in Section IX cannot be carried out immediately, essentially for two reasons. The quantity w as mentioned before, is here treated phenomenologically, while it will be evaluated on a strictly atomistic basis in the following paper.[26] Secondarily, it so happens that experimental papers in the field do not contain precise information on the deviation from saturation, which determines according to, e.g., (7.1), the depolarization constant p. Still, a few general statements of a semi-quantitative nature can be made.

The earliest experiments[28] were mostly carried out with a magnetization which probably did not exceed 70 percent. It is clear without any detailed calculation that the value of p in this case becomes so large that no sensible value of w could lead to an observable polarization. This is the more true since it will be shown in the following investigation[26] that even for ideal saturation the theoretical value of w is rather small.

A similar objection must be raised against later experiments[29] in which also poor saturation $\Delta M/M_0 > 10$ percent was obtained. One is forced to the conclusion that the observations are theoretically inexplicable for any reasonable value of w.

The most detailed observations so far reported are those by Powers[30] who studied single as well as double transmission effects with various samples of iron and under various conditions of magnetization. His single transmission experiments made with Armco iron were carried out with a deviation from saturation which, according to the author, amounted to approximately 1.5 percent. According to formulae (9.5), (9.6) and (7.1a), and with the experimentally well-established value[27] for the crystal size the reduction factor due to depolarization should have been $\frac{1}{3}$ or smaller.

Powers' double transmission experiments were carried out with Swedish iron and a value of $\Delta M/M_0 \sim 8\times 10^{-2}$. The great sensitivity of double transmission experiments to deviations from saturation (cf. (9.9) and (9.10)) makes it hard to understand how under such conditions a double transmission should have been observable. (9.9), (9.10) and (7.1b) indicate that for any reasonable value of the most accurately known crystal size in Swedish iron, the observed effect should have been a fraction of a percent of the value obtainable with complete saturation.

If the picture of the constitution of ferromagnets and of the neutron's magnetic moment as used in this paper should be maintained, we are forced to conclude that the experimental data need revision. It may be that the saturation achieved in some of the experiments is far better than reported, though it is not easy to see how the theoretically required value of $\Delta M/M_0 \sim 10^{-3}$ can be reconciled with the reported value of $\Delta M/M_0 \sim 10^{-1}$.

The authors are indebted to Professor E. Fermi for the discussion of an interesting possibility, which, though not actually helpful, deserves analysis in this difficult situation. Obviously (cf. (7.1b)) the depolarization would be diminished if the number of incompletely magnetized domains could be diminished or, in other words, the size of the domains increased. In the present paper the size of each domain was identified with the size of the crystallite which, in turn, is in certain cases[27] experimentally determined. This seemed almost inevitable since every crystallite has its own direction of easy magnetization which lies nearest to the direction of the magnetizing field.

The new assumption would introduce blocks comprising many crystallites with the direction of easiest magnetization being determined *for the whole block* by internal stresses. Obviously, the existence of such sufficiently large blocks would diminish depolarization strongly.

There exist, on the other hand, difficulties which make the assumption of such blocks rather impossible. It is not easy to see how the existence of such large stresses which overcome the crystalline energies, will affect the magnetization only, without influencing appreciably the elastic and crystallographic structure. Furthermore, the saturation curve of polycrystalline iron can be semi-quantitatively understood by using the magnetization curve for single crystals of iron and averaging over all directions of the

[28] Reported in Frisch, von Halban and Koch, Phys. Rev. **53**, 719 (1938).
[29] Hoffman, Livingston and Bethe, Phys. Rev. **51**, 214 (1937).
[30] P. N. Powers, Phys. Rev. **54**, 827 (1938).

crystalline axis. This fact seems to indicate that "the turning of the magnetization into the direction of the field" has to overcome mainly crystalline forces. Finally it has been pointed out by Becker and Doering[31] that stresses sufficiently large to overcome the crystal orientation energy cannot be realized in iron since they would have to exceed the breaking strength of the material.

[31] R. Becker and W. Doering, *Ferromagnetismus* (Julius Springer, Berlin, 1939), p. 104.

It should be emphasized as a guide for future experiments that it is not at all necessary to use completely polarized neutron beams for the investigation of the properties of ferromagnets. Polarizations as claimed to be present in the various experiments discussed would be amply sufficient to allow investigations of ferromagnetic structures.

The authors wish to express their thanks to Dr. T. D. Yensen of Westinghouse Research Laboratories for a very instructive communication.

JUNE 15, 1941 PHYSICAL REVIEW VOLUME 59

The Passage of Neutrons Through Crystals and Polycrystals

O. HALPERN, M. HAMERMESH AND M. H. JOHNSON
New York University, University Heights, New York, New York

(Received August 28, 1940)

We investigate in this paper phenomena, occurring in the passage of neutrons through matter, which originate from the crystalline or polycrystalline constitution. While the procedure is in many respects closely similar to that followed in the theory of x-rays, important and quantitatively decisive differences arise from the complicated coherence properties of the *atomic* scattering. The theoretical formulae developed in the first two paragraphs permit us to interpret in a quantitative manner a series of experiments which show deviations from the so far almost always assumed additivity of nuclear cross sections. We also obtain information concerning the relative phases of the scattering amplitudes of nuclear isotopes. We next show for illustrative purposes how the Larmor precession of the spin of the neutron passing through the magnetized medium, and the well-known differentiation between the action of the vectors "B" and "H" can be explained as a simple dispersion phenomenon. The preceding formulae permit us to determine quantitatively the transmission and polarization of neutron beams passing through ferromagnetic bodies. The main uncertainties which enter into attempts to evaluate experiments, arise from our incomplete knowledge of the velocity distribution of the incident beam and of the form factor which enters into the formulae for magnetic scattering. We present a detailed discussion of these uncertainties. Even neglecting depolarization effects which are due to incomplete saturation and which would still further diminish the theoretical value for transmission effects, we find that the observed values are considerably higher than those theoretically predicted and are not in good agreement with each other.

INTRODUCTION*

CONTINUING earlier investigations[1] on the transmission of neutrons through macroscopic bodies, and in particular on macroscopic and microscopic magnetic effects, we present in this paper a discussion of the influence of crystal structure on scattering and polarization of neutrons. It has been the accustomed procedure to consider the nuclear cross section for the scattering of slow neutrons as a strictly additive property independent of the physical state or the chemical constitution of the sample investigated. On this basis the total cross section of a chemical compound could, for example, be determined from a knowledge of the cross sections of the constituent elements.

Such a procedure is valid only if we are dealing with a substance of strictly amorphous structure (a gas). In all other cases the crystalline structure of the material becomes significant; it will turn out to be of importance even for substances

* A preliminary report of this work appeared in the abstract: Halpern, Hamermesh and Johnson, Phys. Rev. **55**, 1125A (1939).

[1] I. O. Halpern and M. H. Johnson, Phys. Rev. **51**, 992 (1937); II. *ibid.* **52**, 52 (1937); III. *ibid.* **55**, 898 (1939); IV. Halpern and Holstein, *ibid.* **55**, 601 (1939); V. *ibid.* **59**, 960 (1941) (this issue). These are referred to throughout the paper by the corresponding Roman numerals.

composed of small microcrystals, and to change completely the scattering results for macroscopic crystals. The theory leading to these results is in its essentials the same as that for x-ray scattering, but shows great quantitative differences due to peculiarities which are characteristic of the interaction between neutron and atoms.

In discussing any crystal phenomenon it is essential to separate the coherent and incoherent scattering processes which have previously been found to play so great a part in the theory of x-ray scattering; but while the theory of x-ray scattering by a single chemical element had to take into account only those incoherent processes which are produced by inelastic collision of the incident particles with the lattice vibrations (strictly inelastic scattering), we have in the case of neutrons two more causes for incoherent processes. These are: first, the existence of spin dependent forces between the neutron and the atom, which may be of a nuclear or magnetic type; and secondly, the disorder in the lattice caused by the random distribution of the isotopes, which in general will produce scattered neutron waves, whose amplitude and phase will show no correlation for the various isotopes.

The second part of the paper is concerned with the quantitative evaluation of polarization experiments. We have previously[2] pointed out that the existing[3] theories of polarization effects, which fail to take into account the crystalline structure as well as the various types of scattering, have no direct field of application, and that it is also necessary to calculate in detail the effect of incomplete ferromagnetic saturation on the intensity of the scattered and transmitted beam. We find that the previous estimates of polarization effects are of a higher order of magnitude than those obtained by the rigorous theory. These calculations of course have to be used together with the results of IV and V on magnetic depolarization.

Among previous investigations of the passage of neutrons through crystals, papers by Wick[4] and Pomeranchuk[5] may be mentioned. Pointing out that the elastic scattering of neutrons does not offer much interest, since it is closely analogous to the problem in x-ray scattering, Wick shows that an essential difference arises in the inelastic scattering due to the interaction with the lattice vibrations. This difference arises from the nonrelativistic motion of the neutron (energy = momentum $\times V/2$, not momentum $\times V$ as in the x-ray case), which tends to reduce the inelastic scattering. Similarly, Pomeranchuk discusses mainly the slowing down of neutrons in crystals for neutrons of long wave-length. The physical aspects which are relevant in our paper have not been treated by these authors.

I. The General Scattering Formulae for Atoms

Before considering the effect of the crystalline structure of the scatterer on the results of transmission experiments we wish to review briefly the theory of the passage of neutrons through a material consisting of independent scatterers.

We shall be dealing throughout with slow neutrons, so that only the "s" wave need be considered; also inelastic nuclear scattering can be excluded since the energy of the neutron is too small to excite the nucleus to higher states. If one takes account of the different isotopes present in the scattering sample, the amplitude of the coherent scattering from a single nucleus is given by:[6]

$$C=\sum_p |b_p|^2(2i_p+1)^{-1}[i_p a_0{}^p+(i_p+1)a_1{}^p], \quad (1.1)$$

where $|b_p|^2$ gives the relative abundance of the pth isotope, i_p is the nuclear spin of the pth isotope, and $a_0{}^p$ and $a_1{}^p$ are the amplitudes of the scattered wave for total angular momenta $i_p-\frac{1}{2}$ and $i_p+\frac{1}{2}$, respectively (neutron spin $=\frac{1}{2}$).

The intensity of the incoherent nuclear scattering is proportional[6] to:

$$E^2=\sum_p |b_p|^2(2i_p+1)^{-1} \times[i_p(i_p+1)(a_1{}^p-a_0{}^p)^2]. \quad (1.2)$$

In addition to this purely nuclear scattering, there will be an interaction between the magnetic moment of the neutron and the magnetic field due to the current distributions of the electrons in the atom. Since in most cases one deals with

[2] Cf. V.
[3] F. Bloch, Phys. Rev. **50**, 259 (1936); J. Schwinger, Phys. Rev. **51**, 544 (1937).
[4] G. C. Wick, Physik. Zeits. **38**, 403, 689 (1937).
[5] I. Pomeranchuk, Physik. Zeits. Sowjetunion **13**, 65 (1938).
[6] See Sections III and VI of III.

materials in the crystalline state, the orbital currents are either absent (ground state S), or almost completely quenched by the crystalline field, so that the magnetic properties of the atom are due almost entirely to spin currents. For the amplitude of the magnetically scattered wave we have:[6]

$$\psi_m=\left(\frac{2\pi M_0}{hk}\right)^{\frac{1}{2}}\left(\frac{2e^2\gamma}{mc^2}F^{\frac{1}{2}}\right)\frac{e^{ikr}}{r}$$
$$\times[(\mathbf{e}\cdot\mathbf{s})(\mathbf{e}\cdot\mathbf{S})-(\mathbf{s}\cdot\mathbf{S})]\cdot X_s\Omega_M, \quad (1.3)$$

where M_0 = mass of the neutron; γ = its magnetic moment in nuclear magnetons;

$$\mathbf{e}=(\mathbf{k}-\mathbf{k}')/|\mathbf{k}-\mathbf{k}'|, \quad (1.4)$$

where $\mathbf{k}$ and $\mathbf{k}'$ are the initial and final propagation vectors of the neutron; $\mathbf{s}$ is the spin of the neutron in units of $h/2\pi$; X_s is the spin wave function of the incident neutron; $F^{\frac{1}{2}}$ is the form factor of the spin distribution of the ion, and Ω_M is the spin function describing the orientation of the spin S of the ground state of the ion. (The incident flux has been normalized to 1.)

In the case of ferromagnets at saturation, the spins of all the ions are rigidly aligned along a direction given by the unit vector $\mathbf{k}$.

In this case only elastic collisions in which the spin state of the ion is unchanged are possible, and the expression for the magnetically scattered wave becomes:[6]

$$\psi_m=(2\pi M_0/hk)^{\frac{1}{2}}2Dr^{-1}e^{ikr}(\mathbf{q}\cdot\mathbf{s})X_s, \quad (1.5)$$

where

$$D=\frac{e^2\gamma S}{mc^2}F^{\frac{1}{2}}, \quad (1.6)$$

$$\mathbf{q}=\mathbf{e}(\mathbf{e}\cdot\mathbf{k})-\mathbf{k}. \quad (1.7)$$

Then the total coherently scattered wave (including both magnetic and nuclear scattering) becomes:[6]

$$\psi_{sc}=(2\pi M_0/hk)^{\frac{1}{2}}r^{-1}e^{ikr}(C+2D\mathbf{q}\cdot\mathbf{s})X_s. \quad (1.8)$$

In addition to the above scattering processes, there will be possible capture of the neutron which would lead to a decrease in intensity of the transmitted beam. The cross section σ_{cap} for this straight absorption will for slow neutrons follow the $1/v$ law.

II. Scattering by Crystals and Aggregates of Crystals

Before proceeding with calculations, we wish to fix the nomenclature to be used throughout.

The basic unit in the crystal is the unit cell which, by the repetition of a set of translations, fills out the whole space, forming a microcrystal.

The microcrystal is a composite of unit cells which are in perfect arrangement and scatter coherently.

A single crystal is composed of microcrystals all of which are oriented approximately the same, but whose relative positions are fixed only within a distance of the order of the lattice spacing. (Mosaic single crystal.) The single crystal will act macroscopically as a homogeneous body, but in the propagation of de Broglie waves of the order of the lattice spacing, the separate microcrystals will not scatter coherently. To calculate the scattering from the single crystal, we must first calculate the scattered amplitude for each of its microcrystals and then sum the intensities.

A polycrystalline material is composed of many small single crystals, or crystallites, oriented at random. The crystallites in general contain many microcrystals. To calculate the scattering from a polycrystalline sample, one must average the scattering of its sub-units over all orientations of the crystallites.

By the perfectness of a crystal we mean the linear dimension of the microcrystals composing it.

To calculate the total scattering from a polycrystalline sample, we must integrate the usual diffraction integral over all final directions of the neutron, and then average over all orientations of the constituent microcrystals.

We consider the nuclear scattering of neutrons of wave-length λ by a material having simple cubic structure with lattice distance a, and only one type of nucleus in the lattice. Using the well-known relation

$$2\cos\theta_0=|l|\lambda/a \quad (2.3)$$
$$l=(l_x^2+l_y^2+l_z^2)^{\frac{1}{2}};\quad l_i \text{ Miller indices},$$

one obtains[7] for the scattering due to "reflection"

[7] A. H. Compton and S. K. Allison, *X-Rays in Theory and Experiment* (Van Nostrand, 1935).

from the plane l_i

$$I_l=\frac{\sigma}{4\pi}\frac{N_1N_2N_3}{4}\left(\frac{\lambda}{a}\right)^3\frac{1}{\cos\theta_0}$$

$$=\frac{N_1N_2N_3}{8\pi}\sigma\left(\frac{\lambda}{a}\right)^2\frac{1}{|l|}. \quad (2.6)$$

In (2.6) σ is the cross section for the coherent scattering $=4\pi C^2$ (Section 1.1); N_1, N_2, N_3 are the numbers of planes in the microcrystal along each of the crystal axes. Finally this is to be summed over all triples for which $|l|<2a/\lambda$.

$$I=\frac{N\sigma}{8\pi}\left(\frac{\lambda}{a}\right)^2\sum_{1}^{|l|<2a/\lambda}\frac{1}{|l|}, \quad (2.8)$$

where N is the total number of unit cells.

Before considering this fundamental formula in detail, we wish to examine the case where the initial beam is sharply defined and is incident exactly at the Bragg angle, and calculate the total scattering for this fixed orientation of the crystal. In this case we expect the scattering to be large. This is of interest in examining the influence of secondary extinction, a term which refers to the fact that the incident beam, in going through the specimen, is being depleted due to scattering from individual microcrystals, so that low lying microcrystals are shielded from the full intensity of the beam by microcrystals lying above them. This effect will be noticeable if the scattering of the given wave-length in the specimen is large, so to estimate its importance we choose this most favorable case of incidence at the Bragg angle. Also, for simplicity, we consider the microcrystals to be perfectly aligned, but nevertheless scatter incoherently. Slight variations in orientation would produce a broadening of the range of reflection, but have little effect on the final result.

This calculation seems impossible to perform analytically, but for our purposes only a rough estimate is needed. Each term in (2.8) represents the scattering for a given reflection averaged over all possible orientations. Since the range of initial directions in which scattering occurs appreciably is $\sim\lambda/a_iN_i$, we can take as a rough estimate of the scattering at the Bragg angle

$$N_i^4\frac{\sigma}{8\pi}\frac{\lambda}{a}\frac{1}{|l|} \quad (2.9)$$

so, for a beam incident exactly at the Bragg angle, the total scattered intensity should be proportional to N_i^4. If the microcrystals have sides l, then the scattering will be

$$\sim\frac{l^4\sigma}{8\pi}\frac{\lambda}{a^5}\frac{1}{|l|}. \quad (2.10)$$

If the single crystal (crystallite) is L cm on a side, the ratio of scattered to initial beam will be:

$$\frac{I}{I_0}=\frac{1}{L^2}\left(\frac{L}{l}\right)^3\frac{l^4}{8\pi}\frac{\sigma\lambda}{a^5}\frac{1}{|l|}$$

$$=\frac{Ll\sigma\lambda}{8\pi a^5}\frac{1}{|l|}\sim N^2\sigma\lambda^2lL. \quad (2.11)$$

For Fe, a rough estimate of the effect can be made: l is 10^{-5} cm, while the size of the crystallites is $L\sim2\times10^{-3}$ cm.

$\sigma=7.3\times10^{-24}$ cm^2 (the reason for this choice will be seen in Section III).

$$a=2.9\times10^{-8}\text{ cm},\quad \lambda=1.5\times10^{-8}\text{ cm}.$$

Using these values we obtain:

$$I/I_0=Ll(1.2/4)\times10^6\sim6\times10^{-3}. \quad (2.12)$$

So even in this favorable case of reflection exactly at the Bragg angle, the secondary extinction will be very small for polycrystalline iron. Only for large single crystals ($L\sim1$ cm) will it be important. In what follows we shall deal chiefly with polycrystalline samples for which we may neglect the extinction.

Equation (2.8) has been obtained for the scattering of neutrons of a single wave-length by crystals of simple cubic structure. In (2.8) we have not included the effect of the temperature motion of the nuclei in the crystal. The theory of this temperature motion has been given by Debye and Waller.[8] The effect of the thermal vibration is to decrease the coherent scattering of a crystal of cubic symmetry by the factor

[8] P. Debye, Ann. d. Physik **43**, 49 (1914); I. Waller, Zeits. f. Physik **51**, 213 (1928); Dissertation Uppsala (1925).

$\exp(-2M_w)$ where:

$$M_w=\frac{6h^2}{m_a k\Theta}\left[\frac{\varphi(x)}{x}+\frac{1}{4}\right]\frac{\sin^2\frac{1}{2}\theta}{\lambda^2}, \qquad (2.13)$$

where θ is the angle between final and initial direction of the beam, m_a = mass of the atom forming the lattice, k is the Boltzmann constant, $\varphi(x)/x$ is the Debye function, and $x=\Theta/T$, where Θ is the Debye temperature and T the absolute temperature of the crystal. For the reflection corresponding to index $|l|$, we have $|l|\lambda/2a=\sin\frac{1}{2}\theta$, so the factor giving the decrease in coherent scattering from the crystal becomes

$$\exp(-A|l|^2), \qquad (2.14.1)$$

where

$$A=\frac{3h^2}{m_a k\Theta}\frac{1}{a^2}\left[\frac{\varphi(x)}{x}+\frac{1}{4}\right]. \qquad (2.14.2)$$

It should be noted that the temperature factor does not depend on the wave-length; for a given Debye ring (definite $|l|$) it is the same for all wave-lengths. The $\frac{1}{4}$ represents the effect of the zero-point vibration.

For Fe, $\Theta=453°$,

and taking $T=302°$, $x=1.5$,

$$\varphi(x)=0.70, \quad \frac{\varphi(x)}{x}\sim 0.46; \quad \left[\frac{\varphi(x)}{x}+\frac{1}{4}\right]\sim 0.71.$$

Also for Fe, taking $a=2.86$A; $m_a=56\times 1.661\times 10^{-24}$ g we get $A=0.0194$ so the temperature factor for iron becomes

$$\exp(-0.0194|l|^2). \qquad (2.14.3)$$

As the index $|l|$ of the Debye ring increases the coherent scattering is cut down more and more; for $|l|=4$, the factor is already 0.73.

In the case of Fe, a second correction must be made. Fe, at room temperature, forms a body-centered cubic lattice, with two atoms to each unit cell. This introduces a crystal structure factor which has the following effect:

All reflections for which $\sum_i l_i$ is odd disappear; all for which $\sum_i l_i$ is even are quadrupled in intensity. (We shall refer to these as odd and even $|l|$, respectively.)

In our scattering formula for simple cubic lattice the factor N which gave the number of unit cells represented also the total number of atoms in the crystal, whereas for the body-centered case, the number of unit cells $=\frac{1}{2}$ the number of atoms. Our formulae will be correct for body-centered lattices if we use N to designate the number of atoms in the lattice and take

$$2\sum_{\text{even } |l|<2a/\lambda}.$$

Then the final scattering formula becomes for simple cubic lattice:

$$\frac{N\sigma}{8\pi}\left(\frac{\lambda}{a}\right)^2\sum_{|l|<2a/\lambda}\frac{\exp(-A|l|^2)}{|l|} \qquad (2.15)$$

and for body-centered lattice (e.g. Fe)

$$2\cdot\frac{N\sigma}{8\pi}\left(\frac{\lambda}{a}\right)^2\sum_{\text{even } |l|<2a/\lambda}\frac{\exp(-A|l|^2)}{|l|}. \qquad (2.16)$$

We see that the contributions to the total coherent scattering of the polycrystal from different rings decreases with increasing $|l|$ due to each of the factors in the summand. A given value of $|l|$ can be realized in many different ways; e.g., $|l|=\sqrt{2}$ can be gotten for (0, 1, 1); we must count all permutations and changes of sign in finding the multiplicity $j(|l|)$ of a term in the sum; for

$$|l|=\sqrt{2}, \quad j(|l|)=12.$$

Since there have not yet been made significant experiments with monochromatic beams of slow neutrons it is necessary to generalize the formulae given for the case of rather wide velocity spectra. We shall in this section present some calculations *made for illustrative purposes only* by using a Maxwellian distribution. In Sections VI and VII calculations will be presented using empirically determined distribution functions.

In the case of a Maxwell distribution, the calculations can be carried out analytically; we so find for the scattered intensity produced by a body-centered lattice:

$$2\cdot\frac{N\sigma}{4\pi}\left(\frac{\lambda_A}{a}\right)^2 \times\sum_{\text{even } |l|}\frac{\Phi(\lambda_A|l|/2a)\exp(-A|l|^2)}{|l|}, \qquad (2.17)$$

where

$$\Phi(x)=\frac{2}{\sqrt{\pi}}\int_x^\infty \exp(-y^2)dy \qquad (2.17.1)$$

and

$$\lambda_A=h/(2M_0kT)^{\frac{1}{2}}, \qquad (2.17.2)$$

where T is the temperature of the neutron source.

So the effective coherent cross section $\bar{\sigma}$ of the crystal, as determined by using a beam of thermal neutrons, will be related to the coherent cross section for independent nuclei σ by:

$$\frac{\bar{\sigma}}{\sigma}=2\cdot\frac{1}{4\pi}\left(\frac{\lambda_A}{a}\right)^2 \times\sum_{\text{even }|l|}\frac{\Phi(\lambda_A|l|/2a)\exp(-A|l|^2)}{|l|}. \qquad (2.18)$$

These scattering formulae will be applied to the evaluation of experimental results in Section III.

Let us consider limiting cases for the various scattering formulae. (We consider only simple cubic lattices; similar arguments hold for crystals with basis.)

In (2.8), we can approximate the lattice sum by an integral; this gives

$$\frac{\bar{\sigma}}{\sigma}=\frac{1}{8\pi}\left(\frac{\lambda}{a}\right)^2\int_0^{2a/\lambda}4\pi l dl=1.$$

The validity of this approximation by integral increases with increasing number of lattice points, i.e., decreasing λ. So for small λ, we find the effect of the crystal structure disappearing, as is to be expected from general reasoning.

In Eq. (2.15), where the effect of the temperature vibration is included, this limiting case gives a quite different result. Here replacing the sum by an integral gives

$$\frac{\bar{\sigma}}{\sigma}=\left(\frac{\lambda}{2a}\right)^2\frac{1}{A}(1-\exp(-(2a/\lambda)^2A)),$$

so that as $\lambda\to0$, $\bar{\sigma}/\sigma\to0$. Again this result is easily interpreted. The inclusion of the temperature effect means the introduction of a form factor for the nuclear position in the crystal; any form factor $\to0$, for $\lambda\to0$.

In the expression for simple cubic crystals corresponding to (2.18), let us consider the case where $\lambda_A\to0$. The approximation by integral gives

$$\frac{\bar{\sigma}}{\sigma}=\frac{1}{4\pi}\left(\frac{\lambda_A}{a}\right)^2\int_0^\infty 4\pi l^2\frac{\Phi(\lambda_A l/2a)}{l}dl$$

$$=4\int_0^\infty v\Phi(v)dv$$

and integration by parts gives $\bar{\sigma}/\sigma=1$.

Let us consider (2.8) as λ increases. With increasing λ the number of terms in the sum decreases, but the intensity of each ring increases as λ^2. As λ increases, there will be definite points at which Debye rings disappear. (The $|l|$'th will disappear at $\lambda=2a/|l|$), and a discontinuous drop in intensity occurs; then because of the λ^2 factor, the intensity increases until the next Debye ring is cut out. If $\lambda>a$, only the first Debye ring is left and

$$\frac{\bar{\sigma}}{\sigma}\longrightarrow\frac{1}{8\pi}4\cdot e^{-A}\times j(1)=\frac{3e^{-A}}{\pi}, \quad \text{as} \quad \lambda\to2a.$$

For $\lambda>2a$, the coherent scattering disappears completely.

Apart from the coherent scattering we have to discuss two types of incoherent scattering which form a background between the Debye rings. There is first the inelastic scattering originating from processes involving energy transfer between the neutron and the lattice. This inelastic scattering is, in the case of x-rays, given by formulae analogous to:

$$\sigma(1-e^{-2M_w})d\Omega. \qquad (2.19)$$

In the case of neutrons conditions are more difficult, as mentioned already in the introduction. The inelastic cross section which would already be small for x-rays in case the Debye temperature is considerably larger than the temperature of observation becomes of even less significance for the scattering of slow neutrons.

The incoherent background due to the presence of isotopes constitutes a phenomenon which, with x-rays, is not of great importance numerically. It is due to the fact that the scattering amplitudes of various isotopes constituting the crystal have, in general, different magnitude as well as different sign. The spherically symmetrical background is produced with a scattering cross section

given by[9]

$$\sum_p |b_p|^2\left[\frac{i_p a_0{}^p+(i_p+1)a_1{}^p}{2i_p+1}\right]^2 - \left(\sum_p |b_p|^2\left[\frac{i_p a_0{}^p+(i_p+1)a_1{}^p}{2i_p+1}\right]\right)^2 + \sum_p |b_p|^2 \frac{i_p(i_p+1)(a_1{}^p-a_0{}^p)^2}{(2i_p+1)^2}. \quad (2.20)$$

We shall see later on that it probably accounts for the larger part of incoherent scattering occurring in so well-analyzed a substance as Fe.

III. Discussion of Scattering Experiments

The deliberations of Section II contain the theoretical basis for the explanation and evaluation of scattering experiments. In particular, they give account of certain characteristic phenomena which were observed when neutrons were scattered from the same substances present either in different crystal forms or in different chemical combinations.[10]

We shall first discuss the observations made with Fe, since they will turn out to be of great importance not only for the evaluation of scattering experiments, but also for the quantitative determination of the polarization effects in ferromagnets as given in Section VI.

Experiments were performed first on a polycrystalline sample ($\sigma_{\text{polycr.}}=12.0\pm0.2\times10^{-24}$ cm^2) and then on a single crystal of Fe ($\sigma_{\text{single cr.}}=7\times10^{-24}$ cm^2), using a thermal distribution of neutrons at room temperature. The case of the single crystal may be described as follows: The resolving power of the microcrystals, which are all oriented in approximately the same direction, will limit the scattering to small regions in the neighborhood of those wave-lengths for which Bragg reflection occurs. These neutrons, for which the coherent scattering is large, represent only a small fraction of the total incident neutron intensity; hence for the entire incident neutron beam, the effective coherent scattering will be negligibly small.

Thus the difference between the results in the two cases represents just the coherent scattering of the incident distribution by the polycrystalline sample. This gives for the effective coherent cross section $\bar{\sigma}=5\times10^{-24}$ cm^2.

The ratio $\bar{\sigma}/\sigma$ with the temperature factor included has been calculated numerically for iron, with thermal neutrons. Using this calculated ratio $\bar{\sigma}/\sigma=0.81$, and the experimental value of Whitaker and Beyer $\bar{\sigma}=5\times10^{-24}$ cm^2 we find $\sigma=6.25\times10^{-24}$ cm^2, so the nuclear amplitude

$$C=(\sigma/4\pi)^{\frac{1}{2}}=7.05\times10^{-13}\text{ cm}.$$

We can similarly understand on the basis of our formulae the small deviations found by Whitaker and Beyer when the cross section of certain molecules was compared with the sum of the cross sections of the components. No general predictions can be made as to the sign of this effect, but since the crystal cross section for reasonable velocity distributions of the neutrons may differ by approximately 20 percent from the value for the amorphous state we can readily see that change of lattice, of basis, and of temperature factor can lead to cross-section changes of the order of magnitude of 10 percent. One must also keep in mind that some of the components (e.g., Cu) may possess rather large microcrystals and therefore show a partial extinction effect which will disappear when Cu enters into the chemical compound.

Similarly, in the case of alloys (e.g., Permalloy investigations by Whitaker and Beyer,[10] and Nix, Beyer, and Dunning[11]) the presence of an ordered crystalline structure should produce marked changes in the coherent scattering, and give rise to deviations from additivity; changes in the percentage composition, or treatment which break up the ordered crystalline structure should then lead back to the value given by additivity.

On the basis of our previous discussion, the current belief that the scattering cross section for slow neutrons is independent of the neutron energy can no longer be accepted. The ratio $\bar{\sigma}/\sigma$ has been calculated by use of expression (2.16) for Fe for monochromatic beams of vary-

[9] The first two terms alone represent the incoherent scattering due to isotope disorder; the last term is due to spin dependence of nuclear forces. (See Section III of III; and reference 5.)

[10] M. D. Whitaker and H. G. Beyer, Phys. Rev. **55**, 1101 (1939).

[11] Nix, Beyer and Dunning, Phys. Rev. **57**, 566A (1940).

ing wave-length. The results are plotted in Fig. 1. As already mentioned in Section II, increasing wave-length will mean a decrease in the number of Debye-Scherrer rings, but the intensity of each remaining ring goes up as λ^2. Iron with lattice distance 2.86A is body-centered, so that the lowest order appearing will be (1, 1, 0) with $|l|=\sqrt{2}$ and $j(|l|)=12$; the coherent scattering from iron disappears for $\lambda>2a/\sqrt{2}=4.04$A. The limiting value for the coherent scattering at room temperature as $\lambda\to 4.04$A is, from (2.18)

$$\bar{\sigma}/\sigma=(2/8\pi)2\cdot e^{-2A}\cdot 12=1.29.$$

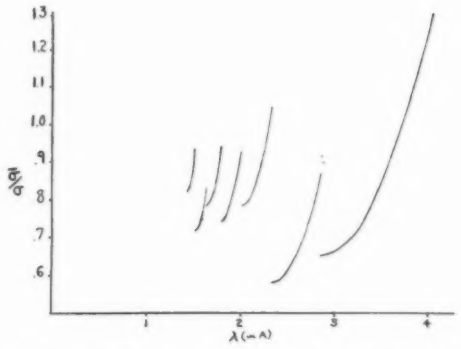

FIG. 1. Variation of crystalline cross section as a function of neutron wave-length.

IV. Discussion of the Size of Microcrystals and Estimate of the Scattering Amplitude of Fe Isotopes

It is of interest to see that the preceding formulae, together with the observations of the difference in cross sections for the crystal and polycrystalline state of iron, enable us to draw some conclusions about the size of the microcrystals and the scattering amplitudes of the Fe isotopes.

For a rough discussion, it is sufficient to describe the weakening of a beam passing through an aggregate of crystallites as follows: The beam will be reduced in intensity by the factor $\exp(-\mu')$ where $\mu'=Ll\sigma\lambda/8\pi a^5$ (see (2.11)) when it strikes a crystallite at the Bragg angle. The probability of such an event is given by a/l, which represents the resolving power of the perfect microcrystal. This probability must be multiplied by a factor which gives the number of possible strong reflections for one and the same wave-length. Although only a *rough estimate* of this factor can be made, it is sufficiently accurate for our purposes to put it equal to 15. The total weakening of a beam is now determined by the various mutually exclusive alternatives that the beam strike 0, 1, 2, etc., properly oriented crystallites when passing through a thickness d of the substance. The probability of n favorable encounters is given by: $P_n=e^{-\alpha}\alpha^n/n!$ where $\alpha=15ad/lL$ (Poisson formula). Denoting the size of one crystallite by L, we obtain for the intensity transmitted:

$$I=I_0\sum_{n=0}^{\infty}P_n\exp(-n\mu')$$
$$=I_0\exp[-\alpha(1-\exp(-\mu'))]. \quad (4.1)$$

This must be compared with the experimentally found absorption law $I=I_0\exp(-N\bar{\sigma}d)$ where $\bar{\sigma}$ refers only to the coherent cross section of the polycrystal. Now two alternatives are possible: Case (1): $\exp(-\mu')\to 0$ (large extinction). In this case $I=I_0e^{-\alpha}$ so $15ad/lL=N\bar{\sigma}d$. Using the empirically determined value $\bar{\sigma}=5$ (see Section III), we obtain as an upper limit, $l\sim 5\times 10^{-4}$ cm.

This upper limit for the size of the perfect microcrystal is, of course, highly exaggerated. It takes its maximum in the case of large extinction since the weakening of the beam by passing through one crystal grain is then almost complete. *It is also of interest to point out that in the case of marked extinction no polarization effect could be observed*, since it is due to the slight increase or decrease of the atomic cross section produced by the interference of nuclear and magnetic scattering. If the nuclear scattering is already so large as to produce extinction, a slight change in the total atomic cross section cannot be of importance. A single crystal as distinguished from a polycrystalline body has complete extinction, and therefore cannot give an observable polarization effect.

Case (2): This corresponds to the absence of extinction or, quantitatively speaking, $\exp(-\mu')\sim 1$. Since the numerator in

$$\exp[-15(ad/lL)(1-\exp(-\mu'))]$$

is now very much smaller, the number of layers of the perfect microcrystal must be correspondingly reduced in order to keep the value for the scattering constant, and equal to the observed $\exp[-N\bar{\sigma}d]$. In the limiting case $\exp(-\mu')=1-\mu'$, the expression for the absorption reduces

to $\exp(-\alpha\mu')=\exp(-15\sigma\lambda d/8\pi a^4)$, and so becomes, as was to be expected, independent of the size of the microcrystal. This case corresponds to the condition found in nature, and leads to a value of $\sigma=17\times10^{-24}$ cm^2. Since this case is precisely the one which we considered in Section II, the fact that the values of σ obtained by both arguments agree so closely, considering the roughness of the estimate, would indicate that our choice of some of the constants used is correct.

Recently, Miller and Du Mond[12] have given estimates of the length of perfect lattice in Ag and Al of approximately 500 lattice distances. They also find that after distortion and working the length is reduced to 150 to 200 lattice distances. Similar behavior in Fe would lead to negligible extinction.

We can also attempt to evaluate *approximately* the coherent cross section of the two iron isotopes which are present in the ratio of 92 : 8.[13] Since the total *cross section of iron* is found to be 12 nuclear units (i.e., $12\times10^{-24}\times$cm^2) and the capture cross section to be approximately 3.5 n.u., we have to account for 8.5 units as being due to coherent and incoherent scattering. Of this, 5 n.u. are found to be coherent scattering, while the incoherent contribution of 3.5 n.u. is due to three causes: inelastic scattering by the lattice, incoherent nuclear scattering, and background due to isotope disorder. The inelastic scattering is small, while the incoherent nuclear scattering also probably does not contribute much to the total background. The isotope Fe^{56} has probably no spin, being a $4n$ nucleus, while the isotope Fe^{54} would have to have an anomalously large cross section to contribute a large portion of the observed background since it forms only 8 percent of the element. Lumping together these first two causes, and ascribing to them for purposes of a rough estimate a cross section of one nuclear unit, we obtain a value of 2.5 nuclear units for the disorder contribution as given by $\sum C_p f_p^2-(\sum C_p f_p)^2$ where C_p is the concentration and $f_p=(4\pi)^{\frac{1}{2}}\times$ the coherent amplitude of the pth isotope, which for the case of two isotopes reduces to

$$C_1C_2(f_1-f_2)^2. \tag{4.2}$$

According to Section III, a crystalline cross section of five nuclear units corresponds to an amorphous cross section of approximately seven nuclear units. We can, with these data, attempt to determine the scattering amplitude and phase for the two isotopes. The equations are:

$$(0.92f_1+0.08f_2)^2=7 \quad (0.92)(0.08)(f_1-f_2)^2=2.5.$$

There is no restriction of generality in assuming that the amplitude of the abundant isotope shall have the positive sign. We then obtain the following two sets of solutions for the amplitudes:

either (a) $f_1=3.11$; $f_2=-2.72$

or (b) $f_1=2.18$; $f_2=8.01$.

(b) may be excluded as being highly improbable; it would lead to an unusually high cross section of 65 n.u. for the less abundant isotope Fe^{54}. We finally obtain the following estimate for the coherent cross sections of the two nuclei:

Fe^{56}: $\sigma\sim9.7$ n.u.
Fe^{54}: $\sigma\sim7.4$ n.u.

In addition to this, it should be noted *that the amplitudes have opposite signs.*

V. An Interpretation of the Larmor Precession of the Spin During Passage through Magnetized Media

We wish now to apply our results to the propagation of neutrons in a ferromagnetic medium (Fe), magnetized to saturation, with the spins of all ions rigidly aligned along the direction of a unit vector $\mathbf{k}$.

The total scattered wave from an ion will be given by (1.8):

$$\psi_{sc}=(2\pi M_0/hk)^{\frac{1}{2}}r^{-1}e^{ikr}(C+2D\mathbf{q}\cdot\mathbf{s})X_s.$$

The presence of the magnetic term introduces the possibility of changes in polarization due to the difference in scattering of the two spin states of the neutron. To put the possibility of such rotation of the plane of polarization clearly in evidence, let us consider a neutron beam of wavelength λ traversing a lattice whose spacing is less

[12] P. H. Miller and J. W. M. Du Mond, Phys. Rev. **57**, 198 (1940).

[13] Actually, Fe has four stable isotopes. The concentration of Fe^{58} is negligible; Fe^{54} and Fe^{57} have been lumped together and are referred to as "Fe^{54}."

than $\frac{1}{2}\lambda$. Then no Bragg maxima can occur and the coherent scattering is confined to the forward direction. We shall resolve the spin along the direction of the magnetization, which is the most convenient representation.

Suppose $\mathbf{k}$ along the x axis; then $\mathbf{q}$ has components $(e_x^2-1, e_xe_y, e_xe_z)$. Then, in summing over the lattice, the cross terms drop out because of the symmetry of the crystal, and only the x component ($\|$ to $\mathbf{k}$) remains. We conclude that no depolarization can be produced by this process.

Nevertheless, the two polarization states are scattered differently. We shall treat the propagation of each of the polarization states as in classical dispersion theory by adding to the incident wave at any point the scattered waves from the centers in the medium, and determine an index of refraction. For simplicity, let the plane OXY contain one scattering center per unit area (see Fig. 2). Let $\mathbf{k}$ be along the z axis. We must calculate the total wave at the field point P, where $OP=a$.

$\mathbf{k}=(0, 0, 1) \quad dxdy=a^2\sec^2\theta\tan\theta d\theta d\varphi$
$\mathbf{e}=(1/2\sin\frac{1}{2}\theta)(-\sin\theta\sin\varphi, -\sin\theta\cos\varphi, 1-\cos\theta)$
$\mathbf{q}=\frac{1}{2}(-\sin\theta\sin\varphi, -\sin\theta\cos\varphi, -\{1+\cos\theta\}).$

The magnetically scattered wave from plane OXY is:

$$2D\int\int\frac{e^{ikr}}{r}(\mathbf{q}\cdot\mathbf{s})dxdyX_s=$$

where $r=QP$

$$=2Da^2\int\int\sec^2\theta\tan\theta d\theta d\varphi\frac{e^{ika\sec\theta}}{a\sec\theta}(\mathbf{q}\cdot\mathbf{s})X_s.$$

As we have seen previously, only the z component remains, giving:

$$2D\pi a\int_0^{\pi/2}\sec\theta\tan\theta d\theta e^{ika\sec\theta}(1+\cos\theta)(\pm\tfrac{1}{2})$$

$$=\pm\frac{D\pi}{ik}\int_0^{\pi/2}d(e^{ika\sec\theta})(1+\cos\theta).$$

The integral will be oscillatory at the upper limit, as in all Fresnel diffraction problems, but just as in the optical case, such convergence difficulties can be eliminated by the introduction of a weight factor. Partial integration gives:

$$\pm D\left[\frac{2\pi}{ik}e^{ika}+\frac{\pi}{ik}\int_0^{\pi/2}e^{ika\sec\theta}\sin\theta d\theta\right].$$

The second term

$$=-\frac{\pi a}{i}\int_{ka}^{\infty}\frac{e^{iy}}{y^2}dy;$$

we proceed neglecting this term. If we had included the nuclear part, this scattered wave from plane OXY would be:

$$e^{ika}\frac{2\pi}{ik}\left(C\pm\frac{e^2\gamma S}{mc^2}\right)\psi_{\text{inc}}$$

for the two polarization states. But the total wave at point P will be the sum of the incident wave at P and the scattered waves from all planes below P. If the phase of the incident wave at P is taken at zero, its phase at OXY is e^{-ika}. So for a thickness d, the amplitude of the total wave is

$$I\left(1+\frac{2\pi d}{ik}\left\{C\pm\frac{e^2\gamma S}{mc^2}\right\}\right)$$

$$=I\exp\left[-2\pi i\frac{d}{k}\left(C\pm\frac{e^2\gamma S}{mc^2}\right)\right],$$

where I is the incident wave, and we have assumed one scattering center per unit volume. This gives for the index of refraction:

$$n_\pm=\frac{2\pi}{k}\left(C\pm\frac{e^2\gamma S}{mc^2}\right)$$

and for the rate of rotation of the direction of polarization: (n_+-n_-) (velocity of the beam)

$$=\frac{2\pi}{k}\cdot\frac{2e^2\gamma S}{mc^2}\frac{hk}{M_0}=\frac{4\pi e^2\gamma Sh}{M_0mc^2}. \tag{5.1}$$

From the macroscopic viewpoint, this rate of rotation should be given by the velocity of the Larmor precession of the neutron in the macroscopic field of the crystal. The magnetic moment/unit volume is $\mathbf{M}=ehS/mc$ so that (5.1) becomes:

$$4\pi e\gamma\mathbf{M}/M_0c. \tag{5.2}$$

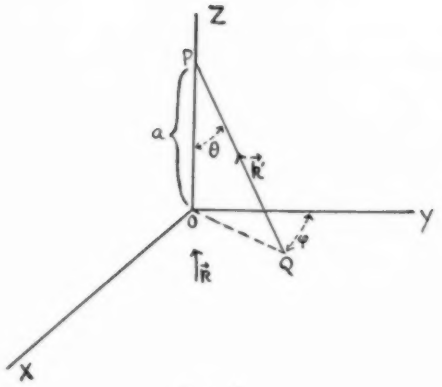

FIG. 2.

The total rotation of the plane of polarization is, of course, obtained by adding to (5.2) the precession due to the over-all magnetic field H. After adding this term which cannot be specified without knowledge about accidental outside fields, as well as the shape of the body, we can summarize the results by saying that it is the vector:

$$\mathbf{B}=\mathbf{H}+4\pi\mathbf{M}, . \qquad (5.3)$$

which determines the total Larmor frequency of precession. Our derivation allows some insight into the manner and the mechanism by which the inhomogeneous magnetic field of the individual atoms averages out and leads to the well-known result for the rotation of the plane of polarization.

It can be shown easily that an analogous result holds when the direction of magnetization is no longer assumed to be parallel to the direction of incidence but allowed to make an arbitrary angle with it.

VI. Polarization Experiments with Ferromagnets; General Principles and Choice of Form Factor

Polarization effects accompanying the passage of neutrons through ferromagnets are due solely to the *interference* between nuclear and magnetic scattering. Since it was proven that the magnetic scattering by free electronic spins is always incoherent[14] we have to limit the discussion to the case in which the electronic spin remains unchanged during the collision process. This is the case only for ferromagnets, and neutrons of sufficiently small velocity. Similarly, only the coherent part of the purely nuclear scattering is relevant. Neither the incoherent nuclear scattering (i.e., transition with change of spin of nucleus) nor the background due to isotope disorder contribute anything to the magnetic polarization phenomenon; this is true for the latter since the magnetic scattering amplitude is the same for all isotopes, and therefore disappears from $\sum C_p f_p^2-(\sum C_p f_p)^2$. We can therefore limit ourselves to the experimentally determined coherent nuclear cross section.[15] From the preceding remarks it becomes apparent that the consideration of the crystalline structure of the material is decisive in any calculation of polarization effects. Not only does it allow us to take properly into account the coherent and incoherent contributions, but it is also, as previously remarked, essential in the introduction of the form factor for the magnetic scattering.

It would be permissible (cf. Section II and Fig. 1) to approximate the crystalline aggregate by an amorphous body for sufficiently small wave-length. But since the distribution of the magnetically active currents in an atom extends over a domain which is not small even compared with the wave-length of thermal neutrons, the case of small wave-length would become uninteresting, since the atomic form factor would almost annihilate the effect to be expected. Choosing, on the other hand, sufficiently large wave-lengths, we are no longer allowed to neglect the crystal structure. Coherent scattering disappears in the case of Fe for wave-lengths larger than 4.04A. There does not therefore exist a range in which the theory based on an amorphous structure is even approximately correct.

A quantitative evaluation of polarization phenomena requires, therefore, knowledge of the wave-length of the incident neutrons, as well as of the form factor of the scattering atom which is a function of wave-length and scattering angle. We shall, in this section, assume, first, that

[14] See II and III.

[15] The background produced by inelastic collisions between the neutron and the lattice vibrations should, strictly speaking, also be considered. We neglect it in the following discussion because, it would be very small even for x-rays, still smaller for neutrons (cf. reference 4) and mostly present for large scattering angles, where its effect is strongly cut down by the form-factor.

monochromatic neutrons are incident, and discuss choice and influence of the form factor. Section VII contains the more general treatment of an incident spectrum together with a numerical evaluation of the results.

Polarization effects can be observed through experiments on the scattered or transmitted beam; only experiments of the second type have so far been performed, for reasons of available intensity. We shall therefore limit ourselves to this group of phenomena; the treatment of the scattered beams can easily be carried out with the aid of the formulae presented here and in previous notes.

As the incident beam is resolved along the direction of magnetization denoted by $\mathbf{k}$, the additional scattering per unit solid angle for the two spin states is given by[16]

$$d\Phi_{\text{additional}} = \pm 2CD(\mathbf{q}\cdot\mathbf{k})d\Omega = \pm 2CDq^2 d\Omega. \quad (6.1)$$

This can be taken over to the crystalline case immediately since both the amplitudes C and D refer to coherent processes *only*. The magnetization is assumed to be perpendicular to the direction of incidence, as is the case in all experiments. In the crystalline case, for a ring of index $|l|$, the average of q^2 over azimuth gives

$$\langle q^2\rangle_{Av} = \tfrac{1}{2}(1+\sin^2\tfrac{1}{2}\theta) = \tfrac{1}{2}(1+|l|^2\lambda^2/4a^2). \quad (6.2)$$

The form factor F which is contained in D is function of $|l|$ only. (From now on we shall write the form factor separately: $D = e^2\gamma S/mc^2$.)

The final result for the additional cross section p, for the case of a simple cubic crystal, including temperature effect, is:

$$\begin{aligned} p &= CD\cdot\tfrac{1}{2}\left(\frac{\lambda}{a}\right)^2 \sum_{|l|<2a/\lambda} \frac{\exp(-A|l|^2)}{|l|} \\ &\qquad \times F(|l|)\left(1+\frac{|l|^2\lambda^2}{4a^2}\right) \\ &= 4\pi C^2\cdot\frac{D}{C}\cdot\frac{1}{8\pi}\left(\frac{\lambda}{a}\right)^2 \sum_{|l|<2a/\lambda} \frac{\exp(-A|l|^2)}{|l|} \\ &\qquad \times F(|l|)\left(1+\frac{|l|^2\lambda^2}{4a^2}\right) \end{aligned} \quad (6.3)$$

and comparing with

$$\bar{\sigma}_{\text{nuclear effective}} = \sigma\cdot\frac{1}{8\pi}\left(\frac{\lambda}{a}\right)^2 \sum_{|l|<2a/\lambda} \frac{\exp(-A|l|^2)}{|l|}, \quad (2.15)$$

we obtain:

$$\begin{aligned} p &= \bar{\sigma}_{\text{nuc eff}}\cdot\frac{D}{C} \\ &\qquad \times \sum_{|l|<2a/\lambda} f(|l|)F(|l|)\left(1+\frac{|l|^2\lambda^2}{4a^2}\right), \end{aligned} \quad (6.4)$$

where $f(|l|)$ is the fraction of the scattered neutrons in the ring of index $|l|$.

The same formula will apply to any other case (average over velocity distribution; body-centered crystal). The "p" is always given by:

$$\bar{\sigma}_{\text{coherent}}(D/C)[\text{average over the rings of } F(|l|)(1+|l|^2\lambda^2/4a^2)].$$

To find the additional scattering w for a centimeter thickness, we multiply by the number N of atoms/cc (for iron $N = 8.48\times10^{22}$); $w = Np$. Then the fractional increase in transmission on magnetization is:

$$(\tfrac{1}{2}e^{-N\sigma x-wx}+\tfrac{1}{2}e^{-N\sigma x+wx}-e^{-N\sigma x})/e^{-N\sigma x}, \quad (6.5)$$

where σ contains the cross sections for all other causes of weakening of the beam (capture, incoherent scattering, nuclear coherent scattering), and x is the total thickness traversed. This gives for the fractional change in transmission

$$\tfrac{1}{2}w^2x^2. \quad (6.6)$$

This result applies to both single and double transmission experiments.

While the amplitude C of nuclear scattering is independent of the scattering angle, D will depend on it through the magnetic form factor. Its determination offers a certain difficulty due to our incomplete knowledge of the constitution of the magnetically active 3-*d* shell of Fe. For the purposes of a rough estimate we have previously[17] used Slater's[18] hydrogenic function for the wave function of the electrons in question. This method, which was also adopted with even

[16] See III, Section VI. We here neglect small effects proportional to D^2.

[17] See Section VII of III.

[18] J. C. Slater, Phys. Rev. **36**, 57 (1930).

steeper decrease towards the outside by Van Vleck,[19] does not seem to lead to reliable quantitative values as successfully as it might have for other applications reported by Slater.

Bethe[20] used the well-tabulated density function of Hartree for the 3-d shell of Cu^+, which was derived by the method of the self-consistent field. To adapt this density distribution to the case of iron with a smaller central charge, Bethe "expanded" the effective radius of iron with respect to copper in the inverse ratio of the effective charges and calculated the form factor by numerical integrations.

In the present paper we also use the Hartree distribution which has so far proved to be of higher accuracy than our demands would require. But in place of the slightly rough numerical integration carried out by Bethe, we use the analytic expression for the Hartree distribution as adapted by Slater.[21] It is interesting to observe that the actual density distribution can be well represented by the sum of three hydrogenic functions of which only two are really significant. The result of this analytic calculation agrees with Bethe's formula for sufficiently small values of $(\sin\frac{1}{2}\theta)/\lambda$, but our probably more correct method gives a decidedly sharper decrease of the form factor at large angles.

For a Cu^+ 3-d electron, the (radial density)$^{\frac{1}{2}}$

$$\sqrt{\rho}=r\psi=r^3(ae^{-br}+ce^{-dr}+fe^{-gr}).$$

The unit of length is the Bohr radius a_0. $b=6.29$; $d=2.65$; $g=1.28$. Slater gives the following data:

inner intersection $=3.78$; i.e.,

$$ae^{-(3/3.78)(6.29)}=ce^{-(3/3.78)2.65}$$

and outer intersection $=1.15$; i.e.,

$$ce^{-2.65(3/1.15)}=fe^{-1.28(3/1.15)}.$$

This gives $a=17.975c$

$f=0.02804c$.

So we can write:

$$\sqrt{\rho}=r\psi=r^3[17.975e^{-6.29r}+e^{-2.65r}+0.02804e^{-1.28r}].$$

To calculate the form factor, we must evaluate:

$$F=\int e^{ipr\cos\theta}\sin\theta d\theta\rho dr, \qquad (6.7)$$

where $p=2k\sin\frac{1}{2}\theta$; $k=2\pi/\lambda$; λ in Bohr units. F will consist of six terms:

$$F=\sum_{i=1}^{6} f_i$$

where f_i is of the form:

$$f_i=\int e^{ipr\cos\theta}\sin\theta d\theta\cdot l_i\exp(-m_ir)r^6dr,$$

i	1	2	3	4	5	6
l_i	323.1	35.95	1.008	1.0	0.0561	0.00079
m_i	12.58	8.94	7.57	5.30	3.93	2.56

$$f_i=\frac{l_i}{ip}\int_0^\infty dr\cdot r^5\exp(-m_ir)[e^{ipr}-e^{-ipr}]$$

$$=\frac{5!\,l_i}{ip}\left[\frac{1}{(m_i-ip)^6}-\frac{1}{(m_i+ip)^6}\right]$$

$$=\frac{2\cdot 6!\,l_i}{m_i^7}\cdot\frac{1-(10/3)(p/m_i)^2+(p/m_i)^4}{[1+(p/m_i)^2]^6}.$$

Normalization is obtained by requiring that for $p\to 0$, $F\to 1$. So we must divide by the normalization factor $\sum_1^6 2\cdot 6!\,l_i/m_i^7$. When this is done, we obtain the form factor: $F=\sum_1^6 F_i$, where

$$F_i=n_i\left[\frac{1-(10/3)(p/m_i)^2+(p/m_i)^4}{[1+(p/m_i)^2]^6}\right]. \qquad (6.8)$$

i	1	2	3	4	5	6
n_i	0.227	0.276	0.025	0.298	0.136	0.038
m_i	12.58	8.94	7.57	5.30	3.93	2.56

The form factor consists of these six terms, each similar to the single-term expression given in III. Figure 3 gives a comparison between F and the form factor F_B as given by Bethe. They coincide for small values of p, but F falls below F_B and decreases more rapidly for large p.

For a Debye-Scherrer ring of index $|l|$, $p=2\pi a_0|l|/d$. We see that F is a function only of $|l|$. For application to Fe, we have reduced the wave-length to 75 percent to take account of the contraction of the charge. The values of p for the first few rings are indicated in Fig. 3.

[19] J. H. Van Vleck, Phys. Rev. **55**, 924 (1939).
[20] Hoffman, Livingston and Bethe, Phys. Rev. **51**, 214 (1937).
[21] J. C. Slater, Phys. Rev. **42**, 33 (1932).

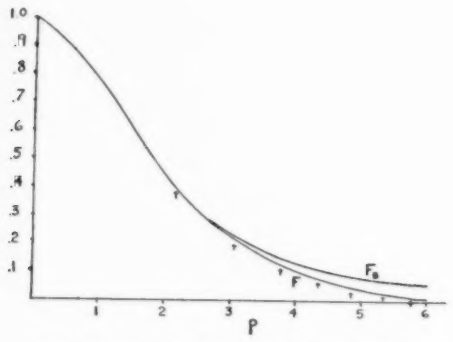

FIG. 3. Form-factor of $3d$ shell of iron.

VII. Evaluation of Polarization Experiments Continued; Velocity Distribution of the Incident Neutrons

The strong dependence of the scattering into rings of different values of $|l|$ on the wave-length, as it becomes apparent from the formula (2.16) and from the discussion at the end of Section III, makes it necessary to refine the calculations of Section II, as far as the velocity distribution is concerned. It has been frequently observed that the Maxwellian distribution used in paragraph 2 for the purpose of illustration cannot really claim to be an accurate representation of the velocities present in the incident beam of "thermal neutrons." Neither are the long wave-lengths (small velocities) really present, since the inelastic transitions are far too slow to produce them (cf. Pomeranchuk[5]); nor can it be expected that the curve falls off at high velocities in an exponential manner, since the whole spectrum should extend even beyond the Cd absorption limit.

Absorption experiments with "cooled" neutrons also fail to show real agreement with the $1/v$ law, when temperatures of the neutron source are used for comparison.

We have therefore made use of the velocity curve which has been obtained by Dunning[22] and collaborators giving the frequency of neutrons as a function of their mechanically determined speed. The result is contained in Fig. 4, where a Maxwell distribution has been included for comparison. (The distributions as shown are not normalized; their maxima have been made to coincide, in order to show clearly the difference in shape.) This choice brings with it the disadvantage of a numerical integration since no analytic representation of this velocity distribution is available. The velocity distribution shows qualitatively all the features to be expected.

A second point to be taken into account is the change in the velocity distribution while the neutrons pass through iron. The coherent scattering as well as the background are *approximately* velocity independent; the capture on the other hand follows the $1/v$ law, and therefore removes the low velocity neutrons preferentially. Since it is the long wave-length, low velocity neutrons which determine the polarization, this correction will turn out to be of significance.

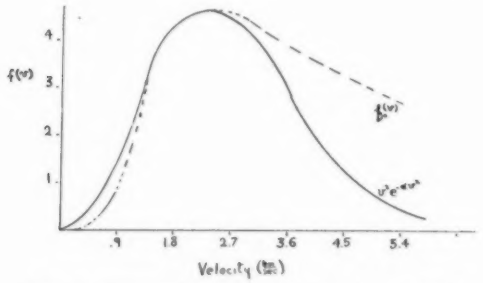

FIG. 4. Comparison of velocity-selector and Maxwellian distributions.

In order to determine the velocity distribution of the neutrons as a function of the thickness of sample traversed, we have proceeded as follows:

The observed capture cross section $\bar{\sigma}_{\text{cap}}$ of Fe for thermal neutrons is $\sim 3.5\times10^{-24}$ cm^2. This represents an average of the capture cross section $\sigma_{\text{cap}}=\sigma_0/v$ over the thermal distribution, i.e.,

$$\bar{\sigma}_{\text{cap}}=3.5\times10^{-24}\text{ cm}^2 = \int \frac{\sigma_0}{v} f_0(v)dv \Big/ \int f_0(v)dv, \quad (7.1)$$

where $f_0(v)$ is the neutron distribution indicated in Fig. 4 and tabulated in Table I. This gives, after numerical integration,

$$\sigma_0=8.9\times10^{-19}; \quad \sigma_{\text{cap}}=\sigma_0/v. \quad (7.2)$$

The velocity distribution $f_x(v)$, after a thickness x has been traversed is given by:

$$f_x(v)=f_0(v)\exp(-N\sigma_0 x/v). \quad (7.3)$$

Using Eq. (7.3), the velocity distribution has

[22] Dunning, Pegram, Fink, Mitchell and Segrè, Phys. Rev. **48**, 704 (1935).

been calculated for thicknesses of 1, 2, 3 and 4 cm, and then a normalization factor introduced so that

$$\int_0^{5.4} f_x(v)dv = 1.$$

The function $f_x(v)$ is tabulated in Table I.

We must also replace the calculation of $\bar{\sigma}/\sigma$ given in Section III on the basis of Eq. (2.17), by a similar calculation using the correct neutron distribution $f_0(v)$. From Eq. (2.16) we obtain:

$$\bar{\sigma}/\sigma = \int_0^\infty f_0(v)dv \cdot \frac{2}{8\pi}\left(\frac{\lambda}{a}\right)^2 \times \sum_{\text{even } |l|<2a/\lambda} \frac{\exp(-A|l|^2)}{|l|}, \quad (7.4)$$

where $f_0(v)$ has been assumed to be normalized. The order of summation and integration may be reversed, giving

$$\frac{\bar{\sigma}}{\sigma} = \sum_{\text{even } |l|} \frac{\exp(-A|l|^2)}{|l|} \cdot \frac{2}{8\pi}\left(\frac{h}{Ma}\right)^2 \times \int_{|l|h/2Ma}^\infty \frac{f_0(v)dv}{v^2}. \quad (7.5)$$

TABLE I. *Values of* $f_x(v)$.*

v(km/sec.)	$f_0(v)$	$f_1(v)$	$f_2(v)$	$f_3(v)$	$f_4(v)$
0.9	0.88	0.38	0.164	0.071	0.031
1.1	1.64	0.826	0.416	0.210	0.105
1.3	2.72	1.521	0.852	0.476	0.266
1.5	3.78	2.286	1.382	0.836	0.505
1.7	4.20	2.694	1.728	1.109	0.711
1.9	4.42	2.972	1.998	1.343	0.903
2.1	4.55	3.175	2.215	1.545	1.078
2.3	4.62	3.328	2.397	1.727	1.244
2.5	4.63	3.423	2.531	1.871	1.383
2.7	4.58	3.462	2.616	1.977	1.494
2.9	4.48	3.455	2.663	2.054	1.584
3.1	4.30	3.369	2.639	2.068	1.620
3.3	4.12	3.277	2.606	2.075	1.648
3.5	3.96	3.191	2.571	2.071	1.669
3.7	3.81	3.107	2.534	2.066	1.685
3.9	3.66	3.015	2.483	2.045	1.686
4.1	3.52	2.929	2.436	2.027	1.686
4.3	3.39	2.843	2.384	1.999	1.677
4.5	3.25	2.748	2.322	1.963	1.660
4.7	3.12	2.656	2.261	1.925	1.639
4.9	3.00	2.572	2.205	1.890	1.620
5.1	2.87	2.475	2.135	1.841	1.588
5.3	2.74	2.377	2.063	1.789	1.552
$\int_0^{5.4} f_x dv =$	16.63	12.408	9.562	7.284	5.256

* *More* figures have been included in these tables than are *physically* significant. This has been done to assist the reader in following a sample calculation and in reproducing the graphs smoothly.

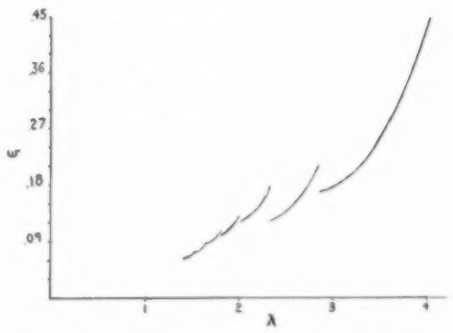

FIG. 5. Variation of polarization effect as a function of neutron wave-length.

From Eq. (7.5) we see that $\bar{\sigma}/\sigma$ consists of a sum of terms for different $|l|$, each involving a numerical integration of $f_0(v)/v^2$ from $v = |l|h/2Ma$ to ∞. This has been carried out, giving $\bar{\sigma}/\sigma = 0.75$, which corresponds to $C = 7.33 \times 10^{-13}$ cm.

Using $\gamma = 1.93$;[24] $S = 1.07$, giving $D = e^2\gamma S/mc^2 = 5.8 \times 10^{-13}$, $N = 8.48 \times 10^{22}$, we have calculated w for monochromatic beams of various wave-lengths, using Eq. (6.4) and the ratio $\bar{\sigma}/\sigma$ given in Fig. 1.

The values of w obtained are shown in Fig. 5. The breaks in the curve occur at wave-lengths where a Debye-Scherrer ring is cut out, as has already been described in connection with Fig. 1.

For an incident beam of thermal neutrons, Eq. (6.6) will no longer apply, but will be replaced by

$$\tfrac{1}{2}\left[\int_0^d w(x)dx\right]^2 \quad (7.6)$$

for the transmission effect of a sample of thickness d; we write $w(x)$ because the polarization will now vary with distance traversed, since the velocity distribution $f_x(v)$ is changing because of preferential absorption of low velocity neutrons.

To evaluate the polarization effect, we have calculated $w(x)$ for $x = 0, 1, 2, 3, 4$, cm using the values of $f_x(v)$ tabulated in Table I and using Eq. (6.4). The fraction $f^{(|l|)}$ is here given by the $|l|$th term in Eq. (7.5), divided by the total value of that sum. The results are shown in Table II. It should be pointed out that the polarization factor $(1+|l|^2\lambda^2/4a^2)$ depends on the wave-length. We have throughout used an

[24] L. W. Alvarez and F. Bloch, Phys. Rev. **57**, 111 (1940).

TABLE II. *Values of* $w(x)$.*

$\lvert l\rvert^2$	$A=1+\frac{\lvert l\rvert^2\lambda^2}{4a^2}$	$F(\lvert l\rvert)$	$f_0(v)$ $f(\lvert l\rvert)$	$fF(A)$	$f_1(v)$ $f(\lvert l\rvert)$	$fF(A)$	$f_2(v)$ $f(\lvert l\rvert)$	$fF(A)$	$f_3(v)$ $f(\lvert l\rvert)$	$fF(A)$	$f_4(v)$ $f(\lvert l\rvert)$	$fF(A)$
2	1.14	0.39	0.281	0.125	0.252	0.112	0.231	0.103	0.207	0.092	0.193	0.086
4	1.29	.22	.076	.022	.071	.020	.068	.019	.063	.018	.061	.017
6	1.43	.13	.183	.034	.181	.034	.178	.033	.171	.032	.170	.032
8	1.57	.08	.061	.008	.062	.008	.062	.008	.061	.008	.062	.008
10	1.71	.047	.086	.0069	.089	.0071	.092	.0074	.092	.0074	.095	.0076
12	1.86	.027	.021	.0011	.022	.0011	.023	.0012	.023	.0012	.024	.0012
14	2.00	.013	.094	.0024	.098	.0025	.106	.0028	.109	.0028	.115	.0030
16	2.00	.010	.009	.0002	.010	.0002	.010	.0002	.011	.0002	.012	.0002
18	2.00	.008	.043	.0007	.046	.0007	.050	.0008	.052	.0008	.056	.0009
		Remainder	0.0004		0.0005		0.0004		0.0004		0.0005	
		Total =	.200		.186		.176		.163		.156	
		$w(x)$ =	.0676		.0627		.0588		.0549		.0529	

* *More* figures have been included in these tables than are *physically* significant. This has been done to assist the reader in following a sample calculation and in reproducing the graphs smoothly.

average value for $\lambda = 1.53$A. This is justified since it is a slowly varying function of λ. Also, as the distribution changes while passing through the sample, the average wave-length decreases, so that, at worst, we are over-estimating the polarization effect.

We obtain from the data of Table II for the transmission effect the results shown in Table III where experimental results[24,25] are listed for comparison:

TABLE III.

Thickness	0.8	1.3	1.95	4.0
% Effect	0.14	0.35	0.75	2.9
Experimental	0.76	1.78	3.32	6.0

As can be seen from the table, there exists a considerable discrepancy between theoretical and observed values for the transmission. We have also, in our comparison, to take into account the marked depolarization effect due to deviation from saturation.[2] The data given by the experimenters do not allow us to draw any very definite conclusion about the state of saturation obtained, and we shall therefore defer the more detailed discussion of that effect until later. The presence of the depolarization effect is clearly indicated by the marked deviation from the law:

$$\text{polarization effect} \propto (\text{thickness})^2.$$

We do not, at the moment, see any possibility of reconciling the observed data with the present accepted views about the magnetic interaction between neutron and iron atom, and the constitution of the iron crystals. We intend to return to a fuller discussion of the questions involved in this field in a later paper.[26]

[25] P. N. Powers, Phys. Rev. **54**, 827 (1938).

[26] O. Halpern and M. H. Johnson, Phys. Rev. **57**, 160 (1940).

Studies of a Ring Discharge

CHARLES G. SMITH
Raytheon Manufacturing Company, Newton, Massachusetts
(Received April 12, 1941)

A driving e.m.f. of 890 cycles per second was employed to energize a ring discharge in mercury vapor in the pressure region near 2×10^{-4} mm. The ring was a secondary of one turn about a transformer core. E.m.f. per turn was usually near 5 volts. Probe measurements revealed a true electronic temperature with values ranging up to about 300,000°K at the peak of the wave of energization. Only 13 percent of the atoms were ionized at the maximum of the cycle of ionization. The highest electronic temperatures were not found at the lowest pressures. At a given e.m.f. the rate of build-up of the field of ions and the electronic temperature was lower at lower pressures. The energization reached a peak near the end of a half-cycle of the input voltage even though the current started at the zero of voltage. Stroboscopic and other spectral observations afforded qualitative confirmation of the probe measurements. Strong lines of Hg I–II–III together with faint lines of Hg IV were observed. The forbidden line $1^1S_0-2^3P_2$ was definitely observed and the forbidden line $1^1S_0-2^3P_0$ possibly observed, under conditions yielding the highest electronic temperatures but not otherwise. A probable rate of ion production in an electronic atmosphere of given density and temperature is calculated in accordance with accepted factors and found to be greatly in excess of that apparently prevailing in the present work. To explain the observed limitation upon degree of ionization, a hypothesis involving recombination of ion and electron with conservation of electrical energy is brought forward.

WITH the exception of astronomical work, there seems to have been only very limited study of a highly energized gas in the region of pressure below 0.001 mm. Observations in the laboratory have dealt mostly with transient conditions. It was an object of the present experiment to extend the parameters of a mercury vapor plasma into regions of lower pressure and higher degree of excitation under conditions making possible detailed study. Interest centers particularly upon the means of interchange of energy among the electrons and the rate of production and loss of ions. Plasma oscillations[1] have been postulated as a means of the interchange of energy, but quantitative support for the idea is apparently lacking though observational evidence[2] for oscillations of the expected frequency has been brought out. The calculated rate of production of ions in the ordinary plasma as previously carried out does not lead to agreement[3] with the observed rate.

These points of immediate interest are apparently aspects of things of a broad fundamental nature to be encountered in an extensive study of the low pressure plasma by the device herein employed.

An electromagnetically induced ring discharge was chosen for our studies because it has no space charge limitations of current, and because it has no electrodes to influence the distribution of velocities among the electrons. A tube with electrodes would yield a space charge limited current near the cathode for pressures below approximately 0.001 mm and would necessarily require an anode capable of dissipating the heat of condensation of the electrons. In a tube with electrodes there is a pronounced tendency in the positive column for the gas to be driven toward the anode,[4] especially under conditions of low pressure and high current. Within an electronic free path of the cathode there is not a good approach to a Maxwellian distribution of velocities among the electrons. At a pressure of 10^{-4} mm there would seem to be required a discharge tube about ten meters long, more or less, if we expected to insure a study of the plasma in a region not strongly disturbed by the cathode. The ring discharge yields a plasma without ends, and any pumping of gas along lines of current flow is of no observable consequence.

A low frequency ring discharge was chosen in order that the time of a half-cycle would be very long in comparison to the time taken for an electron to describe a mean free path. This was to avoid phase displacement between applied e.m.f.

[1] L. Tonks and I. Langmuir, Phys. Rev. **33**, 195 (1928).
[2] H. J. Merrill and H. W. Webb, Phys. Rev. **55**, 1191 (1939).
[3] B. Klarfeld, Tech. Phys. U.S.S.R., Vol. V, No. 12 (1938).
[4] Carl Kenty, J. App. Phys. **9**, 765 (1938).

and current resulting from the mass of the electrons, since it was hoped to realize very simple conditions for all the electrical measurements.

Figure 1 is a schematic representation of the toroidal discharge tube D, and a laminated iron core structure C. D was made from a spherical Pyrex flask of 22 liters capacity, through which a tube four inches in diameter was sealed. The core was made of iron laminations R, in ribbon form 2.7 meters long (the length of C) arranged

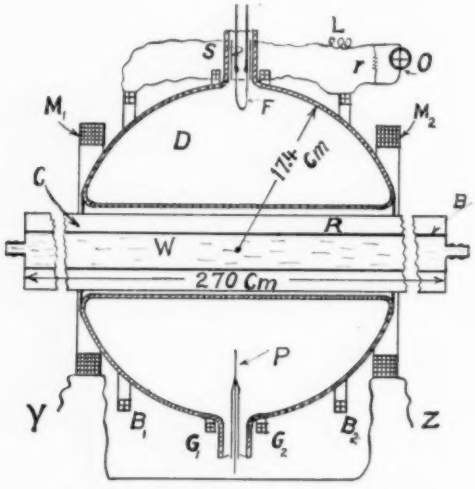

FIG. 1. Diagram of discharge tube.

radially around a brass tube B. Cooling water W was circulated in B. M_1 and M_2 are primary windings of 50 turns each. They were connected in series and the terminals Y and Z went directly to a 900-cycle 3600-r.p.m. motor generator of 10-kw capacity normally supplying power at 500 volts. The core was made long so that large magnetic flux density for linking D could be realized with a minimum of ampere turns in the primary windings. The core had a reluctance equivalent to an air gap of 1.44 mm having the cross section of the iron, which was 33 sq. cm.

Stray magnetic fields in the discharge region interfered with current flow. With the long core and the primary windings arranged symmetrically as shown, the very weak stray fields seemed to be negligible in their effect upon the discharge. In other words, magnetic linkage of the discharge region was made as large as possible but actual invasion of the discharge space by the magnetic field was avoided almost completely.

A tungsten wire probe is shown at P and a 20-mil tungsten filament at F. S represents a metallic can shielding all but the heated portion of F from the discharge. Use was made of these terminals in initiating the discharge or in probe measurements.

D was connected by way of a vapor trap to two mercury diffusion pumps in series. No stopcocks were employed on the low pressure side of the pumps. The pumps operated continuously while observations were being made. Usually a second trap was sealed to the tube D on the side opposite from the pump connection. The supply of vapor to D was controlled by the temperature of the traps.

The e.m.f. tending to impel the electrons around the circuit D was essentially the same as the e.m.f. per turn applied to the primary windings. This was ordinarily of the order of five volts and was incapable of starting the discharge unaided. An electronic current of a few milliamperes was drawn from F to S by an independent, or ionizing circuit, not shown. The ionizer was employed only in initiating the main discharge, and was not used after the main ring discharge arrived at a steady state condition.

The initial stages of operation are of significance in themselves but will be described only briefly, to point out the relation to some "reversible clean-up" phenomena. Given an e.m.f. of 5 volts and a pressure in the traps of 2×10^{-4} mm Hg, the ionizer is energized and a brilliant flash occurs in the toroid D, and this is followed by a cessation of ring current and a diminution or extinction of the ionizing current. After a short time, $\frac{1}{2}$ second more or less, another flash occurs. This is followed by darkness and another flash and so on, the flashing continuing for 30 seconds more or less. Then the ring discharge flows without apparent interruption, starting at a low mean value and building up slowly to a value of several hundred amperes as we shall see later. After the flashing stage, the ionizer and its filament current are disconnected. The ring current meantime continues. Pressure measurements with an ionization gauge show that the first flash practically evacuates the region D of all mercury vapor. A wall population of the vapor is built up by vapor coming in from the traps and is held upon the

walls while the discharge is flowing. The wall robs the volume until its own population is built up, after which steady operation ensues.

If the ring current is permitted to flow for some minutes and then interrupted, the pressure rises rapidly to a value above that in the traps, showing a great evolution of vapor from the walls. These phenomena are in agreement with those of Kenty.[4] It was also noted that any increase in degree of excitation of the vapor caused a release of some of the wall population. The converse was true, showing clearly that a wall previously heated by a prolonged and energetic discharge could immediately take on an additional population of condensed mercury. The wall population could be increased or decreased at will by varying the e.m.f. inducing the ring discharge or by any other means that changed the relative degree of excitation of the vapor. The observations indicate a lifetime for an atom constituting the wall population that is shorter the more energetic the discharge. This peculiar wall population merits a thorough investigation, since it is readily produced, and presents reproducible characteristic effects. There seems to be no ready theory of it, and its whole behavior is of an unexpected nature. We pass on to other matters which have been more carefully investigated.

The current in the gas and its wave form was determined. Coils B_1B_2 and G_1G_2, all of an equal number of turns, were connected in series with an inductance L and a resistance r. The B coils opposed the G coils, and no net voltage was generated to drive current through r and L until current flowed in the tube D. When the gaseous current flowed there was a magnetic flux linking the B coils that was larger than that linking the G coils. The voltage tending to force current i through the inductance L and resistance r was proportional to the time rate of change of the current I in the gas. Hence $Ldi/dt+ri=KdI/dt$, $K=$constant. The fundamental frequency was 890 cycles/sec. We chose $Lw=20r(w=2\pi\times890)$.

We neglect ri in the differential equation and obtain approximately $Li=KI$.

Terminals of a cathode-ray oscillograph O were connected to the ends of r. The oscillograph yielded the fundamental wave form of i and hence of I, the gaseous current.

Figure 2 shows two typical cases. $N_a=$ Number of atoms per cc.

The wave form was taken from oscillographic readings. The magnitude was obtained from a reading of the average power in watts expended in the gas, together with the average in comparison to the peak value of the power. Comparison of the average and the peak was from graphical integration of the product of the instantaneous current and voltage values given by the oscillograph. Oscillographic tests substantiated by stroboscopic observations showed the zero of current coincided with the zero of driving e.m.f.

Stroboscopic observations of the spectra were obtained by causing a spot of light from the tube to move along the slit of the spectroscope. A Bakelite disk about 45 cm in diameter, having fifteen radial slots, was fastened rigidly to the shaft of the generator supplying the energy to the

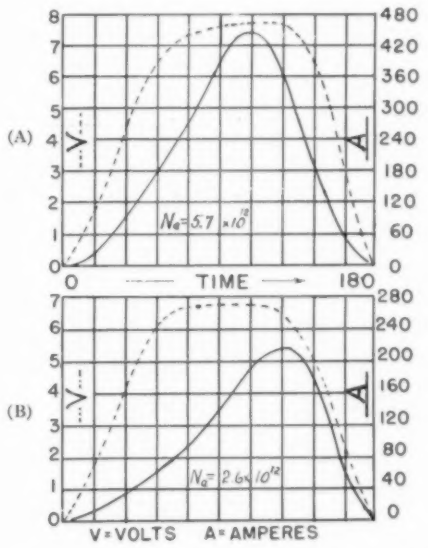

FIG. 2. Wave form of the current and voltage.

discharge tube. An image of a slot was focused upon the slit of the spectroscope, the image being a narrow line at right angles to the slit. Synchronism of the rotating disk and the light source was necessarily perfect regardless of variations in speed of the generator. Since there were thirty poles to the generator and fifteen slots in the disk the photographed spectrum was that for a current in only one direction in the discharge tube. Photographs are shown in Fig. 3. Time progresses

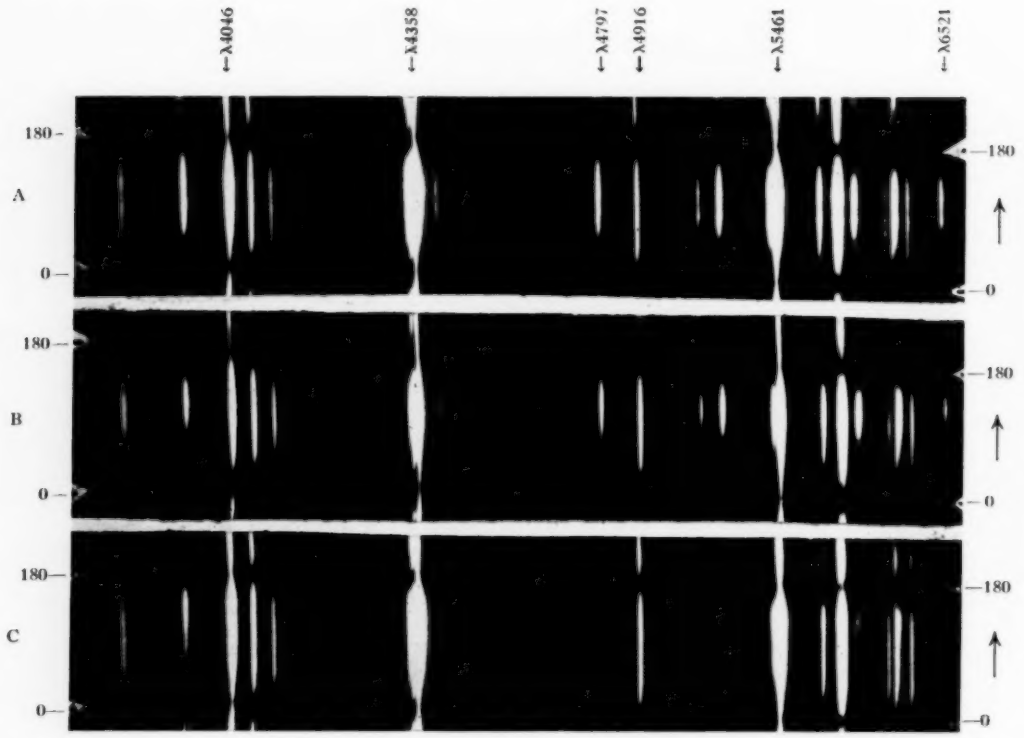

FIG. 3. Stroboscopic spectra arranged in order of electronic temperature; *A* is highest.

upward. Between 0° and 180° on the scale is the time of one half-cycle, 5.6×10^{-4} sec., approximately. Since the stroboscope was in perfect synchronism with the light source, we must conclude that the light of λ5461 was really quite perceptible even through the zero of time, and the minimum of illumination. The zero on the scale is the time of the zero of driving e.m.f. as determined by independent means, description of which must be omitted. Note the behavior of λ4797, a line of Hg III, in comparison to λ4916 of Hg I. The Hg III line begins late in the cycle and its maximum occurs well past the middle of the cycle. Lower pressure or lower driving e.m.f. sends this maximum further toward the 180° mark.

Direct spectral observations without the stroboscope showed Hg I predominant and Hg II–III–IV of apparently lesser intensity. The forbidden line $1^1S_0-2^3P_2$(λ2269.8) was readily observable at the higher electronic temperatures, but never at the lower electronic temperatures even though neighboring lines of Hg I were made to show in greater strength by longer exposures. Under the conditions that brought out λ2269.8 there was a faint line at λ2655.8 which could be the forbidden line $1^1S_0-2^3P_0$. More certainty in regard to this was not attainable due to the great strength of the neighboring strong Hg I line λ2655.

Evidently the energization of the plasma builds up to its maximum relatively slowly. We will first show that a simple ballistic consideration of the electronic motion does not lead us to an explanation. Consider an e.m.f. of 7 volts peak value applied around the toroid.

The average length around the toroid along a line of current flow is approximately 70 cm. The voltage gradient impelling an electron is 0.1 $\sin\omega t$, approx. An electron will experience an acceleration $a=e\sin\omega t/3000m=1.7\times10^{14}\sin\omega t$ cm/sec.^{2}.

Inspection shows that for $\sin\omega t$ as great as 0.2, the acceleration, if continuously operative on a given electron for only 10^{-5} sec., would impart to it a velocity of 3.4×10^8 cm/sec. Thus through more than 0.9 of the voltage wave, the e.m.f. is sufficient to impart the observed average speed to the electrons in 1/50 of a half-cycle or in a

time much smaller. (The observed speeds we infer from measurements of electron temperature discussed below.) Furthermore, if the lag in energization were a pure ballistic effect, then the current should persist and lag behind the zero of voltage. The observations show the current to be zero at the zero of voltage within the limit of resolution of the measurements, considered to be within a percent of a half-cycle.

The electronic temperature was measured by probe methods. A cylindrical probe is shown at P in Fig. 1. In the measurements of temperature to follow, a plane probe with plane parallel to the magnetic axis and to the current of the toroid was used. The other electrode is a hot tungsten filament F shielded by box S as shown, so that only the emitting portion was exposed to the discharge. The wires connecting F and P went out to the end of the core C, remaining in a plane including the axis of the core. Hence the 890-cycle magnetic flux generated no voltage between the filament and the probe. Filament and probe, though spatially separated as far as possible, are in regions of identical potential, and the metallic circuit between them is not disturbed by the induced e.m.f.'s.

A plot of the logarithm of probe current, measured at the peak, against values of voltage in the probe circuit yielded very good straight lines in the region used for temperature measurements. The straight line shows the velocity distribution among the electrons is Maxwellian. The inverse slope is a measure of electronic temperature. One would normally be surprised to find a true electronic temperature in a laboratory region having pressures as low as those employed here. The toroid, however, is in effect a plasma of infinite length and, as previously pointed out, avoids the disturbance to electronic velocity distribution normally caused by conditions near the electrodes. Besides the effective infinite length of the plasma there is no potential difference between any two points on a line of current flow, the electrons being subjected to a driving e.m.f.

Table I shows electronic temperature θ at various e.m.f.'s applied to the torus and at two different vapor pressures in the trap.

The higher pressure yields the higher temperatures. The reverse would have been expected. The explanation is contained in the data showing a slower build-up of energy at the lower pressure as revealed by the current wave form and the stroboscopic spectral observations. The observed variation of maximum temperature with pressure shows the high electronic speeds observed are not simply the result of each electron in question making a number of excursions around the circuit. At the lower pressure and longer mean free path the electron would be expected to make more turns around the circuit, and hence gain more speed. The spectra and the measurements of temperature show the speeds are less at the lower pressure. Evidently the electronic temperature reaches its maximum toward the end of the half-cycle. A longer half-cycle would give more time for the build-up of the energy, and doubtless a lower frequency could be found for which the pressure temperature relation would be reversed and hence behave normally.

It is desirable for later analysis to know besides the temperature θ, the number N of electrons per cc.

N was measured by using a cylindrical probe as a collector of electrons when charged to various positive potentials with respect to the hot cathode.[5] The very large random currents and high electronic temperatures made it impossible to use a continuously applied voltage in the probe circuit without quickly melting the tungsten collector. A rotating interrupter was used to energize the probe circuit only momentarily. The instantaneous probe currents were measured by using a cathode-ray oscillograph. The applied voltage in the probe circuit was supplied by a battery. The circuit had negligible inductance. The voltage between the electrodes was deducible from the current and resistance of the circuit when the battery voltage was known. The

TABLE I. *Electronic temperature.*

E.M.F.	TRAP 0°, $p=0.000185$ MM θ°K	TRAP 7.6°, $p=0.000395$ MM θ°K
3	93,000	115,000
3.5	141,000	180,000
4	145,000	236,000
4.5	160,000	279,000
4.6	159,000	323,000

[5] H. M. Mott-Smith, Gen. Elec. Rev. **27**, 617 (1924).

observed current was divided by the area of the probe. A plot was made of the squares of these values as ordinate, and the voltage as abscissa. A straight line over a large portion of the curve was obtained with slope S. The number of electrons per cc is $N=3.32\times10^{11}\sqrt{S}$. The method does not require a knowledge of the electronic temperature. Results are shown in Table II.

The number of electrons at the maximum seems to vary only slightly with the applied e.m.f., but for a given e.m.f. varies directly as the pressure of the vapor. It shows that 13 percent of the atoms are ionized at the maximum.

Measurements of N at the zero of voltage in a number of cases show that the number is about 11 percent of the maximum. The behavior of λ5461 and other lines of Hg I at the minimum of illumination gives a qualitative check to the minimal N. The current wave form exhibiting the start of current practically at the zero of voltage is also a qualitative check. Later we shall deal more at length with the rate of build-up of ionization from the observed minimum.

At this point we can employ the observed maximum N together with the electronic temperature to calculate the rate at which a normal atom of mercury vapor is subjected to an ionizing collision.

We take a Maxwellian velocity distribution among the electrons and an observational curve of probability of the number of ionizing collisions

TABLE II. *Number of electrons per cc (N) and the number of* Hg *atoms per cc (N_a).*

PEAK VOLTS	PEAK AMP.	$N\times10^{-11}$	$N_a\times10^{-12}$	N/N_a
7.8	445	7.3	5.7	0.13
6.7	302	4.3	4.0	0.11
7.5	303	4.4	3.7	0.12
6.7	212	3.6	2.6	0.14

one electron of given energy makes in traveling one centimeter in mercury vapor of one-mm pressure under standard conditions. This probability P_i is taken from a curve by Nottingham.[6]

Let $N_v dv$ = number of electrons in velocity interval v to $v+dv$.

The number of ionizing collisions experienced per second by one mercury atom in a field of N electrons of temperature θ we write as[7]

$$Nf(\theta)=\int_0^\infty \frac{P_i v N_v}{3.53\times10^{16}}dv$$

or

$$f(\theta)=\int_0^\infty \frac{P_i}{3.53\times10^{16}}\times4\pi\left(\frac{m}{2\pi kT}\right)^{\frac{3}{2}}V^3\mathcal{E}^{-mv^2/2kT}dv.$$

Changing variable to volts and writing $T=\theta$ we have

$$f(\theta)=\frac{0.00236}{\theta^{\frac{3}{2}}}\int_0^\infty P_i E\mathcal{E}^{-11,600E/\theta}dE.$$

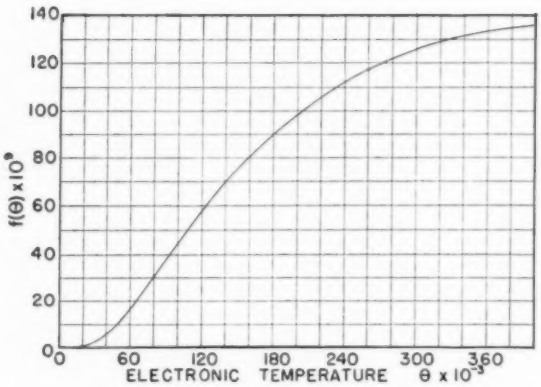

FIG. 4. Values of $f(\theta)$. The number of ionizing collisions per sec. in a field of N electrons is $Nf(\theta)$.

Graphical integration was carried out for values of θ between zero and 400,000°K. The resulting values for $f(\theta)$ are shown by the curve of Fig. 4, and some values below $\theta=20{,}000°$ are shown in Table III. $Nf(\theta)$ gives the number of ionizing collisions (resulting in removal of at least one electron) experienced per second by a normal mercury atom immersed in an electronic gas having N electrons per cm and a temperature θ°K.

For a temperature of 260,000° $f(\theta)=118\times10^{-9}$.

Let $N=6\times10^{11}$; $Nf(\theta)=7\times10^{4}$.

The values of N and θ are approximately those of an actual case.

A normal mercury atom should be ionized 7×10^4 times per second. In mercury vapor at 500°C the average velocity of an atom is 2.85×10^4 cm/sec. Hence the atom could move on the average about 0.41 cm between ionizing colli-

[6] W. B. Nottingham, Phys. Rev. **55**, 203 (1939).

[7] Values of essential constants are taken from E. H. Kennard, *Kinetic Theory of Gases* (McGraw-Hill Book Company, Inc., New York, 1938).

sions. Obviously, if this be true, practically all the atoms should be ionized since the life in the normal state is so limited; unless perchance under the conditions prevailing there is a probability of recombination of the same order of magnitude as the probability of ionization. Recombination in a plasma of mercury vapor in the region of low pressure here employed is considered to be negligible.

Our observations show only 13 percent of the atoms are ionized at the maximum. The expected value is practically 100 percent, if we admit the values of θ and N as observed. If recombination is assumed, two difficulties immediately arise. First, regions of strong continuous spectrum would be expected near the series limits. No appreciable continuum can be found on numerous spectrum plates taken with a quartz spectrometer. Second, the necessary power for producing ions at the calculated rate is greater than the power being put into the discharge. Let W be the least possible power expended per cc in the ionizing process under consideration. We have $W=V_i eN_a Nf(\theta)$; V_i = ionizing potential; N_a = number of atoms of Hg/cc = $8N$ approx; N and $f(\theta)$ are the same as above; $W=0.56$ watts/cc approx.

The active volume of gas is approximately 15,000 cc. Hence it would seem to require at least 8.4 kw to supply the power for ion production at the calculated rate. The observed power input at the peak was approximately 4 kw.

Let us leave this for a time and consider other points of view, namely the current expected and the rate at which the field of ions is created.

At any given point of a cycle, we should expect the current and voltage to follow a formula due to Langevin.

$$I=aEN\lambda_e/\sqrt{\theta}=\text{current amp./sq. cm},$$

E = volts per cm; N = number of electrons per cc; λ_e = electronic free path; a = constant whose value is approximately 3.43×10^{-10}.

This formula is for steady current flow, but the frequency used in the present work is so low that such a formula would be expected to apply.

Using our case of Fig. 2(A) and assuming the peak current density to average about 2.2 amperes per sq. cm and θ to be approximately 300,000°K, we find λ_e to be 45 cm. The expected λ_e in the absence of ions would be about 100 cm and in the actual case, in which account of the ions is taken, the expected value is reasonably near 45 or somewhat lower. The agreement is as good as the data can be expected to yield.

The spectral and other observations clearly indicate that θ increases to relatively enormous values toward the end of a half-cycle, while N rises only to a value resulting from the ionization of less than 13 percent of the mercury atoms.

Let us write $dN/dt=\alpha NN_a-Nl$. α is a factor somewhat larger than $f(\theta)$, since some atoms are multiply ionized and also various factors besides single encounters are at work. l is a loss factor including losses at the walls and recombination. N_a = number of mercury atoms per cc.

The relation indicates that lower values of N_a should lead to a lower rate of creation of ions as observed.

However, the magnitudes involved merit careful consideration insofar as the data permit. When the power expended in ionization was calculated above, we used 10.4 electron volts lost per ion. If we assume the ions to be lost at the walls, the energy per ion should be approximately 160 electron volts, since the walls were observed to be approximately 150 volts negative with respect to the gas. The net result is that ions lost at the walls are apparently less numerous by a factor of twenty or more than they could be if the calculated rate of ionization prevails. If the factor Nl above is only a loss at the walls, then we can neglect it in comparison to αNN_a. If Nl is neglected, then dN/dt turns out to be many times the slow rate of build-up apparently prevailing. The slow rate of creation of the ionic field indicated by the observations calls for a loss factor that is apparently of the order of magnitude of twenty times the losses at the walls.

TABLE III.

θ°K	$f(\theta)$	θ°K	$f(\theta)$
5,000	1.24×10^{-18}	15,000	2.51×10^{-11}
10,000	3.86×10^{-13}	20,000	1.96×10^{-10}

Again we arrive at the same dilemma; too few ions actually created in comparison to the expected value. We cannot conclude that we expect too much unless we simply say that the observed values of one or more of the factors N, θ and N_a

are in error. We have spectroscopic evidence indicating clearly that θ is high, and the electrical measurements of θ were relatively simple. The observed currents and the values expected from the Langevin relation were in sufficient agreement to add confidence to our measurement of N. The stroboscopic spectral observations show that the number of un-ionized mercury atoms at all points of the cycle must be greatly in excess of the ionized atoms. There seems to be no reason to believe there could be a scarcity of un-ionized atoms.

The dilemma is quickly resolved if we postulate recombination of ion and electron in the volume of the discharge tube, and that later, either spontaneously or due to the near approach of another electron, the atom gives up an electron and part or all of the energy of recombination. We will not outline the details of the influence of such phenomena on the electrical characteristics, but will merely point out that recombination varying as N^2 and ionic production varying as N lead to an expected limitation upon N. Also the postulate leads to an immediate visualization of a means of interchange of energy among electrons.

A somewhat similar postulate was advanced by Holst[8] to account for certain phenomena in the low voltage arc, but the hypothesis was shown by Druyvestyn[9] to be apparently inadequate and unnecessary. It must be remarked, however, that the cross section for collision giving rise to the induced emission if taken somewhat larger would have removed the conclusion of inadequacy. Mohler[10] has in fact adduced evidence of a relatively large cross section for a type of collision in caesium vapor involving two electrons and an ion that approximates to the encounters postulated above. In Druyvestyn's communication the electronic exchange of energy was in large part that caused by direct collisions of electrons. There has been a need for additional means of interchange of energy to explain some results of Langmuir, Dittmer[11] and others. The postulate we have made was not to explain the interchange of energy but was demanded from a rate of ionization, the energy exchange being a consequence.

The present postulate of recombination followed by spontaneous or induced ionization accounts for many of our observed phenomena, and fits readily into the postulate of Holst[8] to explain the low voltage arcs.

Obviously, the hypothesis, if tenable, is of fundamental atomic consequence, and evidence for and against it will require more consideration than the writer is prepared to adduce at this time.

The observations show the desirability of extending the factors in the plasma by working with frequencies below 890 cycles; and they reveal a challenge from the curious reversible clean-up.

This work was done in the laboratories of Harvard University. The author wishes especially to express gratitude for aid and encouragement from Professor T. Lyman and other members of the Physics Department of Harvard.

[8] G. Holst and E. Oosterhuis, Physica **4**, 42 (1924).
[9] M. J. Druyvesteyn, Zeits. f. Physik **64**, 782 (1930).
[10] F. L. Mohler, Bur. Stand. J. Research **10**, 771 (1933).
[11] I. Langmuir, Phys. Rev. **26**, 585 (1925); A. F. Dittmer, Phys. Rev. **28**, 507 (1926).

The Magnetostriction, Young's Modulus and Damping of 68 Permalloy as Dependent on Magnetization and Heat Treatment

H. J. Williams, R. M. Bozorth and H. Christensen
Bell Telephone Laboratories, New York, New York

(Received April 4, 1941)

This paper describes measurements of the changes in certain physical properties of 68 Permalloy that result from different thermal and mechanical treatments and considers them in relation to the domain theory. The magnetostriction varied with heat treatment from 2.5×10^{-6} to 22×10^{-6}. The change in Young's modulus with magnetization to saturation varied from 0.09 to 10.5 percent. The damping of mechanical vibrations was also measured as dependent on magnetization and heat treatment. Young's modulus and the damping constant were determined by measuring the natural frequency of vibration and the width of the resonance curve of a hollow rectangle magnetized parallel to its sides so that the magnetic circuit was complete without air gaps or end effects.

THE magnetostriction, Young's modulus and vibrational energy loss have been determined as a function of the magnetization for specimens of 68 Permalloy each of which had been given one of five different mechanical or heat treatments.

The alloy studied was chosen because it has a very small magnetic anisotropy constant[1] and is especially sensitive to heat treatment. The results were expected to help in elucidating the domain structure of ferromagnetic materials. On the basis of a theory[2] of the heat treatment in magnetic fields, proposed previously, it was predicted that the magnetostriction at saturation after heat treatment in a longitudinal field would be zero and after treatment in a transverse field would be $\frac{3}{2}$ times the value obtained after the usual treatments. As pointed out to us by Mr. J. S. Marsh, the change in Young's modulus caused by magnetizing to saturation should, according to this theory, be very small after heat treating in a longitudinal field, as compared to the changes in the material heat treated in other ways. In a qualitative way the measurements of magnetostriction conform well to the predictions—the magnetostriction of the specimen heat treated in a longitudinal field is only a few percent of the normal value for intensities of magnetization below 90 percent of saturation, and at saturation rises to approximately 12 percent of the normal value. A similar statement may be made for the variations of Young's modulus with magnetization. For each property the theory is quantitatively inadequate.

The magnetostriction was determined by measuring the change in length of the rectangular specimen, using a mirror attached to a roller pressed against the specimen. An increase in amplification is attained by inclining the axis of the specimen to the direction in which the roller is constrained to move. The change in Young's modulus with magnetization was determined by measuring the change in frequency of mechanical vibration in the fundamental longitudinal mode, and the logarithmic decrement by measuring the width of the resonance curve. The methods are described below in more detail.

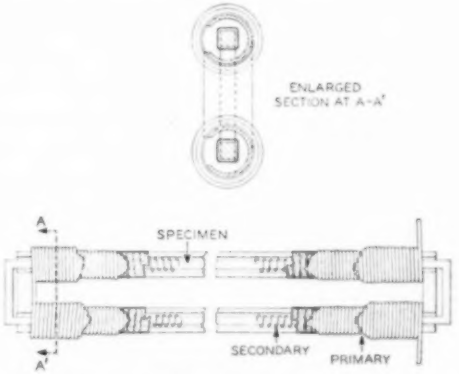

FIG. 1. Specimen, with windings, used for measuring magnetostriction and magnetization for various applied field strengths. The over-all length of the specimen is 30.4 cm, its width 2.54 cm, and its cross section 0.318 cm square.

[1] E. M. Grabbe and L. W. McKeehan, Phys. Rev. **55**, 1142 (1939); E. M. Grabbe, Phys. Rev. **57**, 728 (1940); H. J. Williams and R. M. Bozorth, Phys. Rev. **55**, 673 (1939).

[2] R. M. Bozorth and J. F. Dillinger, Physics **6**, 285 (1935); see also reference 11, p. 217.

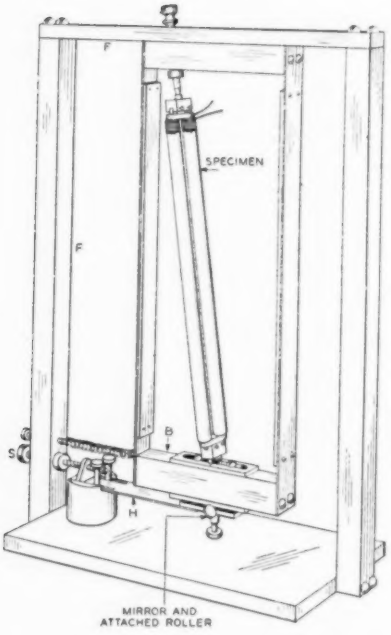

FIG. 2. Apparatus for measuring magnetostriction. *F* is a solid framework, *B* (supported by flexible strips) the bar upon which the specimen rests, *H* a flexible strip held against roller by spring, *S* an adjusting screw. Expansion of specimen moves *B* to right, turns roller and mirror and deflects beam.

SPECIMENS AND TREATMENT

In previous measurements of Young's modulus as affected by magnetization, closed magnetic circuits have not been used and it has been necessary to correct for the demagnetizing influence of the ends of the specimen and to tolerate non-uniformity of magnetization even in the strongest fields. This difficulty has been overcome in the present investigation by cutting the specimen in the form of a hollow rectangle to form a closed magnetic circuit, as shown in Fig. 1. Magnetizing windings were wound around the long sides of the specimens but were supported by tubes to prevent the winding from touching the specimen. A negligible error is attributable to the four corners where the flux executes a rather sharp bend.

The alloy was made from iron and nickel of high commercial purity, melted in a high frequency induction furnace and cast as a $\frac{3}{4}$-inch plate. This was rolled cold to $\frac{1}{8}$-inch and the specimens cut with a length of 12 inches, a width of 1 inch and cross section of $\frac{1}{8}$ inch square. In addition to a nickel content of 68 percent, 0.3 percent manganese was added to make the alloy form easily. The mechanical and heat treatments were as follows: (a) Hard rolled, 83 percent reduction in thickness. Unannealed. (b) Annealed at 1000°C in hydrogen for one hour, cooled slowly (about 5°C/minute through 500°C). (c) Treatment (b), then heated to 600°C and cooled rapidly in air (about 1000°C/minute through 500°C). (d) Treatment (b) then heated to 600°C in hydrogen and subjected to a magnetic field of 10 oersteds which was maintained during slow cooling. The applied field was *longitudinal*, that is, its direction was parallel to the direction of the field applied later for measurement. (e) The same as (d) except that the field was *transverse*. This was applied by passing a current of 30 amperes through the specimen from end to end. The field strength was thus about 15 oersteds at the surface and zero at the middle of the cross section.

METHODS

Magnetostriction

The change in length was measured with the aid of the well-known combination of a roller and mirror. As shown in Fig. 2, the specimen is held about 8° from the vertical with its upper

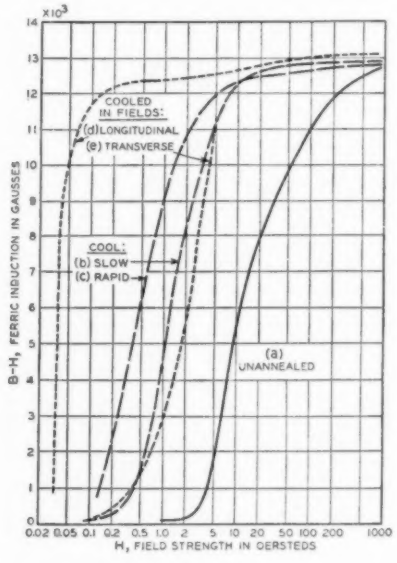

FIG. 3. Magnetization curves of specimens treated in ways indicated. Initial permeabilities are 54 for (a), 5700 for (c) and 3300 for (e); measurements were not made for the other specimens but data on similar materials indicate that they are 3000 to 3500.

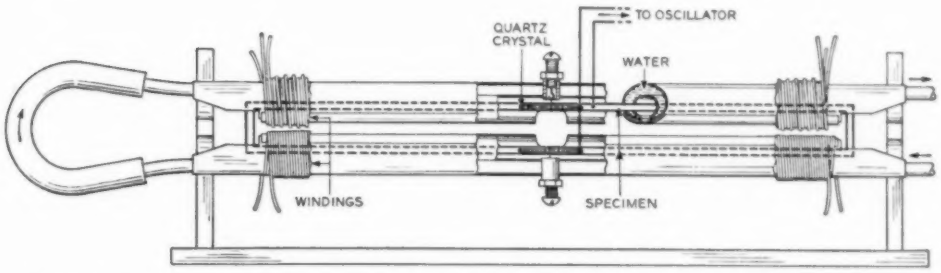

FIG. 4. Apparatus for measuring Young's modulus. Specimen is held by threads at middle and vibrated by quartz crystals. Magnetization is controlled by current in winding. Constant temperature is maintained by water cooling.

point fixed with respect to a heavy frame F. Suspended from this frame are two vertical bars with flexible strips at each end, and these support a heavy horizontal bar B upon which the lower end of the specimen rests. The roller, 1 mm in diameter, is held between two plates, one of which is fastened to the bar B, and the other of which is fastened to the frame F, by a horizontal flexible strip H. The plates were milled lengthwise and lapped, and a strip down the middle was cut to a greater depth so that the roller made contact only along the edges of the plates. The roller and plates were of hardened steel and were held in contact by a spring not shown. Another spring exerted a slight pull on the bar B, so that the specimen would remain in

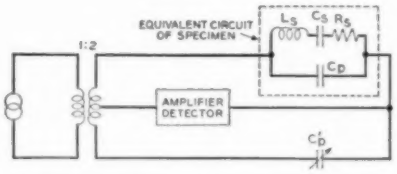

FIG. 5. Electrical measuring circuit for vibrating specimen and measuring its relative amplitude. The oscillator is at the left. C_p is the capacity of the quartz electrodes; C_p' the capacity for balancing C_p; L_s, R_s, and C_s the effective inductance, resistance and capacity of the specimen.

contact at the proper points; tests showed that varying the tension made no difference in the results. The contacts at the two ends of the specimen were steel cones fitting into conical holes having a considerably larger angle. The magnetizing coil was wound on a frame fitting loosely around the specimen so that the expansion of the latter was not restricted.

Because of the fact that the length of the specimen made a large angle with the direction of the displacement of the bar, a change in the length of the specimen caused a seven times larger displacement of the bar B than it would if the specimen were parallel to the displacement. However, the fact that the bar was constrained to move in a definite path by its supports did not permit the magnification by this factor of any errors due to irregularities in the dimension of the roller. A beam of light was reflected from the mirror onto a scale 2 meters distant. A scale reading of 1 mm corresponded to a fractional change in length of 1.47×10^{-7}. The mirror could be rotated into the desired position by means of the screw S. Readings were obtained by first demagnetizing the specimen and then applying a certain magnetizing force. Measurements of magnetization were made simultaneously by means of a fluxmeter. Because of the large thermal lag it was possible to obtain the deflection due to magnetostriction before the heat generated in the windings caused the specimen to expand on account of its change in temperature. Magnetization curves of all specimens are shown in Fig. 3.

Young's modulus

The change in Young's modulus with magnetization was determined from measurements of the natural period of longitudinal vibration before and after magnetization. As shown in Fig. 4, the specimen was held by two stretched threads, one above and one below the specimen, and was excited in the longitudinal mode by impressing an alternating voltage on four quartz crystal plates, each $25\times3\times0.5$ mm, placed on opposite sides of the two long arms of the specimen, at the middle. The quartz crystals were cut in the usual way in the $(11\bar{2}0)$ plane

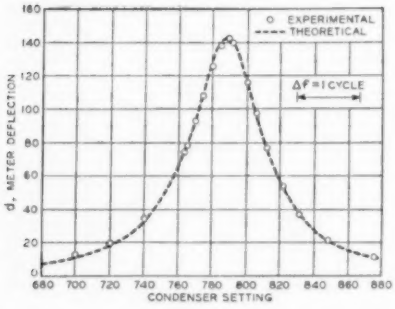

FIG. 6. A typical resonance curve. The unit of the condenser setting is 0.60×10^{-6} microfarad. The calculated curve is adjusted for maximum height and for width at half-maximum. The ordinate (read as microamperes) is proportional to the square of the amplitude of motion of the specimen. A change in frequency of one cycle corresponds to a change in condenser setting of 37 units.

with the mechanical axis $[1\bar{1}00]$ parallel to the long dimension and were covered on their largest surfaces by aluminum deposited from the vapor. They were cemented to the specimen with a thin layer of sealing wax. As shown in Fig. 5, leads from the aluminum-covered surfaces connected the crystals in parallel to the rest of the circuit. This method of excitation and measurement were suggested to us by Mr. R. F. Wick of these laboratories. Magnetizing windings were wound around water-cooled supports which surrounded the specimen and were maintained at a constant temperature.

The oscillator, able to cover the range from 20 to 100,000 cycles per second, was connected to a transformer with primary and secondary impedances in the ratio 1 : 2. A tap in the middle of the secondary was connected to an amplifier having a gain of 90 decibels, the output of the amplifier to a rectifier and this to a microammeter, the readings of which were proportional to the mean square voltage at the amplifier input. The electrical effect of the quartz plates and specimen are simulated by capacity, inductance and resistance as shown. The capacity was balanced by adjusting the condenser in the other arm of the bridge when the frequency was far from the resonant frequency and the output of the amplifier-detector was measured as the frequency was changed in small steps in a range including the resonance.

Changes in frequency were determined accurately in terms of the setting of a carefully calibrated variable air condenser of total capacity 0.0015 microfarad, placed in parallel with the main condenser of the oscillator. The smallest division on this condenser corresponded to a change in frequency of one part in 3,000,000 at 7000 cycles per second. The over-all error in measuring fractional changes in frequency is estimated as less than one part in 1000.

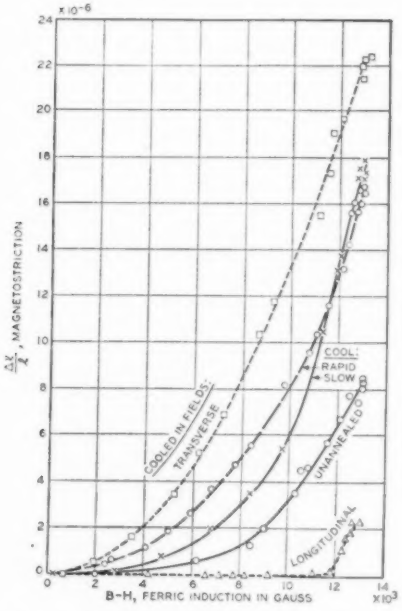

FIG. 7. Magnetostriction as a function of magnetization for specimens treated as indicated.

The frequency of resonance f permits calculation of Young's modulus E by means of the relation

$$f=(n/2l)(E/\rho)^{\frac{1}{2}} \qquad (1)$$

appropriate for longitudinal modes with a node at the middle. Here l is the effective length of the specimen, ρ is the density and n an odd integer. Because of the added weight on the end of the specimen the effective length l was not the measured length l_0. The ratio of these lengths was determined by comparing the resonant frequency of the hollow rectangular specimen with that of a single straight square rod cut from one side of the same specimen, and found to be

$$l/l_0=1.048. \qquad (2)$$

The frequencies were determined accurately in the manner described by Stansel.[3]

[3] F. R. Stansel, Bell Lab. Record **19**, 98 (Nov. 1940).

The effect of the quartz crystals on the stiffness of the composite bar was investigated by driving the unannealed specimen first in the usual way described above, and then, after removing the crystals, by driving magnetically in the manner described by Wegel and Walther[4] using the specimen itself as one of the magnetic elements. The difference in the frequencies obtained by the two methods was less than 0.05 percent, and led to the conclusion that the modulus measured was, in fact, that of the magnetic specimen and that no appreciable error was caused by the presence of the quartz.

Damping

The decrement δ was derived from the width of the resonance curve at half-maximum. The deflection d of the meter at the output of the amplifier, is proportional to the square of the amplitude of vibration of the specimen, and the frequency f of the oscillator is inversely proportional to the square root of the capacity C in its tuning circuit. Thus we have the following relation between δ and Δf, the full width of the d *vs.* f curve at its half-maximum value, $d_0/2$:

$$\delta=\pi(\Delta f/f_0)=(\pi/2)(\Delta C/C_0).$$

Here f_0 and C_0 are the frequency and capacity for resonance, ΔC is the change in capacity between the two points at which d is $d_0/2$, and Δf is the change in frequency corresponding to ΔC. A typical resonance curve is shown in Fig. 6. The points are observed, the curve is that calculated from the relation

$$C-C_0=(C_0/\pi)[(d_0-d)/d]^{\frac{1}{2}}\delta$$

in which δ is adjusted for best agreement.

Measurements of δ were all made with the specimens vibrating with approximately the same amplitude at resonance. This was accomplished by adjusting the output of the oscillator until the value of d at resonance was about 200 microamperes. The amplitude of the bar was measured by Bragg's method[5] when an unusually high voltage was applied to the crystals, and extrapolation to the low power used in the experiments indicated that under these conditions the amplitude was about 10^{-9} cm/cm.

[4] R. L. Wegel and H. Walther, Physics **6**, 141 (1935).
[5] W. H. Bragg, J. Sci. Inst. **6**, 196 (1929).

Results and Discussion

Magnetostriction

Figure 7 shows the magnetostriction for the various specimens as dependent on the magnetization. The magnetostriction at saturation is greatest for the specimen heat treated in a transverse field and smallest for the one heat treated in a longitudinal field. The magnetostriction for the latter is negligible up to a flux density of approximately 12,000 gauss and then increases to only 2.3×10^{-6}. According to domain theory, when a specimen is heat treated in a longitudinal field the domains tend to lie in the direction of the applied field and after demagnetization they are either parallel or antiparallel to this direction. When a field is applied in the direction of the original field, magnetization consists of 180° reversals which are not accompanied by any change in length. This corresponds closely to the observations.

A large contraction of the specimen heat treated in a longitudinal field was effected by passing a current of several amperes along the axis. This is also in accordance with the domain theory outlined above.

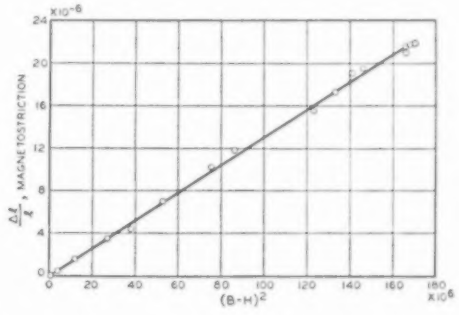

FIG. 8. Magnetostriction of specimen (2) heat treated in a transverse field, plotted against the square of the ferric induction.

In a specimen that has been heat treated in a transverse field the domains lie perpendicular to the direction of the field applied during subsequent measurement. For such an arrangement the expected magnetostriction is thus $\frac{3}{2}$ of that for a random distribution such as may be expected after the usual anneal followed by slow or rapid cooling. This is an effect similar to the unusually large magnetostriction in nickel under

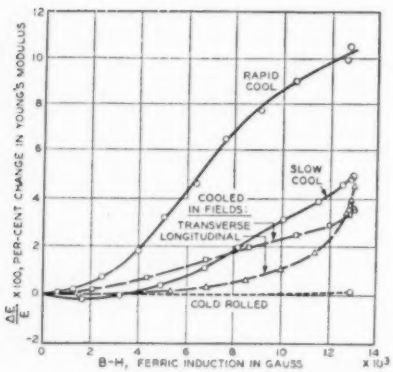

FIG. 9. Percent increase of Young's modulus as dependent on the magnetization for the specimens treated in various ways.

tension, predicted by Becker and Kersten[6] and observed by Kirchner.[7] Lack of perfect agreement with our observations is probably due to nonperfection of alignment, especially of those domains lying near the axis of the bar where the field present during the heat treatment was very small.

The magnetostriction of this specimen is proportional to the square of the magnetization, as shown in Fig. 8. This relation is to be expected if the domains are oriented at right angles to the axis before magnetization and parallel afterwards. If θ is the angle between the axis of the specimen and the direction of magnetization in a domain, the change in magnetization due to the reorientation by the field is proportional to $\cos\theta$ while the change in length is proportional to $\cos^2\theta$; thus the change in length is proportional to the square of the change in magnetization.

The difference in the lengths of a specimen in the demagnetized state and at remanence was found to be only 5 to 10 percent of the change in length that occurred when magnetized originally to saturation. This is commonly observed in magnetic materials generally and is to be expected because the difference in the lengths in the two states (demagnetized and at remanence) is accomplished by 180° reversals of domains which contribute nothing to the length.

The magnetostriction at saturation of the unannealed specimen is considerably less than that of the annealed specimens cooled slowly (b) or rapidly (c). Similar observations on iron have been made by Brown,[8] while Schulze[9] has observed a greater magnetostriction in unannealed than in annealed nickel. These may be due to non-uniform distributions of the orientations of domains resulting, perhaps, from a preponderance of axial strains, but sufficient experiments have not been reported to give a definite conclusion.

Previous to this work, Kaya[10] measured the magnetostriction of various iron-nickel alloys as a function of the magnetization for specimens which had been cooled in a magnetic field, cooled rapidly, cooled slowly, and aged. For the 70 Permalloy, the magnetostriction at saturation was 2.7×10^{-6} for the specimen cooled in the magnetic field, and 11×10^{-6} for the other three specimens. The former value is in good agreement with our result; the latter value is considerably less than our result and also less than that given in Marsh's compilation.[11]

Young's modulus

The variations of Young's modulus with magnetization are given in Fig. 9 for all of the specimens except the hard-worked one, the data for which are shown on a different scale in Fig. 10. The increase in Young's modulus for saturation is slightly over 10 percent for the rapidly cooled specimen and is only 0.088 percent for the cold-rolled specimen. This is in qualitative accord with the theory that this increase in Young's

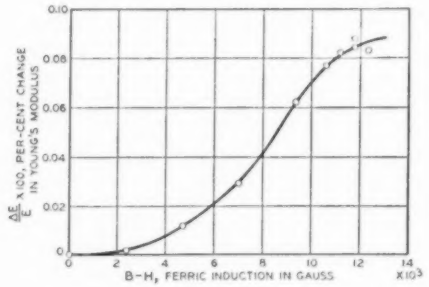

FIG. 10. Percent change of Young's modulus of the unannealed specimen.

[6] R. Becker and M. Kersten, Zeits. f. Physik **64**, 660 (1930).
[7] H. Kirchner, Ann. d. Physik **27**, 49 (1936).
[8] W. F. Brown, Jr., Phys. Rev. **50**, 1165 (1936).
[9] A. Schulze, Ann. d. Physik **11**, 937 (1931).
[10] S. Kaya, J. Faculty Sci., Hokkaido Imp. Univ. **2**, 29 (1938).
[11] J. S. Marsh, *Alloys of Iron and Nickel: I, Special-Purpose Alloys* (McGraw-Hill Book Company, Inc., New York, 1938).

modulus should vary inversely as the internal strain, the latter being measured by the initial permeability. In the case of the rapidly cooled specimen the domains are not "frozen in"—the internal strains are small—and therefore a stress will rotate them easily and Young's modulus for the demagnetized state will be considerably below that for saturation.

The internal strains for the cold-rolled specimen are large and any applied stress has comparatively little effect on rotating the domains. The theory of Kersten[12] may be applied in a quantitative way to this specimen. It gives a relation between the value of $\Delta E/E_0$ attained at saturation, $\Delta E_s/E_0$, and the magnetostriction at saturation, λ_s, the initial permeability, μ_0, and the saturation magnetization, I_s:

$$\Delta E_s/E_0=(9/20\pi)\lambda_s^2\mu_0E_0/I_s^2.$$

According to our observations, $\lambda_s=9\times10^{-6}$, $\mu_0=54$, $E_0=1.82\times10^{12}$, $4\pi I_s=13{,}100$ and the calculated value of $\Delta E_s/E_0$ is, therefore, 0.10 percent, a value to be compared with the experimental value, about 0.088 percent. Although in our measurements the magnetization has been carried closer to saturation, and still maintained uniform, than in previous measurements on any hard-worked material, a fact made possible by the closed magnetic path, there is still some uncertainty in $\Delta E_s/E_0$ because heating of the specimen by the high magnetizing current is likely to occur and change the modulus. With this reservation in mind, it may be stated that the agreement between theory and experiment is good.

TABLE I. *Values of Young's modulus of specimens in the demagnetized (E_0) and saturated (E_s) conditions, after various treatments. Units are dyne-cm^{-2}.*

TREATMENT	$E_0\times10^{-12}$	$E_s\times10^{-12}$	$\Delta E_s/E_0$
(a) Unannealed	1.8145	1.8161	0.00088
(b) Cooled slowly	1.783	1.870	0.049
(c) Cooled rapidly	1.654	1.826	0.104
(d) Cooled in longitudinal field	1.843	1.930	0.047
(e) Cooled in a transverse field	2.105	2.181	0.036

[12] M. Kersten, Zeits. f. Physik **85**, 708 (1933); Zeits. f. Metallkunde **27**, 97 (1935). See also N. Akulov and E. Kondorsky, Zeits. f. Physik **78**, 801 (1932); **85**, 661 (1935); and reference 15, p. 339.

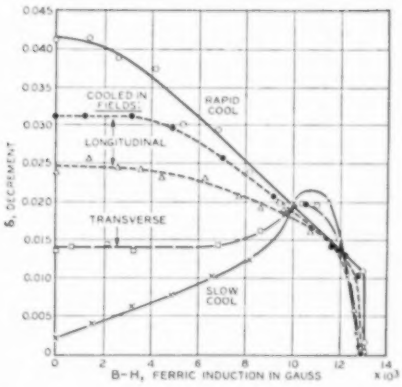

FIG. 11. The decrement as dependent on the magnetization for the heat treated specimens. The decrement of the unannealed specimen at $B=0$ is 0.00053.

The absolute values of Young's modulus for the specimens in the demagnetized state E_0 are given in the second column of Table I. Since the lengths of the specimens were all the same the moduli were proportional to the squares of the natural frequencies of vibration, and the constant of proportionality was determined from Eq. (1). The fractional changes when magnetized to saturation, $\Delta E_s/E_0$, are given in the third column, and the modulus at saturation, $E_s=E_0+\Delta E_s$, in the last column. It will be noted that E_s does not have the same value after the various treatments, as it would be expected to have according to the domain theory. The reason for this requires investigation. A considerable difference in the values of E_s for the unannealed and the annealed states has also been observed by Cooke[13] who found that in iron the modulus of saturated unannealed iron (1.86×10^{12}) was less even than that of demagnetized annealed iron (1.99×10^{12}). On the other hand a decrease in the modulus on annealing has been observed for nickel.[14]

Our values of E_0 and $\Delta E_s/E_0$ for the slowly cooled alloy are close to those observed by Nakamura[15] for a slowly cooled alloy containing 70 percent nickel. His values were 1.90×10^{12} and 3.6 percent, respectively.

Little can be said regarding the way in which $\Delta E/E_0$ changes with magnetization since our

[13] W. T. Cooke, Phys. Rev. **50**, 1158 (1936).
[14] E. Giebe and E. Blechschmidt, Ann. d. Physik **11**, 905 (1931).
[15] K. Nakamura, Sci. Rep. Tohoku Imp. Univ. **24**, 303 (1935).

measurements of reversible permeability and reversible change of magnetization with tension were not complete enough to deduce from the observed quantities the values of $\Delta E/E_0$ corresponding to zero eddy-current shielding.

Decrement

Figure 11 shows the logarithmic decrement δ as a function of the magnetization for the various specimens. Two different specimens were similarly treated in a longitudinal magnetic field and measured to see how well results could be duplicated. As shown by the two curves the decrements differed by about 20 percent at inductions well below saturation, the general shape of the curve remaining the same. As pointed out by Becker[16] there are three kinds of magnetomechanical losses in energy that occur when magnetic materials are subjected to mechanical vibrations: macro-eddy-current losses, micro-eddy-current losses, and magnetomechanical hysteresis. When the net magnetization over the specimen is zero there will be no macro-eddy-current loss; thus the initial points on our experimental curves refer to the combined losses of micro-eddy-currents and magnetomechanical hysteresis. Some preliminary experiments of ours in which δ was measured as a function of frequency, indicate that at the frequency ($f=7300$) used for the experiments of Fig. 10, about two-thirds of the losses in the slowly cooled specimen (treatment (b)) are due to micro-eddy-currents, and that the domain size calculated from these losses by Becker's method are approximately 10^{-8} cm^3, a size lying just in the middle of the range of sizes determined for a variety of materials by previous measurements[17] of the Barkhausen effect.

The courses of the δ *vs.* $B-H$ curves may be compared with those previously observed for iron and nickel. For annealed iron[13] measured at $f=56{,}000$ the curve rises to a high maximum at about three-fourths of saturation and then falls to a low value at saturation; this course corresponds roughly to our curve for the slowly cooled specimen. For annealed nickel,[18] on the other hand, the value of δ decreases continually as $(B-H)$ increases; this corresponds to our rapidly cooled specimen. What factors determine the shapes of the δ *vs.* $B-H$ curves is not now understood, but we expect that such an understanding will be helped by the separation of the losses into their components.

A calculation of macro-eddy-current losses in the rapidly cooled specimen (c) shows that at high intensities of magnetization these losses comprise the major portion of the total losses observed. The unusually high decrement of this specimen at $B=0$ is what would be expected from its high initial permeability of 5700, assuming the loss to be due mainly to micro-eddy-currents. The low decrement, 0.00053, of the unannealed specimen (a) in the unmagnetized condition may similarly be attributed to its low initial permeability, 54. The intermediate values of the decrements of the other specimens at $B=0$ are to be expected, but in view of the lack of the proper data necessary for a separation of micro-eddy-current and magnetomechanical hysteresis losses the different values of the decrement cannot be attributed with any assurance to differences in domain size or magnetomechanical hysteresis constant. As mentioned above we have already made some experiments to obtain the data necessary for a separation of these losses into their components.

We wish to express our indebtedness to Messrs. R. L. Wegel and R. F. Wick of these laboratories for the benefit of discussions concerning the methods of measurements of Young's modulus and damping, and to Professor W. F. Brown, Jr., of Princeton University for a discussion of eddy-current shielding in bars of square cross section.

[16] R. Becker and W. Döring, *Ferromagnetismus* (J. Springer, Berlin, 1939), p. 357.
[17] R. M. Bozorth and J. F. Dillinger, Phys. Rev. **35**, 733 (1930).
[18] S. Siegel and S. L. Quimby, Phys. Rev. **50**, 1165 (1936) and reference 14.

Theory of Liquid He II

HSIEN-YÜ HSÜ, *Department of Mathematics, Yenching University, Peiping, China*

AND

WILLIAM BAND, *Department of Physics, Yenching University, Peiping, China*

(Received February 11, 1941)

It is assumed that atoms in the surface of a liquid can be in energy states appropriate to a two-dimensional monolayer, determined wave-mechanically from the area and shape of the surface. It is then proved that in Bose-Einstein statistics there exists a tendency for atoms to pass over into such states in preference to the three-dimensional states normally occupied, when the temperature reduces to the Einstein λ-point given by T_0 where

$$nh^3(2\pi mkT_0)^{-3/2}=2.612,$$

n being the number of atoms per unit volume. It is supposed that if a single monolayer has almost completely passed over into the two-dimensional states, then a new surface at once presents itself, accessible to the formation of another monolayer. In this case the change-over from three-dimensional states to two-dimensional states can pass almost to completion, so that at temperatures sufficiently below T_0, nearly the entire liquid is arranged in concentric shells which contain atoms in mutually independent sets of two-dimensional energy states. Essentially, it is an order-disorder transformation. Two parameters appear in the analysis: the proportion of the space actually occupied at any stage of the transition by monolayers which is also accessible to atoms in the three-dimensional states, and the relative numerical density per cm² of atoms in a monolayer. By reasonable choices of these parameters a good fit is obtained with the shape of the experimental specific heat curve plotted against (T/T_0), although the theory still predicts too high a value for T_0, namely 3.09°K. The theory explains the thermomechanical or "fountain" effect, and suggests a reasonable interpretation of the surface transfer phenomena.

INTRODUCTION

THE, for the most part, unexplained properties of liquid helium have been well reviewed by H. Jones;[1] they will not be described here. Fröhlich[2] pointed out that the transformation from He II to He I at the λ-point is very similar to an order-disorder transformation, but there seems to have been no precise suggestion as to how such a transformation could occur in a liquid. On the other hand London[3] pointed out that the Einstein critical point in Bose-Einstein statistics falls very close to the observed λ-point in the case of helium. However Fowler and Jones[4] proved that no discontinuity, such as that actually observed in the value of the specific heat, can possibly occur at the Einstein point for a simple Bose-Einstein system; the theoretical discontinuity is only in the temperature gradient of the specific heat.

From the experimental data, however, it is quite clear that He II is not a simple one-phase system; there is always a mobile film—presumably built up from monolayers—in equilibrium with the main body of the liquid. Atoms of the liquid may have energy states given by the usual expression

$$\epsilon_l=h^2(s^2+t^2+u^2)/8mV^{\frac{2}{3}},\quad s,t,u=1,2,\cdots,\quad (1)$$

where V is the volume of the liquid. Atoms in the monolayers, assumed plane of area A, will have states given instead by

$$\epsilon_m=h^2(s^2+t^2)/8mA,\quad s,t=1,2\cdots.\quad (2)$$

The correct statistical argument should include a discussion of the equilibrium between these two competing sets of states; and this was not done in the work of Fowler and Jones.[4]

In specific heat measurements it is not usual to provide the special surface required for the formation of mobile films. Nevertheless, the container itself (and the free surface of the liquid if in equilibrium with its vapor) constitutes a surface area accessible to monolayer states. It is shown below that at the Einstein critical temperature there exists a tendency for atoms to pass over into the monolayer states in preference to the three-dimensional states normally occupied. It is supposed that when the surface atoms

[1] H. Jones, *Reports on Progress in Physics* **6**, 280–296 (1939).
[2] H. Fröhlich, Physica **4**, 639 (1937).
[3] F. London, Proc. Roy. Soc. **A153**, 576 (1936).
[4] R. H. Fowler and H. Jones, Proc. Camb. Phil. Soc. **34**, 573–576 (1938).

have almost completely passed over into the two-dimensional states, the monolayer so formed at once presents a new surface accessible to the formation of another monolayer, and so on. In this way the change-over from the three-dimensional states (1) to the two-dimensional states (2) could ideally pass to completion, so that at temperatures sufficiently below T_0 nearly the entire liquid would be arranged in concentric shells with mutually independent sets of two-dimensional states.

If the region occupied by the multi-layer of atoms in two-dimensional states were completely inaccessible to atoms in the three-dimensional states, then we should be faced with a true isothermal phase change, with a latent heat at the critical temperature: In other words, the specific heat curve would have an infinity at T_0 while remaining normal elsewhere. But in practice the space occupied by the multi-layer cannot be so completely shut off; it must be possible for atoms in the three-dimensional states to penetrate them to some extent. In this case we shall have a gradual change-over with an anomalous specific heat beginning with a finite discontinuity at T_0.

Essentially the phenomena are due to an order-disorder transformation; the multi-layer condition is relatively ordered, each monolayer being practically an independent unit with relatively simple structure. But while previous order-disorder transformations have been due to inter-atomic forces and depended essentially on the presence of a definite lattice structure, here the interatomic forces play no part whatever, and indeed the entire absence of a definite lattice structure seems to be a necessary condition for the existence of the ordered multi-layer condition, whose energy states are in resonance with the surface of the container.

General Theory

Consider N structureless mass particles divided between two phases, the one contained in a box of volume V, the other confined to a plane surface of area A. The stationary states of a particle in the box will be given by[5]

$$\epsilon_l = h^2(s^2+t^2+u^2)/8mV^{\frac{2}{3}}, \quad s, t, u = 1, 2, \cdots, \quad (1)$$

while those of a particle in the surface will be

$$\epsilon_m = h^2(s^2+t^2)/8mA, \quad s, t = 1, 2, \cdots. \quad (2)$$

The numbers in the two phases can be found in the same way as in the problem of a single separate phase:[5]

$$N_l = \sum_{s,t,u} \sum_{j=1}^{\infty} \lambda^j \exp(-jh^2(s^2+t^2+u^2)/8mkTV^{\frac{2}{3}}), \quad (3)$$

where λ is the statistical parameter determined by (8) below and

$$N_m = \sum_{s,t} \sum_{j=1}^{\infty} \lambda^j \exp(-jh^2(s^2+t^2)/8mkTA). \quad (4)$$

In the treatment given by Fowler and Jones[4] of the first of these sums, the series is evaluated by means of a θ function transformation applied to a finite set of the terms, and the remainder series is shown to vanish when $N_l \to \infty$, as long as $\lambda < 1$. The result is

$$N_l = (2\pi mkT)^{\frac{3}{2}} Vh^{-3} \sum_{j=1}^{\infty} \lambda^j/j^{\frac{3}{2}}. \quad (5)$$

When $T < T_0$ defined by

$$(N_l/V)h^3(2\pi mkT_0)^{-\frac{3}{2}} = 1 \quad (6)$$

then $\lambda \to 1$ and the remainder terms, neglected from (5), have to be taken into consideration. The corresponding result for the two-dimensional states is easily shown to be

$$N_m = 2\pi mkTAh^{-2} \sum_{j=1}^{\infty} \lambda^j/j, \quad (7)$$

the analysis being an obvious adaptation of that given by Fowler and Jones.[4]

When both sets of states are possible, the total number of atoms N is shared between them, and the equation determining λ is then

$$N = N_l + N_m. \quad (8)$$

But with this relation, when $T < T_0$, it is the N_m term which becomes significant instead of the remainder terms neglected from (5). In fact λ never becomes near enough to unity to vitiate the approximations in (5) and (7).

The above expressions do not take into account the fact that, at least with arrangements used in specific heat measurements, the two sets of states are competing for atoms in one and the same enclosure. To do this, let σ be the fraction

[5] R. H. Fowler, *Statistical Mechanics* (University Press, Cambridge and Macmillan Company, New York, 1936), second edition, 2.5, 2.7.

of the volume occupied by the multi-layer of two-dimensional states which is excluded from the volume accessible to the atoms in three-dimensional states. Then if V stands for the total volume of the container, and we write

$$\phi_0 \equiv (2\pi mk)^{\frac{1}{2}} V h^{-3}, \tag{9}$$

the correct form in place of (5) will be

$$N_l = \phi_0 T^{\frac{3}{2}} \Big(\sum_{j=1}^{\infty} \lambda^j / j^{\frac{3}{2}}\Big)[1-\sigma(N-N_l)/N]. \tag{10}$$

Here $(N-N_l)V/N$ is the volume occupied by the multi-layer states assuming no appreciable change in bulk density. Writing

$$\alpha = \sum_{j=1}^{\infty} 1/j^{\frac{3}{2}}$$

so that

$$T_0^{\frac{3}{2}} = N/\alpha\phi_0 \tag{11}$$

and solving (10) for N_l: one obtains

$$\left.\begin{aligned} &N_l = N\left(\frac{T}{T_0}\right)^{\frac{3}{2}}\left[\frac{\sum\lambda^j/j^{\frac{3}{2}}}{\alpha}\right]\Psi, \\ &\text{where} \\ &\Psi = \left[1+\left(\frac{\sigma}{1-\sigma}\right)\left\{1-\left(\frac{T}{T_0}\right)^{\frac{3}{2}}\left[\frac{\sum\lambda^j/j^{\frac{3}{2}}}{\alpha}\right]\right\}\right]^{-1}. \end{aligned}\right\} \tag{12}$$

Comparison of (12) and (10) shows that evidently Ψ is the correction factor on the volume accessible to the three-dimensional states, expressed as a function of T.

Again the area accessible to the two-dimensional states is increased by the presence of each monolayer. If the number of atoms per monolayer is N_1, write

$$\mu = N^{\frac{1}{2}}/N_1 \tag{13}$$

and Eq. (7) should be replaced by

$$N_m = \phi_m T\Big(\sum_{j=1}^{\infty} \lambda^j/j\Big)[1+\mu N_m/N^{\frac{1}{2}}], \tag{14}$$

where

$$\phi_m = 2\pi mkAh^{-2}. \tag{15}$$

Here $\mu N_m/N^{\frac{1}{2}}$ is the number of monolayers, and this multiplied by A is the added area, since each monolayer provides a new area. This formula neglects the fact that the area of inner monolayers will be less than A in a manner depending on the shape of the container. Putting

$$\phi_m = \gamma(\phi_0)^{\frac{1}{2}} \quad \text{where} \quad \gamma = A(\alpha V)^{-\frac{1}{2}}, \tag{16}$$

and solving (14) for N_m, one obtains

$$\left.\begin{aligned} &N_m = \gamma N^{\frac{1}{2}}\left(\frac{T}{T_0}\right)\log\left(\frac{1}{1-\lambda}\right)\Theta, \\ &\text{where} \\ &\Theta = \left[1-\mu\gamma\left(\frac{T}{T_0}\right)\log\left(\frac{1}{1-\lambda}\right)\right]^{-1}. \end{aligned}\right\} \tag{17}$$

Comparison of (17) and (14) again shows that Θ is the correction factor for the accessible area, expressed as a function of T.

The equation determining λ now becomes

$$1 = \left(\frac{T}{T_0}\right)^{\frac{3}{2}}\left[\frac{\sum\lambda^j/j^{\frac{3}{2}}}{\alpha}\right]\Psi + \gamma N^{-1/3}\left(\frac{T}{T_0}\right)\log\left(\frac{1}{1-\lambda}\right)\Theta. \tag{18}$$

So long as $T > T_0$, the value of λ is very accurately given by

$$\sum_{j=1}^{\infty} \lambda^j/j^{\frac{3}{2}} = \alpha(T/T_0)^{-\frac{1}{2}}. \tag{19}$$

This makes $\Psi = 1$, and the coefficient of Θ in (18) remains practically zero due to the factor $N^{-\frac{1}{3}}$, which in practice is around 10^{-8}. But as soon as $T \leqslant T_0$, λ must approach unity near enough to make the Θ term appreciable; this is because neither Ψ nor $[(\sum\lambda^j/j^{\frac{3}{2}})/\alpha]$ can ever be greater than unity. From (17) Θ can become very large—about 10^7 is required—only by making

$$\log\left(\frac{1}{1-\lambda}\right) \doteqdot T_0/T\mu. \tag{20}$$

This gives, from (17)

$$N_m = N^{\frac{1}{2}}\Theta/\mu. \tag{21}$$

Equation (20) must remain true for all T less than T_0, and may thus be differentiated to give, for this range,

$$Td\lambda/dT \doteqdot -T_0(1-\lambda)/T\mu\gamma. \tag{22}$$

Because in practice $\mu \sim 0.1$, Eq. (20) also requires $1-\lambda \ll 1$ for $T < T_0$, so that (18) may, for

this range, be written approximately as

$$1=\left(\frac{T}{T_0}\right)^{\frac{1}{2}}\Psi+\gamma N^{-\frac{1}{2}}\left(\frac{T}{T_0}\right)\log\left(\frac{1}{1-\lambda}\right)\Theta. \quad (23)$$

Also

$$\Psi=\left[1+\left(\frac{\sigma}{1-\sigma}\right)\left\{1-\left(\frac{T}{T_0}\right)^{\frac{3}{2}}\right\}\right]^{-1}, \quad (24)$$

and hence

$$\Psi+\frac{2}{5}T\frac{d\Psi}{dT}=\Psi\left[1+\frac{3}{5}\Psi\left(\frac{T}{T_0}\right)^{\frac{3}{2}}\left(\frac{\sigma}{1-\sigma}\right)\right]. \quad (25)$$

These results will be needed in the next section.

Differentiation of (23) gives

$$0=1+\left(\frac{T}{T_0}\right)^{\frac{1}{2}}\left(T\frac{d\Psi}{dT}\right)+\frac{1}{2}\left(\frac{T}{T_0}\right)^{\frac{1}{2}}\Psi+\frac{1}{\mu}N^{-\frac{1}{2}}\left[T\frac{d\Theta}{dT}-\Theta\right]. \quad (26)$$

Using (24) and (25) this leads to

$$\Theta-T\frac{d\Theta}{dT}=\mu N^{\frac{1}{2}}\left[1+\frac{1}{2}\Psi\left(\frac{T}{T_0}\right)^{\frac{3}{2}}\left\{1+3\Psi\left(\frac{\sigma}{1-\sigma}\right)\right\}\right]. \quad (27)$$

On the other hand (18) and (20) lead to

$$\Theta=\mu N^{\frac{1}{2}}\left\{1-\left(\frac{T}{T_0}\right)^{\frac{3}{2}}\Psi\right\}, \quad (28)$$

so that

$$\Theta+\frac{1}{2}T\frac{d\Theta}{dT}=\mu N^{\frac{1}{2}}\left[1-\Psi\left(\frac{T}{T_0}\right)^{\frac{3}{2}}\left\{\frac{7}{4}+\frac{3}{4}\Psi\left(\frac{\sigma}{1-\sigma}\right)\right\}\right], \quad (29)$$

and, near T_0, using (27), (28) and $(\sigma/1-\sigma)\gg 1$:

$$T\frac{d\Theta}{dT}=-\mu N^{\frac{1}{2}}\left(\frac{T}{T_0}\right)^{\frac{3}{2}}\frac{3}{2}\Psi^2\left(\frac{\sigma}{1-\sigma}\right). \quad (30)$$

Equations (29) and (30) will also be needed later.

The Specific Heat

The mean energy per atom in either set of states is given by the known formulae. Thus for the three-dimensional states we have[5] the total energy for a volume V

$$E_l=kT^2\frac{\partial}{\partial T}\left[\sum_{s,t,u}\sum_{j=1}^{\infty}\frac{1}{j}\lambda^j \times\exp(-jh^2(s^2+t^2+u^2)/8mV^{\frac{2}{3}}kT)\right].$$

This series can be summed, leading to

$$E_l=\tfrac{3}{2}kT(2\pi mkT)^{\frac{3}{2}}(V/h^3)\sum_{j=1}^{\infty}\lambda^j/j^{5/2}. \quad (31)$$

Comparison with (5) gives the mean energy per atom

$$E_l/N_l=\tfrac{3}{2}kT(\sum\lambda^j/j^{5/2})/(\sum\lambda^j/j^{3/2}). \quad (32)$$

Similarly, the energy for the two-dimensional states in an area A is

$$E_m=kT^2\frac{\partial}{\partial T}\left[\sum_{s,t}\sum_{j=1}^{\infty}\frac{1}{j}\lambda^j \times\exp(-jh^2(s^2+t^2)/8mkTA)\right], \quad (33)$$

which can again be summed by similar methods, giving

$$E_m=kT(2\pi mkT)(A/h^2)\sum_{j=1}^{\infty}\lambda^j/j^{\frac{3}{2}}. \quad (34)$$

Comparing this with (7) gives the mean energy per atom as

$$E_m/N_m=kT(\sum\lambda^j/j^{\frac{3}{2}})/(\sum\lambda^j/j). \quad (35)$$

The volume and area corrections involved in (12) and (17) evidently do not affect the mean energy per atom in either case, so the total energy of the system is now given by (12) and (17) with (32) and (35) as

$$E=\frac{3}{2}NkT\left(\frac{T}{T_0}\right)^{\frac{3}{2}}\left[\frac{\sum\lambda^j/j^{5/2}}{\alpha}\right]\Psi+\gamma kN^{\frac{1}{2}}T\left(\frac{T}{T_0}\right)(\sum\lambda^j/j^{\frac{3}{2}})\Theta. \quad (36)$$

Above $T>T_0$, the Θ or N_m term can be neglected, and the specific heat is the same as that given by Fowler and Jones[4] for this range,

approaching, at $T=T_0$, the value

$$C_v=(15/4)(\beta/\alpha)Nk=1.92Nk. \tag{37}$$

Below $T\leqslant T_0$ we use (25) and (29), and in (36) write $\lambda\doteqdot 1$, so that, say,

$$\sum_{j=1}^{\infty}\lambda^j/j^{\frac{3}{2}}\doteqdot\sum_{j=1}^{\infty}1/j^{\frac{3}{2}}=\beta. \tag{38}$$

Thus

$$C_v=dE/dT=\frac{15\beta}{4\alpha}Nk(T/T_0)^{\frac{3}{2}}\left[\Psi+\frac{2}{5}T\frac{d\Psi}{dT}\right]+2N^{\frac{2}{3}}k(T/T_0)\alpha\gamma\left[\Theta+\frac{1}{2}T\frac{d\Theta}{dT}\right] \tag{39}$$

$$=\frac{15\beta}{4\alpha}Nk(T/T_0)^{\frac{3}{2}}\Psi\left[1+\frac{3}{5}\Psi\left(\frac{\sigma}{1-\sigma}\right)\left(\frac{T}{T_0}\right)^{\frac{3}{2}}\right]$$

$$+2\alpha\mu\gamma Nk(T/T_0)\left[1-\Psi\left(\frac{T}{T_0}\right)^{\frac{3}{2}}\left\{\frac{7}{4}+\frac{3}{4}\Psi\left(\frac{\sigma}{1-\sigma}\right)\right\}\right]. \tag{40}$$

Evidently the specific heat curve depends on the two parameters σ, and $\mu\gamma$. To see the physical significance of the latter, refer to (13) and (16), which give

$$\mu\gamma=\eta\alpha^{-\frac{3}{2}} \quad \text{where} \quad \eta=(N/V)^{\frac{2}{3}}/(N_1/A). \tag{41}$$

Thus η is the ratio between what may be regarded as the ordinary density per cm² in the liquid—say the density in the surface of He I—and the density per cm² in a single monolayer of He II. Putting the numerical values of α and β in (40), this equation can be written in the form

$$C_v/1.92Nk=1.45\eta(T/T_0)$$

$$+\Psi\left\{1-2.52\eta\frac{T}{T_0}\right\}\left(\frac{T}{T_0}\right)^{\frac{3}{2}}$$

$$+\Psi^2\left\{1-1.8\eta\left(\frac{T}{T_0}\right)^{-\frac{3}{2}}\right\}\left(\frac{T}{T_0}\right)^3\frac{3}{5}\left(\frac{\sigma}{1-\sigma}\right). \tag{42}$$

The best fit with the experimental points was found with $(1.8)\eta=1/11$, $\sigma=11/12$, see curve (A) in Fig. 1. This curve is not steep enough between $(T/T_0)=0.99$ and 1.00, and too steep between 0.99 and 0.95. Some improvement in this respect is shown by curve (B), where $(1.8)\eta=\frac{1}{4}$, $\sigma=25/26$, but this curve has too large a discontinuity at T_0. This trouble could be eliminated by taking σ and η as functions of T. Physically such a procedure would mean that the first few monolayers were practically impenetrable to atoms in the three-dimensional states, with $\sigma/(1-\sigma)$ very large indeed and $(1.8)\eta$ almost unity to maintain the discontinuity at T_0 at the desired value. Inner monolayers, however, would have to be more penetrable, to let $\sigma/(1-\sigma)$ reduce when $T<0.99T_0$, so flattening out the curve.

But in any case the values of η seem unfortunately small, requiring too large a density in the monolayers, and the theory still requires too large a value of T_0, namely 3.09°K. The above procedure for improving the shape of the curve would, therefore, probably be forcing the model too far. Perhaps the correct way to improve it would be to include structure in the mass particles, so that internal energy states would appear in the expressions (1) to (4). In general, the above agreement is as good as can be expected with the simple model used.

Thermomechanical and Transfer Phenomena

Consider two box enclosures connected only by capillaries, whose total area is large enough to compare with the surface of the two boxes. Suppose the temperature of both is just below T_0, so that the change-over from three-dimensional states to two-dimensional states has just set in, only a relatively few monolayers having been formed. Formulae (12), (14) and (17) still apply, with A interpreted as the larger (fixed) area, with a correspondingly larger value of γ. From (21) one derives

$$\frac{d}{dT}\left(\frac{N_m}{A}\right)=\frac{N_m}{A}\frac{1}{\Theta}\frac{d\Theta}{dT}, \tag{43}$$

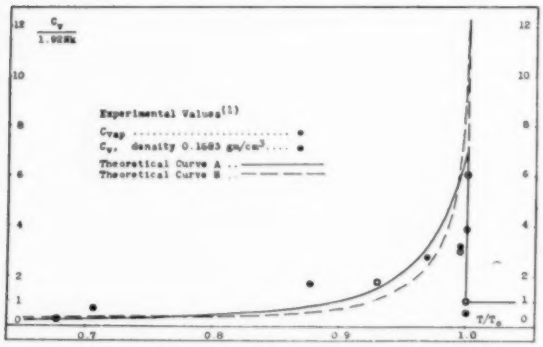

FIG. 1. Specific heat of He II near the λ point.

which by (30) near T_0 becomes, with $\Psi \doteqdot 1$,

$$T\frac{d}{dT}\log\left(\frac{N_m}{A}\right) = -\frac{3}{2}\left(\frac{T}{T_0}\right)^{\frac{1}{2}}\left(\frac{\sigma}{1-\sigma}\right)\left[1-\left(\frac{T}{T_0}\right)^{\frac{1}{2}}\right]^{-1}. \quad (44)$$

The infinity at T_0 is, of course, due to the approximations made in deducing (28): but it is nevertheless true that the density N_m/A is enormously sensitive to minute temperature changes slightly below T_0.

If one of the box enclosures is now maintained at a very slightly lower temperature than the other, both slightly lower than T_0: $T_A < T_B < T_0$, then the film close to "A" will tend to be enormously more densely populated than that close to "B"; a rapid diffusion must then be expected in the film from A to B, as actually observed in the "fountain" effect.[1]

Mean energies per atom in the two sets of states are approximately given by (32) and (35) using (20):

$$E_l/N_l = \tfrac{3}{2}kT\beta/\alpha; \quad E_m/N_m = kT\left(\frac{T}{T_0}\right)\alpha\mu\gamma. \quad (45)$$

Their ratio depends only on the product $\mu\gamma$, which, as seen above, depends only on the relative density of the individual monolayers. Thus, using (41)

$$(E_m/N_m) \div (E_l/N_l) = \tfrac{2}{3}\eta\alpha^{4/3}T/\beta T_0. \quad (46)$$

Taking $\eta = 1/20$, consistently with the values used above, this gives roughly

$$(E_m/N_m) \div (E_l/N_l) \doteqdot 0.04. \quad (47)$$

The total difference in heat content per gram for atoms in the two conditions works out as about 0.6 calorie, which is of the same order as the specific heat of He I, and thus sufficient to account for the observed thermal effects of flow through capillaries.[1]

The surface transfer through capillaries under slight level differences[1] in the connected containers appears to be impossible to explain in great detail without a full discussion by means of perturbation theory of mobile films. However this much seems worth noting: The monolayers must exert a tremendous linear pressure tending to cause occupation of all accessible areas; equal in fact to $N_m kT/A$ which, with $N_m \sim 10^{20}$, is of the order 10^6 dynes per cm! Since accessible area is increased by subdivision of volumes, this tendency will qualitatively account for the observed spreading phenomena. From this point of view the small level differences between the connected enclosures are merely incidental, the true cause of the transport being the very much larger intrinsic linear pressure of the film.

On the Theory of the Thermal Diffusion Coefficient for Isotopes. II

R. CLARK JONES*
Research Laboratory of Physics, Harvard University, Cambridge, Massachusetts
(Received March 11, 1941)

The temperature dependence of the thermal diffusion constant α of a mixture of isotopes is determined for the 9,5 Lennard-Jones model of intermolecular forces by the use of the Chapman-Enskog theory of transport phenomena in gases. The treatments of the Sutherland model and the special Lennard-Jones model given in the first paper of this series were subject to the drastic restriction that the depth ϵ of the potential energy minimum must be small compared with kT. The present treatment of the 9,5 model is valid to all orders of ϵ/kT; this advantage is gained, however, at the expense of substituting laborious numerical methods for the analytical methods that were used in the previous paper. The results indicate that the thermal diffusion constant first increases slightly as the temperature decreases, and then decreases rapidly, passing through zero and becoming negative at a temperature about 1.5 times the critical temperature. The constant becomes strongly negative as the temperature decreases still further, and then approaches zero as the absolute temperature approaches zero. When the theoretical results are modified to account for the fact that the neon molecule is much harder than is indicated by a repulsive force index of 9, a quantitative agreement is obtained with Nier's experimental data on mixtures of the neon isotopes. Fair agreement is obtained with the data of Atkins, Bastick, and Ibbs on mixtures of the noble gases. An approximate method is presented which permits one to obtain from the results for the inverse power model, the first two terms of the series development of α in powers of ϵ/kT for the general Lennard-Jones model of intermolecular forces.

THE present paper is a continuation of the previous one of the same title,[1] and is devoted primarily to a treatment of the Lennard-Jones 9,5 model which is not restricted by the requirement that the attractive force be weak. Although this model of intermolecular forces is more specialized than any of those treated in I, it has turned out to be of much greater interest because the results are free of the restriction just mentioned.

In order to avoid too extensive reference to I, the general formulae will be given briefly in Section I.

I. INTRODUCTION

The equation of diffusion, with the effect of thermal diffusion included, may be written in the form

$$c_1(\mathbf{v}_1-\mathbf{v})=c_1c_2(\mathbf{v}_1-\mathbf{v}_2)=c_2(\mathbf{v}-\mathbf{v}_2)$$
$$=D_{12}(-\text{grad}c_1+\alpha c_1c_2\,\text{grad}\log T) \quad (1)$$

for a mixture of two gases. In Eq. (1), c_1 is the fractional particle density of the first gas, and c_2 is the fractional particle density of the second gas; $\mathbf{v}_1$ and $\mathbf{v}_2$ are the convection velocities of the molecules of the first and second gases, respectively, and $\mathbf{v}$ is defined as

$$\mathbf{v}=c_1\mathbf{v}_1+c_2\mathbf{v}_2; \quad (2)$$

D_{12} is the coefficient of diffusion; and α is the thermal diffusion constant.

It is to be noted that since $\mathbf{v}$ is obtained by averaging with respect to the *number* of the molecules of each kind, the total mass flux is not given by $\rho\mathbf{v}$, where ρ is the density, but is rather given by $\rho\mathbf{v}_m$, where $\mathbf{v}_m$ is defined by

$$\mathbf{v}_m=\frac{c_1m_1\mathbf{v}_1+c_2m_2\mathbf{v}_2}{c_1m_1+c_2m_2}, \quad (3)$$

where m_1 and m_2 are the masses of the molecules of the first and second gas. A confusion between $\mathbf{v}$ and $\mathbf{v}_m$ led to the publication of an incorrect formula in a previous paper.[2]

From here on, we restrict our discussion to the case in which the two gases represent different isotopes of what is chemically the same gas. In this case it is a close approximation to replace D_{12} by D, the coefficient of self-diffusion of either gas.

The rigorous Chapman-Enskog theory of transport phenomena in gases yields the value of the

* National Scholar, Harvard University.
[1] R. Clark Jones, Phys. Rev. **58**, 111 (1940). This paper will be referred to as I.
[2] W. H. Furry, R. Clark Jones and L. Onsager, Phys. Rev. **55**, 1083 (1939). Equation (10) of this paper is correct only if ρ is regarded as the density the gas would have if all of the molecules were of species 1.

thermal diffusion constant in terms of certain cross section integrals which refer to collisions between molecules of the first and second gas. Let the impact parameter of such a collision be indicated by b, and the relative velocity at infinity by g. Now let us reduce b and g to dimensionless form by means of the transformation:

$$g=(2kT/m)^{\frac{1}{2}}\gamma,$$
$$b=s\sigma(\gamma)\beta, \tag{4}$$

where $m=m_1m_2/(m_1+m_2)$ is the reduced mass, s is an arbitrary constant length, and $\sigma(\gamma)$ is an arbitrary function of γ and therefore of g. Finally, let $\theta(\beta,\gamma)$ be the angle of deflection suffered by either molecule when it is deflected by the field of force of another, as measured in the center-of-gravity coordinate system.

We may now define the quantities

$$\Theta^{(l)}(\gamma)=\int_0^\infty\{1-P_l(\cos\theta)\}\beta d\beta \tag{5}$$

and in turn the quantities

$$\Omega^{(l,k)}=\int_0^\infty\exp(-\gamma^2)\sigma^2(\gamma)\gamma^k\Theta^{(l)}(\gamma)d\gamma. \tag{6}$$

The Ω's are dimensionless collision cross sections suitably averaged over β and γ.

In first approximation, the Chapman-Enskog theory yields the following general formula:

$$R_T=\frac{177}{7}\cdot\frac{(2\Omega^{(1,7)}-5\Omega^{(1,5)})(15\Omega^{(1,5)}+2\Omega^{(2,7)})}{\Omega^{(2,7)}(165\Omega^{(1,5)}-60\Omega^{(1,7)}+12\Omega^{(1,9)}+16\Omega^{(2,7)})}, \tag{7}$$

where R_T is the ratio of α to the value predicted by the theory for molecules which behave as hard smooth elastic spheres:

$$R_T=\alpha/\alpha_{\text{hard spheres}}, \tag{8}$$

$$\alpha_{\text{hard spheres}}=\frac{105}{118}\frac{m_2-m_1}{m_2+m_1}. \tag{9}$$

Equation (7) cannot be given in any more explicit form without specifying the nature of the intermolecular forces.

The material presented thus far is given in much greater detail in the first three pages of I.

It seems worth while to indicate the general formulae for the first approximations to the coefficients of viscosity and of diffusion in terms of the Ω's; we have

$$\eta=\frac{15}{32s^2\Omega^{(2,7)}}\left(\frac{mkT}{\pi}\right)^{\frac{1}{2}} \tag{10}$$

and for the coefficient of self-diffusion:

$$D=\frac{3}{16\rho s^2\Omega^{(1,5)}}\left(\frac{mkT}{\pi}\right). \tag{11}$$

In Eqs. (10) and (11), and only in these two equations, m is the mass of the molecules, rather than the reduced mass. The elimination of s^2 between (10) and (11) leads to the useful formula

$$D=\left\{\frac{2}{5}\frac{\Omega^{(2,7)}}{\Omega^{(1,5)}}\right\}\frac{\eta}{\rho}. \tag{12}$$

We may now obtain the result (29,I), which was stated without proof, by substituting (26,I) in (12).

Note added in proof.—As we pointed out in I, Eq. (7) is an approximation in the further sense that the expression on the right is the first term of a power series expansion in the relative mass difference $(m_2-m_1)/(m_2+m_1)$. The equation is approximately correct, however, even when the ratio of the masses m_2/m_1 is large compared with unity. In a recent paper[2a] Chapman has discussed numerically the dependence of R_T on the relative mass difference for the special case of the inverse power model.

His results may be summarized as follows. For the sake of specificity we assume that $m_2\geqslant m_1$. When the concentration of the heavier molecules is small, we find by inspection of Chapman's Table 6 that R_T is essentially independent of the relative mass difference for all values of the force index ν. When the concentration of the heavier molecules is not small, however, we find from Tables 4 and 5 that R_T decreases as the relative mass difference increases from zero to

[2a] S. Chapman, Proc. Roy. Soc. **A177**, 38–62 (1940).

unity, and that the amount of the decrease is greater the greater the value of c_2 and the greater the value of ν. In the most extreme case, when the mass ratio and ν are both infinite, the value of R_T decreases by the factor 2.3 as the concentration of the heavier molecules rises from zero to unity. The corresponding factor is much closer to unity, however, for the isotopic mixtures which one meets in practice. For example, when $m_2=2m_1$ and ν is infinite, the factor is 1.2; and when $\nu=15$ with the same mass ratio, the factor is 1.1.

In the same paper, Chapman points out that the values of $A_1^{(3)}$ and $A_2^{(3)}$ which he had previously given and which were used in I, 0.812 and 1.825, are incorrect. He states that the correct values are 0.796 and 1.584. As a consequence of this change, the first line of Table I in I should read

0.796	1.584	1.327	1.592	0.807

The next line, which was obtained by interpolation, should be modified, and the first line of Table V should also be changed in an obvious manner. The correction of these errors removes a noticeable discontinuity in the functions $f(\nu)$ and $C(\nu)$.

Ternary and Higher Order Mixtures

Note added in proof.—Further on in this paper it is suggested that measurements of the thermal diffusion constant of xenon are desirable, and this suggestion brings squarely before us the question of mixtures of more than two isotopes. The results presented below have been known to the author for some time on the basis of plausibility arguments, but only recently have they been derived from the rigorous general theory.

The general theory of thermal diffusion in ternary and higher order gas mixtures has been given by Hellund.[2b] In his article Hellund stresses quite properly that thermal diffusion in ternary and higher order mixtures contains essentially new features, and that the results, therefore, cannot be obtained by extrapolation from the theory of binary mixtures. In the special case, however, in which the molecules differ only with respect to their mass, the equations of thermal diffusion in higher order mixtures may be written in terms of the binary thermal diffusion constants.

In order to indicate the nature of the generalization, it is convenient first to rewrite Eq. (1) in the following form:

$$\mathbf{v}_1-\mathbf{v}=D(-\text{grad}\,\log c_1+\alpha_{12}c_2\,\text{grad}\,\log T) \quad \text{(A)}$$

where α_{12} is the value of α defined by Eqs. (7)–(9). We see that the presence of the second gas occurs explicitly only in the combination $\alpha_{12}c_2$. It is plausible to suppose that in a mixture of three isotopes the factor $\alpha_{12}c_2$ would be replaced by $\alpha_{12}c_2+\alpha_{13}c_3$, and similarly for the case of more than three isotopes. This suggestion has been confirmed by the general theory of ternary and higher order mixtures.

The following relations have been derived from Hellund's general theory for a mixture whose component gases are all isotopic with respect to one another. Let the number of components be N, and let the fractional particle density of the ith component be c_i, where

$$\Sigma_k c_k=1. \quad \text{(B)}$$

The remaining relations in this section are valid only to terms of the first order in the relative mass differences $(m_i-m_j)/(m_i+m_j)$. We have

$$\alpha_{ij}=-\alpha_{ji}, \quad \alpha_{ii}=0, \quad \text{(C)}$$

$$\alpha_{ij}+\alpha_{jk}=\alpha_{ij}-\alpha_{kj}=\alpha_{ik}. \quad \text{(D)}$$

The equation of diffusion for the ith component is

$$\mathbf{v}_i-\mathbf{v}=D(-\text{grad}\,\log c_i+(\Sigma_k\alpha_{ik}c_k)\,\text{grad}\,\log T) \quad \text{(E)}$$
$$k=1, 2, \cdots, N$$

where

$$\mathbf{v}\equiv\Sigma_k c_k\mathbf{v}_k \quad \text{(F)}$$

is the particle convection velocity of the gas as a whole. The equation for $\mathbf{v}_i$ which has just been given involves all of the c's. From Eqs. (B), (C) and (D), however, we find that the expression for $\mathbf{v}_i-\mathbf{v}_j$ contains only c_i and c_j:

$$\mathbf{v}_i-\mathbf{v}_j=D(-\text{grad}\,\log c_i/c_j+\alpha_{ij}\,\text{grad}\,\log T). \quad \text{(G)}$$

This equation is identical in form with the equation for a mixture of only two isotopes.

In application to the Clusius-Dickel thermal separation column, we find by the use of (E) that the equations for the *equilibrium* concentration

[2b] E. J. Hellund, Phys. Rev. **57**, 328 (1940).

distribution are of the form

$$dc_i/dy = c_i \Sigma_k \alpha_{ik} c_k \qquad \text{(H)}$$

where y is proportional to the coordinate along the column. In analogy with Eq. (G), we find from (H)

$$d \log(c_i/c_j)/dy = \alpha_{ij}. \qquad \text{(I)}$$

The Eqs. (H) or (I) form a set of simultaneous, nonlinear differential equations for which the general solution may be found as follows: Integration of (I) yields $N-1$ independent equations of the form

$$\log(c_i/c_j) = \alpha_{ij}(y - y_{ij}). \qquad \text{(J)}$$

The $N-1$ constants y_{ij} may be determined from the $N-1$ independent conditions that the total mass of each component be conserved.

II. The General Lennard-Jones Model

General formulation

Lennard-Jones has proposed[3] and used extensively[4] in theoretical treatments a law of intermolecular force of the form

$$F = \kappa/r^{\nu} - \kappa'/r^{\nu'}, \qquad (13)$$

where r is the distance between the centers of the molecules, and where κ, κ', ν and ν' are positive constants. A positive value of F corresponds to a repulsive force.

The modern quantum theory of van der Waals forces suggests that ν' should have the value seven; quantum theory further suggests that the first term of (13) should be replaced by a term involving the radius exponentially. For the ranges of radii which are concerned in molecular collisions at ordinary temperatures, however, an exponential term can be approximated closely by a term involving a large inverse power of the radius.

As in I, we use a polar coordinate system r, ϕ, with its plane in the plane of motion of the two molecules whose collision we wish to study, and with its origin at one of the two molecules. In terms of the reciprocal radius $u = 1/r$, the first integral of the equation of motion in a spherically symmetrical field of force may be written

$$\left(\frac{du}{d\phi}\right)^2 = \frac{1}{b^2} - u^2 - \frac{2}{mg^2b^2}\int_r^{\infty} F dr. \qquad (14)$$

We now substitute (13) in (14), and subject b and g to the transformation (4) with

$$s = (\kappa/2kT)^{1/(\nu-1)}, \quad \sigma(\gamma) = \gamma^{-2/(\nu-1)}. \qquad (15)$$

With the further substitution

$$x = bu, \qquad (16)$$

Eq. (14) becomes

$$\left(\frac{dx}{d\phi}\right)^2 = 1 - x^2 - \frac{2}{\nu-1}\left(\frac{x}{\beta}\right)^{\nu-1} + \frac{2p}{\nu'-1}\left(\frac{x}{\beta}\right)^{\nu'-1} \qquad (17)$$

where we have used the abbreviation

$$p = \frac{\kappa'}{\kappa^{(\nu'-1)/(\nu-1)}(2kT\gamma^2)^{(\nu-\nu')/(\nu-1)}}. \qquad (18)$$

The quantity p is important because it is the means by which the temperature dependence is introduced into the final results.

The physical significance of p is more easily grasped when it is expressed in terms of ϵ, the depth of the potential energy minimum expressed as a positive quantity. When $\nu > \nu'$, such a minimum exists for the law of force (13), and is easily shown to have the value

$$\epsilon = \frac{(\nu-\nu')}{(\nu-1)(\nu'-1)} \cdot \frac{\kappa'^{(\nu-1)/(\nu-\nu')}}{\kappa^{(\nu'-1)/(\nu-\nu')}}. \qquad (19)$$

The elimination of the κ's between (18) and (19) leads to the result

$$p = \left[\frac{(\nu-1)(\nu'-1)}{2(\nu-\nu')} \cdot \frac{\epsilon}{kT\gamma^2}\right]^{(\nu-\nu')/(\nu-1)}. \qquad (20)$$

The appearance of the temperature at this stage of the derivation is somewhat fictitious, of course; it appears explicitly because of the substitution (4). According to (4), $kT\gamma^2$ is equal to $\frac{1}{2}mg^2$, so that p is a quantity which is proportional to a power of the ratio of ϵ to the kinetic energy of the molecules at infinity.

[3] J. E. Lennard-Jones, Proc. Roy. Soc. **A106**, 441 (1924).
[4] See, for example, R. H. Fowler and E. A. Guggenheim, *Statistical Thermodynamics* (Cambridge, 1939), Chapters VII and VIII; or R. H. Fowler, *Statistical Mechanics* (Cambridge, 1936), Chapter X.

By exactly the same procedure that was used for the case of the inverse power model in I, we find from (17) for the angle of deflection

$$\theta(\beta,\gamma)=\pi-2\int_0^{x_0}\left\{1-x^2-\frac{2}{\nu-1}\left(\frac{x}{\beta}\right)^{\nu-1}+\frac{2p}{\nu'-1}\left(\frac{x}{\beta}\right)^{\nu'-1}\right\}^{-\frac{1}{2}}dx, \quad (21)$$

where $x_0(\beta, p)$ is the smallest positive root of the equation obtained by setting the right-hand side of (18) equal to zero.

The integration indicated in (21) cannot be performed in terms of known functions for the general case, so that it is usually necessary to resort to numerical methods from here on.

Specialization to the 9,5 case

The Sutherland model ($\nu=\infty$) and the special Lennard-Jones model ($\nu'=3$) represent special cases of the general Lennard-Jones model, and have been worked out as far as terms of the first order in ϵ/kT. Subject to this limitation, the derivation of the value of α for these models was given in I.

For the 9,5 model, Hassé and Cook[5] have proceeded from Eq. (21) by purely numerical methods, and have obtained the values of $\Theta^{(1)}$ and $\Theta^{(2)}$ for 18 different values of p. The authors exhibited admirable foresight in computing the values of both $\Theta^{(1)}$ and $\Theta^{(2)}$, inasmuch as they were interested in the coefficient of viscosity, which involves only $\Theta^{(2)}$.

The work of Hassé and Cook appeared only a year before London[6] showed by a simple calculation that the interaction energy of two molecules without permanent moments would fall off as the inverse sixth power of the distance; it was later shown quite generally by Lennard-Jones[7] that the leading term in the energy of mutual polarization is always of the form $-\mu r^{-6}$, where μ is positive. We may feel quite certain, therefore, that Hassé and Cook would have performed their computations for the 13,7 model if they had done their work slightly later, inasmuch as the trigonometrical substitution which they used to facilitate the numerical evaluation of (21) is equally effective for any pair of values of ν and ν' which satisfy the relation $\nu=2\nu'-1$. The 13,7 model has since found extensive use in the statistical-mechanical treatment of the properties of fluids and solids.[4]

Because a substantial part of the task of computing the Ω's has already been accomplished for the 9,5 model, it seems worth while to determine the temperature dependence of α for this model before proceeding to the working out of the 13,7 model from the beginning. This order of procedure is further justified by the expectation that the results for the 13,7 model will not be greatly different.

For the special case $\nu=9$, $\nu'=5$, Eqs. (15) and (20) reduce to

$$s^2=(\kappa/2kT)^{\frac{1}{2}}, \quad \sigma^2(\gamma)=\gamma^{-\frac{1}{2}} \quad (22)$$

$$p=\frac{2}{\gamma}\left(\frac{\epsilon}{kT}\right)^{\frac{1}{2}}. \quad (23)$$

The relation between the notation used by Hassé and Cook and that used here is given in Table I for the convenience of those who wish to refer to the paper of Hassé and Cook.*

The values of $\Theta^{(1)}$ and $\Theta^{(2)}$ determined by Hassé and Cook are given in Table II. The values of θ were determined to an accuracy of one second of arc, and the writers state that the Θ's

TABLE I. *Comparison of the notation used by Hassé and Cook, and by Jones, I and II.*

H AND C	J	H AND C	J	H AND C	J
θ	χ	λ	κ		
θ	ϕ	μ	κ'	*For the (9,5) model only:*	
$\pi-2\theta$	θ	n	ν	$1/s$	q
V	g	m	ν'	$I_1(k)/2\pi=(2k)^{\frac{1}{2}}Y_1(k)$	$\Theta^{(1)}(\gamma)$
z	γ	a	β	$I_2(k)/2\pi=(2k)^{\frac{1}{2}}Y_2(k)$	$\frac{1}{2}\Theta^{(2)}(\gamma)$
p	b	$\xi=ay$	x	$I(s)$	$\frac{1}{2}\Omega^{(2,7)}$
R	k	at	x_0		
		k	p		

[5] H. R. Hassé and W. R. Cook, Proc. Roy. Soc. **A125**, 196 (1929).

[6] F. London, Zeits. f. physik. Chemie **B11**, 222 (1930).

[7] J. E. Lennard-Jones, Proc. Phys. Soc. London **43**, 461 (1931).

* It may also be helpful to point out the few typographical errors which occur in their paper: 1. The statement on p. 207 that $I(s)$ is the integral with respect to z in (13) should be replaced by the statement that $I(s)$ is $1/2\pi$ times the integral with respect to z in (12); 2. The variable of integration in (12) should be changed from k to z; and 3. The four polynomial approximations on p. 207 which are indicated as expressions for $I_2(k)$ are actually approximations to $I_2(k)/2\pi$.

TABLE II. *The exact values of $\Theta^{(1)}$ and $\Theta^{(2)}$, and the values given by the approximate formulae.*

p	$\Theta^{(1)}$ EXACT	$\Theta^{(1)}$ EQ. (25)	$\Theta^{(1)}$ EQ. (32)	$\Theta^{(1)}/(2p)^{\frac{1}{2}}$ EXACT	$\frac{1}{3}\Theta^{(2)}$ EXACT	$\frac{1}{3}\Theta^{(2)}$ EQ. (26)	$\frac{1}{3}\Theta^{(2)}$ EQ. (33)	$\frac{1}{3}\Theta^{(2)}/(2p)^{\frac{1}{2}}$ EXACT
0.00	0.38080	0.38080			0.16520	0.16520		
0.25	0.35947	0.35947			0.15108	0.15110		
0.50	0.34766	0.34766			0.14435	0.14431		
0.75	0.34972	0.34988			0.14929	0.14931		
1.00	0.37066	0.37066			0.17059	0.17059		
1.25	0.41584	0.41450			0.21165	0.21262		
1.50	0.49001	0.48592			0.27171	0.27988		
1.75	0.59603	0.58944			0.34269	0.37686		
2.00	0.73297	0.72956	0.95377	0.36648	0.40754	0.50802	0.38640	0.20377
2.3835	0.98228		1.06480	0.44990	0.44926		0.42190	0.20577
2.8563	1.23697		1.18818	0.51754	0.44778		0.46189	0.18735
3.4641	1.32953		1.33076	0.50511	0.50824		0.50866	0.19309
4.0	1.44530		1.44530	0.51099	0.54659		0.54658	0.19325
6.0	1.81155		1.81153	0.52295	0.66923		0.66927	0.19319
8.0	2.11888		2.11658	0.52972	0.77264		0.77264	0.19316
10.0	2.38356		2.38357	0.53298	0.86366		0.86368	0.19312
∞	∞		∞	0.55260	∞		∞	0.19257

are accurate to five significant figures. The values of the Ω's are now to be determined by performing the integration with respect to γ which is indicated in Eq. (6). In this integration the dependence on γ is, of course, eliminated, so that the Ω's are functions of the quantity

$$q=p\gamma=2(\epsilon/kT)^{\frac{1}{2}}. \tag{24}$$

The temperature dependence of the Ω's will enter through their dependence on q.

Before proceeding to the numerical evaluation of the Ω's, we shall derive expressions for the Ω's which are valid for the two limiting cases of q small, and q large, compared with unity.

For values of p lying between zero and unity, the following polynomials are very close approximations to the data given in Table II:

$$\Theta^{(1)}=0.38080-0.09834p+0.04004p^2+0.04816p^3, \tag{25}$$

$$\tfrac{1}{3}\Theta^{(2)}=0.16520-0.06507p+0.02268p^2+0.04778p^3. \tag{26}$$

It happens that (25) fits the data in Table II to within two percent for values of p between unity and two, but such is not the case for (26).

For small values of q, we may obtain the Ω's by substituting (25) and (26) in (6). This procedure may at first seem questionable, since the integral involves large values of q as well as the small values for which (25) and (26) are good approximations. The error would be expected to be greatest for small values of γ, which correspond to large values of q. It is easily confirmed, however, that the factor γ^k in the integrand of (6) vanishes so strongly at the origin that the error is inappreciable for sufficiently small values of q, when k takes values as large as 5, 7 or 9. We find

$$\Omega^{(1,5)}=0.30623-0.05571q+0.01840q^2+0.02183q^3, \tag{27}$$

$$\Omega^{(1,7)}=0.84213-0.12535q+0.03220q^2+0.02728q^3, \tag{28}$$

$$\Omega^{(1,9)}=3.15801-0.40738q+0.08855q^2+0.06139q^3, \tag{29}$$

$$\tfrac{1}{3}\Omega^{(2,7)}=0.36534-0.08294q+0.01824q^2+0.02707q^3. \tag{30}$$

If now the expressions (27–30) are regarded, not as polynomial approximations, but as power series expansions of the Ω's about the point $q=0$, they may be substituted in (7), and the result expanded in ascending powers of q. One finds at length

$$\begin{aligned}R_T&=0.43241\{1+0.4026q-0.1392q^2-0.1616q^3+\cdots\}\\&=0.43241\{1+0.8052(\epsilon/kT)^{\frac{1}{2}}-0.5568\epsilon/kT-1.2930(\epsilon/kT)^{\frac{3}{2}}+\cdots\}.\end{aligned} \tag{31}$$

This expression is compared with the precise result in Fig. 1.

Similarly, for values of p greater than four, the following expressions are very close ap-

proximations

$$\Theta^{(1)}=0.78149_5 p^{\frac{1}{2}}-0.03621-0.16295p^{-\frac{1}{2}}, \quad (32)$$

$$\tfrac{1}{3}\Theta^{(2)}=0.27234p^{\frac{1}{2}}+0.00344-0.00309p^{-\frac{1}{2}}. \quad (33)$$

For sufficiently large values of q, the values of the Θ's for which (32) and (33) are not good approximations will not contribute appreciably to the integrals (6). Substituting (32–33) in (6) yields

$$\Omega^{(1,5)}=0.51944q^{\frac{1}{2}}-0.02912-0.16295q^{-\frac{1}{2}}, \quad (34)$$

$$\Omega^{(1,7)}=1.29859q^{\frac{1}{2}}-0.08008-0.48885q^{-\frac{1}{2}}, \quad (35)$$

$$\Omega^{(1,9)}=4.5451q^{\frac{1}{2}}-0.3003-1.9554q^{-\frac{1}{2}}, \quad (36)$$

$$\tfrac{1}{3}\Omega^{(2,7)}=0.45254q^{\frac{1}{2}}+0.00761-0.00927q^{-\frac{1}{2}}. \quad (37)$$

If now we substitute these expressions in (7), and expand the result in descending powers of $p^{\frac{1}{2}}$, we find that the constant term is identically zero, and we are left with

$$\begin{aligned} R_T &= -0.03390q^{-\frac{1}{2}}-0.37935q^{-1}+\cdots \\ &= -0.02397(kT/\epsilon)^{\frac{1}{2}} \\ &\qquad -0.18968(kT/\epsilon)^{\frac{1}{2}}+\cdots. \end{aligned} \quad (38)$$

This expression is also compared with the precise result in Fig. 1.

Numerical results

The values of the Ω's have been obtained by purely numerical methods from the data given in Table II. The values of $\Omega^{(2,7)}$ for $0.25 \leqslant q \leqslant 20$ were determined by Hassé and Cook;[5] the remainder of the entries in Table III were determined by the writer.

The method of integration used by Hassé and Cook was to split the range of the variable p into four parts, and to find accurate polynomial approximations to $\Theta^{(2)}$ for each of these ranges. The integration was then accomplished by use of tables on the incomplete gamma-function.

The writer used a different method, which was essentially ordinary numerical integration. Instead of integrating $\Theta^{(1)}$ itself, however, the integration was actually performed using as the integrand the difference between (25) or (32) and the exact value of $\Theta^{(1)}$ as given in Table II. The numbers obtained were then applied as corrections to the approximate values of the Ω's obtained from (27–29) or from (34–36). This method has the advantage that the quantity obtained by numerical integration was nearly always a small fraction of the final value of the Ω in question.

For values of q equal to or less than four, the correction to (27–29) was determined, whereas for values of q equal to or greater than five, the correction to (34–36) was determined by numerical integration. The interval used in the integration (6) with respect to γ was 0.25; in only one case, that of $q=5$, it was necessary to subdivide the interval of integration over part of the range. It was usually sufficient to carry the numerical integration out to $\gamma=5.0$. All of the calculations were carried to six significant figures although the accuracy of the results did not always warrant such precision.

The one drastic limitation on the accuracy of the results obtained lies in the fact that because of the great labor of the calculations, Hassé and Cook computed only three values of $\Theta^{(1)}$ and $\Theta^{(2)}$ in the range $2<p<4$. Although these values were computed to an accuracy of five significant figures, the function behaves so irregularly in this interval that the interpolated values may be in error by as much as one percent. The irregularity is more apparent in the values of $\Theta/(2p)^{\frac{1}{2}}$, which are also given in Table II. Accordingly, the values of the Ω's for which the main contribution comes from Θ's in this range have a probable error of something less than one percent. The

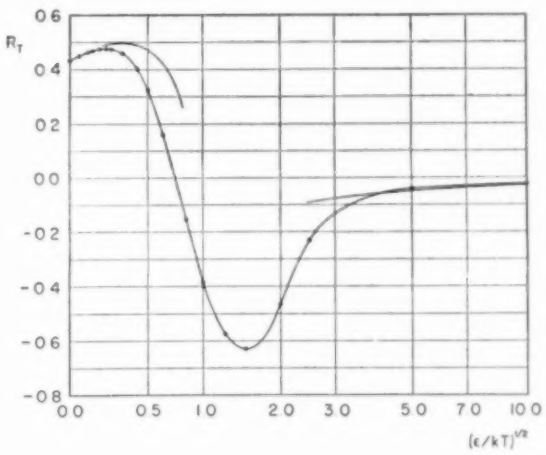

FIG. 1. Showing the dependence of R_T on ϵ/kT for the Lennard-Jones 9,5 model. For approximate purposes, the abscissa may be considered as the square root of T_c/T, where T_c is the critical temperature. The two shorter curves represent the results yielded by the approximate formulae (31) and (38).

TABLE III. *Values of the* Ω*'s.*

$1/q$	$\Omega^{(1,1)}$	$\Omega^{(1,2)}$	$\Omega^{(1,3)}$	$\frac{1}{3}\Omega^{(2,2)}$
∞	0.30623	0.84213	3.1580	0.36534
20.0	0.30349	0.83595	3.1379	0.36124
10.0	0.30086	0.82994	3.1182	0.35726
8.0	0.29960	0.82702	3.1097	0.35531
6.0	0.29756	0.82230	3.0928	0.35215
5.0	0.29600	0.81857	3.0806	0.34970
4.0	0.29379	0.81323	3.0626	0.34617
3.0	0.29051	0.80494	3.0343	0.34072
2.4	0.28779	0.79746	3.0081	0.33590
2.0	0.28570	0.79092	2.9841	0.33181
1.6	0.28390	0.78303	2.9530	0.32722
1.2	0.28484	0.77581	2.9156	0.32445
1.0	0.28982	0.77621	2.9006	0.32735
0.8	0.30485	0.78895	2.9072	0.34138
0.6	0.35051	0.84733	3.0101	0.39214
0.5	0.40624	0.93189	3.1899	0.45523
0.4	0.51020	1.12014	3.6433	0.57470
0.3333	0.63116	1.37246	4.3201	0.70133
0.25	0.86044	1.95803	6.1680	0.90432
0.2	1.03951	2.48879	8.1644	1.02595
0.1	1.56006	3.87286	13.4659	1.44991
0.05	2.25604	5.61808	19.5888	2.02936
0.025	3.22935	8.05563	28.1362	2.86826
0.0125	4.59797	11.48021	40.1337	4.05421
0.005	7.30491	18.25020	63.8389	6.40684

TABLE IV. *Table of* R_T *as a function of* ϵ/kT.

$1/q$	ϵ/kT	R_T	$1/q$	ϵ/kT	R_T
∞	0.0	0.43241	0.8	0.3906	0.1617
10.0	0.0025	0.44898	0.6	0.6944	−0.153
5.0	0.01	0.46304	0.5	1.0	−0.384
4.0	0.0156	0.4687	0.4	1.5625	−0.573
3.0	0.0277	0.4753	0.3333	2.25	−0.629
2.4	0.0434	0.4771	0.25	4.0	−0.465
2.0	0.0625	0.4753	0.2	6.25	−0.232
1.6	0.0977	0.4605	0.1	25.0	−0.040
1.2	0.1736	0.4036	0.05	100.0	−0.023
1.0	0.25	0.3243	0.0	∞	0.000

TABLE V. *Quantities for the special Lennard-Jones model.*

ν	$G(\nu)$	$H(\nu)$
3	1.000	0.000
5	0.833	0.833
7	0.392	0.557
9	0.156	0.293
11	0.030	0.120
15	−0.0928	−0.0833
∞	−0.2662	−0.4822

relative accuracy of the Ω's is much higher, of course.

The Ω's given in Table III were then substituted in Eq. (7). The values of R_T so obtained are given in Table IV as well as in Fig. 1.

We shall defer the discussion of these results to Section IV.

III. THE SPECIAL LENNARD-JONES MODEL ($\nu'=3$)

This model has already been treated in I.* The result, however, can be presented more simply and in a more useful form than was done in I. Furthermore, the present formulation is better adapted for the generalization which will be attempted in Section IV.

Equation (45,I) may be written in the form

$$\Theta^{(l)} = A_l^{(\nu)} + B_l^{(\nu)} \left(\frac{\nu-1}{\nu-3} \cdot \frac{\epsilon}{kT\gamma^2} \right)^{(\nu-3)/(\nu-1)}, \tag{39}$$

where $A_l^{(\nu)}$ and $B_l^{(\nu)}$ are the quantities tabulated in Tables I and V of I. The expression (39) is valid only to the terms of the first order in $(\epsilon/kT)^{(\nu-3)/(\nu-1)}$. From (6) and (39) we find the formula corresponding to (47,I):

$$\Omega^{(l,k)} = \tfrac{1}{2} A_l^{(\nu)} \Gamma\left(\frac{k+1}{2} - \frac{2}{\nu-1} \right) + \tfrac{1}{2} B_l^{(\nu)} \Gamma\left(\frac{k-1}{2} \right) \cdot \left(\frac{\nu-1}{\nu-3} \cdot \frac{\epsilon}{kT} \right)^{(\nu-3)/(\nu-1)}. \tag{40}$$

The substitution of this expression in (7) now leads to

$$R_T = C(\nu) \frac{\left[\frac{\nu-5}{\nu-1} + G\left(\frac{\epsilon}{kT} \right)^{(\nu-3)/(\nu-1)} \right] \left[1 - G \frac{15+4B_2/B_1}{15+6f} \left(\frac{\epsilon}{kT} \right)^{(\nu-3)/(\nu-1)} \right]}{\left[1 - G \frac{2B_2}{3fB_1} \left(\frac{\epsilon}{kT} \right)^{(\nu-3)/(\nu-1)} \right] \left[1 - G \frac{117+32B_2/B_1}{177+48(f-1/(\nu-1)+1/(\nu-1)^2)} \left(\frac{\epsilon}{kT} \right)^{(\nu-3)/(\nu-1)} \right]}, \tag{41}$$

$$\cong C(\nu) \left[\frac{\nu-5}{\nu-1} + H(\nu) \left(\frac{\epsilon}{kT} \right)^{(\nu-3)/(\nu-1)} \right]. \tag{42}$$

* The writer is aware of two errors in I, both of which involve the special Lennard-Jones model: 1. The κ immediately preceding the $D(\nu)$ in Eq. (IV) should be κ', and 2. The value of $D(15)$ in Table V should be 0.012 instead of 0.088.

The function $G(\nu)$ is defined by

$$G(\nu)=-\left(\frac{\nu-3}{\nu-1}\right)^{-(\nu-3)/(\nu-1)}\cdot\frac{B_1^{(\nu)}}{A_1^{(\nu)}\Gamma(3-2/(\nu-1))}.$$

The second expression for R_T is equivalent to the first as far as terms of the first order in $(\epsilon/kT)^{(\nu-3)/(\nu-1)}$. The functions $C(\nu)$ and $f(\nu)$ are tabulated in Table I of I; $G(\nu)$ and $H(\nu)$ are tabulated in Table V of this paper.

IV. Discussion of Results

The results indicated in Fig. 1 were derived explicitly for the Lennard-Jones 9,5 model. In the absence of evidence to the contrary, however, it seems reasonable to assume that the qualitative features of the result will be much the same for other molecular models which are similar to the 9,5 model. In particular, we shall suppose for the present that the behavior indicated in Fig. 1 is typical of Lennard-Jones models in which the attractive force index is about half of the repulsive force index, and we know that such molecular models have had considerable success in explaining the properties of fluids and solids.

The negative portion

By far the most striking aspects of the results given in Fig. 1 and Table IV are the rapid decrease of R_T as $(\epsilon/kT)^{\frac{1}{2}}$ increases beyond one-half, and the large negative values of R_T as the temperature decreases still further. This behavior of R_T was quite unexpected, and it has not yet received any definite confirmation from experiment. The negative portion, if it exists, should not be at all difficult to observe, as we shall now indicate.

The theoretical results can be more easily understood when they are expressed in terms of the critical temperature of the gas in question. Since the critical temperature is the temperature at which the attractive forces are just able to overpower the disrupting effects of thermal agitation, it is clear that the critical temperature is given approximately by the relation $kT_c=\epsilon$. Using the Lennard-Jones 13,7 model, and a simplified model of a liquid, Lennard-Jones and Devonshire[8] have found by detailed calculation the more precise result

$$T_c=(z/9)\cdot(\epsilon/k), \tag{43}$$

where z is the number of nearest neighbors of any given molecule in the liquid. Fowler and Guggenheim[9] suggest in this connection that a suitable value of z is 11. With $z=11$, Eq. (43) reduces to

$$T_c=1.22\epsilon/k. \tag{44}$$

If now we use the relation (44) to interpret the results in Fig. 1, we find that R_T is positive for temperatures greater than $1.54T_c$, and negative for temperatures less than $1.54T_c$. We also find that the minimum of R_T occurs at the temperature $0.36T_c$.

Now it is not at all difficult to work with gases at temperatures less than $1.54T_c$. In Table VI we have given the boiling points at atmospheric pressure and the critical temperatures of the noble gases and a few others chosen at random. From this table we may draw the very rough but rather general conclusion that at atmospheric pressure one may work with gases at temperatures greater than about $0.6T_c$.

For xenon, the range of temperature from the boiling point to $1.54T_c$ is the range from -109°C to 173°C. An experimental determination of the thermal diffusion constant of xenon in this temperature range would thus provide a useful and highly desirable check on this theory.

Application to isotope separation

It is clear that the attempt to separate isotopes with a thermal separation column having $1.54T_c$ as its mean temperature would meet with disappointing results, since the integral[10] yielding the value of H would be nearly zero as a consequence of the reversal of the sign of α. As we have just seen, however, there is usually a comfortable range of temperature between the temperature of condensation and $1.54T_c$. If, therefore, it is

[8] J. E. Lennard-Jones and A. F. Devonshire, Proc. Roy. Soc. **A163**, 53 (1937); Proc. Roy. Soc. **A165**, 1 (1938).

[9] See Fowler and Guggenheim, reference 4, p. 345.

[10] W. H. Furry, R. Clark Jones, and L. Onsager, Phys. Rev. **55**, 1083 (1939); R. Clark Jones and W. H. Furry, Rev. Mod. Phys., to be published.

TABLE VI. *Values of the critical temperature and the boiling point at atmospheric pressure for the noble gases and for a few others chosen at random.*

GAS	B.P. AT ATMOS. PRESS.	T_c	B.P./T_c
He	4.3	5.3	0.81
Ne	27	44	0.61
A	88	151	0.58
Kr	121	211	0.58
Xe	164	290	0.57
Cl_2	239	417	0.57
CCl_4	349	556	0.63
O_2	90	154	0.58
CH_4	108	191	0.57

inconvenient or impossible to operate the column over the range of temperature in which α is positive, it should usually be possible to operate the column so that it utilizes the negative portion of the curve shown in Fig. 1.

The hardness function

It will be noted that the initial slope of the curve in Fig. 1 is positive. This corresponds to the fact that the coefficient of $(\epsilon/kT)^{\frac{1}{3}}$ in (31) is positive. We shall find it convenient to use the term "initial slope" in a more general sense in connection with the general Lennard-Jones model; more generally, we shall mean by the "initial slope" the initial slope of the plot of R_T against $(\epsilon/kT)^{(\nu-\nu')/(\nu-1)}$. We then find that the initial slope for the special Lennard-Jones model is also positive when ν is less than about 15; according to Table V, the function $H(\nu)$ is positive for values of ν less than about 15.

In I, this positive "initial slope" was felt to be a defect of the special Lennard-Jones model, since the experiments seemed to indicate a negative slope. This difficulty has been resolved by the results in Fig. 1, which indicate that the initial slope is only a small part of the whole story.

The writer also stated in I that he did not know whether the positive initial slope was due to the choice of $\nu'=3$, or whether the "difficulty is more deeply seated." The writer now believes that he knows the reason for the positive initial slope, and that it can be explained on the basis of the inverse power model. Since Frankel[11] has shown that the essential properties of the inverse power model can be derived from elementary considerations, the argument to be given below furnishes another crumb of information about the thermal diffusion constant that can be obtained from elementary considerations.

The argument itself is somewhat arbitrary and approximate, and derives its real justification from the fact that its result is in good agreement with the results already obtained for the special Lennard-Jones model and for the 9,5 model. The argument follows.

Let r_0 be the distance of separation which corresponds to the minimum of the potential energy. Then, for values of r greater than r_0, the force is an attractive one, whereas for smaller values of r the force is repulsive. We propose that these two ranges of r make opposing contributions to the initial slope.

In the case of the Sutherland model r cannot be less than r_0, so that we are concerned only with the effect of the first of these two ranges. We saw in I that, for the Sutherland model, the initial slope is negative for all values of ν'. It therefore appears that the contribution of the first range to the initial slope is negative.

In order to discuss the contribution of the second range let us first recall some of the results for the inverse power model. This model is the special case of the Lennard-Jones model in which κ' is zero. For the inverse power model, we found in I that R_T is given by

$$R_T=C(\nu)(\nu-5)/(\nu-1), \tag{45}$$

where $C(\nu)$ is a slowly varying function of ν which increases from 0.8 to 0.9 as ν rises from 5 to 15. R_T thus increases as ν increases, or as the "hardness" of the molecule increases. The derivative $d\log F/d\log r$ is constant for the inverse power model, and is equal to $-\nu$. Let us therefore introduce a "hardness function"

$$\mu(r)=-d\log F/d\log r. \tag{46}$$

For the general Lennard-Jones model, we find the hardness function to be

$$\mu(r)=(\nu-Q\nu')/(1-Q)$$
$$=\nu+Q(\nu-\nu')+O(Q^2), \tag{47}$$

where Q is the ratio of the attractive to the repulsive term in (13):

$$Q(r)=\kappa'/(\kappa r^{\nu-\nu'}). \tag{48}$$

[11] S. P. Frankel, Phys. Rev. **57**, 661L (1940).

Now for all values of r in the second range, Q is positive and less than unity. This means that for all values of r in the second range, $\mu(r)$ is greater than ν; *the effect of the second term in (13) is to increase the hardness of the repulsive force.* We should thus expect that the presence of a weak attractive force would increase the value of R_T.

In order to put this argument in a more quantitative form, it is necessary to perform some sort of an averaging process on $\mu(r)$ in order to eliminate the dependence on r. We shall perform this averaging by the arbitrary device of evaluating Q at the distance of separation which corresponds to an energy of interaction equal to $\frac{1}{2}kT$. We shall also approximate by treating Q as a number small compared with unity.

As a first approximation, we find

$$Q \cong \frac{\kappa'}{\kappa}\left(\frac{2\kappa}{(\nu-1)kT}\right)^{(\nu-\nu')/(\nu-1)} = \left(\frac{\nu'-1}{\nu-\nu'}\cdot\frac{2\epsilon}{kT}\right)^{(\nu-\nu')/(\nu-1)}. \tag{49}$$

If now we substitute (49) in (47), and then substitute the average value of μ so obtained for ν in (45), we find after a little manipulation

$$R_T = C(\nu)\left(\frac{\nu-5}{\nu-1} + \left\{4\frac{\nu-\nu'}{(\nu-1)^2}\left(\frac{2(\nu'-1)}{\nu-\nu'}\right)^{(\nu-\nu')/(\nu-1)}\right\}\left(\frac{\epsilon}{kT}\right)^{(\nu-\nu')/(\nu-1)}\right). \tag{50}$$

This is the result toward which we have been working. The quantity in the curly bracket (multiplied by $C(\nu)$) is the value of the initial slope predicted by the argument just presented.

In Table VII we compare the value of the curly bracket in (50) with the value of the corresponding coefficient as given by the results for the special Lennard-Jones model and for the 9,5 model. The agreement is satisfying; the approximate treatment yields substantially correct results as long as the second range is not too small in extent; that is to say, as long as ν is not too great a multiple of ν'.

The precise value of the initial slope obtained by this approximate treatment depends, of course, on the particular method of averaging which is used to eliminate the dependence of μ on r. Any method of averaging which is physically reasonable will yield about the same result, however, so that the writer feels that Eq. (50) affords a reliable approximate evaluation of the "initial slope" for the general Lennard-Jones model, subject to the restriction that ν may not be too great a multiple of ν'.

It is interesting to contemplate that if the van der Waals forces were non-existent for any molecule, and if the only energy of interaction were an overlap energy of the asymptotic form

$$E = \alpha e^{-\beta r}, \tag{51}$$

then the hardness function would be given by

$$\mu(r) = \beta r. \tag{52}$$

According to (52), R_T would *rise* monotonically as the temperature decreased, and would approach unity as the absolute temperature approached zero.

The approximate formulae (31) and (38)

These formulae are indicated by the dotted lines in Fig. 1. Equation (31) affords the correct initial slope, but it is clear that the second- and third-order terms are far from correct. The error

TABLE VII. *Comparison of the results yielded by the use of the hardness function with the results of detailed calculation.*

ν	ν'	EXACT COEFFICIENT	CURLY BRACKET IN EQ. (50)
3	3	0.000	0.0000
3.25	3		0.2688
3.50	3		0.4850
4	3		0.7055
5	3	0.833	0.7071
7	3	0.557	0.4444
9	3	0.293	0.2767
11	3	0.120	0.1838
15	3	−0.0833	0.09551
9	5	0.4026	0.35355

TABLE VIII. *The temperature dependence of n according to the 9,5 model.*

ϵ/kT	n	ϵ/kT	n	ϵ/kT	n	ϵ/kT	n
0.0	0.75	0.20	0.77	0.50	0.98	1.50	1.30
0.01	0.73	0.25	0.80	0.60	1.04	2.0	1.28
0.02	0.73	0.30	0.84	0.70	1.10	2.5	1.24
0.05	0.72	0.35	0.87	0.80	1.15	3.0	1.19
0.1	0.73	0.40	0.91	1.00	1.22	∞	1.00
0.15	0.75	0.45	0.94	1.25	1.27		

is due to the impropriety of considering the polynomial approximations as series expansions. The approximate relation (38) is quite accurate for values of q greater than about 20.

Viscosity

By substituting (22) and the numerical values of $\Omega^{(2,7)}$ given in Table III in Eq. (10), one obtains the temperature dependence of the coefficient of viscosity according to the Lennard-Jones 9,5 model. Hassé and Cook have compared with experiment the theoretical predictions so obtained.

During the time since the work of Hassé and Cook was published, Trautz and his associates[12] have measured the temperature dependence of the viscosity of a large number of gases. We do not intend to make here any detailed examination of these more recent data. We should like to point out, however, that with nearly all of their data, Trautz and his associates have given also the experimentally determined values of

$$n = d\log\eta/d\log T \tag{53}$$

as a function of the temperature. The quantity n is important because of its simple interpretation in terms of the inverse power model, as we pointed out in detail in I.

The writer has determined n as a function of ϵ/kT for the 9,5 model. The results are given in Table VIII. The predictions of Table VIII are in qualitative agreement with the experimental data; the data show a general tendency for n to increase as the temperature decreases. Values of n as large as 1.30, however, have not been observed; the value $n=1.14$ for SO_2 in the range 287°–370°K is the largest found by Trautz *et al.*

In conclusion, we may say that the 9,5 model is in qualitative agreement with the tendency of nearly all molecules to become, with respect to viscosity, more "soft" as the temperature decreases.

[12] For references, see Table II of reference 1.

TABLE IX. *Values of α determined experimentally by Nier.*

MIXTURE	TEMP. RANGE	α	$\bar{R}_T$
$C^{12}H_4-C^{13}H_4$	296°–728°K	0.0080±~5%	0.30
	296°–573°K	0.0074±~5%	0.27
$Ne^{20}-Ne^{22}$	283°–617°K	0.0302±2%	0.71
	90°–294°K	0.0188±2%	0.44
	90°–195°K	0.0165±8%	0.39

There is remarkable agreement between the values of R_T given in Table IV, and those obtained from Table VIII by the approximate relation (32,I):

$$R_T = 1.7(1-n), \tag{54}$$

which was derived on the basis of the inverse power model. To two significant figures, the two methods agree in predicting a maximum of 0.48 at $\epsilon/kT=0.05$, and they both indicate that R_T changes sign at $\epsilon/kT=0.53$. Equation (54), however, predicts a minimum of -0.51 at $\epsilon/kT=1.5$, whereas Table IV indicates a minimum of -0.63 at $\epsilon/kT=2.2$. In the opinion of the writer, the close correspondence between the values of R_T obtained by the two methods should be considered as fortuitous, since the use of (54) in the present connection has no theoretical justification.

If such a close correspondence should turn out to hold for other Lennard-Jones models, however, the existence of an empirical relation of the form (54) should have considerable practical utility, since it would be possible to obtain an estimate of the value of R_T at any given temperature by a naïve application of the inverse power model to viscosity data for the gas in question.

The fact that values of n as large as 1.3 are not found experimentally, however, may be taken to suggest that negative values of R_T as large as those indicated by Table IV will also not be found experimentally.

V. COMPARISON WITH EXPERIMENT

The only direct experimental determinations of α for isotopic mixtures which have been published up to the present are those of Nier.[13]

[13] A. O. Nier, Phys. Rev. **56**, 1009 (1939); Phys. Rev. **57**, 338 (1940).

His results are given in Table IX, which is reprinted from I.

The values of $\bar{R}_T$ given in Table IX are "average" values over the temperature interval in question; that is to say, they are the values of R_T which would give the observed separations if R_T were independent of the temperature. The relation between $\bar{R}_T$ and R_T for the "two-bulb" method used by Nier is

$$\bar{R}_T = \int_{T_1}^{T_2} R_T \, d \log T \Big/ \log T_2/T_1. \qquad (55)$$

For the Sutherland model, with the approximate expression for R_T given by Eq. (43,I), Brown[14] has shown by the use of (55) that for any values of T_1 and T_2, $\bar{R}_T$ is equal to the value of R_T at the temperature

$$T_r = \frac{T_1 T_2}{T_2 - T_1} \log \frac{T_2}{T_1}. \qquad (56)$$

When R_T cannot be expressed analytically, however, it is possible to use a simple graphical method: R_T is plotted against $\log T$; the value of $\bar{R}_T$ is then the average value of the ordinate between the abscissae corresponding to T_1 and T_2.

Neon

In attempting to compare Nier's data for neon with our theoretical results for the 9,5 model, we are immediately faced by the difficulty that the largest experimental value of R_T is much greater than any of those found in Table IV. This difficulty simply corresponds to the fact that neon is much harder than $\nu = 9$. The experimental value $\bar{R}_T = 0.71$ is in good agreement with the high temperature viscosity data of Trautz and Sorg, which according to Table II of I, predict the value $\bar{R}_T = 0.69$ at the temperature $T = 1030°$ on the basis of the inverse power model; at such a high temperature, the inverse power model should be adequate for neon because of the small magnitude of the attractive forces.

In order to take account of the greater hardness of neon, we take the bold step of increasing the scale of the results given in Table IV so that the maximum value of R_T is 0.74 instead of 0.48. We then find by the graphical method just described that with $\epsilon/k = 42.5°$, the theoretical values of $\bar{R}_T$ corresponding to the three temperature ranges for neon are 0.71, 0.45, and 0.36. These values agree with the experimental values within the experimental error, and the value $\epsilon/k = 42.5°$ is in fair agreement with (44), since we find in Table VI that the critical temperature is 44°.

Now we should not like to lay too much stress on the excellence of the agreement between theory and experiment. After all, anyone can fit three experimental points, two of them close together, with a curve involving two adjustable constants. The important fact is that the large decrease in R_T, which occurs at temperatures well above the critical temperature, can be explained by the use of a value of ϵ/k which is in substantial agreement with the value indicated by other methods of approach.

It should be remembered in this connection that we found in I that the Sutherland model in the approximate form (43,I) could be made to fit the neon data, but that the required value of ϵ/k was about 350°, a value nearly ten times the critical temperature!

Methane

The methane molecule is far from being spherically symmetrical, so that Chapman-Enskog theory does not strictly apply.

If we use the value of ϵ/k indicated by Eq. (44) and the critical temperature:

$$\epsilon/k = 191°/1.22 = 156°,$$

then we find by the graphical method that the theoretical values of $\bar{R}_T$ which correspond to the temperature ranges in Table IX are 0.212 and 0.168. If these numbers are multiplied by $0.71/0.48 = 1.48$, they become 0.31 and 0.25. The fact that the necessary multiplicative factor is slightly smaller than in the case of neon suggests

TABLE X. *Values of $\bar{R}_T$ for mixtures of the noble gases over the temperature range 0°–100° C.*

	Ne	A	Kr	Xe
He	0.80	0.65	0.63	0.59
Ne		0.54	0.51	0.43
A			0.19	0.17
Kr				0.08

[14] Harrison Brown, Phys. Rev. **58**, 661L (1940).

TABLE XI. *Comparison of the theoretical and experimental values of R_T for certain mixtures of the noble gases.*

MIXTURE	$\bar{T}_e$	ϵ/k	$\bar{R}_T$(THEORY)	$\bar{R}_T$(EXP.)
He-Ne	25	20	0.74	0.80
Ne-A	98	80	0.51	0.54
A-Kr	181	148	0.15	0.19
Kr-Xe	250	205	−0.12	0.08

that the methane molecule is slightly softer than the neon molecule.

We may also use the alternative procedure, and find the value of ϵ/k which permits the best check between experiment and the predictions of the 9,5 model without the use of a correction factor. It is found that the value $\epsilon/k=120°$ leads to a better check than was found in the last paragraph. It is difficult, however, to justify the smaller value of ϵ/k.

Other evidence, both pro and con

Atkins, Bastick and Ibbs[15] have measured the thermal diffusion constant of all of the ten different binary mixtures of the five noble gases. The measurements were all made in the same series of experiments in the same apparatus. The lower and upper temperatures in every case were 0° and 100°C. The results obtained by these authors are given in Table X.

The general formula (7), upon which all of the results derived in the present paper depend, was derived upon the explicit assumption that the molecules of the two gases differed from one another only in that their masses were different. The theory does not strictly apply, therefore, to mixtures of dissimilar molecules, even when they are as much alike as the molecules of the noble gases. There can be little doubt, however, that the mass difference accounts for all but a small part of the observed separations. We shall therefore attempt to compare the experimental results of Atkins, Bastick and Ibbs with the predictions of the Lennard-Jones 9,5 model.

It is, of course, necessary to determine a suitable value of ϵ, which is now the depth of the potential energy minimum for the interaction of the two dissimilar molecules. It is well known[16] that the magnitude of the van der Waals attractive force is proportional to the product of the polarizabilities of the two atoms. If then we should assume that the fields of force of all the noble gases differed only by a multiplicative constant, it is clear that the value of ϵ for the interaction between two dissimilar molecules would be the mean proportional of the values of ϵ for each of the two molecules interacting with molecules of its own kind. Actually the assumption at the beginning of the last sentence is not strictly justified, and we shall omit all detailed considerations by evaluating ϵ from the arithmetic mean of the critical temperatures of the two gases which make up the mixture. Of the four mixtures which we shall discuss, only the first (He−Ne) provides an appreciable ambiguity in the proper choice of ϵ, and in this case any reasonable value of ϵ will lie on the broad maximum of Fig. 1, so that there is no ambiguity in the predicted value of R_T even for this mixture.

We shall discuss only the mixtures of adjacent members of the family of noble gases. We have given in Table XI the value of the mean critical temperature of each of these mixtures, and the value of ϵ/k determined from (44). We then determined from Table IV the value of R_T at the temperature $T=323°$, and have multiplied this value by 0.74/0.48, the factor that was found necessary in the case of the neon isotopes; the result is given as the theoretical value of $\bar{R}_T$.

The comparison between theory and experiment is, for the first three mixtures, better than we might have expected. The discrepancy in the case of the krypton-xenon mixture may be ascribed to a lack of applicability of the 9,5 model, or it may be written off as experimental error. The authors reported considerable difficulty in making the measurement in this case. Since the observed change in concentration was only 0.098 percent, and since the concentrations were estimated from the thermal conductivity of the mixture, it is conceivable that the discrepancy can be attributed to experimental error. The authors do not estimate the probable errors of any of their results.

A serious objection to the present theoretical results is offered by the work of Groth and

[15] B. E. Atkins, R. E. Bastick and T. L. Ibbs, Proc. Roy. Soc. **A172**, 142 (1939).

[16] See, for example, F. Seitz, *Modern Theory of Solids* (McGraw-Hill, 1940), p. 84.

Harteck,[17] who obtained a partial separation of the mercury isotopes by means of a thermal separation column of the hot-wire type, operating between the temperatures 350°C and 1800°C. Since the free mercury atom is in a spherically symmetrical singlet S state, and since the critical temperature of mercury vapor is about 1650°C, the present theory would indicate that the value of α would be negative, and that therefore the lighter fraction would be concentrated at the bottom of the column. Actually, however, the light fraction was collected at the top of the column. The writer has no explanation for the discrepancy.

Conclusion

The small amount of experimental data which is so far available lends considerable support to the accuracy of the predictions of the 9,5 model for positive values of R_T. There is, however, no experimental evidence for the large negative values predicted, and the work of Groth and Harteck, as well as the failure of the viscosity predictions to be borne out for larger value of ϵ/kT, suggests that the large negative values of R_T may not be found experimentally.

Our theoretical understanding of the temperature dependence of α has increased significantly since the publication of the first paper of this series. It will be remembered that we closed in I on a rather pessimistic note, with the unstated but implied suggestion that the general Lennard-Jones model would turn out to be inadequate for the explanation of Nier's data. This pessimism, the writer now realizes, was founded upon an incomplete realization of the sad inadequacy of the "initial slope" determinations.

Ideally, work on this problem in the near future should proceed along two lines. There is a need for more experimental data on the thermal diffusion constant of isotopic mixtures, particularly at temperatures in the neighborhood of the critical temperature. In order that the Chapman-Enskog theory be capable of application, the measurements should preferably be made on the noble gases and on those metallic vapors whose atoms have a spherically symmetrical ground state. Secondly, we must work out the detailed predictions of other Lennard-Jones models, preferably of the ν,7 type. The necessary numerical calculations are discouragingly onerous, and it is to be hoped that the scientific methods of machine computation, which are just beginning to be developed at this late stage of scientific progress, will be of assistance in the execution of the computations.

Acknowledgment

The writer would like to thank Professor W. H. Furry for helpful comments on the manuscript, and he is indebted to his wife, Lois Kathryn Jones, for assistance in the numerical computations involved in the investigation of the 9,5 model.

[17] W. Groth and P. Harteck, Naturwiss. **27**, 584L (1939).

A New Technique for Preparing Monocrystalline Metal Surfaces for Work Function Study. The Work Function of Ag(100)

PAUL A. ANDERSON
State College of Washington, Pullman, Washington
(Received April 14, 1941)

A new method of experimental attack upon the problem of the structural dependence of the work functions of the metals is described. The method utilizes the results of recent electron diffraction studies which show that many cubic lattice metals when thermally vaporized and condensed on heated cleavages of rocksalt form films which are in effect single crystals with a (100) plane parallel to NaCl (100). With silver as a typical metal of this class, there has been developed a technique of preparing an Ag(rocksalt) film in the measuring tube itself and of then determining its contact difference of potential against (1) polycrystalline silver films deposited on glass at room temperature, and (2) a reference metal of known work function, barium. The silver was fractionally distilled and only the middle fractions deposited on the glass and rocksalt targets, the barium fractionally and multiply distilled and its discarded fractions used to getter the tubes in which the measurements were made. The contact p.d. between Ag(rocksalt) and Ag(glass) has been found to range from 0.12 v in a preliminary measurement to 0.32 ± 0.03 v in final measurements made after the technique of preparing the Ag(rocksalt) films had been perfected. The contact p.d. for Ag(glass) —Ba is found to be 1.95 v, in close agreement with our earlier results at liquid-air temperature. Work function values computed from these measurements and the work function of Ba, 2.52 ev, are 4.47 ev for Ag(glass) and 4.79 ev for Ag(rocksalt). Since two independent electron diffraction investigations, both especially complete for silver, indicate that Ag(rocksalt) films formed under the conditions of the present experiments invariably approximate closely to the ideal (100) structure, and since the contact potential method measures the average work function of a surface without weighting vestigial regions of imperfect symmetry, our Ag(rocksalt) work function value is identified tentatively with the work function of Ag(100). Our Ag(100) value is in good agreement with Farnsworth and Winch's recent photoelectric measurements on a massive single crystal but Winch's earlier value of 4.74 ev for the work function of a heat-treated silver wire is probably characteristic of the crystal faces of preferred orientation developed by thermal etching rather than of randomly oriented polycrystalline silver. The method developed in the present work for measuring Ag(100) appears to be directly applicable to the (100) orientations of Ni, Cu, Au, Pd and Al.

A MAJOR problem in the experimental and theoretical study of work functions concerns the influence of the crystalline structure of a metal surface upon its work function. There is now abundant evidence for the existence of such a structure dependence but few quantitative data are available for surfaces of definitely known structure. Progress has been hampered by the extraordinary technical difficulties involved not only in preparing monocrystalline surfaces which are free from serious structural defects but in satisfying simultaneously the requirement, demanded of all work function measurements, that these surfaces shall be free from adsorbed gases and vapors. With the exception of studies on tungsten,[1] by methods applicable only to the ultra-high melting point metals, previous work[2] has been done with massive single crystal ingots and it has been necessary to prepare the required crystal faces by grinding, followed by chemical or electrolytic etching. Surface contaminations then have to be removed as completely as is possible in an outgassing in which the maximum permissible outgassing temperature is limited by the onset of thermal etching, with attendant development of unwanted crystal facets. The method is necessarily laborious and there is some question as to the quality of the faces which can be prepared by its use. Rose,[2] in measuring the contact p.d. between the (100) and (111) orientations of a copper crystal prepared by this method, observed extraneous reflections on the finished faces and concluded that his final values were characteristic of crystal faces contaminated with gas and with unwanted crystal facets.

A relatively simple method of preparing gas-free single crystal surfaces in the measuring tube itself, without atmospheric exposure, mechanical working or chemical etching, is suggested by

[1] R. P. Johnson and W. Shockley, Phys. Rev. **49**, 436 (1936); C. E. Mendenhall and C. F. DeVoe, Phys. Rev. **51**, 346 (1937); S. T. Martin, Phys. Rev. **56**, 947 (1939); M. H. Nichols, Phys. Rev. **57**, 297 (1940).

[2] H. E. Farnsworth and B. A. Rose, Proc. Nat. Acad. **19**, 777 (1933); B. A. Rose, Phys. Rev. **44**, 585 (1933); H. E. Farnsworth and R. P. Winch, Phys. Rev. **58**, 812 (1940).

Brück's observation[3] that many isometric metals, e.g., Cu, Au, Ag, Ni and Pd, when thermally vaporized and condensed on heated rocksalt cleavages, form films which exhibit electron diffraction patterns characteristic of the (100) faces of single crystals of these metals. With the purpose of testing this possibility, experiments on the contact difference of potential between silver films condensed on glass and on rocksalt were started by the author early in 1936. The first experiments were vitiated by the use of natural rocksalt which, even after prolonged heating near the sublimation point, could not be outgassed sufficiently to allow the maintenance of an adequate vacuum in a sealed-off tube. This difficulty was removed by the use of artificial rocksalt crystals,[4] which are free from impounded water and hygroscopic impurities and give exceptionally good cleavages. Other difficulties have been encountered in the tendency of silver films, deposited on rocksalt at too slow a rate, to show an erratic electrical conductivity and in the problem of making electrical contact to these films, much more fragile than films of similar thickness laid down on glass. Throughout the preliminary measurements, made with a variety of different tube designs and techniques, the silver films on rocksalt, to be designated Ag(rocksalt), were consistently electronegative to silver films on glass, Ag(glass), but reproducibility within satisfactorily narrow limits has been obtained only in the most recent measurements. Unlike the results reported in previous papers of this series and based on the measurement of twenty or thirty duplicate surfaces, the present "final" results are based on measurements of only two Ag(rocksalt) films, prepared and measured in different tubes. The present report is to be regarded primarily as a description of a new method of attack rather than as an exhaustive study of the work function of Ag(100).

Method of Measurement

Except for modifications dictated by the special requirements of the problem and described in detail below, the method of preparing and measuring the metal surfaces was similar to that developed in the study of the contact differences of potential between different metals deposited on a single substrate. This method, for the details of which the reader is referred to the earlier papers of this series,[5] may be summarized briefly as follows. (1) Specimens of the two metals under investigation, of high chemical purity but containing absorbed and adsorbed gases, are outgassed by repeated fusion while the measuring tube is undergoing a thorough baking and high frequency treatment on the pumps. One member of the metal pair is always barium; the other is the "unknown." Barium, which gives vaporized films of highly reproducible and constant work function, is used both to getter the tube and to prepare the standard reference surface of known work function to which all our contact potential measurements are referred. (2) The tube is sealed from the pumps and each metal specimen fractionally distilled. A middle fraction of one of the metals is finally condensed on a movable target. (3) Immediately after the deposition of a fresh metal film upon it, the target is moved before an electron gun which supplies a constant energy (about 10 ev), constant intensity electron beam, and the retarding potential required to establish a given reference current is determined. This reference current is so selected as to be near the middle of the straight-line portion of the current-potential characteristic. (4) Step three is repeated for a succession of films of the first metal and the reproducibility of the potential setting for this metal thus determined. (5) Steps three and four are repeated for the second metal of the pair. The contact difference of potential between the two metals, or between films of a given metal deposited on different substrates, is then equal to the difference between the potential settings, i.e., to the shift of the current-potential characteristic with change of surface.

Tube Design

Figure 1 is a sketch of the most satisfactory of the tubes used in the present measurements. The barium vaporizer, connected at *B* but not shown, was identical in design to a vaporizer previously

[3] L. Brück, Ann. d. Physik **26**, 233 (1936).

[4] These crystals, grown from fused NaCl, were furnished to me through the kindness of Dr. H. C. Kremers of the Harshaw Chemical Company, Cleveland, Ohio.

[5] P. A. Anderson, Phys. Rev. **47**, 958 (1935); **49**, 320 (1936); **54**, 753 (1938); **57**, 122 (1940).

described[6] and now being incorporated as a standard part in all of our tubes. It provides for both fractional distillation of the barium and for revaporization of any selected fraction, and contains a rotatable glass shutter which eliminates any possibility of contaminating the silver with barium during the preliminary vaporizations of the metals. The efficiency of this shielding has been checked repeatedly by operating the barium vaporizers with shield closed during the measurement of metal surfaces of high work function. Although such a surface is extremely sensitive to a slight barium contamination, no change in work function has been observed in any one of these tests. The silver vaporizer was a simple conical spiral of 20-mil tungsten wire. The important question of the efficacy of the vaporization method for producing gas-free silver surfaces is given special consideration in another section of this paper. The mounting of the rocksalt target *R* was such as to leave its surface entirely free of contacts or clamping lugs during the deposition of silver upon it, a precaution which is probably essential if structural disturbances in the silver film are to be avoided. As shown in the sketch, the rocksalt cleavage was carried on an inclined glass platform fitted with short glass stops. This design had the further advantage of permitting a fresh cleavage to be introduced into the tube quickly, immediately after it was prepared. To avoid errors originating in tube geometry, the clearance between the electron gun and each of the two targets was equalized carefully during the construction of the tube. In this adjustment a glass "dummy" took the place of the rocksalt cleavage and the cleavage was then made to match the dimensions of the dummy. The rocking contact *C* was designed after simple brush-type contacts had been found unsatisfactory. The lightest practicable brushes, e.g., a whisker of 3-mil tungsten wire, were found to scratch the Ag(rocksalt) films so seriously as to destroy electrical contact between film and brush. During the centering of the target before the gun, *C* was raised clear of the target path by traction on the armature *N*. The contact was then lowered carefully on to the edge of the target and a positive contact pressure maintained by the weight of the armature.

[6] Reference 5, 1940 paper.

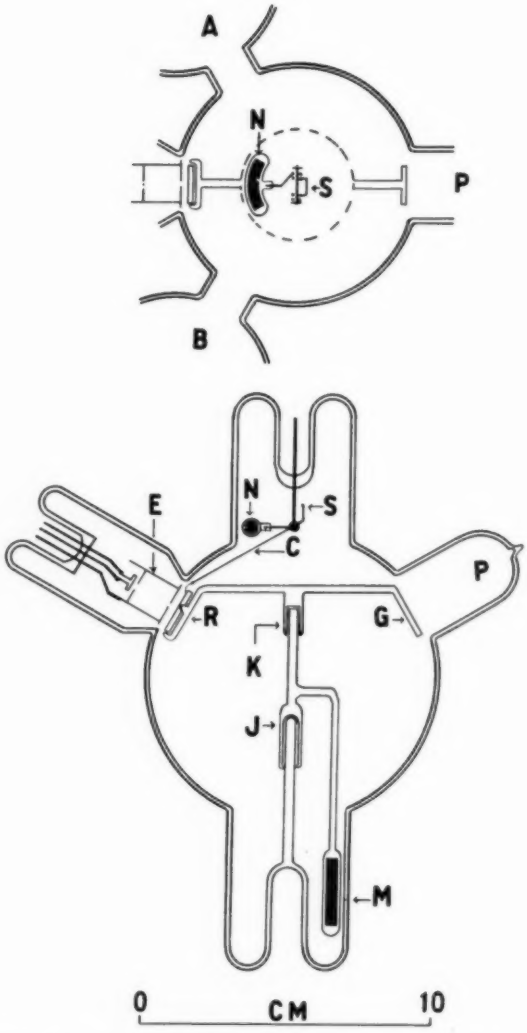

FIG. 1. The tube. The target assembly *RGKJ* is all-glass, driven on bearing *J* by magnetic traction on the glass-enclosed armature *M*. The rocksalt target, lying loosely on the glass platform *R*, and the glass target *G* are both 2×18×20 mm. *K* is a wedge-in-slot separable junction to facilitate mounting. The rocking contact assembly *NCS* comprises the 20-mil (0.5-mm) tungsten wire *C* tipped with a 2-mm loop of 12-mil Pt wire, a four-turn bearing of 30-mil Ta wire, with stop *S*, close wound on the 60-mil W lead-wire, and the glass-enclosed armature *N*. The electron gun *E* is of 4-mil Ta foil; emitter, 1-mil W foil 1.5 mm wide. For the silver and barium vaporizing chambers *A* and *B*, see text.

MATERIALS

The silver was Hilger's "spectroscopically pure" material, supplied with an analysis showing the total impurity content to be 0.001 percent or less. (Hilger Laboratory No. 9696.) Since the contact potential method measures the average work function of a surface and the silver was

fractionally distilled in the measuring tube, errors due to solid impurities on the final silver surfaces must have been entirely negligible. The barium was taken from the same stock used in previous measurements and previously described.[5]

Procedure

The pumping and outgassing procedure was similar, in the main, to that followed in the earlier studies of this series. An initial baking at 500–550°C was carried out before the rocksalt target and barium charge were introduced into the tube. The vacuum was then relieved by dried air or dried helium (no advantage in the use of the latter could be observed) and the rocksalt and barium quickly introduced through suitably placed side tubes, not shown in the sketch. The final cleavage on the rocksalt specimen was made immediately before it was placed in the tube. The side tubes were then sealed off quickly and the tube immediately repumped. After baking for at least 72 hours at 350°C, with repeated high frequency heating of the electron gun to temperatures at which the tantalum began to vaporize, the silver and barium charges were melted down and the tube then sealed from the pumps. Before starting the measurements, or depositing any metal on either of the targets, the silver and barium were melted down repeatedly. During these preliminary fusions and vaporizations about 50 percent of the silver, and 80 percent of the barium, charge was discarded. Both the Ag(rocksalt) and Ag(glass) films were prepared and measured against each other before barium was deposited upon either target and before any barium vapor was allowed to enter the measuring chamber. To minimize the possibility of silver vapor condensing on the rocksalt before this target was heated, the Ag(rocksalt) film was deposited first. In the case of the tube sketched in Fig. 1, the rocksalt target was brought to the temperature selected for deposition, 200°C, by placing the whole tube in a small oven fitted with Calrod stove unit and mica windows. In earlier tubes the rocksalt cleavages were heated by radiation from tungsten wire grids mounted within the tube. This method shortens the time lapse between deposition and measurement of a film to the time required to swing the target to the measuring position and take a galvanometer reading, i.e., to about 10 seconds. It was an essential preliminary to the simpler technique and was discontinued only after it was found that neither the Ag(rocksalt) or Ag(glass) films showed any significant change of work function over a period extending from ten seconds to several hours after deposition. After securing the potential setting for the Ag(rocksalt) film, a succession of silver films was laid down on the glass target at room temperature and each film measured immediately after it was formed. After establishing the contact difference of potential between Ag(rocksalt) and Ag(glass), barium was deposited upon each of the targets with the purpose of checking our value[7] for the work function of Ag(glass) and determining the effect, if any, of the structure of the silver substrate upon the work function of barium.

Appraisal of Gas Contaminations at Vaporized Silver Surfaces

As mentioned above, the silver was fractionally distilled in the sealed-off measuring tube and only the middle fractions condensed on the targets. During vaporization of the first discarded fractions the small silver globule was melted and solidified[8] at least sixteen times. Between fusions, and in order to utilize the slow diffusion of gas through the solid metal, the silver was held at a temperature just below that at which vaporization was noticeable. Barium fusions, each accompanied by vaporization, were interspersed between the silver fusions and the entire post-seal-off outgassing regime extended over a period of several weeks to allow thorough clean-up after each barium vaporization. Before this outgassing treatment was completed the silver ceased to emit any detectable quantity of gas upon remelting, an observation which indicates that equilibrium between the gases dissolved in the silver and the residual gas in the tube was

[7] Reference 5, 1936 paper.

[8] Since much of the gas which remains dissolved in a molten metal is segregated and forced out upon solidification, alternate fusion and solidification is an especially effective means for outgassing a metal. The efficacy of fusion in removing gas is due, of course, not only to a rapid increase in the diffusion rate with temperature but to convective stirring of the molten metal.

established or at least approached very closely.[9] When such an equilibrium is established the silver contains the minimum quantity of absorbed gas possible for a given residual gas pressure. The main constituent of the dissolved gas, and the constituent most likely to form a contamination active in altering the work function, was probably oxygen. Since the oxygen evolved during outgassing reacted, in effect irreversibly, with the barium getter, the equilibrium pressure of oxygen must have been vanishingly small. If, now, silver thus outgassed is vaporized and condensed on a cool surface, the dissolved gas content will be temporarily reduced below the equilibrium value provided that, as is generally true for most gas-metal systems, the restitution coefficients for the gases are greater than the restitution coefficient for silver at a silver surface. Given a silver specimen outgassed to equilibrium, it is clear that a multiple distillation can be more effective than a single vaporization only if the dissolved gas equilibrium is thus disturbed, and such a disturbance must be followed by reestablishment of the equilibrium during the aging of the film. If it alters the work function measurably, i.e., if it is extensive enough to be significant in a work function determination, this process must be detectable in a series of work function measurements started within a time interval which is short compared to the time required for the redeposition of an equilibrium layer of gas, a layer which becomes the source for any rediffusion of gas into the metal. In the present investigation, work function measurements started within 10 seconds of the formation of a fresh silver film showed no drift over aging periods extending to several hours. At the residual pressure obtaining in a barium gettered tube the redeposition of an equilibrium gas layer requires a time period far in excess of 10 seconds[10] and we have, therefore, some reason to conclude that the equilibrium gas film which must have formed eventually was either (1) too dilute to have a measurable influence on the work function, or (2) was composed of gases to which the work function of silver is insensitive. In this connection it should be pointed out that the common assumption that an equilibrium gas layer is always a completed "monomolecular layer" is not born out by kinetic analysis.[10] If the residual gas pressure is sufficiently low and the time of sojourn of an adsorbed gas molecule sufficiently small, the covering factor may be much less than unity for the equilibrium layer. In a barium gettered tube the residual gas available for deposition on a freshly vaporized metal surface is the gas which is in equilibrium with the barium. Not only is the residual gas pressure extremely low; the residuum must be composed of gases which are not strongly adsorbed by metal surfaces.

[9] The dissociation pressure of Ag_2O is 388 mm at 773°K and increases with temperature. The combined oxygen must have been released in the first stages of the outgassing treatment.

[10] Reference 5, 1940 paper.

The Structure of Silver Films Deposited on Rocksalt

The results of the most recent structural studies[11] on silver-rocksalt films, insofar as they bear directly upon the present problem, may be summarized briefly as follows. (1) When a stream of silver vapor[12] impinges upon a rocksalt cleavage heated to a temperature of 150–200°C, condensation starts with the formation of nuclei which have the orientation of a silver lattice twinned on any one of the four possible octahedral (111) planes with respect to a silver lattice paralleling the lattice of the rocksalt substrate. As Menzer[11] shows in detail, this structure satisfies the condition which requires approximate matching of interatomic spacings in the contiguous NaCl and Ag layers. Since no one of the four possible orientations is favored, nuclei with all these orientations form at random on the (100) rocksalt surface. (2) As the condensation of silver proceeds, the nuclear crystals form, by interpenetration, a lattice which parallels NaCl (100) and which has the full cubic symmetry of Ag(100). (3) If the deposition of silver is stopped at a film thickness of the order of a few hundred A.U. there remain on the surface, in addition to the interpenetration regions of (100) symmetry,

[11] G. Menzer, Zeits. f. Krist. **99**, 410 (1938); O. Goche and H. Wilman, Proc. Roy. Soc. **51**, 648 (1939).

[12] In the structural studies little attention has been given the well-known fact that the condensation of a metal vapor upon a dielectric is conditioned by the rate at which vapor is supplied to the surface as well as by surface temperature. Although only the target temperatures are specified, the order of vapor stream intensities can be inferred from descriptions of the deposition periods for films of specified thickness.

relatively small areas of lower symmetry in which the interpenetration has not been completed. These "interstitial" areas account for the satellites characteristic of electron diffraction photographs taken on extremely thin Ag(rocksalt) films. If the deposition is carried to film thicknesses greater than about 1000A the satellites disappear and the diffraction pattern becomes characteristic of Ag(100) alone.

It is to be noted especially that in none of the independent structural investigations was precaution taken to deposit the thicker silver films under exactly controlled conditions. The fact that the thick films nevertheless gave undistorted (100) diffraction patterns in all cases warrants the conclusion that the technique is quite reliable. Since the contact potential method of determining work functions measures the average work function of a surface without weighting regions of abnormally high or low work function, vestiges of the original interstitial regions persisting in a thick film might be expected to have little influence upon measurements made by this method.

Most of our preliminary measurements were made before the more definitive structural results appeared. The conditions under which silver films of good electrical conductivity are formed, a consideration which did not enter into the structural work, were determined empirically. In the first tube to be constructed after the more obvious requirements for a satisfactory technique had been determined, the Ag(rocksalt) film was deposited at such a low vapor stream intensity that a 90-minute exposure was required to form a semi-opaque film at a target temperature of 200°C. The electrical conductivity of this film was somewhat erratic; it behaved as if composed of a mosaic of large patches separated by crevasses extending to the rocksalt surface. For a position of the contact which established a conducting path through the film, a contact p.d. of 0.12 v was observed between this film and the Ag(glass) films.[13] In our latest measurements, the results of which are described below, the rate of deposition of the Ag(rocksalt) films has been so increased as to form an opaque film in from 20 to 30 minutes at a target temperature of 200°C, i.e., at a rate comparable to that employed in the later electron diffraction studies. These films showed a normal conductivity and, except for their fragility, could be measured with all the ease and precision of silver films on glass.

[13] P. A. Anderson, Phys. Rev. **56**, 850 (1939).

The Contact p.d. Between Ag(Rocksalt) and Ag(Glass)

Measurements on two Ag(rocksalt) films, prepared in two different tubes at the higher deposition rates described above, against two series of Ag(glass) films have given contact potential values lying within the extreme limits of 0.29–0.35 v. As in all the preliminary as well as final measurements, the Ag(rocksalt) films were electronegative with respect to the Ag(glass) surfaces. The reproducibility was of the same order as that found in previous measurements on Ag(glass)—barium.[7] Deviations from the mean value of 0.32 v appeared to be due largely to work function variations between the fourteen individual Ag(glass) films included in the final set of measurements. As described above, barium was deposited on both the Ag(glass) and Ag(rocksalt) surfaces after these surfaces had been measured against each other. The contact difference of potential Ag(glass)—Ba so determined was 1.95 $\pm$0.02 v, in close agreement with our previous value of 1.94 v obtained with both silver and barium at liquid-air temperature.[7] Since the difference between the room and liquid-air temperature values is less than the reproducibility of either set of measurements it cannot, of course, throw light on the temperature dependence of this contact p.d., except to indicate that the temperature coefficient is probably very small. The contact p.d. between barium and Ag(rocksalt) differed from that for Ba-Ag(glass) by values which fell within the limits of reproducibility for Ag(glass)-Ag(rocksalt). This result indicates that the structure of the silver substrate had no profound effect upon the structure, or at least on the work function, of a thick barium film deposited upon it at room temperature. During the preliminary measurements an interesting incidental observation was made on a Ag(glass) film deposited at a target temperature of 200°C. The silver film thus prepared had the characteristic "milky" appearance associated with partial

agglomeration and was 0.09 v electronegative with respect to a mirror-like silver film formed by condensation on glass at room temperature.

The Work Function of Polycrystalline Silver

Combination of our value for the contact p.d. between Ag(glass) and vaporized barium, 1.95 v, with the work function of vaporized barium, established at 2.52 ev by the careful work of Jamison and Cashman,[14] assigns the value 4.47 ev to the work function of Ag(glass) films deposited and measured at room temperature. Although this value agrees closely with our previous value of 4.46 ev for silver films deposited at liquid-air temperature, a recent paper by Farnsworth and Winch[2] makes necessary a re-examination of the question of the work function which is to be assigned to polycrystalline silver. As has been pointed out previously,[7] the "polycrystalline state" appears to have distinctive meaning in work function measurements only when defined as a microcrystalline aggregate in which the crystallites, especially those crystallites exposed at the surface of the specimen, are oriented entirely at random. That such a definition is imperative is indicated by the fact that any group of crystallites which expose only faces of a single orientation must give the work function characteristic of that orientation alone. When silver is deposited on glass at liquid-air temperature, the condition of random orientation is probably satisfied as closely as is possible in practice. But in discussing our work function value for silver films thus prepared, Farnsworth and Winch compare it directly with Winch's early value of 4.74 ev, obtained for a silver wire outgassed by heating for 1200 hours at temperatures up to 850°C.[15] They assume implicitly that agreement between these two values is to be expected. It should be pointed out, in the first place, that Farnsworth and Winch's suggestion that the discrepancy in question may be due to a diffusion of barium through our silver films is rendered untenable by our measuring technique. As described explicitly in our previous paper,[7] the potential setting for silver was obtained not from measurement of a single silver film laid down on barium but from a succession of silver-on-silver films. Each silver film, measured as laid down, showed no significant deviation from the potential setting for films preceding and succeeding it in the series. This procedure completely excludes any possibility of errors originating either in the diffusion of barium or in the persistence of incompletely covered patches of the substrate. Incidentally to the present work, furthermore, the silver films were deposited directly on glass and measured before any barium was introduced into the measuring chamber. In our earlier paper[7] the discrepancy was attributed tentatively to a difference in surface structure between (1) silver deposited from the vapor at liquid-air temperature, and (2) silver with the structure of Winch's heat-treated wire. Considered in the light of crystal growth theory,[16] now well established and known to determine the development of crystal faces by thermal etching as well as by atom-by-atom growth, Farnsworth and Winch's own recent measurements lend strong support to this conclusion. The prolonged heating of Winch's silver wire must have produced extensive recrystallization with growth of a relatively small number of crystallites of preferred orientation. Furthermore, and as remarked by Winch, extensive thermal etching occurred. The Kossel-Stranski theory, as applied to the face-centered cubic metals, shows that the crystal facets developed by the thermal etching of any metal of this class will consist predominantly of the crystal planes of densest packing. It is probable, therefore, that the surface of Winch's wire consisted predominantly of facets bounded by (111) planes. If, now, we compare Winch's work function value, 4.74 ev, with the value of Farnsworth and Winch for the (111) face of a single crystal of silver, 4.75 ev, we have strong evidence for the conclusion that Winch's value is to be identified with Ag(111) rather than with randomly oriented polycrystalline silver. It should be remarked that Farnsworth and Winch's recent work indicates that both their value for Ag(111) and that of

[14] N. C. Jamison and R. J. Cashman, Phys. Rev. **50**, 624 (1936).
[15] R. P. Winch, Phys. Rev. **37**, 1269 (1931).
[16] W. Kossel, *Leipziger Vorträge* (Hirzel, Leipzig, 1928); I. N. Stranski, Zeits. f. physik. Chemie **B11**, 342 (1930); A. Smekal, *Handbuch der Physik* (Julius Springer, Berlin, 1933), Vol. 24, No. 2, p. 809.

Winch refer to surfaces contaminated by an equilibrium layer of gas.

The Work Function of Ag(Rocksalt); of Ag(100)

A simple computation, similar to that described above for Ag(glass) films, assigns the value 4.79 ev to the work function of silver films deposited on rocksalt. As described in detail earlier in this report, electron diffraction studies have shown that thick Ag(rocksalt) films give undistorted (100) patterns when they are deposited under conditions similar to, but less favorable than, those realized in the present work. We are justified therefore in tentatively identifying the work function observed for Ag(rocksalt) with the work function of Ag(100). It is conceivable that vestigial regions with symmetry lower than (100) may persist even in a thick Ag(rocksalt) film to a degree insufficient to be detectable in electron diffraction photographs but sufficient to affect a work function measurement. Since it is, of course, impossible to obtain an ideal crystal face by any experimental means whatever, the question of the magnitude of errors originating in deviations from the ideal structure can be answered only by independent measurements on a large number of surfaces known to approximate this structure. The deviations in question must be to some extent accidental and if it is found eventually that satisfactory reproducibility can be obtained for a sufficiently large number of surfaces it may be possible to conclude that the error involved in identifying the observed work function with ϕ_{100} is negligible.

In their thorough study of a massive single crystal of silver, Farnsworth and Winch[2] obtain the value 4.81 ev for the work function of a (100) face. From observations on the effect of depositing vaporized silver upon it, they conclude that this face was contaminated with gas and that the value 4.81 ev is therefore characteristic of Ag(100) so contaminated. The deposition of the fresh silver film lowered the work function and, considering only the effects of gas contamination, their measurements could be interpreted as indicating that the true value of ϕ_{100} is in fact lower than 4.81 ev. But the surface formed by the deposition of silver vapor, apparently on the cold monocrystal, was found to deviate markedly from the (100) structure and the complications introduced by simultaneous changes in both structure and gas contamination make it difficult to appraise the influence of either factor alone. The agreement between the two values for ϕ_{100} is better than the probable experimental error involved in either set of measurements would lead us to expect and is probably, to some extent at least, fortuitous. The main significance of the present work is its indication that the condensation of metal vapors on monocrystalline dielectrics promises to furnish a convenient and reliable method for preparing, in the measuring tube itself, metal surfaces of known and reproducible structure which are free from contaminations and the effects of mechanical working. The method appears to be immediately applicable to Ni, Cu, Pd, Al and Au.

Letters to the Editor

PROMPT publication of brief reports of important discoveries in physics may be secured by addressing them to this department. Closing dates for this department are, for the first issue of the month, the eighteenth of the preceding month, for the second issue, the third of the month. Because of the late closing dates for the section no proof can be shown to authors. The Board of Editors does not hold itself responsible for the opinions expressed by the correspondents.

Communications should not in general exceed 600 words in length.

Mechanism of Deuteron-Induced Fission

N. BOHR
Institute of Theoretical Physics, University of Copenhagen, Copenhagen, Denmark
May 8, 1941

IN nuclear transformations initiated by deuteron impact, two types of processes are, as well known, to be taken into consideration. In the process of the first type (process I), the intermediate state is formed by the capture of the whole deuteron by the nucleus; in the process of the second type (process II), the deuteron breaks up during the impact with the result that the proton escapes and only the neutron is taken up in the compound nucleus. As originally pointed out by Oppenheimer and Phillips[1] and more closely discussed by Bethe,[2] the cross section for the formation of the compound system may, under certain circumstances, be considerably larger in process II than in process I. Still, a clear discrimination between the two types of processes by means of ordinary nuclear transformations seems so far to have met with difficulties, and it may, therefore, be of interest to point out that the study of deuteron-induced fission of heavy nuclei offers new possibilities for such a discrimination.

Not only is fission easily distinguished from other possible transformations but, in particular, a certain critical excitation energy different for different nuclei is necessary for fission to occur. Just as regards the excitation of the compound nucleus, the processes I and II differ essentially. While the excitation obtained by process I will be far greater than the neutron binding energy for all nuclei concerned, it will, in process II, on the average be smaller than this energy. Since, for the abundant uranium isotope, as well as for thorium, the critical fission energy is higher than the neutron binding energy, it was concluded[3] that a considerable output of nuclear fission in thorium and uranium could only be expected in processes of type I. Even if, in certain deuteron energy regions, processes of type II should be more probable, they would almost entirely result in a permanent capture of a neutron with formation of radioactive uranium and thorium isotopes with well-known periods.

One of the possibilities of testing these arguments is offered by a comparison between the fission yields in uranium and thorium. This is possible because the probability of fission of the compound nucleus in process I may be estimated with a high degree of approximation. In fact, the excitation energy in process I will not only be sufficient for fission to occur in competition with neutron escape, but even the excitation of the residual nucleus left after the escape of a neutron will be large enough to make a fission quite probable. The total probability for fission of the compound nucleus in such successive transformations was thus estimated[4] to be nearly 1 for uranium and about 0.8 for thorium. These expectations seemed confirmed by the experiments reported by Jacobsen and Lassen[5] who found that the ratio of the fission cross sections in uranium and thorium at 9-Mev deuteron energy was approximately 0.7.

In a later discussion of these experiments,[6] however, it has been realized that the cross section for the formation of the compound system in process I, because of the smaller nuclear charge, must be expected to be 25 percent greater in thorium than in uranium. If the whole fission effect in both elements was due to processes of this type, the theoretically estimated ratio of the fission yields in thorium and uranium should, consequently, instead of 0.8, be about 1.0. The difference between this last figure and the measured value 0.7 seems too great to be explained, unless it is assumed that a considerable part of the effect, at any rate in uranium, is due to processes of type II. A support of this conclusion is also offered by a closer comparison of the fission effects in thorium and uranium for smaller deuteron energies. Thus, in the experiments of Jacobsen and Lassen the fission cross section for deuteron energies about 8 Mev is relatively higher in uranium than in thorium, as would be expected if a part of the effect in uranium sets in for lower energy values.

A contribution of process II to the fission effects which is relatively greater in uranium than in thorium may be expected from the fact that the critical fission energy of the compound nucleus for thorium is almost 2 Mev higher than the neutron binding energy, while, for the abundant uranium isotope (238), the difference is smaller than 1 Mev. Moreover, in the energy region concerned, where the fission cross section is less than 1 percent of the geometrical nuclear cross section, it is possible that a not inconsiderable contribution is due to the lighter rare uranium isotope (235). Since, for this isotope, the critical fission energy of the compound nucleus in process II is about 1 Mev lower than the neutron binding energy, the probability of fission may, for the low excitations obtained by such a process, be far greater than for the heavy isotope.

To clear up the different questions raised, it would be very desirable that experiments on deuteron-induced fission be extended to a region of greater deuteron energies, and, especially, that such experiments be performed with separated uranium isotopes and with protactinium, for which the critical fission energy of the compound nucleus is nearly equal to the neutron binding energy.[7]

[1] J. R. Oppenheimer and M. Phillips, Phys. Rev. **48**, 500 (1935).
[2] H. A. Bethe, Phys. Rev. **53**, 39 (1938).
[3] N. Bohr and J. A. Wheeler, Phys. Rev. **56**, 449 (1939).
[4] N. Bohr, Phys. Rev. **58**, 864 (1940).
[5] J. C. Jacobsen and N. O. Lassen, Phys. Rev. **58**, 867 (1940).
[6] J. C. Jacobsen and N. O. Lassen, Det Kgl. Danske Vidensk. Selsk. Math.-fys. Medd. (Math.-phys. Comm., Acad. Sci. Copenhagen), in print.
[7] N. Bohr and J. A. Wheeler, Phys. Rev. **56**, 1065 (1939).

Fission Cross Section in Uranium and Thorium for Deuteron Impact

J. C. JACOBSEN AND N. O. LASSEN
Institute of Theoretical Physics, University of Copenhagen, Copenhagen, Denmark
May 8, 1941

AS reported in a previous note,[1] experiments have been carried out with the cyclotron in this institute to investigate the cross section for fission in thorium and uranium produced by impact of deuterons with different energies. The fission outputs were determined by collecting the radioactive fragments on aluminum foils facing the targets and screened from the deuteron beam. Because of the difficulty of estimating the number of fission processes from the β-radioactivity of these foils, a considerable uncertainty, however, was involved in the determination of the absolute value of the fission cross section.

In continued experiments, this uncertainty has been reduced by a calibrating procedure in which two thin uranium targets were exposed to neutron impact. One of the targets was placed in a small ionization chamber and the number of fission particles emitted from this target counted by a linear amplifier. The fission particles from the second target were collected on a thin lead foil; the distance between the two targets was sufficiently small to ensure that the neutron intensity was very nearly the same. By measuring the activity of the collecting foil with the same counting arrangement as in the experiments with deuterons, the ratio between the foil activity and the number of fission particles emitted during the irradiation could thus be determined.

Instead of the preliminary value of $0.5\cdot10^{-26}$ cm^2 given in the previous note, the measurements thus calibrated gave now the value $(2.2\pm1)\cdot10^{-26}$ cm^2 for the fission cross section in uranium at 9-Mev deuteron energy. The results found for the variation of the cross section with deuteron energy and the ratio between the cross sections in thorium and uranium given in the note remain, of course, unaltered. From the value 0.7 for the last ratio, which agrees with the independent determination by Krishnan and Banks,[2] we obtain in consequence, $(1.5\pm0.7)\cdot10^{-26}$ cm^2 for the fission cross section in thorium at 9-Mev deuteron energy.

Details of the experiments are described in a paper in print in the *Communications of the Copenhagen Academy of Sciences* where, also, a description of the cyclotron has just been published.[3]

[1] J. C. Jacobsen and N. O. Lassen, Phys. Rev. **58**, 867 (1940).
[2] R. S. Krishnan and T. E. Banks, Nature **145**, 860 (1940).
[3] J. C. Jacobsen, Det Kgl. Danske Vidensk. Selsk. Math.-fys. Medd. **19**, 2 (1941).

The Resistivity of Interstellar Space

FRED L. MOHLER
National Bureau of Standards, Washington, D. C.
May 5, 1941

IN a paper by Foster Evans on "Electric fields produced by cosmic rays,"[1] the conductivity of interstellar space has been computed on the assumption that electrons are scattered by neutral atoms with a collision radius of 10^{-8} cm. He assumes that there are two neutral atoms, one ion and one electron per cm^3 and that the electron temperature is 10,000°K. For these conditions the collision radius for a collision between an electron and a positive ion[2] is 50×10^{-8} cm so that the scattering by neutral atoms is entirely negligible. The mean free path is about 5×10^{13} cm and not 10^{15} cm as estimated by Evans.

The resistivity is given by the equation for an ionized gas[2]

$$R=\frac{1.48\times10^4}{T_e^{\frac{3}{2}}}\log 0.72\times10^6\frac{T_e^{\frac{3}{2}}}{N_+^{\frac{1}{2}}},$$

where R is resistivity in ohm-centimeters, T_e is electron temperature and N_+ is the number of ions per cm^3. The above numerical values give the resistivity of interstellar space as 0.2 ohm-centimeter; a value comparable with the resistivity of an intense low pressure discharge. The resistivity is extremely insensitive to variations in the number of ions or in the degree of ionization provided more than 1 percent of the atoms are ionized, and it remains of the same magnitude even within a stellar atmosphere. While this is a higher resistivity than assumed by Evans, it does not change the general conclusion of his paper that interstellar space is an equipotential region and that no conceivable energy source can change the potential of a star by more than a few volts.

[1] Foster Evans, Phys. Rev. **59**, 1 (1941).
[2] S. D. Gvosdover, Physik. Zeits. Sowjetunion **12**, 164 (1937).

Are There Spin One Mesotrons?

H. SNYDER
Department of Physics, Northwestern University, Evanston, Illinois
May 27, 1941

THE work of Christy and Kusaka[1] shows that the mesotrons which are mainly responsible for bursts at low altitudes cannot be particles of spin one, probably have spin zero, though possibly spin one-half. If mesotrons are responsible for nuclear forces, and if they do not have spin one-half, then the known spin dependence of nuclear forces demands that, in addition to mesotrons of spin zero, there must be particles of spin one. The experiments of Schein, Jesse and Wollan[2] indicate that the incident radiation is protonic and that the mesotrons are probably produced in multiple nuclear processes. If these things are true, it is extremely difficult to believe that mesotrons of spin one are not produced in addition to those of spin zero. Since such particles are not present in appreciable amounts at low altitudes, they must be highly absorbable. The radiative cross sections for particles of spin one are not adequate to account for so high an absorption. However, if spin one mesotrons disintegrate with a lifetime of about 10^{-8} second there is no contradiction with cosmic-ray evidence. This lifetime would be satisfactory for the mesotron theory of β-decay.

[1] R. F. Christy and S. Kusaka, Phys. Rev. **59**, 414 (1941).
[2] Learned in conversation with M. Schein.

On Secondary Slow Mesotrons

V. I. Veksler and N. A. Dobrotin
Physical Institute, Academy of Sciences of the USSR, Moscow, USSR
March 28, 1941

RECENTLY many investigators[1] have reported that observations at high elevations (8–9 km) point to an unexpectedly large amount of slow mesotrons in the cosmic radiation. These observations indicate that the processes of production of mesotrons play an important role, not only in the stratosphere but also at considerably lower elevations. Rossi and Regener[2] have recently performed some very elaborate experiments which enabled them to detect the formation of secondary penetrating particles at a height of only 4200 meters above sea level.

It ought to be mentioned that our experiments, carried out on Mount Elbrus, Caucasus, at a height of 4250 m, according to a completely different method yielded similar results as early as 1937.[3]

In 1936 we developed a method based on the utilization of the so-called proportional counters for observing the heavily ionizing particles of the cosmic radiation. The sensitivity of the counters used was such that the only particles recorded with a probability close to unity were those which caused an ionization exceeding by at least 3 to 6 times the value corresponding to the minimum of the ionizing agents; i.e., an ionization at least 3–6 times greater than that of fast electrons with energies of the order of several Mev.[4]

Coincidences in two groups of such counters, placed one above the other (the counters of each group were connected in parallel and placed inside thin-walled metallic boxes), were registered as usual. These coincidences are caused by showers as well as by slow ionizing particles. The coincidences caused by single slow mesotrons can be eliminated by interposing a thin layer between the boxes.[5] Thus, the number of coincidences eliminated by the layer determines the number of these slow mesotrons.

Observations on Elbrus[6] in 1938 and 1939 showed that the number of particles absorbed by a layer 0.5 g/cm² thick comprise approximately 0.1 percent of the total number of the penetrating particles. By examining the shape of the absorption curve and the dependence of the number of particles absorbed on the sensitivity of the counters, we conclude that the particles thus counted are, in the main, slow mesotrons at the end of their paths and that they possess kinetic energy of the order of 10^7 ev.[7]

The value of percentage of these particles per one penetrating particle (0.1 percent) excludes the possibility that we are dealing with the ends of the paths of the primary mesotrons themselves.

It is essential to point out that, according to our data, the number of slow mesotrons remains practically unchanged when the whole arrangement is placed under 30 cm of Pb.

In order to check directly the hypothesis of the secondary nature of the registered particles, and also to obtain data on the distribution of their total ranges, observations were carried out at the same height in the summer of 1940. The arrangement employed is shown in Fig. 1.

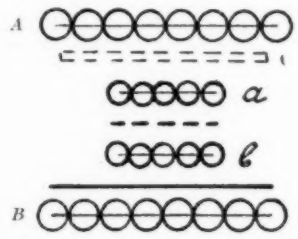

FIG. 1. Arrangement of counters.

In order to reduce the number of pulses due to showers, we employed an anticoincidence circuit. The particles under investigation, recorded previously by means of a layer introduced between the two proportional counters *a* and *b*, were now absorbed by a screen (0.7 g/cm²) interposed between *b* and *B* and did not cause impulses in the anticoincidence counter *B*, whereas showers actuated this counter as well.

In distinction to the previous circuit, only threefold coincidences *Aab* were recorded (with and without the layer) which did not coincide with impulses in *B*, in other words, the coincidences *Aab*−*B*. We note here that *A* and *B* are not proportional counters. Filters of various thicknesses were introduced between *A* and *a*.

The results of these observations are summarized in Table I. They give a direct proof of the secondary nature of the particles observed; their amount decreases rapidly when the thickness of the layer between *A* and *a* increases.

The experiments described here do not permit us to conclude with absolute certainty that the particles we observed are generated by a non-ionizing penetrating component. However, they are in complete accord with this hypothesis which we arrived at as a result of some of our previous observations.[6, 8]

It is possible that the phenomenon we observed is identical with that observed recently by Rossi and Regener[2] under different conditions. However, whereas the observa-

TABLE I. *Summary of data.*

	Without Interlayer between *A* and *α*		0.85 g/cm² Cu between *A* and *α*		17 g/cm² Pb between *A* and *α*	
	Without Interlayer between *a* and *b*	1.35 g/cm² between *a* and *b*	Without Interlayer between *a* and *b*	1.35 g/cm² between *a* and *b*	Without Interlayer between *a* and *b*	1.35 g/cm² between *a* and *b*
No. of impulses per min.	0.916 ±0.03	0.630 ±0.62	0.803 ±0.03	0.515 ±0.03	0.805 ±0.03	0.697 ±0.025
Difference	0.285 ±0.04		0.188 ±0.042		0.108 ±0.037	

tions of these investigators do not yield direct evidence on the nature of the recorded particles (they could have been protons as well as mesotrons) it can be asserted that in our experiments mesotrons were observed. Our experiments also bring to light an essential singularity—the predominance of secondary slow particles with exceedingly small ranges.

The authors express their gratitude to Professor D. V. Skobelzyn for helpful suggestions and valuable discussions of results.

[1] G. Herzog, Phys. Rev. **57**, 337 (1940); M. Schein, E. O. Wollan, G. Groetzinger, Phys. Rev. **58**, 1027 (1940); G. Herzog, Phys. Rev. **59**, 117 (1941); G. Herzog and W. H. Bostick, Phys. Rev. **59**, 122 (1941).
[2] B. Rossi and H. Regener, Phys. Rev. **58**, 837 (1940).
[3] V. Veksler and B. Isajev, Comptes rendus Acad. Sci. USSR **17**, 189 (1937); V. Veksler and N. Dobrotin, Comptes rendus Acad. Sci. USSR **19**, 479 (1938).
[4] The probability of such electrons having been recorded by our counters is exceedingly small.
[5] The cathodes of the counters were made of brass nets; the walls of the boxes which enclosed the counters were 0.09 g/cm² thick.
[6] V. Veksler, K. Alekseeva and N. Reynov, Comptes rendus Acad. Sci. USSR **21**, 122 (1938); V. Veksler and N. Dobrotin, Bull. Acad. Sci. USSR, Série Physique **4**, 260 (1940).
[7] These observations also pointed to the existence of heavily ionizing particles with essentially longer ranges of the order of a few grams per cm², i.e., apparently slow secondary protons.
[8] V. Veksler and N. Dobrotin, Comptes rendus Acad. Sci. USSR **25**, 103 (1939).

Time Lags in Geiger-Müller Counter Discharges

C. G. MONTGOMERY AND D. D. MONTGOMERY
Sloane Physics Laboratory, Yale University, New Haven, Connecticut
June 2, 1941

SOME time ago we reported[1] the existence of delayed counts in Geiger-Müller counters in which the appearance of a potential on the counter wire did not take place until several microseconds after the formation of the primary ions responsible for the discharge. We suggested that the cause of this long time lag was the capture of the electrons of the primary ion pairs, forming negative molecular ions which moved relatively slowly into the region of the counter wire. In this region of high field strengths, the molecular ions were broken up and the electrons released were multiplied by the ordinary processes of ionization by collision. These long-time lags are not to be confused with the shorter ones which represent the periods necessary for the building up of the space charge around the counter wire.

Some new experiments have been performed to establish the correctness of this explanation, and to measure the capture probabilities. A counter 18 mm in diameter and 120 mm long, with an oxidized copper cathode, was used. Ultraviolet light could strike the interior of the cathode by passing through a quartz window and a small hole in the cathode, and eject photoelectrons. The light was produced by a spark which caused, at the same time, an electrical pulse. The difference in time between the occurrence of this pulse and the beginning of the change of potential of the counter wire was measured by a vacuum-tube circuit of the type previously described.[1]

If n is the average number of photoelectrons produced by a spark, then the fraction f of the number of sparks which cause a counter discharge is $f=1-e^{-n}$. If α is the probability that an electron be captured in such a manner as to produce a time lag greater than a given amount τ, then the probability p that the spark will give rise to a delayed counter discharge is

$$P=\sum_{m=1}^{\infty}\alpha^m\frac{e^{-n}n^m}{m!}=(e^{\alpha n}-1)e^{-n},$$

since all of the electrons must be captured if the count is to be delayed. Hence, by measuring p and f, n and α may be determined. If the proposed explanation for the delayed counts is correct, then the values α calculated in this way should be independent of n for a given pressure and composition of the gas in the counter. Thus, measuring α provides a sensitive test of the correctness of the picture.

TABLE I. *Values of the probability α that an electron will be captured so as to produce a time lag greater than τ.*

ELECTRONS PER SPARK, n	0.22	0.41	0.64	MEAN
τ, microseconds				
1.4	0.40	0.42	0.39	0.40
2.3	0.19	0.17	0.18	0.18
3.7	0.08	0.10	0.08	0.08

An example of the results of such a test is shown in Table I. The counter was filled with a mixture of argon with six percent oxygen at a pressure of 104.5 mm of mercury. For a given time lag the values of α are the same within the accuracy of the observations.

Other observations show that α increases with increasing pressure. From the knowledge of the time of travel of the negative molecular ions, we can estimate the capture cross section of an electron by an oxygen molecule to be of the order of 10^{-18} cm². This is in agreement with the results of Rose and Ramsey,[2] and other more direct determinations.

If the primary ions are produced within the gas of the counter, as when gamma-rays or cosmic rays are being counted, then both n and α increase with the pressure of the counter gas. Hence, as the pressure is increased, the probability of a delayed count p first increases, reaches a maximum value, and then decreases again.

[1] C. G. Montgomery, W. E. Ramsey, D. B. Cowie and D. D. Montgomery, Phys. Rev. **56**, 635 (1939).
[2] M. E. Rose and W. E. Ramsey, Phy. Rev. **59**, 616 (1941).

Superconducting Films as Radiometric Receivers

D. H. ANDREWS, W. F. BRUCKSCH, JR., W. T. ZIEGLER AND E. R. BLANCHARD
The Johns Hopkins University, Baltimore, Maryland
May 31, 1941

THREE years ago a series of experiments was undertaken to investigate the usefulness of superconducting films as resistance thermometers in the measurement of small quantities of energy[1] and in particular as receivers in radiometers. The latter application has since been suggested independently by A. Goetz.[2] Because of the interest in the optical properties of superconducting surfaces and the possibilities of this new radiometric method in the infrared, we are presenting a few preliminary results at this time.

Lead films were prepared[3] by evaporating the metal on clean glass in a high vacuum giving a bright metallic

mirror-like surface. The glass was in the form of a ribbon 1.5 cm long, 1 mm wide and 25μ thick, fused to a glass plate at the ends in such a way that the ribbon bowed up slightly in the middle. Contacts were made by means of platinum wires sealed into the glass at the ends of the ribbon. This "receiver" was placed on a thin copper base-plate suspended on quartz fibers attached to a small heavy-walled copper vessel in which the liquid helium was made by the Simon expansion method. Our most sensitive film had a transition zone roughly 0.02° wide in which the resistance varied from 100 ohms (normal) to 10^{-3} ohm (superconducting). The estimated thickness of the film was 10 mμ. Other films studied varied in thickness up to 500 mμ and had correspondingly lower resistances. By means of a small electrical heating coil attached to the base-plate, the temperature of the film was maintained in the middle of the "steep" portion of the transition during the radiation measurement. Judging from the observed fluctuation in resistance of the lead film, the temperature was maintained effectively constant to within 10^{-6} degree.

The source of radiation was a blackened copper disk, electrically heated and with thermocouple attached. It was suspended about 5 cm above the receiver, with shutter and diaphragms in between so that measured amounts of energy could be transmitted.

The potential drop across the film was measured with a potentiometer circuit, the galvanometer beam having a deflection of 1 cm per μv. Radiation was flashed on the receiver from the radiator at a series of temperatures from 15°K to 150°K. The receiver was at a temperature of about 7°K and the shutter at 14°K.

The largest ratio of potential drop to input of radiant energy was obtained with the unblackened 10 mμ film. This receiver (glass+lead) had a heat capacity of about one erg deg.$^{-1}$. A beam of radiant energy, 6 erg sec.$^{-1}$, produced a galvanometer deflection corresponding to about 6 millivolts in less than 1 sec. This is equivalent to a sensitivity of 10^{-4} erg sec.$^{-1}$ per mm deflection. Blackening the lead surface with a thin layer of cobalt oxide produced no appreciable increase in sensitivity.

Because of temperature fluctuations in the receiver, this sensitivity of 10^{-4} erg sec.$^{-1}$ per mm deflection was too high to permit accurate measurements. The highest precision obtained was in an experiment with the radiator at 35°K. A beam of 2×10^{-3} erg sec.$^{-1}$ gave a deflection of 7 mm. The probable error corresponded to 1.5 mm, giving a precision of measurement of 4×10^{-3} erg sec.$^{-1}$.

It appears that the ratio of potential drop to radiant energy input is several orders of magnitude higher than in the other methods for measuring radiation in the infra-red region, and that the possibilities for sensitivity and precision are correspondingly high. It is probable that, with superconducting receivers of higher resistance, more sensitive galvanometer systems, and better temperature control, the precision can be improved considerably beyond the results reported here.

We wish to express our appreciation to Professor A. H. Pfund for helpful advice and suggestions. Grateful acknowledgment is made of a grant-in-aid from Research Corporation.

[1] D. H. Andrews, Am. Phil. Soc. Year Book (1938), p. 132.
[2] A. Goetz, Phys. Rev. **55**, 1270 (1939).
[3] W. F. Brucksch, Jr., W. T. Ziegler, E. R. Blanchard and D. H. Andrews, Phys. Rev. **59**, 688 (1941).

Production of Radioactive Hydrogen by Neutron Bombardment of Boron and Nitrogen

R. Cornog and W. F. Libby
Radiation Laboratory, Department of Chemistry, University of California, Berkeley, California
May 13, 1941

SATURATED water solutions containing an excess of boric acid crystals, or of ammonium nitrate crystals, were bombarded for several thousand microampere hours by fast neutrons produced by the $Be^9(d, n)B^{10}$ reaction, with 16.5-Mev deuterons. In all cases the water surrounding the crystals, when placed as water vapor in a Geiger-Müller counter, showed an activity of approximately 10^4 counts per mole per second. Control samples of distilled water had less than five percent as much activity.

The following reactions are energetically possible, with 20 Mev as the upper limit of the neutrons used:

$$_5B^{10}+{}_0n^1\rightarrow[{}_5B^{11}]^*\rightarrow{}_4Be^8+{}_1H^3+Q_1 \qquad (1)$$
$$_4Be^8\rightarrow 2{}_2He^4$$
$$_5B^{11}+{}_0n^1\rightarrow[{}_5B^{12}]^*\rightarrow{}_4Be^9+{}_1H^3+Q_2 \qquad (2)$$
$$_7N^{14}+{}_0n^1\rightarrow[{}_7N^{15}]^*\rightarrow{}_6C^{12}+{}_1H^3+Q_3 \qquad (3)$$
$$_7N^{14}+{}_0n^1\rightarrow[{}_7N^{15}]^*\rightarrow 3{}_2He^4+{}_1H^3+Q_5 \qquad (3a)$$
$$_7N^{15}+{}_0n^1\rightarrow[{}_7N^{16}]^*\rightarrow{}_6C^{13}+{}_1H^3+Q_4 \qquad (4)$$

where $Q_1=+0.2$ Mev; $Q_2=-9.6$ Mev; $Q_3=-4.3$ Mev; $Q_4=-10.1$ Mev; $Q_5=-11.5$ Mev.

Reaction (1) might be expected, since the compound nucleus formed has already been observed to yield radioactive hydrogen.[1]

Since only 0.38 percent of the bombarded nitrogen was N^{15}, it is not likely that reaction (4) was primarily responsible for the observed activity.

The total neutron output of the 60-inch cyclotron has been recently measured by Dr. Emilio Segrè and Mr. Hubert Yockey. Using their unpublished and preliminary result of one neutron per 200 deuterons, and 31 years as the half-life,[2] one may obtain a rough value for the reaction cross sections. Assuming that (1) and (2) are involved for boron, and (3) and (3a) are involved for the nitrogen, one obtains for both elements approximately 10^{-26} cm^2 as the fast neutron cross section for the production of hydrogen three. It is estimated that these values for both cross sections may be in error by a factor of five.

We wish to thank Professor E. O. Lawrence and the entire staff of the Radiation Laboratory for their interest and cooperation in all phases of this work.

[1] R. D. O'Neal and M. Goldhaber, Phys. Rev. **57**, 1086 (1940).
[2] R. D. O'Neal and M. Goldhaber, Phys. Rev. **58**, 574 (1940).

Author Index to Volume 59

References with (A) are to abstracts of papers presented at meetings of the American Physical Society. References with (L) are to Letters to the Editor and those with (T) designate title only.

Adams, F. W., Lee Devol and H. R. Letner. Instrument for studying the topographies of fine textured surfaces—684(A)

Adel, Arthur. Equivalent thickness of the atmospheric nitrous oxide layer—944(A)

—— Grating map of the infra-red solar spectrum: 14 mu to 2 mu—915(A)

Allen, James S. Measurement of the intensity of x-rays of wave-length 0.14A to 1.0A by means of an electron multiplier tube—110(A)

Allis, W. P. (see Brown, Sanborn C.)—932(A)

Allison, Samuel K., Leonard C. Miller, Lester S. Skaggs and Nicholas M. Smith, Jr. Electrostatic deflection studies of alpha-particles; the alphas from Li^6 (p,α) He^3—108(A)

Amdur, I. and H. Pearlman. Estimation of interaction potentials from molecular scattering experiments—689(A)

Anderson, E. E. (see Mack, J. E.)—683(A)

—— **and J. E. Mack.** Low terms in Co VII and Ni VIII—106(A), 717

Anderson, H. H. (see Valley, G. E.)—113(A)

Anderson, H. L., E. Fermi and A. V. Grosse. Branching ratios in the fission of uranium (235)—52

Anderson, Paul A. New technique for preparing monocrystalline metal surfaces for work function study. The work function of Ag (100)—1034

Andrews, D. H. (see Brucksch, W. F., Jr.)—688(A)

——, **W. F. Brucksch, Jr., W. T. Ziegler and E. R. Blanchard.** Superconducting films as radiometric receivers—1045(L)

Arakawa, H. (see Nishina, Y.)—679(L)

Atanasoff, John V. and Philip J. Hart. Dynamical determination of the elastic constants and their temperature coefficients for quartz—85

—— **and Erwin Kammer.** Determination of the c_{44} elastic constant for beta-quartz—97

Atwood, H., Jr. (see Colwell, R. C.)—935(A)

Avrami, Melvin. Granulation, phase change, and microstructure—688(A)

—— Temperature distributions in hollow cylindrical systems—691(A)

Bacher, R. F. (see Baker, C. P.)—332

Bacon, Ralph H., Edgar N. Grisewood and Carel W. van der Merwe. Radioactivity of Mn^{55} and I^{128}—531

Bailey, F. M. (see Fox, G. W.)—174

Bailey, H. H. (see DuMond, J. W. M.)—219(A)

Bailey, J. E. (see Colwell, R. C.)—935(A)

Bailey, L. E. (see Thaxton, H. M.)—474(A)

Bainbridge, K. T. (see Sherr, R.)—937(A)

Baker, C. P. and R. F. Bacher. Experiments with a slow neutron velocity spectrometer—332

Baker, Richard F. (see Cole, Kenneth S.)—685(A)

Ballard, Stanley S. and L. A. Dean. Soil studies with radioactive phosphorus: the phosphate fixation of soils—467(A)

Baltzer, O. J. (see Jauncey, G. E. M.)—699, 908(L)

Bancroft, Dennison. Velocity of longitudinal waves in cylindrical bars—588

—— (see Birch, Francis)—685(A)

Band, William (see Hsü, Hsien-yü)—1013

Banerjee, S. (see Krishnan, K. S.)—770(L)

Banks, Floyd R. Measurement of self-diffusion in zinc—376

—— **and Park H. Miller, Jr.** Measurement of self-diffusion in zinc single crystals—943(A)

Banning, Mary. Reflectivity of thin Al and Cu films in the ultraviolet—914(A)

Baños, Alfredo, Jr. (see Schremp, E. J.)—614(L)

Bardeen, J. Theory of superconductivity—928(A)

Barry, J. G. (see Johnson, T. H.)—470(A)

Barschall, H. H., R. Ladenburg and C. C. Van Voorhis. Elastic and inelastic scattering of 2.5-Mev neutrons—917(A)

Bartlett, J. H., Jr. and T. A. Welton. Scattering of fast electrons by heavy elements. II—281

Batdorf, S. B. and Roy Thomas. Burst production by mesotrons of spin one-half and zero magnetic moment—621

Bauer, W. M. and J. D. Cobine. Recovery of dielectric strength in high pressure a.c. arcs—115(A)

Beams, J. W. (see Stauffacher, Arthur L.)—468(A)

Bearden, J. A. (see Beeman, W. W.)—933(A)

—— (see Shaw, C. H.)—690(A)

—— **and G. Schwarz.** New evaluation of h/e—934(A)

—— **and T. M. Snyder.** X-ray spectra arising from the valence band—L transitions of tungsten, tungsten oxide (WO_3) and platinum—162

Beardsley, Niel F. Change in height of a mesotron-producing layer of air—402(L)

—— Correlation between cosmic-ray intensities and meteorological conditions over Washington for 1939—470(A)

—— Correlation between cosmic-ray intensity at Cheltenham and the air temperatures and pressures for 1939—233

—— Effect of external temperature on cosmic-ray intensity—931(A)

Beck, Clifford. Optimum liquid combinations in cloud chambers—910(A)

Becker, R. A. (see Bonner, T. W.)—215(A)

——, **W. A. Fowler and C. C. Lauritsen.** Short range alpha-particles from $F^{19}+H^1$—217(A)

Beeman, W. W. and J. A. Bearden. K-absorption edges of metal ions in solution—933(A)

Beers, Yardley. Precision method of measuring Geiger counter resolving times—932(A)

Beese, N. C. Radiant energy measurements with thermopiles—922(A)

Bell, M. E. and J. H. Findlay. Molybdenite as a new lubricant—922(A)
Bennett, F. D. (see Ham, W. R.)—939(A)
Bennett, W. E., T. W. Bonner, E. Hudspeth, H. T. Richards and B. E. Watt. Disintegration of carbon by deuterons—781
——, **T. W. Bonner, H. T. Richards and B. E. Watt.** High energy gamma-ray from Li+D—904(L)
——, **T. W. Bonner and Bob E. Watt.** Energy of the γ-rays from the disintegration of fluorine by protons and deuterons—793
Bergmann, Peter G. On relativistic thermodynamics—928(A)
Beringer, Robert and C. G. Montgomery. Collinear emission of annihilation quanta—933(A)
Bessey, William H. Reflection and diffraction of molecular beams at lithium fluoride cleavage surfaces—459(L)
Bethe, H. A. On the theory of secondary emission—940(A)
—— Theoretical extension of large air showers—684(A)
——, **G. Blanch, A. N. Lowan and R. E. Marshak.** Internal temperature-density distribution in the sun—467(A)
Bhabha, H. J. Protons of double charge and the scattering of mesons—100
Birch, Francis and Dennison Bancroft. Rigidity and internal friction of a glass in its softening range—685(A)
Birge, Raymond T. Value of the Rydberg constant—221(A)
Biscoe, J. (see Warren, B. E.)—688(A)
Blake, F. C. Order-disorder questions and certain spinels—477(A)
Blanch, G. (see Bethe, H. A.)—467(A)
Blanchard, E. R. (see Andrews, D. H.)—1045(L)
—— (see Brucksch, W. F.)—688(A)
Blewett, John P. and Simon Ramo. Dielectric constant of a space charge rotating in a magnetic field—922(A)
Bloom, L. R. (see Tykociner, J. T.)—115(A)
Boeker, G. F. (see Reber, R. K.)—938(A)
Bøggild, J. K., K. J. Brostrøm and T. Lauritsen. Range and straggling of fission fragments—275
Bohlke, P. G., T. R. Cuykendall and H. S. Sack. Some measurements of the temperature dependence of Young's modulus of β-brass and certain other metals—940(A)
Bohr, N. Velocity-range relation for fission fragments—270
—— Mechanism of deuteron-induced fission—1042(L)
Bonner, T. W. Precise determination of the energy of the neutrons from the deuteron-deuterium reaction—237
—— (see Bennett, W. E.)—781, 793, 904(L)
——, **R. A. Becker, S. Rubin and J. F. Streib.** Gamma-rays from C+H^2—215(A)
Booth, E. T. (see Grosse, A. V.)—322(L)
Borst, Lyle B. Deuteron-tritium reaction in nitrogen—941(A)
—— (see Newson, Henry W.)—941(A)
Bostick, W. H. (see Herzog, G.)—113(A), 122
Bowman, D. S. Term values in V II and Mn II—386
Bowman, D. W. (see Green, J. B.)—72, 106(A)
—— (see Hurlburt, E. H.)—106(A)
Bozorth, R. M. (see Williams, H. J.)—939(A), 1005
—— **and H. J. Williams.** Calculation of the torque on a ferromagnetic single crystal in a magnetic field—827
Bradner, Hugh (see Houston, W. V.)—219(A)
Brooks, Harvey. Rotational magnetic moments of H_2, HD and D_2—925(A)
Brostrøm, K. J. (see Bøggild, J. K.)—275
Brown, S. Leroy and Lisle L. Wheeler. Solving a type of nonlinear simultaneous equations with a mechanical harmonic synthesizer—468(A)
Brown, Sanborn C. Beta-ray energy of H^3—954
—— Energy of the H^3 beta-ray—687(A)
—— **and W. P. Allis.** Initial avalanche in discharge counter breakdown—932(A)
Brown, William Fuller, Jr. Dislocations and magnetization—528(L)
Browne, S. H. and C. T. Lane. Magnetic properties of antimony-tin crystals at low temperatures—939(A)
—— **and C. T. Lane.** Magnetic properties of antimony-tin monocrystals—476(A)
Broxon, James W. Cosmic-ray recurrences—470(A)
—— Geomagnetic character and cosmic-ray intensity pulses—678(L), 909(L)
—— Recurrence phenomena in cosmic-ray intensity—773
Brucksch, W. F., Jr. (see Andrews, D. H.)—1045(L)
——, **W. T. Ziegler, E. R. Blanchard and D. H. Andrews.** Critical currents in superconducting films—688(A)
Brunings, J. H. M. and J. K. Knipp. Range of intermediate ions—919(A)
Buechner, W. W. (see Van de Graaff, R. J.)—687(A)
Bueso-Sanllehí, F. Rotational analysis of the CO_2^+ band near 2900A—923(A)

Cady, Willoughby M. and D. H. Tomboulian. *L*-emission band of sodium—472(A)
—— **and D. H. Tomboulian.** *L*-emission bands of sodium, magnesium and aluminum—381
—— (see Tomboulian, D. H.)—422
Caldwell, Wallace C. Evaporation of molten metals from hot filaments—940(A)
Carapella, Louis A. and Ralph R. Hultgren. High magnetic saturation value for the copper-manganese-tin Heusler alloy, CU_2MnSn—905(L)
Carlson, J. Franklin and Marcel Schein. On the production of mesotrons—840(L)
Cartwright, C. Hawley, John Daniel and Alex Petrauskas. Infra-red transmission of the human body—475(A)
Christensen, H. (see Williams, H. J.)—1005
Christy, R. F. and S. Kusaka. Burst production by mesotrons—220(A), 414
—— **and S. Kusaka.** Interaction of γ-rays with mesotrons—405
Clancy, Edward P. Induced radioactivity of xenon—686(A)
Clark, J. C. and H. R. Kelly. Absolute determination of the continuous x-ray energy from thin aluminum targets—220(A)
Cleveland, Forrest F. and M. J. Murray. Carbon isotope effect in acetylenes—475(A)
—— **and M. J. Murray.** Raman spectra of alkyl acetylenes—924(A)
—— **and M. J. Murray.** Raman spectra of some ethers containing one or more phenyl groups—107(A)
—— **and M. J. Murray.** Raman spectrum of 6-dodecyn-5-one—478(A)

Clogston, A. M. (see Feshbach, H.)—189
Cobine, J. D. (see Bauer, W. M.)—115(A)
—— (see Easton, E. C.)—473(A)
Code, F. Leslie. Scattering of mesotrons in tungsten—229
Cohee, A. V. (see Miller, E. P.)—468(A)
Cohen, Alvin (see Williams, Dudley)—911(A)
Cole, Kenneth S. (see Cole, Robert H.)—474(A)
—— **and Richard F. Baker.** Impedance of the squid giant nerve fiber during current flow—685(A)
—— **and Robert H. Cole.** Transient current in dielectrics—935(A)
Cole, Peter A. Ultraviolet absorption spectra of different regions of *Trichophyton mentagrophytes* spores—475(A)
Cole, Robert H. Dielectric constants of aliphatic ketones—689(A)
—— (see Cole, Kenneth S.)—935(A)
—— **and Kenneth S. Cole.** Dispersion and absorption in dielectrics—474(A)
Collar, H. W., J. M. Cork and G. P. Smith. Radioactive barium from cesium—937(A)
Collins, George B. (see Feldmeier, J. R.)—937(A)
—— **and B. Waldman.** Energy distribution of continuous x-rays from nuclear excitation—109(A)
Coltman, John W. Capture cross sections for slow neutrons—917(A)
Colwell, R. C., H. Atwood, Jr., J. E. Bailey and C. O. Marsh. Velocity of radio-waves over short distances—935(A)
Compton, A. H. and A. T. Monk. Recurrence pulses in cosmic-ray intensity—112(A)
Constant, F. W. and R. E. Faires. Ferromagnetic impurities in copper, brass and silver—938(A)
Cook, Samuel R. Theory of the geneses of primary x-rays—220(A)
Cooper, E. P. and E. C. Nelson. Lifetimes and ground states of Be^{10} and C^{10}—216(A)
Cooper, John N. Auger effect in the relative intensities of x-ray lines—473(A)
Copeland, Paul L. and W. H. Sparing. Stability of a low pressure mercury arc—115(A)
Corben, H. C. Theory of cascade showers in heavy elements—216(A)
Cork, J. M. Characteristic x-rays produced by deuteron bombardment—934(A)
—— Production of characteristic x-rays by deuteron bombardment—957
—— (see Collar, H. W.)—937(A)
Cornog, R. and W. F. Libby. Production of radioactive hydrogen by neutron bombardment of boron and nitrogen—1046(L)
Cox, Richard T. (see Rosenblith, W. A.)—219(A)
Crane, N. D. (see Herb, R. G.)—111(A)
Crenshaw, C. M. (see Manning, H. P.)—941(A)
Creutz, E. C. (see White, M. G.)—63
—— (see Wilson, Robert R.)—916(A)
—— **and Robert R. Wilson.** Production of mono-energetic protons with the cyclotron—916(A)
Critchfield, Charles L. Excited states of nuclear particles in the meson-pair theory—48
Cummings, Charles S. and Lewi Tonks. Influence of a longitudinal magnetic field on an electrical discharge in mercury vapor at low pressure—514
Cuykendall, T. R. (see Bohlke, P. G.)—940(A)

Daniel, John (see Cartwright, C. Hawley)—475(A)
Danielson, G. C. and K. Lark-Horovitz. Structure of liquid nitromethane—110(A)
Davis, Leverett, Jr. Deviations from Ohm's law at high current densities—474(A)
Dawson, L. H. and E. O. Hulburt. Angular distribution of light scattered in liquids—914(A)
Dean, L. A. (see Ballard, Stanley S.)—467(A)
De Benedetti, Sergio. Simultaneous emission of particles and pair production—463(L)
Delsasso, L. A. (see White, M. G.)—63
Dempster, A. J. (see Sherwin, C. W.)—114(A)
Dessauer, G. and E. M. Hafner. Proton-induced fission—840(L), 940(A)
Deutsch, Martin. Magnetic lens beta-ray spectrometer—684(A)
—— Radiations from $I^{131} \rightarrow Xe^{131}$—940(A)
Devol, Lee (see Adams, F. W.)—684(A)
Diaz, J. T. (see Underwood, N.)—911(A)
Dicke, R. H. and John Marshall. Inelastic scattering of protons—917(A)
Dieke, G. H. (see Ginsburg, N.)—632
Dobrotin, N. A. (see Veksler, V. I.)—1044(L)
Downing, J. R. and A. Roberts. Coincidence study of the decay of Br^{82}—940(A)
Dresden, M., W. T. Scott and G. E. Uhlenbeck. Exact solution of the integral equations for cosmic-ray showers—112(A)
DuMond, J. W. M. (see Panofsky, W. K. H.)—219(A)
——, **H. H. Bailey, W. K. H. Panofsky and A. E. S. Green.** Preliminary report on a redetermination of h/e by the short wave-length limit of the continuous x-ray spectrum—219(A)
Dunning, J. R. (see Grosse, A. V.)—322(L)
Dwyer, Robert J. Energy of dissociation of water vapor—928(A)

Earle, Marshall D. Electrical conductivity of titanium dioxide—942(A)
Easley, M. Adelaide (see Forsythe, W. E.)—921(A)
Easton, E. C. and J. D. Cobine. Timer for spark breakdown studies—473(A)
Ehrhardt, C. H. and E. P. Miller. X-ray determination of the particle size of electro-deposited coatings—472(A)
Eisele, L. J., S. J. (see Weber, A. H.)—473(A)
Elder, Frank R. (see Hull, Albert W.)—115(A)
Eldridge, John A. Scattering of low velocity ion beams—473(A)
Ellickson, R. T. and B. Serin. Determination of diffusion coefficients—922(A)
Elliott, D. R. Nuclear radii of light elements—918(A)
—— (see King, L. D. P.)—108(A)
—— **and L. D. P. King.** Radioactive $_{21}Sc^{41}$, $_{18}A^{35}$, $_{16}S^{31}$—403(L)
Elsasser, Walter M. Measurement of the total infra-red emission of atmospheric water vapor—218(A)

Evans, Foster. Electric fields produced by cosmic rays—1
Evans, Robley D. (see Goodman, Clark)—920(A)
—— (see Kip, Arthur F.)—920(A)
—— **and Clark Goodman.** Radioactivity of rocks—920(A)

Faires, R. E. (see Constant, F. W.)—938(A)
Fedorenko, Nikitin. Soft component and decay of mesotrons at 3000 meters—461(L)
Feenberg, Eugene. General nuclear model—691(A)
—— Non-uniform particle density in nuclear structure—593, 687(A)
—— Note on the density and compressibility of nuclear matter—149
—— (See Phillips, M.)—400(L)
Feldmeier, J. R. and George B. Collins. Excitation of nuclei by x-rays—937(A)
Fermi, E. (see Anderson, H. L.)—52
—— **and E. Segrè.** Fission of uranium by alpha-particles—680(L)
Feshbach, H. and A. M. Clogston. Perturbation of boundary conditions—189
Feynman, R. P. and John Archibald Wheeler. Reaction of the absorber as the mechanism of radiative damping—683(A)
Findlay, J. H. (see Bell, M. E.)—922(A)
Fleming, Gertrude M. and J. E. Henderson. On the energy losses attending thermionic and field emission—907(L)
Flowers, J. W. Radiation of light by high current electrical discharges—685(A)
Foley, H. M. and H. M. Randall. Fine structure in the far infra-red spectrum of NH_3—171
Folsom, T. R. New method for rapidly desiccating human plasma for transfusion purposes—685(A)
Forsythe, W. E. and M. Adelaide Easley. Characteristics of two new photoflash lamps—921(A)
Fowler, Charles A., Jr. New absorption spectra of the alkaline earth fluorides—645
Fowler, W. A. (see Becker, R. A.)—217(A)
—— (see Lauritsen, Tom)—241
—— (see Streib, J. F.)—215(A), 253
Fox, G. W. and F. M. Bailey. Measurement of cathode emission by use of the electron microscope—174
Frank, Philipp. Deflection of light rays by a general anisotropy—475(A)
Frankel, Stanley. Interpretation of fast neutron scattering—216(A)
Frevel, Ludo K. Note on the indexing of powder diffraction patterns—925(A)
Friedlander, G. (see Seaborg, G. T.)—320(L), 400(L)
Furry, W. H. Flow of a radioactive gas through a tube—919(A)

Gamertsfelder, Carl. Atomic distributions in liquid aluminum and lithium—926(A)
Gamow, G. Relative importance of different elements for neutrino production—617(L)
—— **and M. Schoenberg.** Neutrino theory of stellar collapse—539
Gast, Paul F. and D. H. Loughridge. Cosmic rays in the Bering Sea—769(L)
—— **and D. H. Loughridge.** Latitude effect of cosmic rays above 50°N latitude—127
Gautier, T. N. One-tube counter quenching circuit with capacitative feedback—112(A)
Gerjuoy, Edward. Forbidden lines of Pb I—218(A)
Germer, Lester H. (see White, Addison H.)—926(A)
Gerö, L. and R. F. Schmid. Rotational analysis, perturbation and predissociation in the CD and CH bands—528(L)
Getting, I. A. Preliminary results on two new ion sources—467(A)
Gingrich, Newell S. Note on the analysis of liquid x-ray diffraction patterns—290
—— (see Gregg, R. Q.)—619
—— (see Sharrah, P. C.)—472(A)
Ginsburg, N. and G. H. Dieke. Intensity measurements in the molecular spectrum of hydrogen—632
Goetz, Alexander and S. Scott Goetz. Extremely sensitive biophysical indicator for metal ions—219(A)
Goetz, S. Scott (see Goetz, Alexander)—219(A)
Gofman, J. W. (see Seaborg, G. T.)—321(L)
Goldhaber, M. (see O'Neal, R. D.)—102(L)
—— **and R. D. O'Neal.** Absorption cross sections for slow neutrons—109(A)
Good, W. E. and G. Scharff-Goldhaber. Total cross sections for 900-kev neutrons—917(A)
Goodman, Clark (see Evans, Robley D.)—920(A)
——, **Robley D. Evans and Patrick M. Hurley.** Helium age measurements—920(A)
Gorodetzky, S. (see Leprince-Ringuet, L.)—460(L)
Gray, Robert B. and Millard F. Manning. Self-consistent field calculations for nickel—475(A)
Green, A. E. S. (see DuMond, J. W. M.)—219(A)
Green, E. H. (see Kurrelmeyer, B.)—921(A)
Green, J. B. Paschen-Back effect. VII. Configuration interaction—69
—— Spectra of the rare gases—915(A)
—— (see Hurlburt, E. H.)—106(A)
——, **D. W. Bowman and E. H. Hurlburt.** Paschen-Back effect. VIII. Configuration interaction—106(A)
——, **E. H. Hurlburt and D. W. Bowman.** Zeeman effect of xenon—72
Green, M. Vacuum spark spectra of Cd IV and In V—218(A)
Gregg, R. Q. and N. S. Gingrich. Diffuse scattering of x-rays by rocksalt—619
Griffith, R. L. and P. M. Harris. Electron distribution in metallic lithium as determined from x-ray diffraction measurements—110(A)
Grisdale, R. O. Microphonic contacts and the properties of pyrolitic carbon—772(T)
Grisewood, Edgar N. (see Bacon, Ralph H.)—531
Groetzinger, Gerhart, E. O. Wollan and Marcel Schein. Study of the production and adsorption of mesotrons in the substratosphere—113(A)
Gross, B. On the theory of dielectric loss—748
Grosse, A. V. (see Anderson, H. L.)—52
——, **E. T. Booth and J. R. Dunning.** Fourth $(4n+1)$ radioactive series—322(L)
Grover, Horace (see King, Allen)—469(A)

Gunn, Ross. Formation of multiple stars by fission and simultaneous capture—929(A)
—— Formation of the solar system by the rotational fission of a star: The fission being initiated by a passing second star—680(L)
Guth, Eugene. On the excitation of nuclei by x-rays—109(A)
—— Radiative transition probabilities in heavy nuclei. Excitation of nuclei by x-rays—325
—— (see James, Hubert M.)—111(A)
—— (see Mullin, Charles J.)—114(A), 943(A)
—— **and Charles J. Mullin.** Electron emission of metals in electric fields. I. Explanation of the periodic deviations from the Schottky line—575
—— **and Charles J. Mullin.** Electron emission of metals in electric fields. II. Field dependence of the surface photoeffect—867

Haas, Arthur E. Some rules concerning isobaric radioactive nuclei—107(A)
Hafner, E. M. (see Dessauer, G.)—840(L), 940(A)
Haggstrom, E. β-ray spectrum of $_{91}$ekatantalum^{233}—322(L)
Hagstrum, Homer D. and John T. Tate. Ionization and dissociation of diatomic molecules by electron impact—354
—— **and John T. Tate.** On the thermal activation of the oxygen molecule—509
Hall, David B. (see Rossi, Bruno)—223
Halpern, O. and M. H. Johnson. On position measurements of heavy particles—683(A)
—— **and M. H. Johnson.** On the measurement of observables in relativistic quantum mechanics—896
—— **and T. Holstein.** On the passage of neutrons through ferromagnets—960
——, **M. Hamermesh and M. H. Johnson.** Passage of neutrons through crystals and polycrystals—981
Ham, W. R. and F. D. Bennett. Transitions in alloys of cobalt nickel and iron by the hydrogen diffusion method—939(A)
Hamermesh, M. (see Halpern, O.)—981
Hansen, W. Disintegration of nitrogen and oxygen by neutrons—941(A)
Hanson, A. O. (see Herb, R. G.)—111(A)
Hanson, Alvin W. Measurement of the S_{13} elastic constant of zinc—912(A)
Hanstein, Henry B. Interaction experiments with resonance neutrons—489
Hardy, H. C. and W. H. Pielemeier. Velocity of sound in air—934(A)
Hardy, T. C. Nuclear magnetic moment of In^{115}—686(A)
Harris, P. M. (see Griffith, R. L.)—110(A)
Hart, Philip J. (see Atanasoff, John V.)—85
Hartree, D. R. (see Hartree, W.)—299, 306
—— (see Manning, Millard F.)—683(A)
Hartree, W. (see Manning, Millard F.)—683(A)
——, **D. R. Hartree and Millard F. Manning.** Self-consistent field calculations for Ge^{++} and Ge—306
——, **D. R. Hartree and Millard F. Manning.** Self-consistent field calculations for Zn, Ga, Ga^{+}, Ga^{+++}, As, As^{+}, As^{++}, As^{+++}—299
Harvey, G. G. and L. J. Sullivan. Magnetic electron microscope—929(A)
Hatfield, T. N. and R. C. Smith. Alpha-particle range in and relative stopping powers of some gases—911(A)
Hatoyama, Mitio (see Shinohara, Kenichi)—461(L)
Hawkes, John B. Method of making direct measurements of the thermal coefficient of the index of refraction, with some results for distilled water—921(A)
Haworth, L. J. (see Luebke, E. A.)—918(A)
—— (see Manley, J. H.)—109(A)
——, **J. H. Manley and E. A. Luebke.** Voltage distribution on a multi-section accelerating tube—108(A)
Haxby, R. O., W. E. Shoupp, W. E. Stephens and W. H. Wells. Photo-fission of uranium and thorium—57
Hay, Robert H. Nuclear magnetic moments of Ba^{135} and Ba^{137}—686(A)
Haynes, S. K. Effect of neutron energy on the total decay curves of fission products—834(L)
Hazen, Wayne E. Growth of drops in a Wilson cloud chamber—933(A)
Heaps, C. W. Discontinuities of magnetostriction and magnetization in nickel—585
Hebb, M. H. and H. Spone. On the mechanism of the nitrogen afterglow—925(A)
Hecht, Selig, Simon Shlaer and Maurice H. Pirenne. Quantum relationships in vision—772(T)
Heilprin, Laurence B. Apparatus for studying surface tension at high pressures—921(A)
Hellund, E. J. Phase series—395
Helmholz, A. C., Charles Pecher and Perry R. Stout. Radioactive Rb from deuteron bombardment of Sr—902(L)
Henderson, J. E. (see Fleming, Gertrude M.)—907(L)
—— **and Sidney M. Rubens.** Anode spots in oxygen—213(L)
Herb, R. G., C. M. Turner, A. O. Hanson and N. D. Crane. Electrostatic generator with concentric electrodes—111(A)
Hering, K. W. (see Warren, B. E.)—925(A)
Herman, Robert C. and Robert Hofstadter. Photoconductivity of a natural willemite crystal—79
Herring, Conyers. On the thermodynamic interpretation of certain thermionic and thermoelectric phenomena—889
Herzog, G. Cloud tracks of cosmic rays in the substratosphere—117
—— **and W. H. Bostick.** Cloud-chamber pictures of cosmic rays at 29,000 feet altitude—113(A), 122
Hilberry, Norman. Energy distribution and composition of the primary cosmic-ray particles—763
—— Variation of the intensity of extensive cosmic-ray showers with altitude—112(A)
—— **and Victor H. Regener.** Frequency-extension curves for the soft and penetrating components of extensive cosmic-ray showers—471(A)
Hill, R. D. Production of He^3—103(L)
Hippel, A. von and G. M. Lee. Scattering, trapping, and release of electrons in NaCl and in mixed crystals of NaCl-AgCl—691(A), 824
—— **and R. J. Maurer.** Electric breakdown of glasses and crystals as a function of temperature—820

Hirsh, Frederick R., Jr. On the absence of the $M\beta$ satellite intensity anomaly—766(L)
Hofstadter, Robert (see Herman, Robert C.)—79
Hoge, Harold J. Electrical conduction in the glass insulation of resistance thermometers—921(A)
Holstein, T. (see Halpern, O.)—960
—— **and H. Primakoff.** Magnetization near saturation in polycrystalline ferromagnets—388
Horton, Robert E. Hydro-physical approach to the quantitative morphology of drainage basins—478(A)
Horvath, W. J. and E. O. Salant. Absorption of resonance neutrons by boron, chlorine, cobalt and manganese—154
Houston, W. V. and Hugh Bradner. Two-stage electron microscope—219(A)
Hsü, Hsien-yü and William Band. Theory of liquid He II—1013
Hubbard, J. C. Sound velocity and absorption by ultrasonic interferometry—935(A)
Hubbell, Harry H., Jr. Images projected from etched surfaces of quartz crystals—473(A)
Hudspeth, E. (see Bennett, W. E.)—781
—— (see Ramsey, W. E.)—685(A)
Hughes, Donald J. and Volney C. Wilson. Cloud chamber and counter tube cosmic-ray studies under ground—931(A)
Hulburt, E. O. Measurements of some optical properties of atmospheric haze—914(A)
—— (see Dawson, L. H.)—914(A)
Hull, Albert W. and Frank E. Elder. Phase of arc-back in rectifiers—115(A)
Hultgren, Ralph R. (see Carapella, Louis A.)—905(L)
Humphreys, Richard F. (see Pollard, Ernest)—466(A)
—— **and Ernest Pollard.** Alpha-proton reactions of sodium and aluminum—942(A)
Hunter, G. T. and D. C. Swanson. Van de Graaff pressure type electrostatic generator—911(A)
Huntington, H. B. Dislocations in NaCl—942(A)
Hurlburt, E. H. (see Green, J. B.)—72, 106(A)
——, **D. W. Bowman and J. B. Green.** Zeeman effect of xenon—106(A)
Hurley, Patrick M. (see Goodman, Clark)—920(A)
Huxford, W. S. (see Jones, R. W.)—932(A)

Ikawa, M. (see Nishina, Y.)—323(L), 677(L)
—— (see Sagane, R.)—904(L)
Infeld, L. On a new treatment of some eigenvalue problems—737
Inglis, D. R. Motion of the earth's fluid core—469(A)
—— Motion of the earth's fluid core: A geophysical problem—178
Irvine, John W., Jr. (see Roberts, A.)—936(A)

Jacobs, James A. and William L. Whitson. Distribution in angle of alpha-particles from boron bombarded with protons—108(A)
Jacobsen, J. C. and N. O. Lassen. Fission cross section in uranium and thorium for deuteron impact—1043(L)
Jacques, R. B. Automatic frequency control for cyclotron R. F. power supply—918(A)
Jaffé, George. On the joint action of diffusion and recombination of ions—652
James, Hubert M. and Eugene Guth. Theoretical stress-strain curve for rubberlike materials—111(A)
Jauncey, G. E. M. Note on the theory of the modified reflection of x-rays by crystals—456
—— **and O. J. Baltzer.** Non-Laue maxima in the diffraction of x-rays from rocksalt—equatorial maxima—699
——, **O. C. Baltzer and D. C. Miller.** Non-Laue diffraction maxima from rocksalt—non-equatorial maxima—908(L)
Jenkins, F. A. and S. Mrozowski. Interference between quadrupole and magnetic dipole radiation—915(A)
—— **and S. Mrozowski.** Zeeman effect of the forbidden lines of Pb I. I. Pure quadrupole and magnetic dipole lines—808
Jensen, Arthur S. Radiations from radioactive cobalt—936(A)
Jesse, William P. (see Schein, Marcel)—615(L), 930(A)
—— (see Wollan, E. O.)—930(A)
——, **E. O. Wollan and Marcel Schein.** Vertical intensity and the latitude effect of the hard component at high altitudes—930(A)
Johnson, M. H. (see Halpern, O.)—683(A), 896, 981
Johnson, Thomas H. East-west asymmetry of the cosmic radiation in high latitudes and the excess of positive mesotrons—11, 112(A)
——, **J. G. Barry and R. P. Shutt.** Large Wilson cloud chamber for cosmic-ray studies—470(A)
—— (see Pomerantz, Martin A.)—143, 471(A)
—— (see Shutt, R. P.)—113(A)
Jones, R. Clark. Effect of van der Waals forces on the thermal diffusion coefficient of gaseous isotopic mixtures—688(A)
—— Theory of the thermal diffusion coefficient for isotopes: II—1019
Jones, R. W. and W. S. Huxford. Forms of discharge in micro-gaps—932(A)

Kamen, M. D. (see Ruben, S.)—349
Kammer, Erwin (see Atanasoff, John V.)—97
Kanne, W. R. (see Ragan, G. L.)—687(A)
Kaplan, Joseph and S. M. Rubens. Afterglows in nitrogen rare gas mixtures—476(A)
—— **and Sidney M. Rubens.** Excitation of the auroral green line in nitrogen afterglows—218(A)
Kaufmann, A. R. (see Rado, G. T.)—690(A)
—— (see Squire, C. F.)—690(A)
—— (see Starr, C.)—476(A)
—— **and C. Starr.** Magnetization of copper-nickel alloys—690(A)
Kelly, H. R. (see Clark, J. C.)—220(A)
Kendall, H. C. (see Overbeck, C. J.)—934(A)
Kennedy, J. W. (see Seaborg, G. T.)—321(L)
Kerst, D. W. Induction electron accelerator—110(A)
—— Radiations from the induction accelerator—933(A)
Kimura, K. (see Nishina, Y.)—323(L), 677(L)
King, Allen and Horace Grover. Temperature correction methods in calorimetry—469(A)
King, L. D. P. (see Elliott, D. R.)—403(L)
—— **and D. R. Elliott.** Short-lived radioactivities of $_{14}Si^{27}$, $_{16}S^{31}$, $_{18}A^{35}$ and $_{21}Sc^{41}$—108(A)
King, Ronold. Input impedance of a symmetrical antenna—684(A)

Kip, Arthur F. and Robley D. Evans. Improved counting rate meter for radioactivity detection—920(A)
Kirkham, Don. Conjugate potentials of a grid between conducting planes—111(A)
Kirkpatrick, H. A. (see Panofsky, W. K. H.)—219(A)
Kirkpatrick, Paul. X-ray diffraction maxima at other than Bragg angles—452
Knipp, J. K. (see Brunings, J. H. M.)—919(A)
Knipp, Julian and Edward Teller. On the energy loss of heavy ions—659
Kobayasi, M. Distinction between longitudinal and transverse mesons—843(L)
Koehler, J. S. Energy stored during work hardening—943(A)
—— Taylor dislocation near a cylindrical boundary—477(A)
Korff, S. A. Fast neutrons and particles with high specific ionization in the cosmic radiation at high elevations—214(L)
—— Nuclear particles in the cosmic radiation—949
—— (see Rose, M. E.)—467(A), 850
Kratz, H. R. and J. E. Mack. Preliminary study of the doublet structure of the principal series of potassium—915(A)
Krishnan, K. S. and S. Banerjee. Magnetic anisotropy of gadolinium sulphate octahydrate—770(L)
Kurbatov, J. D. (see Law, H. B.)—936(A)
——, **M. L. Pool and H. B. Law.** Isolation of pure radioactive strontium and barium—919(A)
Kuroda, H. (see Okuda, T.)—104(L)
Kurrelmeyer, B., W. H. Mais and E. H. Green. Bridge method for specific heat of wire samples—921(A)
Kusaka, S. (see Christy, R. F.)—220(A), 405, 414
Kyropoulos, S. Crystallization phenomena, crystal structure and fatigue in metallic conglomerates—220(A)

Ladenburg, R. (see Barschall, H. H.)—917(A)
Lagemann, R. T. New measurements on some infra-red bands of methyl iodide—911(A)
Lamb, W. E., Jr. Range of fission fragments—687(A)
—— **and A. Nordsieck.** On the Einstein condensation phenomenon—677(L)
—— **and A. Nordsieck.** On the λ transition in liquid helium—927(A)
Lanczos, C. Dynamics of a particle in general relativity—813
—— Total mass of a particle in general relativity—708
Landé, Alfred. Finite electromagnetic self-energies and nuclear electric forces—927(A)
—— On the magnitude of electronic charges—434
—— On the universal constants h, c, and e—475(A)
Landshoff, R. On the virial theorem in the theory of metals—906(L)
Lane, C. T. Description of the liquid helium equipment at Yale University—477(A)
—— (see Browne, S. H.)—476(A), 939(A)
Laporte, Otto. Term energies in the configuration d^5—684(A)
—— (see Platt, John R.)—684(A)
Lark-Horovitz, K. (see Danielson, G. C.)—110(A)
—— (see Parshall, C. M.)—926(A)
—— **and W. A. Miller.** Fission tracks on the photographic plate—941(A)
Lassen, N. O. (see Jacobsen, J. C.)—1043(L)
Lauritsen, C. C. (see Becker, R. A.)—217(A)
—— (see Lauritsen, Tom)—241
—— (see Streib, J. F.)—215(A), 253
Lauritsen, Tom (see Bøggild, J. K.)—275
——, **C. C. Lauritsen and W. A. Fowler.** Application of a pressure electrostatic generator to the transmutation of light elements by protons—241
Law, H. B. (see Kurbatov, J. D.)—919(A)
——, **M. L. Pool, J. D. Kurbatov and L. L. Quill.** Radioactive isotopes of Nd, Il and Sm—936(A)
Lawson, A. W. Comment on the elastic constants of alpha-quartz—838(L)
—— Determination of the elastic modulus s_{13} of beta-quartz—608
—— Generation of dislocations in polycrystalline copper—943(A)
Lee, G. M. (see Hippel, A. von)—691(A), 824
Lees, Wayne L. (see Ramsey, W. E.)—685(A)
—— (see Swann, W. F. G.)—470(A)
Leet, L. Don. Physical frontiers in seismology—479(A)
Leprince-Ringuet, L., S. Gorodetzky, E. Nageotte and R. Richard-Foy. Direct measurement of the mass of the mesotron—460(L)
Letner, H. R. (see Adams, F. W.)—684(A)
Libby, W. F. (see Cornog, R.)—1046(L)
Liebermann, Leonard N. Rotational analysis of some CS_2 bands in the near ultraviolet—106(A)
Lin, C. C. Note on the normalization of Dirac functions—841(L)
Livingood, J. J. (see Seaborg, G. T.)—320(L)
Livingston, M. Stanley. Neutron shielding—918(A)
Long, V. A. and R. M. Whaley. Fluctuational effects in cosmic-ray ionization—470(A)
Longwell, Chester R. Problems of orogeny—478(A)
Loughridge, D. H. (see Gast, Paul F.)—127, 769(L)
Lowan, A. N. (see Bethe, H. A.)—467(A)
Lowen, Irving S. Lifetimes of nuclear levels with respect to electric multipole radiation—835(L)
Ludloff, H. F. Elasticity in order-disorder transformations—939(A)
—— Simultaneous determination of isothermal and adiabatic elasticities—111(A)
Luebke, E. A. (see Haworth, L. J.)—108(A)
—— (see Manley, J. H.)—109(A)
——, **J. H. Manley and L. J. Haworth.** Velocity dependence of slow neutron capture cross section of boron—918(A)
Lyddane, R. H., R. G. Sachs and E. Teller. On the polar vibrations of alkali halides—673

MacHattie, L. E. High rotational speed with small rotors—468(A)
Mack, J. E. (see Anderson, E. E.)—106(A), 717
—— (see Kratz, H. R.)—915(A)
—— **and E. E. Anderson.** Unexplained irregularities in the Z dependence of the energy differences within the configuration $3d^3$—683(A)

MacNair, D. (see Nix, F. C.)—939(A)
Mais, W. H. (see Kurrelmeyer, B.)—921(A)
Manley, J. H. (see Haworth, L. J.)—108(A)
—— (see Luebke, E. A.)—918(A)
——, **L. J. Haworth and E. A. Luebke.** Neutron capture cross sections of F^{19}, Tl^{203}, and N^{15}—109(A)
Manning, H. P., C. M. Crenshaw and V. J. Young. Distribution with angle of protons from D−D reaction—941(A)
Manning, Millard F. (see Gray, Robert B.)—475(A)
—— (see Hartree, W.)—299, 306
——, **W. Hartree and D. R. Hartree.** Self-consistent field with exchange for Si V and Si IV—683(A)
Margenau, Henry. Attractive forces between ions and neutral molecules—928(A)
—— Interaction of alpha-particles—37
—— Statistical theory of the spacing of nuclear levels—467(A)
—— Statistics of excited energy states of nuclei—627
Marsh, C. O. (see Colwell, R. C.)—935(A)
Marshak, R. E. Highly forbidden transitions in beta-decay—937(A)
—— (see Bethe, H. A.)—467(A)
—— **and V. F. Weisskopf.** On the scattering of mesons of spin $\frac{1}{2}\hbar$ by atomic nuclei—130, 471(A)
Marshall, Fitz-Hugh. Method for obtaining powders of uniform sodium chloride crystals in various size ranges, and the effect of size upon the intensity of x-ray reflection—110(A)
Marshall, John (see Dicke, R. H.)—917(A)
Marton, L. Electron microscopical determination of object thickness—929(A)
Masuda, T. (see Nishina, Y.)—401(L)
Matheson, G. L. (see McAlister, E.D.)—922(A)
Mauchly, J. W. 27-day recurrence tendency in North American precipitation—469(A)
Maurer, R. J. Conductivity of glass as a function of field strength—691(A)
—— (see Hippel, A. von)—820
Maxfield, F. A. and O. A. Mortensen. Use of the radioactive properties of thorium for a quantitative study of phagocytosis—107(A)
McAlister, E. D., G. L. Matheson and W. J. Sweeney. Large recording spectrograph for the infra-red to 15μ—922(A)
McCay, Myron S. Structure of the (0, 4) Angstrom band of CO for high rotational states—911(A)
McCreary, Ralph L. Magnetic beta-ray spectrometer—919(A)
Merwe, Carel W. van der (see Bacon, Ralph H.)—531
Metropolis, N. Explanation of the rotational structure of the λ3800 band system of SO_2—106(A)
—— Vibrational analysis of the absorption system of sulphur dioxide at λ3400–2900—923(A)
Miles, S. H. (see Thaxton, H. M.)—945(A)
Miller, D. C. (see Jauncey, G. E. M.)—908(L)
Miller, E. P. and A. V. Cohee. Use of radioactive materials in measuring the thickness of enamel coatings—468(A)
Miller, E. P. (see Ehrhardt, C. H.)—472(A)
Miller, Leonard C. (see Allison, Samuel K.)—108(A)
Miller, Park H., Jr. Electrical properties of zinc oxide—942(A)
—— (see Banks, Floyd R.)—943(A)
Miller, W. A. (see Lark-Horovitz, K.)—941(A)
Millett, Walter (see Williams, Dudley)—911(A)
Millikan, Robert A. Experimental testing of a hypothetical distribution of energy in the cosmic-ray spectrum—930(A)
Miyamoto, G. (see Sagane, R.)—904(L)
Miyazaki, Y. (see Nishina, Y.)—401(L)
Mohler, Fred L. Resistivity of interstellar space—1043(L)
Møller, C. Nomenclature of nuclear particles—323(L)
Molnar, Julius P. New absorption bands in colored alkali-halide crystals—944(A)
Monk, A. T. (see Compton, A. H.)—112(A)
Montgomery, C. G. (see Beringer, Robert)—933(A)
—— **and D. D. Montgomery.** Time lags in Geiger-Müller counter discharges—932(A), 1045(L)
—— **and D. D. Montgomery.** Transition effect for large showers of cosmic rays—471(A)
Montgomery, D. D. (see Montgomery, C. G.)—471(A), 932(A), 1045(L)
Mooney, Rose C. L. Structure determination of molecules and groups in crystals by means of x-ray diffraction—910(T)
—— X-ray structure analysis of polyvinyl alcohol—925(A)
Morgan, F., M. Muskat and D. W. Reed. Friction phenomena and the stick-slip process—935(A)
Morgan, K. Z. (see Nielsen, W. M.)—547, 910(A)
Morrison, P. Electron capture in white dwarf stars—217(A)
Mortensen, O. A. (see Maxfield, F. A.)—107(A)
Motz, Lloyd. Apsidal motion in binary stars for a point source convective core model with varying guillotine factor—929(A)
—— (see Rothstein, Jerome)—916(A)
Mrozowski, S. Hyperfine structure of ionized mercury lines—104(L)
—— On the spectrum of Hg II—106(A)
—— Rotational analysis of a system of CO_2 bands—923(A)
—— (see Jenkins, F. A.)—808, 915(A)
Mulliken, Robert S. Species classification and rotational energy level patterns of non-linear triatomic molecules—873
—— Species classification and rotational energy level patterns of triatomic molecules—923(A)
Mullin, Charles J. (see Guth, Eugene)—575, 867
—— **and Eugene Guth.** Explanation of the periodic deviations from the Schottky line—114(A)
—— **and Eugene Guth.** Field dependence of the surface photo-effect—943(A)
Murphey, Byron F. Relative abundances of the oxygen isotopes—320(L)
—— **and Alfred O. Nier.** Variations in the relative abundance of the carbon isotopes—771(L)
Murray, M. J. (see Cleveland, Forrest F.)—107(A), 475(A), 478(A), 924(A)
Muskat, M. (see Morgan, F.)—935(A)

Muto, Toshinosuke. Radiative collision of neutrons with protons—837(L)
Myers, F. E. (see Petrauskas, A. A.)—688(A)
—— (see Van Atta, L. C.)—688(A)

Nageotte, E. (see Leprince-Ringuet, L.)—460(L)
Neher, H. V. (see Pickering, W. H.)—930(A)
—— **and W. H. Pickering.** Cosmic-ray radio-sonde—930(A)
Nelson, E. C. (see Cooper, E. P.)—216(A)
Newson, Henry W. and Lyle B. Borst. Determination of nuclear reaction energies for a mixture of copper isotopes—941(A)
Nichols, Myron H. Average thermionic constants for single crystal tungsten wire—944(A)
Nielsen, Alvin H. and Dudley Williams. Some new measurements ν_3 and $\nu_4+\nu_5$ of C_2H_2—911(A)
Nielsen, Harald H. Near infra-red spectrum of water vapor. Part I. The perpendicular bands ν_2 and $2\nu_2$—565
—— Interaction theory and anomalies in the infra-red spectra of polyatomic molecules—910(T)
Nielsen, W. M., C. M. Ryerson, L. W. Nordheim and K. Z. Morgan. Differential measurement of the meson lifetime—547, 910(A)
Nier, Alfred O. (see Murphey, Byron F.)—771(L)
Nishina, Y., Y. Sekido, Y. Miyazaki and T. Masuda. Cosmic rays at a depth equivalent to 1400 meters of water—401(L)
——, **Y. Sekido, H. Simamura and H. Arakawa.** Cosmic-ray intensities and typhoons—679(L)
——, **T. Yasaki, K. Kimura and M. Ikawa.** Fission products of uranium by fast neutrons—323(L), 677(L)
Nix, F. C. and D. MacNair. Thermal expansion of pure metals: iron, nickel, copper, gold and aluminum—939(A)
Nonaka, Itaru. Excitation of gamma-rays by fast neutrons of different energy—681(L)
Nordheim, L. W. Decay radiation and nature of the meson—910(A)
—— Lateral extension of cosmic-ray showers—929(A)
—— On the nature of the meson decay—554
—— (see Nielsen, W. M.)—547, 910(A)
Nordsieck, A. (see Lamb, W. E., Jr.)—677(L), 927(A)
Nottingham, W. B. Remarks on energy losses attending thermionic emission of electrons from metals—906(L)
Nye, H. A. (see Rarita, William)—209

Ogata, K. (see Okuda, T.)—104(L)
Okuda, T., K. Ogata, H. Kuroda, S. Shima and S. Shindo. Isotopic weights of Ni isotopes by the doublet method—104(L)
Olsen, Leonard O. Quenching and depolarization of mercury resonance radiation by helium, neon and argon—914(A)
O'Neal, R. D. Comparative study of photo-neutron sources—919(A)
—— On the activation of chlorine by slow neutrons—109(A)
—— (see Goldhaber, M.)—109(A)
—— **and M. Goldhaber.** Capture cross sections for C neutrons—102(L)
Oppenheimer, J. R. On the selection rules in beta-decay—908(L)
—— On the spin of the mesotron—462(L)
Overbeck, C. J. and H. C. Kendall. Temperature effect on ultrasonic velocities in carbon dioxide—934(A)

Page, Chester H. Analysis of the amplification of exponential pulses—920(A)
Panofsky, W. K. H. (see DuMond, J. W. M.)—219(A)
——, **J. W. M. DuMond, R. R. Yost and H. A. Kirkpatrick.** Design, assembly and preliminary tests of a curved crystal γ-ray spectrometer—219(A)
Pardue, T. Eugene (see Shearin, Paul E.)—933(A)
Parshall, C. M. and K. Lark-Horovitz. Structure of stretched rubber—926(A)
Paul, Fred W. and Harry D. Polster. Extreme ultraviolet spectra of Ne IV, V and VI—424
Pearlman, H. (see Amdur, I.)—689(A)
Pecher, Charles (see Helmholz, A. C.)—902(L)
Pepinsky, R. Twinning in nesquehonite, $MgCO_3 \cdot 3H_2O$—925(A)
Peters, B. and C. Richman. Deuteron disintegration by electrons—804
Petrauskas, Alex (see Cartwright, C. Hawley)—475(A)
Petrauskas, A. A. (see Van Atta, L. C.)—688(A)
——, **F. E. Myers and L. C. Van Atta.** Absorption coefficients in lead for x-rays produced in the voltage range from 0.7 to 2.5 Mv—688(A)
Phillips, M. and E. Feenberg. Coulomb exchange energy in light nuclei—400(L)
Pickering, W. H. (see Neher, H. V.)—930(A)
—— **and H. V. Neher.** Results of a high altitude cosmic-ray survey near the magnetic equator—930(A)
Pielemeier, W. H. (see Hardy, H. C.)—934(A)
—— (see Telfair, D.)—934(A)
Pierce, J. A. Note on ionization by meteors—625
Pietenpol, W. B. Electron, a quantum unit in nuclear disintegrations—466(A)
—— (see Westerfield, E. C.)—466(A)
Pirenne, Maurice H. (see Hecht, Selig)—772(T)
Platt, John R. and Otto Laporte. General considerations concerning term energies of configurations d^x—684(A)
—— **and Ralph A. Sawyer.** New classifications in Au I and Au II—916(A)
Plesset, Ernst H. Studies with a permanent-magnet β-ray spectrograph—936(A)
Plumley, Harold J. Conduction of electricity by dielectric liquids at high field strengths—114(A), 200
Pollard, Ernest (see Humphreys, Richard F.)—942(A)
—— (see Shrader, E. F.)—277
—— (see Smith, Everett C.)—466(A), 942(A)
—— **and Richard F. Humphreys.** Energy levels of Mg^{20} and Si^{30} formed by deuteron bombardment—466(A)
Polster, Harry D. (see Paul, Fred W.)—424
Pomerantz, Martin A. and Thomas H. Johnson. Relative stopping powers of carbon and lead for slow mesons—143, 471(A)
Pompeia, P. A. (see Santos, M. Damy de Souza)—902(L)
Pool, M. L. (see Kurbatov, J. D.)—919(A)
—— (see Law, H. B.)—936(A)

Potapenko, G. New circuit for generating alternating electric pulses of very short duration—220(A)
Powell, Wilson M. Slow protons and mesotrons at 4300 meters—471(A)
Present, R. D. Inflation of heavy nuclei—918(A)
—— Possibility of ternary fission—466(A)
Preston, W. M. Far ultraviolet absorption coefficients—914(A)
Prigogine, J. (see Sack, H. S.)—924(A)
Primakoff, H. (see Holstein, T.)—388
Pugh, Emerson M. Hall e.m.f. and intensity of magnetization—476(A)

Quill, L. L. (see Law, H. B.)—936(A)

Rado, G. T. and A. R. Kaufmann. Saturation magnetization of nickel-antimony and nickel-tantalum alloys—690(A)
Ragan, G. L., W. R. Kanne and R. F. Taschek. Scattering of protons in hydrogen from 200 to 300 kev—687(A)
Ramo, Simon (see Blewett, John P.)—922(A)
Ramsey, W. E. (see Rose, M. E.)—616(L), 691(A)
—— (see Swann, W. F. G.)—931(A)
——, **Emmett Hudspeth and Wayne L. Lees.** Further verification of the Montgomery theory of Geiger counter discharge—685(A)
——, **W. F. G. Swann and Paul Weisz.** Multiple values of the specific ionization produced by cosmic-ray entities—932(A)
Randall, H. M. (see Foley, H. M.)—171
Randars, Gunnar. On the asymmetrical metric in the four-space of general relativity—195
Rao, M. Ramo. Thermal conductivity of liquids—212(L)
Rarita, William and Julian Schwinger. On the exchange properties of the neutron-proton interaction—556
—— **and Julian Schwinger.** On the neutron-proton interaction—436
—— **and Julian Schwinger.** Photo-disintegration of the deuteron—215(A)
——, **Julian Schwinger and H. A. Nye.** Photo-disintegration of the deuteron—209
Rasetti, Franco. Evidence for the radioactivity of slow mesotrons—706
—— Mean life of slow mesotrons—613(L)
Rawcliffe, R. D. Lifetime of fluorescence by an electronic method—915(A)
Read, Thomas A. Damping of mechanical vibrations in copper crystals—477(A)
Reber, R. K. and G. F. Boeker. Measurement of the magnetic susceptibility of vapors—938(A)
Reed, D. W. (see Morgan, F.)—935(A)
Regener, Victor H. and Bruno Rossi. Production of mesotrons by a neutral radiation—113(A)
—— (see Hilberry, Norman)—471(A)
Richard-Foy, R. (see Leprince-Ringuet, L.)—460(L)
Richards, H. T. Photographic plate spectrum of the neutrons from the disintegration of lithium by deuterons—796
—— (see Bennett, W. E.)—781, 904(L)
Richman, C. (see Peters, B.)—804
Rinehart, John S. Behavior of Young's modulus of beta-brass single crystals at low temperature—308
Ringo, Roy. A magnetic α-particle spectrograph—107(A)
Roberts, A. (see Downing, J. R.)—940(A)
—— **and John W. Irvine, Jr.** Radioactive isotopes of iodine—936(A)
Rogers, F. T., Jr. Note on the d. c. characteristics of the string galvanometer—911(A)
—— Note on the energy-range relations—945(A)
Rose, M. E. and S. A. Korff. Investigation of the properties of proportional counters. I—850
—— **and S. A. Korff.** Mechanism of proportional counter action—467(A)
—— **and W. E. Ramsey.** On time lags in coincident discharges of Geiger-Müller counters—616(L)
—— **and W. E. Ramsey.** Time lag studies in Geiger counters—691(A)
Rosen, N. Gravitational field in special relativity—927(A)
Rosenblith, W. A. and Richard T. Cox. Velocity of propagation of the electric impulse along the organs of the electric eel—219(A)
Rossi, Bruno. On the theory of cosmic-ray showers including ionization loss—929(A)
—— (see Regener, Victor H.)—113(A)
—— **and David B. Hall.** Variation of the rate of decay of mesotrons with momentum—223
Rothstein, Jerome and Lloyd Motz. Scattering of high energy neutrons by deuterons—916(A)
Ruben, S. and M. D. Kamen. Long-lived radioactive carbon: C^{14}—349
Rubens, Sidney M. (see Henderson, J. R.)—213(L)
—— (see Kaplan, Joseph)—218(A), 476(A)
Rubin, S. Excitation energy of excited Li^7—216(A)
—— (see Bonner, T. W.)—215(A)
Ruedy, J. E. Crystal structure and surface flow of thin evaporated antimony films—926(A)
Ryerson, C. M. (see Nielsen, W. M.)—547, 910(A)

Sachs, R. G. (see Lyddane, R. H.)—673
Sack, H. S. (see Bohlke, P. G.)—940(A)
—— **and J. Prigogine.** Association of alcohol studies by infra-red spectroscopy—924(A)
Sagane, R., G. Miyamoto and M. Ikawa. Radioactivity produced in germanium—904(L)
Sakmann, B. W. Relaxation time of colloidal particles from measurements of the electro-optical effect—935(A)
Salant, E. O. (see Horvath, W. J.)—154
Santos, M. Damy de Souza, P. A. Pompeia and G. Wataghin. Showers of penetrating particles—902(L)
Sawyer, Ralph A. (see Platt, John R.)—916(A)
—— (see Wheatley, Marshall A.)—916(A)
Scharff-Goldhaber, G. Energy of the hard gamma-rays of radio-yttrium (100 days)—937(A)
—— (see Good, W. E.)—917(A)
Schein, Marcel (see Carlson, J. Franklin)—840(L)
—— (see Groetzinger, Gerhart)—113(A)
—— (see Jesse, William P.)—930(A)
—— (see Wollan, E. O.)—930(A)

——, **William P. Jesse and E. O. Wollan.** Nature of the primary cosmic radiation and the origin of the mesotron —615(L)
——, **William P. Jesse and E. O. Wollan.** Production of mesotrons by ionizing cosmic rays—930(A)
Schiff, I. I. Note on the structure of liquid helium—839(L)
—— On the phase transition in liquid helium—477(A), 758
—— Structure of liquid helium—927(A)
—— Theory of degenerate non-ideal gases—751
Schilling, Harold K. Lattice type acoustic filter—111(A)
—— Lattice type acoustic filter. II—469(A)
Schmid, R. F. (see Gerö, L.)—528(L)
Schoenberg, Mario. Angular momenta of gravitational fields—616(L)
—— (see Gamow, G.)—539
Schremp, E. J. and Alfredo Baños, Jr. On the fine structure pattern of cosmic rays at Mexico City. II—614(L)
Schwarz, G. (see Bearden, J. A.)—934(A)
Schwinger, Julian (see Rarita, William)—209, 215(A), 436, 556
Scott, W. T. (see Dresden, M.)—112(A)
Seaborg, G. T. (see Segrè, E.)—212(L)
—— **and G. Friedlander.** Radioactive isotopes of osmium —400(L)
——, **J. W. Gofman and J. W. Kennedy.** Radioactive isotope of protoactinium—321(L)
——, **J. J. Livingood and G. Friedlander.** Radioactive isotopes of germanium—320(L)
Seely, Samuel. Work function and temperature—75
Segrè, E. (see Fermi, E.)—680(L)
—— **and G. T. Seaborg.** Fission products of uranium and thorium produced by high energy neutrons—212(L)
Seidl, F. G. P. East-west asymmetry of the cosmic radiation at high latitudes—7
Seitz, Frederick. Dislocations and the theory of creep—477(A)
Sekido, Y. (see Nishina, Y.)—401(L), 679(L)
Serin, B. (see Ellickson, R. T.)—922(A)
Shaffer, Wave H. (see Silver, Samuel)—474(A)
Sharrah, P. C. and N. S. Gingrich. Diffraction of x-rays by liquid oxygen—472(A)
Shaw, C. H. and J. A. Bearden. Secondary structure in the absorption limits of gases—690(A)
Shearin, Paul E. and T. Eugene Pardue. Measurement of the electron-electron cross section at energies from 1.3 to 2.6 Mev—933(A)
Sherr, R. and K. T. Bainbridge. Transmutation of mercury by fast neutrons—937(A)
Sherwin, C. W. and A. J. Dempster. Relative abundance of the calcium isotopes—114(A)
Shima, S. (see Okuda, T.)—104(L)
Shindo, S. (see Okuda, T.)—104(L)
Shinohara, Kenichi and Mitio Hatoyama. Pair production in the field of an electron—461(L)
Shlaer, Simon (see Hecht, Selig)—772(T)
Shoupp, W. E. (see Haxby, R. O.)—57
Shrader, E. F. and Ernest Pollard. Protons from the deuteron bombardment of the separated isotopes of chlorine —277
Shutt, R. P. and T. H. Johnson. Wilson cloud chamber study of scattering and stopping of mesotrons in lead—113(A)
—— (see Johnson, T. H.)—470(A)
Sidhu, S. S. (see Worrell, Francis T.)—944(A)
Siegel, Stanley. Experimental study of the diffuse scattering of x-rays by potassium chloride crystals—371
Silver, Samuel and Wave H. Shaffer. Vibration-rotation energies of the planar XY_3 molecular model—474(A)
Simamura, H. (see Nishina, Y.)—679(L)
Sinma, K. and F. Yamasaki. Capture cross sections for slow neutrons—402(L)
Skaggs, Lester S. (see Allison, Samuel K.)—108(A)
Smith, Charles G. Studies of a ring discharge—997
Smith, E. and Ernest Pollard. Energy levels of S^{33} by deuteron bombardment of S^{32}—942(A)
—— **and Ernest Pollard.** Proton distribution in the O. P. process—466(A)
Smith, G. P. Beta-ray spectra of scandium—937(A)
—— (see Collar, H. W.)—937(A)
Smith, Lincoln G. High resolution study of the infra-red bands of cyclopropane—924(A)
Smith, Nicholas M., Jr. (see Allison, Samuel K.)—108(A)
—— (see Van Allen, J. A.)—108(A), 501, 618(L)
Smith, R. C. (see Hatfield, T. N.)—911(A)
Smith, W. V. Surface recombination of hydrogen atoms and hydroxyl radicals at different surfaces—689(A)
Smoluchowski, R. On the molecular-field theory of volume magnetostriction—476(A)
—— On the theory of volume magnetostriction—309
—— Work function and double layer—944(A)
Snoddy, L. B. (see Stauffacher, Arthur L.)—468(A)
Snyder, H. Are there spin one mesotrons?—1043(L)
Snyder, T. M. Effect of chemical combination on x-ray emission lines—689(A)
—— Fluorescent K x-rays from ions in solution and from gases—168
—— (see Bearden, J. A.)—162
Sparing, W. H. (see Copeland, Paul L.)—115(A)
Sponer, Hertha D. E. Absorption spectra of substituted benzenes—910(T)
—— (see Hebb, M. H.)—925(A)
—— **and S. H. Wollman.** Absorption spectrum of fluorobenzene in the near ultraviolet—924(A)
Squire, C. F. and A. R. Kaufmann. Electron configuration change in metallic Zr from magnetic and resistance measurements—690(A)
Starr, C. Paramagnetic dispersion—938(A)
—— Paramagnetic relaxation—690(A)
—— (see Kaufmann, A. R.)—690(A)
—— **and A. R. Kaufmann.** Magnetic susceptibility of metallic lithium—476(A)
Stauffacher, Arthur L., J. W. Beams and L. B. Snoddy. New analytical ultracentrifuge—468(A)
Steigman, Joseph. Concentration method for certain radioactive metals—498
Stephens, W. E. (see Haxby, R. O.)—57
Stevenson, A. F. Influence of end effect on the theoretical shape of intensity curves in radiofrequency spectra—767(L)

—— Note on the "Kepler problem" in a spherical space, and the factorization method of solving eigenvalue problems—842(L)
Stever, H. G. Deadtime of a Geiger counter—219(A)
—— Directional Geiger counter—765(L)
Stout, Perry R. (see Helmholz, A. C.)—902(L)
Straus, Henry A. Abundance ratio Ni^{61} : Ni^{64}—102(L)
—— New mass spectrograph and the isotopic constitution of nickel—430
Streib, J. F. (see Bonner, T. W.)—215(A)
——, **W. A. Fowler and C. C. Lauritsen.** Measurement of the absolute yield of gamma-radiation—215(A)
——, **W. A. Fowler and C. C. Lauritsen.** Transmutation of fluorine by protons—253
Strong, John (see Summerfield, Martin)—217(A)
Stuhlman, Otto, Jr. Correlation between cochlear microphonics and stapes motion—911(A)
Sullivan, L. J. (see Harvey, G. G.)—929(A)
Summerfield, Martin and John Strong. "Ultra-Spectrometer" technique for infra-red absorption bands—217(A)
Swann, W. F. G. Further evidence for a single component in the primary cosmic radiation—836(L)
—— Single component for the primary cosmic radiation—770(L)
—— (see Ramsey, W. E.)—932(A)
—— **and Wayne L. Lees.** Cosmic rays and the nature of the field in magnetized iron—470(A)
—— **and W. E. Ramsey.** Further experiments on mesotron showers—931(A)
Swanson, D. C. (see Hunter, G. T.)—911(A)
Sweeney, W. J. (see McAlister, E. D.)—922(A)

Taft, Robert B. Gamma-radiation from airplane instruments—470(A)
Takamine, T. (see Tanaka, Y.)—613(L), 771(L)
Tanaka, Y. and T. Takamine. Vibrational structure of the $^2\Sigma_g^+ \leftarrow {}^1\Sigma_g^+$ Rydberg series of N_2—613(L)
—— Vibrational structure of the $^4\Sigma_g^-(O_2^+) \leftarrow {}^3\Sigma_g^-$ Rydberg series of O_2—771(L)
Taschek, R. F. (see Ragan, G. L.)—687(A)
Tate, John T. (see Hagstrum, Homer D.)—354, 509
Tatel, H. Proton recoils from high energy neutrons—916(A)
Telfair, D. and W. H. Pielemeier. Supersonic measurements with a new apparatus—934(A)
Teller, Edward. Use of isotopes in molecular spectra—910(T)
—— (see Knipp, Julian)—659
—— (see Lyddane, R. H.)—673
Thaxton, H. M. and S. H. Miles. Phase shifts in the scattering of 100-Mev protons by protons—945(A)
——, **L. E. Bailey and H. E. Webb.** Coulomb wave functions in repulsive fields—474(A)
Thomas, Roy (see Batdorf, S. B.)—621
Tomboulian, D. H. (see Cady, Willoughby M.)—381, 472(A)
—— **and Willoughby M. Cady.** Radiative x-ray transitions within the *L* shell—422
Tomlinson, E. P. Magnetic electron-pair spectrograph—216(A)
Tonks, Lewi. Transmission of an electron density disturbance along a positive column in a longitudinal field—522
—— (see Cummings, Charles S.)—514
Torrey, H. C. Notes on intensities of radiofrequency spectra—293
Tunell, G. Atomic arrangement of sylvanite—472(A)
Turner, C. M. (see Herb, R. G.)—111(A)
Turner, R. N. (see Wilson, V. C.)—931(A)
Tykociner, J. T. and L. R. Bloom. Photoelectric sensitization of metal surfaces in group II by optical dissociation of water vapor—115(A)

Uehling, E. A. Density distribution in the steady-state diffusion of neutrons—136
Ufford, C. W. Interaction of electrons in metals and insulators—598
Uhlenbeck, G. E. (see Dresden, M.)—112(A)
Underwood, N. and J. T. Diaz. Study of the gaseous exchange between the circulatory system and the lungs—911(A)
Urry, William D. Radio-elements in the water and sediments of the ocean—479(A)

Valley, G. E. Internal conversion in rhenium—686(A)
—— Stable isotopes of nickel—836(L)
—— **and H. H. Anderson.** Relative abundance of the stable isotopes of terrestrial and meteoritic iron—113(A)
Van Allen, James A. and Nicholas M. Smith, Jr. Absolute cross section for the photo-disintegration of deuterium by 6.2-Mev quanta—618(L)
—— Absolute number of quanta from the bombardment of fluorine with protons—108(A), 501
Van Atta, L. C. (see Petrauskas, A. A.)—688(A)
——, **F. E. Myers and A. A. Petrauskas.** Variation with angle of the intensity and hardness of x-rays produced at 0.9, 1.6, and 2.35 Mv—688(A)
Van de Graaff, R. J. and W. W. Buechner. Test of the suggested emission of neutrinos due to the impact of electrons on heavy nuclei—687(A)
Vanderberg, R. M. Exact comparison of small currents—114(A)
Van Dyke, K. S. and Maynard C. Waltz. Measured admittances of a Rochelle salt resonator—686(A)
Van Vleck, J. H. Calculation of energy exchange between lattice oscillators—730
—— Note on Liouville's theorem and the Heisenberg uncertainty principle—682(A)
—— On the mechanism of paramagnetic relaxation at helium temperatures—938(A)
—— Paramagnetic relaxation and the equilibrium of lattice oscillators—724
Van Voorhis, C. C. (see Barschall, H. H.)—917(A)
Veksler, V. I. and N. A. Dobrotin. On secondary slow mesotrons—1044(L)
Vinti, John P. Correction: Isotope shift in boron—103(L)

Wait, G. R. Small-ion content of air in a closed room occupied by people—936(A)

Waldman, B. (see Collins, G. B.)—109(A)
Walerstein, I. Absorption spectrum of monobromobenzene—924(A)
Wall, C. N. Atomic distribution curve for liquid argon—927(A)
Waltz, Maynard C. (see Van Dyke, K. S.)—686(A)
Wannier, Gregory H. Statistics of the two-dimensional ferromagnet—683(A)
Warren, B. E. X-ray diffraction in random layer lattices—693
—— **and J. Biscoe.** X-ray diffraction in random layer lattices—688(A)
—— **and K. W. Hering.** Random structure of chrysotile asbestos—925(A)
Wataghin, G. (see Santos, M. Damy de Souza)—902(L)
Watanabe, Kenichi. Resonance broadening of the sodium *D* lines—151
Waterman, A. T. Electron emission from surfaces subject to periodic fluctuations in work function—943(A)
Watt, B. E. (see Bennett, W. E.)—781, 793, 904(L)
Webb, H. E. (see Thaxton, H. M.)—474(A)
Weber, A. H. and L. J. Eisele, S.J. Photoelectric and electric properties of thin bismuth films of measured thickness—473(A)
Weinberg, J. W. Scattering in the pair theory of nuclear forces—776
Weisskopf, V. F. Note on the radiation properties of heavy nuclei—318
—— (see Marshak, R. E.)—130, 471(A)
Weissler, Gerhard L. Point-to-plane corona in very pure N_2 and H_2—217(A)
Weisz, Paul. Rest mass and lifetime of the mesotron as found from cosmic-ray measurements—931(A)
—— Rest mass of the mesotron—845
—— (see Ramsey, W. E.)—932(A)
Welles, S. B. Deuteron bombardment of oxygen—679(L)
—— Partial separation of the oxygen isotopes by thermal diffusion—920(A)
Wells, W. H. (see Haxby, R. O.)—57
Welton, T. A. (see Bartlett, J. H., Jr.)—281
Westerfield, E. C. and W. B. Pietenpol. Quantum likelihood—466(A)
Whaley, R. M. (see Long, V. A.)—470(A)
Wheatley, Marshall A. and Ralph A. Sawyer. New classifications in the spectrum of Cs II—916(A)
Wheeler, John Archibald. Action at a distance between simple atoms—928(A)
—— Alpha-particle model and the properties of the nucleus Be^8—27
—— Interaction between two alpha-particles and the properties of Be^8—108(A)
—— Scattering of alpha-particles in helium—16
—— (see Feynman, R. P.)—683(A)
Wheeler, Lisle L. (see Brown, S. Leroy)—468(A)
White, A. H. Structure of black carbon—772(T)
White, Addison H. and Lester H. Germer. Structure of black carbon—926(A)
White, M. G., E. C. Creutz, L. A. Delsasso and R. R. Wilson. Positrons from light nuclei—63
Whitson, William L. (see Jacobs, James A.)—108(A)
Williams, Dudley (see Nielsen, Alvin H.)—911(A)
——, **Walter Millett and Alvin Cohen.** Wadsworth-Littrow spectrometer for the near infra-red—911(A)
Williams, H. J. (see Bozorth, R. M.)—827
—— **and R. M. Bozorth.** Magnetic domain size determined from measurements of damping in 68 Permalloy—939(A)
——, **R. M. Bozorth and H. Christensen.** Magnetostriction, Young's modulus and damping of 68 Permalloy as dependent on magnetization and heat treatment—1005
Wilson, Robert R. (see Creutz, Edward C.)—916(A)
—— (see White, M. G.)—63
—— **and Edward C. Creutz.** Proton-proton scattering at 8 Mev—916(A)
Wilson, Volney C. (see Hughes, Donald J.)—931(A)
—— **and R. N. Turner.** Latitude effects of the hard and soft components of cosmic rays—931(A)
Wollan, E. O. (see Groetzinger, Gerhart)—113(A)
—— (see Jesse, William P.)—930(A)
—— (see Schein, Marcel)—615(L), 930(A)
——, **Marcel Schein and William P. Jesse.** Nature of the primary cosmic radiation—930(A)
Wollman, S. H. (see Sponer, H.)—924(A)
Woods, L. H. On the silicon oxide bands—922(A)
Worrell, Francis T. and S. S. Sidhu. Contamination of incandescent molybdenum filaments in a vacuum obtained by an oil diffusion pump—944(A)
Wu, Chien-Shiung. Continuous x-rays excited by the beta-particles of $_{15}P^{32}$—481

Yamamoto, Mikio. Young's modulus of elasticity and its change with magnetization in iron-cobalt alloys—768(L)
Yamasaki, F. (see Sinma, K.)—402(L)
Yasaki, T. (see Nishina, Y.)—323(L), 677(L)
Yearian, H. J. New electron diffraction camera for molecular structure investigation—926(A)
Yost, R. R. (see Panofsky, W. K. H.)—219(A)
Young, V. J. (see Manning, H. P.)—941(A)

Zachariasen, W. H. On the diffuse x-ray diffraction maxima observed by C. V. Raman and P. Nilakantan—207
—— On the theory of the temperature diffuse scattering—766(L)
—— Temperature diffuse scattering maxima for rocksalt—909(L)
—— Temperature diffuse scattering of a simple cubic lattice—860
Zener, Clarence. Intrinsic inelasticity of large plates—669
Ziegler, W. T. (see Andrews, D. H.)—1045(L)
—— (see Brucksch, W. F., Jr.)—688(A)
Zwicky, F. Neutron stars as gravitational lenses—221(A)
—— On the morphology of nebulae—218(A)

Analytic Subject Index to Volume 59

References with (A) are to abstracts of papers presented at meetings of the American Physical Society.
References with (L) are to Letters to the Editor.

Absorption coefficient (see also **Scattering of electrons, etc.**; **X-ray, absorption**; **Collision diameter**)
Of primary cosmic rays, W. F. G. Swann—836(L)

Acoustics
Acoustic filter, H. K. Schilling—111(A), 469(A)
Cochlear microphonics and stapes motion, O. Stuhlman, Jr.—911(A)
Supersonic measurements, D. Telfair, W. H. Pielemeier—934(A)
Ultrasonic velocities in CO_2, C. J. Overbeck, H. C. Kendall—934(A)
Velocity and absorption by ultrasonic interferometry, J. C. Hubbard—935(A)
Velocity of sound in air, H. C. Hardy, W. H. Pielemeier—934(A)

Activated gases
Thermal activation of oxygen, H. D. Hagstrum, J. T. Tate—509

Afterglow
Auroral green line, J. Kaplan, S. M. Rubens—218(A)
Mechanism of, M. H. Hebb, H. Sponer—925(A)
N_2 rare gas mixtures, J. Kaplan, S. M. Rubens—476(A)

Astrophysics
Apsidal motion in binary stars, L. Motz—929(A)
Electron capture in white dwarf stars, P. Morrison—217(A)
Formation of multiple stars, R. Gunn—929(A)
Infra-red solar spectrum, A. Adel—915(A)
Morphology of nebulae, F. Zwicky—218(A)
Neutrino theory of stellar collapse, G. Gamow, M. Schoenberg—539; G. Gamow—617(L)
Neutron stars as lenses, F. Zwicky—221(A)
Rotational fission of star, R. Gunn—680(L)
Temperature-density distribution in sun, H. A. Bethe, G. Blanch, A. N. Lowan, R. E. Marshak—467(A)

Atmosphere (see **Meteorology**)

Atmospheric electricity (see **Meteorology**)

Atomic and molecular beams
Reflection at LiF surfaces, W. H. Bessey—459(L)

Atomic and molecular radii (see also **Scattering of electrons**)
And diffusion of ions, G. Jaffé—652

Atomic structure (see also **Spectra**)
Energies of configuration d^5, O. Laporte—684(A)
Energies of configurations d^2, J. R. Platt, O. Laporte—684(A)
Energy diffferences within $3d^3$, J. E. Mack, E. E. Anderson—683(A)
Interaction potentials, I. Amdur, H. Pearlman—689(A)
Self-consistent field for Ge^{++} and Ge, W. Hartree, D. R. Hartree—306
Self-consistent field for Ni, R. B. Gray, M. F. Manning—475(A)
Self-consistent field for Si V and Si IV, M. F. Manning, W. Hartree, D. R. Hartree—683(A)
Self-consistent field for Zn, Ga, Ga^+, Ga^{+++}, As, As^+, As^{++}, As^{+++}, W. Hartree, D. R. Hartree—299

Biophysics
Biophysical indicator for metal ions, A. Goetz, S. S. Goetz—219(A)
Desiccating human plasma, T. R. Folsom—685(A)
Electric impulse along organs of electric eel, W. A. Rosenblith, R. T. Cox—219(A)
Gaseous exchange in lungs, N. Underwood, J. T. Diaz—911(A)
Impedance of squid giant nerve fiber, K. S. Cole, R. F. Baker—685(A)
Infra-red transmission of human body, C. H. Cartwright, J. Daniel, A. Petrauskas—475(A)
Phosphate fixation of soils, S. S. Ballard, L. A. Dean—467(A)
Thorium, study of phagocytosis, F. A. Maxfield, O. A. Mortensen—107(A)
Ultraviolet absorption of spores, P. A. Cole—475(A)

Collision diameter (see **Atomic and molecular radii**)

Colloids
Relaxation time of colloidal particles, B. W. Sakmann—935(A)

Conductivity, electrical (see **Electrical conductivity**; **Discharge of electricity in gases**)

Constants, physical, Standards
Evaluation of h/e, J. A. Bearden, G. Schwarz—934(A)
h, c, and e, relationship, A. Landé—475(A)
Redetermination of h/e, J. W. M. DuMond, H. H. Bailey, W. K. H. Panofsky, A. E. S. Green—219(A)
Rydberg constant, R. T. Birge—221(A)

Cosmic radiation
Burst production by mesotrons, R. F. Christy, S. Kusaka—220(A), 414
Cascade showers, theory of, H. C. Corben—216(A)
Cloud chamber for cosmic-ray studies, T. H. Johnson, J. G. Barry, R. P. Shutt—470(A)
Cloud chamber pictures at 29,000 feet, G. Herzog, W. H. Bostick—113(A), 122; G. Herzog—117
Cloud chamber studies under ground, D. J. Hughes, V. C. Wilson—931(A)
Decay of mesotrons with momentum, B. Rossi, D. B. Hall—223
Decay radiation, L. W. Nordheim—910(A)
At depth of 1400 meters of water, Y. Nishina, Y. Sekido, Y. Miyazaki, T. Masuda—401(L)
East-west asymmetry, high latitudes, F. G. P. Seidl—7
East-west asymmetry, positive mesotrons, T. H. Johnson—11, 112(A)
Effect of temperature, N. F. Beardsley—931(A)
Electric fields in space, F. Evans—1; F. L. Mohler—1043(L)
Energy distribution and composition of primary particles, N. Hilberry—763
Extension of large showers, H. A. Bethe—684(A)

Fine structure pattern at Mexico City, E. J. Schremp, A. Baños, Jr.—614(L)
Fluctuations, V. A. Long, R. M. Whaley—470(A)
Frequency-extension curves, N. Hilberry, V. H. Regener—471(A)
Geomagnetic character and intensity, J. W. Broxon—678(L), 909(L)
Height of mesotron-producing layer of air, N. F. Beardsley—402(L)
High altitude survey near magnetic equator, W. H. Pickering, H. V. Neher—930(A)
High specific ionization at high elevations, S. A. Korff—214(L)
Integral equations for showers, M. Dresden, W. T. Scott, G. E. Uhlenbeck—112(A)
Intensities and meteorological conditions, N. F. Beardsley—470(A)
Intensities and typhoons, Y. Nishina, Y. Sekido, H. Simamura, H. Arakawa—679(L)
Intensity and air temperatures and pressures, N. F. Beardsley—233
Lateral extension of showers, L. W. Nordheim—929(A)
Latitude effect above 50°N latitude, P. F. Gast, D. H. Loughridge—127
Latitude effects, V. C. Wilson, R. N. Turner—931(A)
Life of slow mesotrons, F. Rasetti—613(L)
Mesotron lifetime measurement, W. M. Nielsen, C. M. Ryerson, L. W. Nordheim, K. Z. Morgan—547, 910(A)
Mesotron showers, W. F. G. Swann, W. E. Ramsey—931(A)
Mesotrons, slow, V. I. Veksler, N. A. Dobrotin—1044(L)
Mesotrons by neutral radiation, V. H. Regener, B. Rossi—113(A)
Multiple values of specific ionization, W. E. Ramsey, W. F. G. Swann, P. Weisz—932(A)
Nature of primary radiation, M. Schein, W. P. Jesse, E. O. Wollan—615(L); E. O. Wollan, M. Schein, W. P. Jesse—930(A); W. F. G. Swann—770(L)
Nuclear particles, S. A. Korff—949
Production and absorption of mesotrons, G. Groetzinger, E. O. Wollan, M. Schein—113(A)
Production of He^3, R. D. Hill—103(L)
Production of mesotrons, J. F. Carlson, M. Schein—840(L); M. Schein, W. P. Jesse, E. O. Wollan—930(A)
Protons and mesotrons at 4300 meters, W. M. Powell—471(A)
Radio-sonde, H. V. Neher, W. H. Pickering—930(A)
Rays in Bering Sea, P. F. Gast, D. H. Loughridge—769(L)
Rays in magnetized iron, W. F. G. Swann, W. L. Lees—470(A)
Recurrence phenomena, J. W. Broxon—470(A), 773
Recurrence pulses, A. H. Compton, A. T. Monk—112(A)
Rest mass and lifetime of the mesotron, P. Weisz—845, 931(A)
Showers with altitude variation, N. Hilberry—112(A)
Showers of penetrating particles, M. Damy de Souza Santos, P. A. Pompeia, G. Wataghin—902(L)
Single component for primary radiation, W. F. G. Swann—770(L)
Stopping of mesotrons in Pb, R. P. Shutt, T. H. Johnson—113(A)
Stopping powers of C and Pb for mesons, M. A. Pomerantz, T. H. Johnson—143, 471(A)
Testing of hypothetical distribution of energy, R. A. Millikan—930(A)
Theory of longitudinal and transverse mesons, M. Kobayasi—843(L)
Theory of showers, B. Rossi—929(A)
Transition effect for large showers, C. G. Montgomery, D. D. Montgomery—471(A)
Vertical intensity and latitude effect, W. P. Jesse, E. O. Wollan, M. Schein—930(A)

Crystal structure
Of black carbon, A. H. White, L. H. Germer—926(A)
Of chrysotile asbestos, B. E. Warren, K. W. Hering—925(A)
Of evaporated Sb films, J. E. Ruedy—926(A)
Images from etched surfaces, H. H. Hubbell, Jr.—473(A)
Indexing of powder diffraction patterns, L. K. Frevel—925(A)
Order-disorder, spinels, F. C. Blake—477(A)
Of polyvinyl alcohol, R. C. L. Mooney—925(A)
Random layer lattices, B. E. Warren, J. Biscoe—688(A), 693
Stretched rubber, C. M. Parshall, K. Lark-Horovitz—926(A)
Of sylvanite, G. Tunell—472(A)
Twinning in nesquehonite, R. Pepinsky—925(A)

Crystalline state
Crystallization phenomena, fatigue in metallic conglomerates, S. Kyropoulos—220(A)
Dislocations in polycrystalline copper, A. W. Lawson—943(A)
Energy exchange between lattice oscillators, J. H. Van Vleck—730
Granulation, microstructure, M. Avrami—688(A)
Impurities in Cu, brass and Ag, F. W. Constant, R. E. Faires—938(A)
Interaction of electrons, C. W. Ufford—598
LiF cleavage surfaces, secondary structure, W. H. Bessey—459(L)
Molybdenite as a lubricant, M. E. Bell, J. H. Findlay—922(A)
Polar vibrations of alkali halides, R. H. Lyddane, R. G. Sachs, E. Teller—673
Transitions in alloys, W. R. Ham, F. D. Bennett—939(A)
Virial theorem, theory of metals, R. Landshoff—906(L)

Dielectric constants (see **Dielectrics and dielectric properties**)

Dielectrics and dielectric properties
Of aliphatic ketones, R. H. Cole—689(A)
Breakdown of glasses and crystals, A. von Hippel, R. J. Maurer—820
Conduction at high fields, H. J. Plumley—114(A), 200
Dispersion and absorption, R. H. Cole, K. S. Cole—474(A)
Polar vibrations of alkali halides, R. H. Lyddane, R. G. Sachs, E. Teller—673

Dielectrics and dielectric properties (continued)
NaCl and mixed crystals NaCl-AgCl, A. von Hippel, G. M. Lee—691(A)
Scattering, trapping, and release of electrons in NaCl, A. von Hippel, G. M. Lee—824
Theory of dielectric loss, B. Gross—748
Transient currents, K. S. Cole, R. H. Cole—935(A)
Diffusion (see also **Thermal diffusion**)
Determination of coefficients, R. T. Ellickson, B. Serin—922(A)
And recombination of ions, G. Jaffé—652
Self-diffusion in Zn, F. R. Banks—376; F. R. Banks, P. H. Miller, Jr.—943(A)
Steady-state diffusion of neutrons, E. A. Uehling—136
Discharge of electricity in gases
Anode spots in O_2, J. E. Henderson, S. M. Rubens—213(L)
Light from high current discharges, J. W. Flowers—685(A)
Longitudinal magnetic field; Hg discharge, C. S. Cummings, L. Tonks—514
In micro-gaps, R. W. Jones, W. S. Huxford—932(A)
Phase of arc-back in rectifiers, A. W. Hull, F. R. Elder—115(A)
Point-to-plane corona, G. L. Weissler—217(A)
Recovery of dielectric strength in arcs, W. M. Bauer, J. D. Cobine—115(A)
Ring discharge, C. G. Smith—997
Stability of low pressure Hg arc, P. L. Copeland, W. H. Sparing—115(A)
Theory of Geiger counter discharge, W. E. Ramsey, E. Hudspeth, W. L. Lees—685(A)
Time lags in counters, M. E. Rose, W. E. Ramsey—691(A); C. G. Montgomery and D. D. Montgomery—1045(L)
Transmission of electron density disturbance, L. Tonks—522
Disintegration and excitation of nucleus (see also **Radioactivity**)
α-particles from $F^{19}+H^1$, R. A. Becker, W. A. Fowler, C. C. Lauritsen—217(A)
α-particles from Li, S. K. Allison, L. C. Miller, L. S. Skaggs, N. M. Smith, Jr.—108(A)
α-proton reactions of Na and Al, R. F. Humphreys, E. Pollard—942(A)
β-ray energy of H^3, S. C. Brown—954
Of C by H^2, W. E. Bennett, T. W. Bonner, E. Hudspeth, H. T. Richards, B. E. Watt—781
Deuteron disintegration by electrons, B. Peters, C. Richman—804
Distribution in angle of α-particles from B, J. A. Jacobs, W. L. Whitson—108(A)
Distribution of protons from D-D reaction, H. P. Manning, C. M. Crenshaw, V. J. Young—941(A)
Emission of neutrinos from heavy nuclei, R. J. Van de Graaff, W. W. Buechner—687(A)
Energy of γ-rays from F, W. E. Bennett, T. W. Bonner, B. E. Watt—793
Energy levels of Mg^{26} and Si^{30}, E. Pollard, R. F. Humphreys—466(A)
Energy levels of S^{33}, E. Smith, E. Pollard—942(A)
Energy of neutrons from H^2-H^2, T. W. Bonner—237
Excitation energy of Li^7, S. Rubin—216(A)
Excitation of γ-rays by neutrons, Itaru Nonaka—681(L)
Excitation by x-rays, J. R. Feldmeier, G. B. Collins—937(A)
Of F^{19} by H^1, J. F. Streib, W. A. Fowler, C. C. Lauritsen—253
γ-ray from Li+D, W. E. Bennett, T. W. Bonner, H. T. Richards, B. E. Watt—904(L)
γ-rays from C+H^2, T. W. Bonner, R. A. Becker, S. Rubin, J. F. Streib—215(A)
Lifetimes of excited states of nuclei, I. S. Lowen—835(L)
Neutrons from disintegration of Li by deuterons, H. T. Richards—796
Of N and O by neutrons, W. Hansen—941(A)
$N^{14}(d,H^3)N^{13}$ reaction, L. B. Borst—941(A)
Number of quanta from F, J. A. Van Allen, N. M. Smith, Jr.—108(A)
Of O^{17} by deuterons, S. B. Welles—679 (L)
Photo-disintegration of deuterium, W. Rarita, J. Schwinger—209, 215(A); J. A. Van Allen, N. M. Smith, Jr.—618(L)
Proton distribution in O.P. process, E. C. Smith, E. Pollard—466(A)
Protons from isotopes of Cl, E. F. Shrader, E. Pollard—277
Quanta from bombardment of F with protons, J. A. Van Allen, N. M. Smith, Jr.—501
Reaction energies Cu isotopes, H. W. Newson, L. B. Borst—941(A)
Theory of longitudinal and transverse mesons, M. Kobayasi—843(L)
Transmutation by protons, T. Lauritsen, C. C. Lauritsen, W. A. Fowler—241
By x-rays, G. B. Collins, B. Waldman—109(A); E. Guth—109(A), 325
Dissociation
Of diatomic molecules by electron impact, H. D. Hagstrum, J. T. Tate—354
Of water vapor, R. J. Dwyer—928(A)

Elasticity
c_{44} elastic constant for beta-quartz, J. V. Atanasoff, E. Kammer—97
Damping of vibrations in Cu crystals, T. A. Read—477(A)
Dislocation near plane boundary, J. S. Koehler—477(A)
Dislocations in NaCl, H. B. Huntington—942(A)
Elastic constants, temperature coefficients for quartz, J. V. Atanasoff, P. J. Hart—85; A. W. Lawson—838(L)
Energy of work hardening, J. S. Koehler—943(A)
Intrinsic inelasticity of large plates, C. Zener—669
Isothermal and adiabatic elasticities, H. F. Ludloff—111(A)
Modulus s_{13} of beta-quartz, A. W. Lawson—608
In order-disorder transformations, H. F. Ludloff—939(A)

Rigidity and friction of glass, F. Birch, D. Bancroft—685(A)
S_{12} constant of Zn, A. W. Hanson—912(A)
Stress-strain curve for rubberlike materials, H. M. James, E. Guth—111(A)
Theory of creep, F. Seitz—477(A)
Velocity of waves in bars, D. Bancroft—588
Young's modulus of beta-brass crystals at low temperature, J. S. Rinehart—308
Young's modulus and damping of Permalloy, H. J. Williams, R. M. Bozorth, H. Christensen—1005
Young's modulus and magnetization in Fe-Co alloys, Mikio Yamamoto—768(L)
Young's modulus, temperature dependence, P. G. Bohlke, T. R. Cuykendall, H. S. Sack—940(A)

Electrical circuits
Admittances of Rochelle resonator, K. S. Van Dyke, M. C. Waltz—686(A)

Electrical conductivity and resistance (see also **Photoconductivity**)
Critical currents in superconducting films, W. F. Brucksch, Jr., W. T. Ziegler, E. R. Blanchard, D. H. Andrews—688(A)
Deviations from Ohm's law, L. Davis, Jr.—474(A)
Of dielectric liquids at high fields, H. J. Plumley—114(A), 200
Electron configuration change, metallic Zr, C. F. Squire, A. R. Kaufmann—690(A)
Of glass, R. J. Maurer—691(A)
Glass insulation of resistance thermometers, H. J. Hodge—921(A)
Small-ion content of air, G. R. Wait—936(A)
Superconducting films as radiometers, D. H. Andrews, W. F. Brucksch, Jr., W. T. Ziegler, E. R. Blanchard—1045(L)
Superconductivity, J. Bardeen—928(A)
Of titanium dioxide, M. D. Earle—942(A)
Of zinc oxide, P. H. Miller, Jr.—942(A)

Electromagnetic theory
Dielectric constant of a rotating space charge, J. P. Blewett, S. Ramo—922(A)
Electromagnetic self-energies, A. Landé—927(A)
Reaction of absorber; radiative damping, R. P. Feynman, J. A. Wheeler—683(A)
Velocity of radio-waves, short distances, R. C. Colwell, H. Atwood, Jr., J. E. Bailey, C. O. Marsh—935(A)

Electron diffraction
Camera for molecular structure investigation, H. J. Yearian—926(A)

Electrons
Emission of particles and pair production, S. De Benedetti—463(L)
Pair production in field of electron, Kenichi Shinohara, Mitio Hatoyama—461(L)

Electrons, secondary
Theory of, H. A. Bethe—940(A)

Electrostatics
Conjugate potentials of grid between planes, D. Kirkham—111(A)

Energy states of atoms (see **Atomic structure**)

Energy states of nucleus (see **Nuclear structure**)

Errata
Isotope shift in boron, J. P. Vinti—103(L)
On the energy losses attending thermionic and field emission. G. M. Fleming, J. E. Henderson—907(L)

Excitation of nuclei (see **Disintegration and excitation of nucleus**)

Films, properties of
Properties of Sb films, J. E. Ruedy—926(A)

Fission of nucleus
Branching ratios, U^{235}, H. L. Anderson, E. Fermi, A. V. Grosse—52
By high energy neutrons, E. Segrè, G. T. Seaborg—212(L)
Cross section for deuteron impact, J. C. Jacobsen, N. O. Lassen—1043(L)
Effect of neutron energy, S. K. Haynes—834(L)
Energy loss of heavy ions, J. Knipp, E. Teller—659
Mechanism of deuteron-induced, N. Bohr—1042(L)
Photo-fission of U and Th, R. O. Haxby, W. E. Shoupp, W. E. Stephens, W. H. Wells—57
Proton-induced, G. Dessauer, E. M. Hafner—840(L), 940(A)
Range of fragments, W. E. Lamb, Jr.—687(A)
Range and straggling of fragments, J. K. Bøggild, K. J. Brostrøm, T. Lauritsen—275
Ternary fission, R. D. Present—466(A)
Tracks on photographic plate, K. Lark-Horovitz, W. A. Miller—941(A)
Of U by α-particles, E. Fermi, E. Segrè—680(L)
Of U by fast neutrons, Y. Nishina, T. Yasaki, K. Kimura, M. Ikawa—323(L), 677(L)
Velocity-range relation for fragments, N. Bohr—270

Fluorescence
Lifetime by electronic method, R. D. Rawcliffe—915(A)

Friction
In polycrystalline copper, A. W. Lawson—943(A)
Stick-slip process, F. Morgan, M. Muskat, D. W. Reed—935(A)

Geophysics
Helium age measurements, C. Goodman, R. D. Evans, P. M. Hurley—920(A)
Motion of earth's core, D. R. Inglis—178, 469(A)
Problems of orogeny, C. R. Longwell—478(A)
Problems in seismology, L. D. Leet—479(A)
Radioactivity of rocks, R. D. Evans, C. Goodman—920(A)

Gravitation
Angular momenta of fields, M. Schoenberg—616(L)
Gravitational field in special relativity, N. Rosen—927(A)

Hydrodynamics
Morphology of drainage basins, R. E. Horton—478(A)

Hyperfine structure (see also **Nuclear moments and spin**)
Of ionized Hg, S. Mrozowski—104(L)

Ionization by collision
Of diatomic molecules, H. D. Hagstrum, J. T. Tate—354
Energy loss of heavy ions, J. Knipp, E. Teller—659
Ionization by radiation
By γ-radiation, J. F. Streib, W. A. Fowler, C. C. Lauritsen—215(A)
Ionosphere
Atmospheric haze, E. O. Hulburt—914(A)
Ionization by meteors, J. A. Pierce—625
Ultraviolet absorption, W. M. Preston—914(A)
Isotopes
Of Ca, abundance, C. W. Sherwin, A. J. Dempster—114(A)
Of C, abundance, B. F. Murphey, A. O. Nier—771(L)
Of O, abundance, B. F. Murphey—320(L)
Of Ni, H. A. Straus—102(L), 430; G. E. Valley—836(L)
Of terrestrial and meteoritic Fe, relative abundance, G. E. Valley, H. H. Anderson—113(A)
Weights of Ni isotopes, T. Okuda, K. Ogata, H. Kuroda, S. Shima, S. Shindo—104(L)

Kinetic theory of gases
Einstein condensation phenomenon, W. E. Lamb, Jr., A. Nordsieck—677(L)

Liquids (see also **Hydrodynamics**)
Atomic distribution in Al and Li, C. Gamertsfelder—926(A)
Atomic distribution in liquid A, C. N. Wall—927(A)
Atomic distribution in liquid O, P. C. Sharrah, N. S. Gingrich—472(A)
Electron distribution in Li, R. L. Griffith, P. M. Harris—110(A)
Helium II, theory of liquid, Hsien-yü Hsü, W. Band—1013
Light scattered in liquids, L. H. Dawson, E. O. Hulbert—914(A)
Phase transition in liquid He, L. I. Schiff—477(A), 758; W. E. Lamb, Jr., A. Nordsieck—927(A)
Structure of liquid He, L. I. Schiff—839(L), 927(A)
Structure of nitromethane, G. C. Danielson, K. Lark-Horovitz—110(A)
X-ray diffraction patterns, liquid A, N. S. Gingrich—290

Magnetic fields
In magnetized iron, W. F. G. Swann, W. L. Lees—470(A)
Magnetic properties
Anisotropy of $Gd_2(SO_4)_3 \cdot 8H_2O$, K. S. Krishnan, S. Banerjee—770(L)
Of Sb-Sn monocrystals, S. H. Browne, C. T. Lane—476(A), 939(A)
Of Cu-Ni alloys, A. R. Kaufmann, C. Starr—690(A)
Discontinuities of magnetostriction, C. W. Heaps—585
Dislocations and magnetization, W. F. Brown, Jr.—528(L)
Domain size, H. J. Williams, R. M. Bozorth—939(A)
Electron configuration change, metallic Zr, C. F. Squire, A. R. Kaufmann—690(A)
Hall e.m.f., E. M. Pugh—476(A)
Impurities in Cu, brass and Ag, F. W. Constant, R. E. Faires—938(A)
Magnetostriction of Permalloy, H. J. Williams, R. M. Bozorth, H. Christensen—1005
Molecular-field theory of magnetostriction, R. Smoluchowski—476(A)
Paramagnetic dispersion, C. Starr—938(A)
Paramagnetic relaxation, C. Starr—690(A)
Paramagnetic relaxation, equilibrium of lattice oscillators, J. H. Van Vleck—724, 938(A)
Of polycrystalline ferromagnets, T. Holstein, H. Primakoff—388
Saturation of Ni-Sb and Ni-Ta alloys, G. T. Rado, A. R. Kaufmann—690(A)
Saturation value for Heusler alloys, L. A. Carapella, R. R. Hultgren—905(L)
Susceptibility of metallic Li, C. Starr, A. R. Kaufmann—476(A)
Susceptibility of vapors, R. K. Reber, G. F. Boeker—938(A)
Torque on a ferromagnetic single crystal, R. M. Bozorth, H. J. Williams—827
Volume magnetostriction, R. Smoluchowski—309
Young's modulus and magnetization in Fe-Co alloys, Mikio Yamamoto—768(L)
Magnetostriction (see **Magnetic properties**)
Mean life
Lifetimes of excited states of nuclei, I. S. Lowen—835(L)
Of mesotrons, W. F. G. Swann—836(L)
Mechanics, quantum—general
Coulomb wave functions, H. M. Thaxton, L. E. Bailey, H. E. Webb—474(A)
Eigenvalue problems, L. Infeld—737
Electron, a unit in nuclear disintegrations, W. B. Pietenpol—466(A)
Liouville's theorem and the uncertainty principle, J. H. Van Vleck—682(A)
Magnitude of electronic charges, A. Landé—434
Measurement of observables, O. Halpern, M. H. Johnson—683(A), 896
Neutron-proton interaction, W. Rarita, J. Schwinger—436, 556
Normalization of Dirac functions, C. C. Lin—841(L)
Quantum likelihood, E. C. Westerfield, W. B. Pietenpol—466(A)
Solution of eigenvalue problems, A. F. Stevenson—842(L)
Mechanics, statistical
Theory of degenerate gases, L. I. Schiff—751
Two-dimensional ferromagnet, G. H. Wannier—683(A)
Mesotrons
Burst production by mesotrons, R. F. Christy, S. Kusaka—220(A), 414
Burst production; spin one-half, zero magnetic moment, S. B. Batdorf, R. Thomas—621
Cloud-chamber pictures at 29,000 feet, G. Herzog, W. H. Bostick—113(A), 122; G. Herzog—117
In cosmic radiation at 4300 meters, W. M. Powell—471(A)

In cosmic rays, W. F. G. Swann—770(L)
Decay at 3000 meters, Nikitin Fedorenko—461(L)
Direct measurement of mass, L. Leprince-Ringuet, S. Gorodetzky, E. Nageotte, R. Richard-Foy—460(L)
Evidence for radioactivity, F. Rasetti—706
Life of slow mesotrons, F. Rasetti—613(L)
Lifetime measurement, W. M. Nielsen, C. M. Ryerson, L. W. Nordheim, K. Z. Morgan—547, 910(A)
Mesotron showers, W. F. G. Swann, W. E. Ramsey—931(A)
Nature of, L. W. Nordheim—910(A)
Nature of decay, L. W. Nordheim—554
Origin, M. Schein, W. P. Jesse, E. O. Wollan—615(L)
Production of, J. F. Carlson, M. Schein—840(L)
Production and absorption in substratosphere, G. Groetzinger, E. O. Wollan, M. Schein—113(A)
Production of mesotrons, R. F. Christy, S. Kusaka—405; M. Schein, W. P. Jesse, E. O. Wollan—930(A)
Production by neutral radiation, V. H. Regener, B. Rossi—113(A)
Rate of decay, B. Rossi, D. B. Hall—223
Rest mass and lifetime, P. Weisz—845, 931(A)
Scattering in Pb, R. P. Shutt, T. H. Johnson—113(A)
Scattering of mesons, R. E. Marshak, V. F. Weisskopf—130, 471(A)
Scattering, pair theory of nuclear forces, J. W. Weinberg—776
Scattering in W, F. L. Code—229
Showers in cosmic rays, M. Damy de Souza Santos, P. A. Pompeia, G. Wataghin—902(L)
Slow, evidence for, V. I. Veksler, N. A. Dobrotin—1044(L)
Spin, J. R. Oppenheimer—462(L)
Of spin one, H. Snyder—1043(L)
Stopping powers of C and Pb, M. A. Pomerantz, T. H. Johnson—143, 471(A)
Theory of longitudinal and transverse mesons, M. Kobayasi—843(L)

Metals (see **Crystalline state**)

Meteorology

Atmospheric haze, E. O. Hulbert—914(A)
Atmospheric nitrous oxide layer, A. Adel—944(A)
Cosmic-ray intensities and meteorological conditions, N. F. Beardsley—470(A)
Ionization by meteors, J. A. Pierce—625
Recurrence tendency in precipitation, J. W. Mauchly—469(A)

Methods and instruments

Acoustic filter, H. K. Schilling—111(A), 469(A)
Air and vacuum thermopiles, N. C. Beese—922(A)
α-particle range in gases, T. N. Hatfield, R. C. Smith—911(A)
Analysis of pulses, C. H. Page—920(A)
Analytical ultracentrifuge, A. L. Stauffacher, J. W. Beams, L. B. Snoddy—468(A)
Characteristics of string galvanometer, F. T. Rogers, Jr.—911(A)
Cloud chamber for cosmic-ray studies, T. H. Johnson, J. G. Barry, R. P. Shutt—470(A)
Combinations in cloud chambers, C. Beck—910(A)
Comparison of small currents, R. M. Vanderberg—114(A)
Concentration of radioactive metals, J. Steigman—498
Contamination of incandescent filaments, F. T. Worrell, S. S. Sidhu—944(A)
Cosmic-ray radio-sonde, H. V. Neher, W. H. Pickering—930(A)
Counter resolving times, Y. Beers—932(A)
Counting rate meter, A. F. Kip, R. D. Evans—920(A)
Crystals of NaC, various sizes, F.-H. Marshall—110(A)
Curved crystal γ-ray spectrometer, W. K. H. Panofsky, J. W. M. DuMond, R. R. Yost, H. A. Kirkpatrick—219(A)
Cyclotron R. F. power supply, R. B. Jacques—918(A)
Deadtime of counter, H. G. Stever—219(A)
Directional Geiger counter, H. G. Stever—765(L)
Electric pulses of short duration, G. Potapenko—220(A)
Electron diffraction camera, H. J. Yearian—926(A)
Electron microscope, W. V. Houston, H. Bradner—219(A)
Electron microscopical determination of object thickness, L. Marton—929(A)
Electrostatic generator, T. Lauritsen, C. C. Lauritsen, W. A. Fowler—241
Electrostatic generator with concentric electrodes, R. G. Herb, C. M. Turner, A. O. Hanson, N. D. Crane—111(A)
Electrostatic generator at Florida, G. T. Hunter, D. C. Swanson—911(A)
Energies of hard γ-rays, G. Scharff-Goldhaber—937(A)
Evaporation of molten metals, W. C. Caldwell—940(A)
Flow of a radioactive gas, W. H. Furry—919(A)
Glass insulation of resistance thermometers, H. J. Hodge—921(A)
Growth of drops in cloud chamber, W. E. Hazen—933(A)
High rotational speeds, L. E. MacHattie—468(A)
Index of refraction, thermal coefficient of H_2O, J. B. Hawkes—921(A)
Induction electron accelerator, D. W. Kerst—110(A)
Initial discharge counter breakdown, S. C. Brown, W. P. Allis—932(A)
Intensity of x-rays by electron multiplier tube, J. S. Allen—110(A)
Ion sources, I. A. Getting—467(A)
Isolation of radioactive Sr and Ba, J. D. Kurbatov, M. L. Pool, H. B. Law—919(A)
Liquid He plant at Yale, C. T. Lane—477(A)
Magnetic α-particle spectrograph, R. Ringo—107(A)
Magnetic β-ray spectrometer, M. Deutsch—684(A); R. L. McCreary—919(A)
Magnetic electron microscope, G. G. Harvey, L. J. Sullivan—929(A)
Magnetic electron-pair spectrograph, E. P. Tomlinson—216(A)
Magnetic susceptibility of vapors, R. K. Reber, G. F. Boeker—938(A)
Mass spectrograph, H. A. Straus—430
Molybdenite as a lubricant, M. E. Bell, J. H. Findlay—922(A)

Methods and instruments (continued)
Mono-energetic protons from cyclotron, E. C. Creutz, R. R. Wilson—916(A)
Multi-section accelerating tube, voltage distribution, L. J. Haworth, J. H. Manley, E. A. Luebke—108(A)
Neutron shielding, M. S. Livingston—918(A)
Neutron velocity spectrometer, C. P. Baker, R. F. Bacher—332
One-tube counter quenching circuit, T. N. Gautier—112(A)
Particle size of electro-deposited coatings, C. H. Ehrhardt, E. P. Miller—472(A)
Permanent-magnet β-ray spectrograph, E. H. Plesset—936(A)
Perturbation of boundary conditions, H. Feshbach, A. M. Clogston—189
Photoflash lamps, characteristics of, W. E. Forsythe, M. A. Easley—921(A)
Photo-neutron sources, R. D. O'Neal—919(A)
Properties of proportional counters, M. E. Rose, S. A. Korff—467(A), 850
Resistance thermometer, superconducting films, D. H. Andrews, W. F. Brucksch, Jr., W. T. Ziegler, E. R. Blanchard—1045(L)
Solution of nonlinear simultaneous equations, S. L. Brown, L. L. Wheeler—468(A)
Sound velocity and absorption by ultrasonic interferometry, J. C. Hubbard—935(A)
Specific heat of wires, B. Kurrelmeyer, W. H. Mais, E. H. Green—921(A)
Spectrograph for infra-red to 15μ, E. D. McAlister, G. L. Matheson, W. J. Sweeney—922(A)
Surface tension at high pressures, L. B. Heilprin—921(A)
Temperature correction in calorimetry, A. King, H. Grover—469(A)
Temperature distributions in cylindrical systems, M. Avrami—691(A)
Theory of Geiger counter discharge, W. E. Ramsey, E. Hudspeth, W. L. Lees—685(A)
Thickness of enamel coatings, E. P. Miller, A. V. Cohee—468(A)
Time lags in counters, M. E. Rose, W. E. Ramsey—616(L), 691(A); C. G. Montgomery, D. D. Montgomery—932(A); 1045(L)
Timer for spark breakdown, E. C. Easton, J. D. Cobine—473(A)
Topographies of fine textured surfaces, F. W. Adams, L. Devol, H. R. Letner—684(A)
Ultra-spectrometer for infra-red, M. Summerfield, J. Strong—217(A)
Wadsworth-Littrow spectrometer; infra-red, D. Williams, W. Millett, A. Cohen—911(A)

Molecular beams (see **Atomic and molecular beams**)

Molecular structure and constants (see also **Spectra, molecular** and **Raman spectra**)
Action at a distance between atoms, J. A. Wheeler—928(A)
Energies of planar XY_3 model, S. Silver, W. H. Shaffer—474(A)
Forces between ions and molecules, H. Margenau—928(A)
Magnetic moments of H_2, HD, and D_2, H. Brooks—925(A)

Neutrons
Absorption by B, Cl, Co and Mn, W. J. Horvath, E. O. Salant—154
Capture cross section of B, velocity dependence, E. A. Luebke, J. H. Manley, L. J. Haworth—918(A)
Capture cross section of F^{19}, Tl^{203}, and N^{15}, J. H. Manley, L. J. Haworth, E. A. Luebke—109(A)
Capture cross sections, K. Sinma, F. Yamasaki—402(L); J. W. Coltman—917(A)
Cross sections for C neutrons, R. D. O'Neal, M. Goldhaber—102(L), 109(A)
Excitation of γ-rays by neutrons, Itaru Nonaka—681(L)
Experiments with slow neutrons, C. P. Baker, R. F. Bacher—332
Interaction with resonance neutrons, H. B. Hanstein—489
From Li+H^2, H. T. Richards—796
Neutron shielding, M. S. Livingston—918(A)
Passage through crystals and polycrystals, O. Halpern, M. Hamermesh, M. H. Johnson—981
Passage through ferromagnets, O. Halpern, T. Holstein—960
Photo-neutron sources, R. D. O'Neal—919(A)

Nuclear moments and spin (see also **Hyperfine structure**)
Of Ba^{135} and Ba^{137}, R. H. Hay—686(A)
Of In^{115}, T. C. Hardy—686(A)

Nuclear structure (see also **Disintegration of nucleus; Energy states of nucleus**)
Of α-particles in He, H. Margenau—37
α-particle model, nucleus Be^8, J. A. Wheeler—27, 108(A)
Compressibility of nuclear matter, E. Feenberg—149
Exchange energy in light nuclei, M. Phillips, E. Feenberg—400(L)
Excitation by x-rays, E. Guth—109(A), 325; G. B. Collins, B. Waldman—109(A)
Excited states, lifetime, I. S. Lowen—835(L)
Excited states, meson-pair theory, C. L. Critchfield—48
General nuclear model, E. Feenberg—691(A)
Ground states of Be^{10} and C^{10}, E. P. Cooper, E. C. Nelson—216(A)
Nomenclature of particles, C. Møller—323(L)
Nuclear density, E. Feenberg—593, 687(A)
Production of He^3, R. D. Hill—103(L)
Protons of double charge, H. J. Bhabha—100
Radiation properties of heavy nuclei, V. F. Weisskopf—318
Radii of light elements, D. R. Elliott—918(A)
Spacing of nuclear levels, H. Margenau—467(A)
Statistics of excited states, H. Margenau—627
Volume of heavy nuclei, R. D. Present—918(A)

Optical constants and properties
Deflection by general anisotropy, P. Frank—475(A)
Index of refraction, thermal coefficient of H_2O, J. B. Hawkes—921(A)

Light scattered in liquids, L. H. Dawson, E. O. Hulbert —914(A)
Reflectivity of Al and Cu in ultraviolet, M. Banning—914(A)
Relaxation time of colloidal particles, B. W. Sakmann —935(A)

Optical instruments (see **Methods and instruments**)

Paschen-Back effect (see **Zeeman effect**)

Photo-conductivity
Of willemite crystal, R. C. Herman, R. Hofstadter—79

Photoelectric effect and properties; cells
Field dependence, surface photo-effect, C. J. Mullin, E. Guth—867, 943(A)
Of monocrystalline surfaces, P. A. Anderson—1034
Sensitization of surfaces by dissociation of water vapor, J. T. Tykociner, L. R. Bloom—115(A)
Of thin Bi films, A. H. Weber, L. J. Eisele, S. J.—473(A)

Photo-ionization (see **Ionization by radiation**)

Proceedings of the American Physical Society
Chicago, Illinois, Meeting, November 22–23, 1940—105
Pasadena, California, Meeting, December 20–21, 1940 —215
Philadelphia, Pennsylvania, Meeting, December 26–28, 1940—464
Cambridge, Massachusetts, Meeting, February 21–22, 1941—682
Metropolitan Section, Meeting, March 28, 1941—772
Southeastern Section, Meeting, April 4–5, 1941—910
Washington, D. C., Meeting, May 1–3, 1941—913

Quantum mechanics (see **Mechanics, quantum**)

Radiation
Annihilation quanta, R. Beringer, C. G. Montgomery —933(A)
Quadrupole and magnetic dipole radiation, F. A. Jenkins, S. Mrozowski—915(A)

Radio (see also **Ionosphere; Electrical circuits**)
Input impedance of antenna, R. King—684(A)
Velocity of radio-waves, short distances, R. C. Colwell, H. Atwood, Jr., J. E. Bailey, C. O. Marsh—935(A)

Radioactivity (see also **Disintegration of nucleus**)
Absolute yield of γ-radiation, J. F. Streib, W. A. Fowler, C. C. Lauritsen—215(A)
Activation of Cl by neutrons, R. D. O'Neal—109(A)
α-particle range in gases, T. N. Hatfield, R. C. Smith —911(A)
β-ray spectra of Sc, G. P. Smith—937(A)
Coincidence study of Br^{82}, J. R. Downing, A. Roberts —940(A)
Concentration of radioactive metals, J. Steigman—498
Of $_{91}Et^{233}$, β-ray spectrum, E. Haggstrom—322(L)
Energy of γ-rays of radio-yttrium, G. Scharff-Goldhaber —937(A)
Excitation by x-rays, J. R. Feldmeier, G. B. Collins —937(A)
Forbidden transitions in β-decay, R. E. Marshak—937(A)
Fourth $(4n+1)$ radioactive series, A. V. Grosse, E. T. Booth, J. R. Dunning—322(L)
γ-radiation from airplane instruments, R. B. Taft—470(A)
γ-rays from Au, E. H. Plesset—936(A)
Of Ge isotopes, G. T. Seaborg, J. J. Livingood, G. Friedlander—320(L); R. Sagane, G. Miyamoto, M. Ikawa—904(L)
Half-life of $_{14}Si^{27}$, $_{16}S^{31}$, $_{18}A^{35}$, and $_{21}Sc^{41}$, L. D. P. King, D. R. Elliott—108(A)
Of H^3, R. Cornog, W. F. Libby—1046(L)
H^3 β-ray, S. C. Brown—687(A)
Internal conversion in Re, G. E. Valley—686(A)
Isolation of radioactive Sr and Ba, J. D. Kurbatov, M. L. Pool, H. B. Law—919(A)
Isotope of Pa, G. T. Seaborg, J. W. Gofman, J. W. Kennedy—321(L)
Isotopes of I, A. Roberts, J. W. Irvine, Jr.—936(A)
Isotopes of Nd, Il and Sm; periods, H. B. Law, M. L. Pool, J. D. Kurbatov, L. L. Quill—936(A)
Isotopes of Os, G. T. Seaborg, G. Friedlander—400(L)
Of Mn^{56} and I^{128}, R. H. Bacon, E. N. Grisewood, C. W. van der Merwe—531
Positrons from light nuclei, M. G. White, E. C. Creutz, L. A. Delsasso, R. R. Wilson—63
Production and use of C^{14}, S. Ruben, M. D. Kamen —349
Radiations from Co, A. S. Jensen—936(A)
Radiations from $I^{131} \rightarrow Xe^{131}$, M. Deutsch—940(A)
Radioactive Ba from Cs, H. W. Collar, J. M. Cork, G. P. Smith—937(A)
Radioactivity of rocks, R. D. Evans, C. Goodman—920(A)
Radio-elements in the ocean, W. D. Urry—479(A)
Of Rb, A. C. Helmholtz, C. Pecher, P. R. Stout—902(L)
Rules concerning isobaric nuclei, A. E. Haas—107(A)
Of $_{21}Sc^{41}$, $_{18}A^{35}$ and $_{16}S^{31}$, D. R. Elliott, L. D. P. King —403(L)
Selection rules in β-decay, J. R. Oppenheimer—908(L)
Of slow mesotrons, F. Rasetti—706
Transmutation of Hg by neutrons, R. Sherr, K. T. Bainbridge—937(A)
Of Xe, E. P. Clancy—686(A)

Raman spectra
Of alkyl acetylenes, F. F. Cleveland, M. J. Murray—924(A)
C isotope effect in acetylenes, F. F. Cleveland, M. J. Murray—475(A)
Of ethers, F. F. Cleveland, M. J. Murray—107(A)
Of 6-dodecyn-5-one, F. F. Cleveland, M. J. Murray—478(A)

Recombination
Recombination at different surfaces, W. V. Smith—689(A)

Relativity
Asymmetrical metric of general relativity, G. Randers —195
Dynamics of a particle, C. Lanczos—813
Gravitational field in special relativity, N. Rosen—927(A)

Relativity (continued)
Measurement of observables, O. Halpern, M. H. Johnson—683(A), 896
Relativistic thermodynamics, P. G. Bergmann—928(A)
Total mass of particle, C. Lanczos—708
Resonance radiation
Quenching and depolarization, L. O. Olsen—914(A)

Scattering of electrons, neutrons, and ions (see also **Electron diffraction**)
α-particles in He, J. A. Wheeler—16; H. Margenau—37
Calculation of cross sections, E. J. Hellund—395
Capture cross sections of neutrons, J. W. Coltman—917(A)
Electron-electron cross section, P. E. Shearin, T. E. Pardue—933(A)
Energy loss of heavy ions, J. Knipp, E. Teller—659
Energy-range relations, F. T. Rogers, Jr.—945(A)
Of fast electrons by heavy elements, J. H. Bartlett, Jr., T. A. Welton—281
High energy neutrons by deuterons, J. Rothstein, L. Motz—916(A)
Inelastic scattering of protons, R. H. Dicke, J. Marshall—917(A)
Interpretation of neutron scattering, S. Frankel—216(A)
Of low velocity ions, J. A. Eldridge—473(A)
Of mesons, H. J. Bhabha—100; R. E. Marshak, V. F. Weisskopf—130, 471(A)
Of mesotrons in W, F. L. Code—229
Neutron-proton interaction, W. Rarita, J. Schwinger—436, 556
Neutrons by B, E. A. Luebke, J. H. Manley, L. J. Haworth—918(A)
Of neutrons by various elements, W. E. Good, G. Scharff-Goldhaber—917(A)
Pair theory of nuclear forces, J. W. Weinberg—776
Phase shifts in scattering of protons, H. M. Thaxton, S. H. Miles—945(A)
Proton-proton scattering, R. R. Wilson, E. C. Creutz—916(A)
Proton recoils from neutrons, H. Tatel—916(A)
Of H^1 in H_2, G. L. Ragan, W. R. Kanne, R. F. Taschek—687(A)
Radiative collisions, neutrons on protons, T. Muto—837(L)
Range-velocity relation, J. H. M. Brunings, J. K. Knipp—919(A)
Of 2.5-Mev neutrons, H. H. Barschall, R. Ladenburg, C. C. Van Voorhis—917(A)
Solid state (see **Crystalline state**)
Sound (see **Acoustics**)
Specific heat
Of wire samples, B. Kurrelmeyer, W. H. Mais, E. H. Green—921(A)
Spectra, absorption
Of alkaline earth fluorides, C. A. Fowler, Jr.—645
Analysis of SiO_2 bands, N. Metropolis—923(A)
Broadening of *D* lines, Kenichi Watanabe—151
In colored alkali-halide crystals, J. P. Molnar—944(A)
Of C_6H_5F at 2750–2380A, H. Sponer, S. H. Wollman—924(A)
Infra-red of NH_3, H. M. Foley, H. M. Randall—171
Of methyl iodide, R. T. Lagemann—911(A)
Of monobromobenzene, I. Walerstein—924(A)
Principal series of K, H. R. Kratz, J. E. Mack—915(A)
Ultraviolet absorption, W. M. Preston—914(A)
Spectra, atomic (see also **Atomic structure**)
Of Cd IV and In V, M. Green—218(A)
Of Cs II, M. A. Wheatley, R. A. Sawyer—916(A)
Of Co VII and Ni VIII, low terms, E. E. Anderson, J. E. Mack—106(A), 717
Forbidden lines of Pb I, E. Gerjuoy—218(A)
Of Au I and Au II, J. R. Platt, R. A. Sawyer—916(A)
Isotope shift in B, J. P. Vinti—103(L)
Of Hg II, S. Mrozowski—106(A)
Of Ne IV, V and VI, ultraviolet, F. W. Paul, H. D. Polster—424
Of rare gases, J. B. Green—915(A)
Self-consistent field for Ge^{++} and Ge, W. Hartree, D. R. Hartree, M. F. Manning—306
Self-consistent field for Ni, R. B. Gray, M. F. Manning—475(A)
Self-consistent field for Si V and Si IV, M. F. Manning, W. Hartree, D. R. Hartree—683(A)
Self-consistent field for Zn, Ga, Ga^+, Ga^{+++}, As, As^+, As^{++}, As^{+++}, W. Hartree, D. R. Hartree, M. F. Manning—299
Term values in V II and Mn II, D. S. Bowman—386
Spectra, general
Infra-red solar spectrum, A. Adel—915(A)
Radiofrequency spectra, intensities, H. C. Torrey—293; A. F. Stevenson—767(L)
Spectra, molecular (see also **Molecular structure and constants**)
Of C_2H_2, A. H. Nielsen, D. Williams—911(A)
Analysis of CO_2 bands, S. Mrozowski—923(A)
Analysis of CO_2^+ band, F. Bueso-Sanllehí—923(A)
Association of alcohol, H. S. Sack, J. Prigogine—924(A)
Of CO, high rotational states, M. S. McCay—911(A)
CS_2 bands in ultraviolet, L. N. Liebermann—106(A); N. Metropolis—106(A)
Energy level patterns of triatomic molecules, R. S. Mulliken—873.
Infra-red bands of cyclopropane, L. G. Smith—924(A)
Infra-red emission of water vapor, W. M. Elsasser—218(A)
Intensity measurements in H_2, N. Ginsburg, G. H. Dieke—632
Nitrogen afterglow, M. H. Hebb, H. Sponer—925(A)
Predissociation in CD and CH bands, L. Gerö, R. F. Schmid—528(L)
Rydberg series of N_2, Y. Tanaka, T. Takamine—613(L)
Rydberg series of O_2, Y. Tanaka, T. Takamine—771(L)
Silicon oxide bands, L. H. Woods—922(A)
Species classification of triatomic molecules, R. S. Mulliken—923(A)
Of water vapor, H. H. Nielsen—565

Spectroscopy, technique
Energy measurements with thermopiles, N. C. Beese —922(A)
Spectrograph for infra-red to 15μ, E. D. McAlister, G. L. Matheson, W. J. Sweeney—922(A)
Surface tension
At high pressures, L. B. Heilprin—921(A)

Thermal conductivity
Of liquids, M. R. Rao—212(L)
Temperature distributions in cylindrical systems, M. Avrami—691(A)
Thermal diffusion
Effect of van der Waals forces, R. C. Jones—688(A)
Separation of O isotopes, S. B. Welles—920(A)
Theory of, for isotopes, R. C. Jones—1019
Thermal expansion
Of pure Fe, Ni, Cu, Au and Al, F. C. Nix, D. MacNair —939(A)
Thermionic emission of electrons; Emitting surfaces
Cathode emission, electron microscope, G. W. Fox, F. M. Bailey—174
Constants for single crystal tungsten, M. H. Nichols—944(A)
Deviations from Schottky line, E. Guth, C. J. Mullin—114(A), 575
Energy losses attending emission, W. B. Nottingham, 906(L), G. M. Fleming, J. E. Henderson, 907(L)
Fluctuations in work function, A. T. Waterman—943(A)
Interpretation of certain phenomena, C. Herring—889
Work function and double layer, R. Smoluchowski—944(A)
Work function and temperature of pure metals, S. Seely —75
Thermodynamics
Interpretation of thermionic and thermoelectric phenomena, C. Herring—889
Relativistic thermodynamics, P. G. Bergmann—928(A)

Virial coefficient
Theory of metals, R. Landshoff—906(L)

Wave mechanics (see **Mechanics, quantum, etc.**)
Work function (see **Thermionic emission; Photoelectric effect**)

X-rays, absorption
Absorption coefficients in Pb, A. A. Petrauskas, F. E. Myers, L. C. Van Atta—688(A)
K-absorption edges of ions in solution, W. W. Beeman, J. A. Bearden—933(A)
Secondary structure, limits of gases, C. H. Shaw, J. A. Bearden—690(A)
X-rays, diffraction, scattering, reflection, refraction, and polarization
Analysis of patterns from liquids, N. S. Gingrich—290
Diffraction by liquid O, P. C. Sharrah, N. S. Gingrich —472(A)
Diffraction maxima not at Bragg angles, W. H. Zachariasen—207; P. Kirkpatrick—452; G. E. M. Jauncey—456; W. H. Zachariasen—766(L), 909(L); G. E. M. Jauncey, O. J. Baltzer—699; G. E. M. Jauncey, O. J. Baltzer, D. C. Miller—908(L)
Diffuse scattering by cubic lattice, W. H. Zachariasen —860
Diffuse scattering by KCl crystals, S. Siegel—371
Diffuse scattering by rocksalt, R. Q. Gregg, N. S. Gingrich—619
In random layer lattices, B. E. Warren, J. Biscoe—688(A); B. E. Warren—693
X-rays, emission
Absence of $M\beta$ satellite, F. R. Hirsh, Jr.—766(L)
Absolute determination of x-ray energy, J. C. Clark, H. R. Kelly—220(A)
Auger effect and relative intensities, J. N. Cooper—473(A)
By deuteron bombardment, J. M. Cork—934(A), 957
Effect of chemical combination, T. M. Snyder—689(A)
Excited by β-particles of $_{15}P^{32}$, Chien-Shiung Wu—481
Fluorescent *K* x-rays from ions, T. M. Snyder—168
Geneses of primary x-rays, S. R. Cook—220(A)
Intensity and hardness, variation with angle, L. C. Van Atta, F. E. Myers, A. A. Petrauskas—688(A)
L-emission bands of Na, Mg and Al, W. M. Cady, D. H. Tomboulian—381, 472(A)
Radiations from induction accelerator, D. W. Kerst—933(A)
Transitions within *L* shell, D. H. Tomboulian, W. M. Cady—422
Valence band—*L* transitions, J. A. Bearden, T. M. Snyder—162
X-rays, tubes, apparatus
Intensity of x-rays by electron multiplier tube, J. S. Allen—110(A)

Zeeman effect
Configuration interaction, J. B. Green—69; J. B. Green, D. W. Bowman, E. H. Hurlburt—106(A)
Forbidden lines of Pb I, F. A. Jenkins, S. Mrozowski—808, 915(A)
In Kr and Xe, J. B. Green—915(A)
Of Xe, J. B. Green, E. H. Hurlburt, D. W. Bowman—72, 106(A)

CONTENTS

JANUARY 1, 1941

Electric Fields Produced by Cosmic Rays . . . . . FOSTER EVANS 1
East-West Asymmetry of the Cosmic Radiation at High Latitudes . . . . . F. G. P. SEIDL 7
East-West Asymmetry of the Cosmic Radiation in High Latitudes and the Excess of Positive Mesotrons . . . . . THOMAS H. JOHNSON 11
Scattering of Alpha-Particles in Helium . . . . . JOHN ARCHIBALD WHEELER 16
Alpha-Particle Model and the Properties of the Nucleus Be^8 . . JOHN ARCHIBALD WHEELER 27
Interaction of Alpha-Particles . . . . . HENRY MARGENAU 37
Excited States of Nuclear Particles in the Meson-Pair Theory . . . CHARLES L. CRITCHFIELD 48
Branching Ratios in the Fission of Uranium (235) . . . . . H. L. ANDERSON, E. FERMI AND A. V. GROSSE 52
Photo-Fission of Uranium and Thorium . . . . . R. O. HAXBY, W. E. SHOUPP, W. E. STEPHENS AND W. H. WELLS 57
Positrons from Light Nuclei . . . . . M. G. WHITE, E. C. CREUTZ, L. A. DELSASSO AND R. R. WILSON 63
Paschen-Back Effect. VII. Configuration Interaction . . . . . J. B. GREEN 69
Zeeman Effect of Xenon . . . . . J. B. GREEN, E. H. HURLBURT AND D. W. BOWMAN 72
Work Function and Temperature . . . . . SAMUEL SEELY 75
Photoconductivity of a Natural Willemite Crystal . . . . . ROBERT C. HERMAN AND ROBERT HOFSTADTER 79
Dynamical Determination of the Elastic Constants and Their Temperature Coefficients for Quartz . . . . . JOHN V. ATANASOFF AND PHILIP J. HART 85
Determination of the c_{44} Elastic Constant for Beta-Quartz . . . . . JOHN V. ATANASOFF AND ERWIN KAMMER 97
Protons of Double Charge and the Scattering of Mesons . . . . . H. J. BHABHA 100

Letters to the Editor:

Capture Cross Sections for C Neutrons . . . . . R. D. O'NEAL AND M. GOLDHABER 102
Abundance Ratio Ni^{61} : Ni^{64} . . . . . HENRY A. STRAUS 102
Production of He^5 . . . . . R. D. HILL 103
Correction: Isotope Shift in Boron . . . . . JOHN P. VINTI 103
Hyperfine Structure of Ionized Mercury Lines . . . . . S. MROZOWSKI 104
Isotopic Weights of Ni Isotopes by the Doublet Method . . . . . T. OKUDA, K. OGATA, H. KURODA, S. SHIMA AND S. SHINDO 104

Proceedings of the American Physical Society: Chicago, Illinois, Meeting, November 22–23, 1940: Minutes and Abstracts 1–49; Author Index 105

JANUARY 15, 1941

Cloud Tracks of Cosmic Rays in the Substratosphere . . . . . G. HERZOG 117
Cloud-Chamber Pictures of Cosmic Rays at 29,000 Feet Altitude . . . . . G. HERZOG AND W. H. BOSTICK 122
Latitude Effect of Cosmic Rays Above 50°N Latitude . PAUL F. GAST AND D. H. LOUGHRIDGE 127
On the Scattering of Mesons of Spin $\frac{1}{2}h$ by Atomic Nuclei . . . . . R. E. MARSHAK AND V. F. WEISSKOPF 130
Density Distribution in the Steady-State Diffusion of Neutrons . . . . . E. A. UEHLING 136
Relative Stopping Powers of Carbon and Lead for Slow Mesons . . . . . MARTIN A. POMERANTZ AND THOMAS H. JOHNSON 143
Note on the Density and Compressibility of Nuclear Matter . . . . . EUGENE FEENBERG 149
Resonance Broadening of the Sodium *D* Lines . . . . . KENICHI WATANABE 151
Absorption of Resonance Neutrons by Boron, Chlorine, Cobalt and Manganese . . . . . W. J. HORVATH AND E. O. SALANT 154
X-Ray Spectra Arising from the Valence Band—*L* Transitions of Tungsten, Tungsten Oxide (WO_3) and Platinum . . . . . J. A. BEARDEN AND T. M. SNYDER 162
Fluorescent *K* X-Rays from Ions in Solution and from Gases . . . . . T. M. SNYDER 168
Fine Structure in the Far Infra-Red Spectrum of NH_3 . . . H. M. FOLEY AND H. M. RANDALL 171

Measurement of Cathode Emission by Use of the Electron Microscope . . . . . G. W. Fox and F. M. Bailey 174
Motion of the Earth's Fluid Core: A Geophysical Problem . . . . . D. R. Inglis 178
Perturbation of Boundary Conditions . . . . . H. Feshbach and A. M. Clogston 189
On an Asymmetrical Metric in the Four-Space of General Relativity . . . Gunnar Randers 195
Conduction of Electricity by Dielectric Liquids at High Field Strengths . . . . H. J. Plumley 200
On the Diffuse X-Ray Diffraction Maxima Observed by C. V. Raman and P. Nilakantan . . . . . W. H. Zachariasen 207
Photo-Disintegration of the Deuteron . William Rarita, Julian Schwinger and H. A. Nye 209

Letters to the Editor:

Thermal Conductivity of Liquids . . . . . M. Ramo Rao 212
Fission Products of Uranium and Thorium Produced by High Energy Neutrons . . . . . E. Segrè and G. T. Seaborg 212
Anode Spots in Oxygen . . . . . J. E. Henderson and Sidney M. Rubens 213
Fast Neutrons and Particles with High Specific Ionization in the Cosmic Radiation at High Elevations . . . . . S. A. Korff 214

Proceedings of the American Physical Society: Pasadena, California, Meeting, December 20–21, 1940: Minutes and Abstracts 1–30; Author Index 215

February 1, 1941

Variation of the Rate of Decay of Mesotrons with Momentum . . . . . Bruno Rossi and David B. Hall 223
Scattering of Mesotrons in Tungsten . . . . . F. Leslie Code 229
Correlation Between Cosmic-Ray Intensity at Cheltenham and the Air Temperatures and Pressures for 1939 . . . . . Niel F. Beardsley 233
Precise Determination of the Energy of the Neutrons from the Deuteron-Deuterium Reaction . . . . . T. W. Bonner 237
Application of a Pressure Electrostatic Generator to the Transmutation of Light Elements by Protons . . . . . Tom Lauritsen, C. C. Lauritsen and W. A. Fowler 241
Transmutation of Fluorine by Protons . . J. F. Streib, W. A. Fowler and C. C. Lauritsen 253
Velocity-Range Relation for Fission Fragments . . . . . N. Bohr 270
Range and Straggling of Fission Fragments . . . . . J. K. Bøggild, K. J. Brostrøm and T. Lauritsen 275
Protons from the Deuteron Bombardment of the Separated Isotopes of Chlorine . . . . . E. F. Shrader and Ernest Pollard 277
Scattering of Fast Electrons by Heavy Elements. II . J. H. Bartlett, Jr. and T. A. Welton 281
Note on the Analysis of Liquid X-Ray Diffraction Patterns . . . . . Newell S. Gingrich 290
Notes on Intensities of Radiofrequency Spectra . . . . . H. C. Torrey 293
Self-Consistent Field Calculations for Zn, Ga, Ga^+, Ga^{+++}, As, As^+, As^{++}, As^{+++} . . . . . W. Hartree, D. R. Hartree and Millard F. Manning 299
Self-Consistent Field Calculations for Ge^{++} and Ge . . . . . W. Hartree, D. R. Hartree and Millard F. Manning 306
Behavior of Young's Modulus of Beta-Brass Single Crystals at Low Temperature . . . . . John S. Rinehart 308
On the Theory of Volume Magnetostriction . . . . . R. Smoluchowski 309
Note on the Radiation Properties of Heavy Nuclei . . . . . V. F. Weisskopf 318

Letters to the Editor:

Relative Abundances of the Oxygen Isotopes . . . . . Byron F. Murphey 320
Radioactive Isotopes of Germanium . G. T. Seaborg, J. J. Livingood and G. Friedlander 320
Radioactive Isotope of Protoactinium . G. T. Seaborg, J. W. Gofman and J. W. Kennedy 321
β-Ray Spectrum of $_{91}$Ekatantalum^{233} . . . . . E. Haggstrom 322
Fourth $(4n+1)$ Radioactive Series . . . . A. V. Grosse, E. T. Booth and J. R. Dunning 322
Nomenclature of Nuclear Particles . . . . . C. Møller 323
Fission Products of Uranium by Fast Neutrons . . . . . Y. Nishina, T. Yasaki, K. Kimura and M. Ikawa 323

FEBRUARY 15, 1941

Radiative Transition Probabilities in Heavy Nuclei. Excitation of Nuclei by X-Rays . . . . . EUGENE GUTH 325
Experiments with a Slow Neutron Velocity Spectrometer . . C. P. BAKER AND R. F. BACHER 332
Long-Lived Radioactive Carbon: C^{14} . . . . . S. RUBEN AND M. D. KAMEN 349
Ionization and Dissociation of Diatomic Molecules by Electron Impact . . . . . HOMER D. HAGSTRUM AND JOHN T. TATE 354
Experimental Study of the Diffuse Scattering of X-Rays by Potassium Chloride Crystals . . . . . STANLEY SIEGEL 371
Measurement of Self-Diffusion in Zinc . . . . . FLOYD R. BANKS 376
***L*-Emission Bands of Sodium, Magnesium and Aluminum** . . . . . WILLOUGHBY M. CADY AND D. H. TOMBOULIAN 381
Term Values in V II and Mn II . . . . . D. S. BOWMAN 386
Magnetization Near Saturation in Polycrystalline Ferromagnets . . . . . T. HOLSTEIN AND H. PRIMAKOFF 388
Phase Series . . . . . E. J. HELLUND 395

Letters to the Editor:

Radioactive Isotopes of Osmium . . . . . G. T. SEABORG AND G. FRIEDLANDER 400
Coulomb Exchange Energy in Light Nuclei . . . . . M. PHILLIPS AND E. FEENBERG 400
Cosmic Rays at a Depth Equivalent to 1400 Meters of Water . . . . . Y. NISHINA, Y. SEKIDO, Y. MIYAZAKI AND T. MASUDA 401
Change in Height of a Mesotron-Producing Layer of Air . . . . . NIEL F. BEARDSLEY 402
Capture Cross Sections for Slow Neutrons . . . . . K. SINMA AND F. YAMASAKI 402
Radioactive $_{21}Sc^{41}$, $_{18}A^{35}$ and $_{16}S^{31}$ . . . . . D. R. ELLIOTT AND L. D. P. KING 403

MARCH 1, 1941

Interaction of γ-Rays with Mesotrons . . . . . R. F. CHRISTY AND S. KUSAKA 405
Burst Production by Mesotrons . . . . . R. F. CHRISTY AND S. KUSAKA 414
Radiative X-Ray Transitions Within the *L* Shell . . . . . D. H. TOMBOULIAN AND WILLOUGHBY M. CADY 422
Extreme Ultraviolet Spectra of Ne IV, V and VI . FRED W. PAUL AND HARRY D. POLSTER 424
New Mass Spectrograph and the Isotopic Constitution of Nickel . . . . . HENRY A. STRAUS 430
On the Magnitude of Electronic Charges . . . . . ALFRED LANDÉ 434
On the Neutron-Proton Interaction . . . . . WILLIAM RARITA AND JULIAN SCHWINGER 436
X-Ray Diffraction Maxima at Other Than Bragg Angles . . . . . PAUL KIRKPATRICK 452
Note on the Theory of the Modified Reflection of X-Rays by Crystals . . G. E. M. JAUNCEY 456

Letters to the Editor:

Reflection and Diffraction of Molecular Beams at Lithium Fluoride Cleavage Surfaces . . . . . WILLIAM H. BESSEY 459
Direct Measurement of the Mass of the Mesotron . . . . . L. LEPRINCE-RINGUET, S. GORODETZKY, E. NAGEOTTE AND R. RICHARD-FOY 460
Pair Production in the Field of an Electron . . . . KENICHI SHINOHARA AND MITIO HATOYAMA 461
Soft Component and Decay of Mesotrons at 3000 Meters . . . . . NIKITIN FEDORENKO 461
On the Spin of the Mesotron . . . . . J. R. OPPENHEIMER 462
Simultaneous Emission of Particles and Pair Production . . . . . SERGIO DE BENEDETTI 463

Proceedings of the American Physical Society, Philadelphia, Pennsylvania, Meeting, December 26–28, 1940: Minutes, Abstracts and Author Index 464

MARCH 15, 1941

Continuous X-Rays Excited by the Beta-Particles of $_{15}P^{32}$ . . . . . CHIEN-SHIUNG WU 481
Interaction Experiments with Resonance Neutrons . . . . . HENRY B. HANSTEIN 489
Concentration Method for Certain Radioactive Metals . . . . . JOSEPH STEIGMAN 498
Absolute Number of Quanta from the Bombardment of Fluorine with Protons . . . . . JAMES A. VAN ALLEN AND NICHOLAS M. SMITH, JR. 501
On the Thermal Activation of the Oxygen Molecule . . . . . HOMER D. HAGSTRUM AND JOHN T. TATE 509
Influence of a Longitudinal Magnetic Field on an Electrical Discharge in Mercury Vapor at Low Pressure . . . . . CHARLES S. CUMMINGS AND LEWI TONKS 514
Transmission of an Electron Density Disturbance Along a Positive Column in a Longitudinal Field . . . . . LEWI TONKS 522

Letters to the Editor:

Dislocations and Magnetization . . . . . WILLIAM FULLER BROWN, JR. 528
Rotational Analysis, Perturbation and Predissociation in the CD and CH Bands . . . . . L. GERÖ AND R. F. SCHMID 528

APRIL 1, 1941

Radioactivity of Mn^{56} and I^{128} . . . . . RALPH H. BACON, EDGAR N. GRISEWOOD AND CAREL W. VAN DER MERWE 531
Neutrino Theory of Stellar Collapse . . . . . G. GAMOW AND M. SCHOENBERG 539
Differential Measurement of the Meson Lifetime . . . . . W. M. NIELSEN, C. M. RYERSON, L. W. NORDHEIM AND K. Z. MORGAN 547
On the Nature of the Meson Decay . . . . . L. W. NORDHEIM 554
On the Exchange Properties of the Neutron-Proton Interaction . . . . . WILLIAM RARITA AND JULIAN SCHWINGER 556
Near Infra-Red Spectrum of Water Vapor. Part I. The Perpendicular Bands ν_2 and $2\nu_2$ . . . . . HARALD H. NIELSEN 565
Electron Emission of Metals in Electric Fields. I. Explanation of the Periodic Deviations from the Schottky Line . . . . . EUGENE GUTH AND CHARLES J. MULLIN 575
Discontinuities of Magnetostriction and Magnetization in Nickel . . . . . C. W. HEAPS 585
Velocity of Longitudinal Waves in Cylindrical Bars . . . . . DENNISON BANCROFT 588
Non-Uniform Particle Density in Nuclear Structure . . . . . EUGENE FEENBERG 593
Interaction of Electrons in Metals and Insulators . . . . . C. W. UFFORD 598
Determination of the Elastic Modulus s_{13} of Beta-Quartz . . . . . A. W. LAWSON 608

Letters to the Editor:

Vibrational Structure of the $^2\Sigma_g^+ \leftarrow {}^1\Sigma_g^+$ Rydberg Series of N_2 . . Y. TANAKA AND T. TAKAMINE 613
Mean Life of Slow Mesotrons . . . . . FRANCO RASETTI 613
On the Fine Structure Pattern of Cosmic Rays at Mexico City. II . . . . . E. J. SCHREMP AND ALFREDO BAÑOS, JR. 614
Nature of the Primary Cosmic Radiation and the Origin of the Mesotron . . . . . MARCEL SCHEIN, WILLIAM P. JESSE AND E. O. WOLLAN 615
Angular Momenta of Gravitational Fields . . . . . MARIO SCHOENBERG 616
On Time Lags in Coincident Discharges of Geiger-Müller Counters . . . . . M. E. ROSE AND W. E. RAMSEY 616
Relative Importance of Different Elements for Neutrino Production . . . . . G. GAMOW 617
Absolute Cross Section for the Photo-Disintegration of Deuterium by 6.2-Mev Quanta . . . . . JAMES A. VAN ALLEN AND NICHOLAS M. SMITH, JR. 618

APRIL 15, 1941

Diffuse Scattering of X-Rays by Rocksalt . . . . . R. Q. GREGG AND N. S. GINGRICH 619
Burst Production by Mesotrons of Spin One-Half and Zero Magnetic Moment . . . . . S. B. BATDORF AND ROY THOMAS 621
Note on Ionization by Meteors . . . . . J. A. PIERCE 625
Statistics of Excited Energy States of Nuclei . . . . . H. MARGENAU 627
Intensity Measurements in the Molecular Spectrum of Hydrogen . . . . . N. GINSBURG AND G. H. DIEKE 632
New Absorption Spectra of the Alkaline Earth Fluorides . . . . CHARLES A. FOWLER, JR. 645
On the Joint Action of Diffusion and Recombination of Ions . . . . . GEORGE JAFFÉ 652
On the Energy Loss of Heavy Ions . . . . . JULIAN KNIPP AND EDWARD TELLER 659
Intrinsic Inelasticity of Large Plates . . . . . CLARENCE ZENER 669
On the Polar Vibrations of Alkali Halides . R. H. LYDDANE, R. G. SACHS AND E. TELLER 673

Letters to the Editor:

Fission Products of Uranium by Fast Neutrons . Y. NISHINA, T. YASAKI, K. KIMURA AND M. IKAWA 677
On the Einstein Condensation Phenomenon . . . . . W. E. LAMB, JR. AND A. NORDSIECK 677
Geomagnetic Character and Cosmic-Ray Intensity Pulses . . . . . JAMES W. BROXON 678
Cosmic-Ray Intensities and Typhoons . Y. NISHINA, Y. SEKIDO, H. SIMAMURA AND H. ARAKAWA 679
Deuteron Bombardment of Oxygen . . . . . S. B. WELLES 679
Formation of the Solar System by the Rotational Fission of a Star: the Fission Being Initiated by a Passing Second Star . . . . . ROSS GUNN 680
Fission of Uranium by Alpha-Particles . . . . . E. FERMI AND E. SEGRÈ 680
Excitation of Gamma-Rays by Fast Neutrons of Different Energy . . . . . ITARU NONAKA 681

Proceedings of the American Physical Society: Cambridge, Massachusetts, Meeting, February 21–22, 1941: Minutes and Abstracts 1–47; Author Index 682

MAY 1, 1941

X-Ray Diffraction in Random Layer Lattices . . . . . B. E. WARREN 693
Non-Laue Maxima in the Diffraction of X-Rays from Rocksalt—Equatorial Maxima . . . . . G. E. M. JAUNCEY AND O. J. BALTZER 699
Evidence for the Radioactivity of Slow Mesotrons . . . . . FRANCO RASETTI 706
Total Mass of a Particle in General Relativity . . . . . C. LANCZOS 708
Low Terms in Co VII and Ni VIII . . . . . E. E. ANDERSON AND J. E. MACK 717
Paramagnetic Relaxation and the Equilibrium of Lattice Oscillators . . . J. H. VAN VLECK 724
Calculation of Energy Exchange between Lattice Oscillators . . . . . J. H. VAN VLECK 730
On a New Treatment of Some Eigenvalue Problems . . . . . L. INFELD 737
On the Theory of Dielectric Loss . . . . . B. GROSS 748
Theory of Degenerate Non-Ideal Gases . . . . . L. I. SCHIFF 751
On the Phase Transition in Liquid Helium . . . . . L. I. SCHIFF 758
Energy Distribution and Composition of the Primary Cosmic-Ray Particles . . . . . NORMAN HILBERRY 763

Letters to the Editor:

Directional Geiger Counter . . . . . H. G. STEVER 765
On the Theory of the Temperature Diffuse Scattering . . . . . W. H. ZACHARIASEN 766
On the Absence of the $M\beta$ Satellite Intensity Anomaly . . . . . FREDERICK R. HIRSH, JR. 766
Influence of End Effect on the Theoretical Shape of Intensity Curves in Radiofrequency Spectra . . . . . A. F. STEVENSON 767
Young's Modulus of Elasticity and Its Change with Magnetization in Iron-Cobalt Alloys . . . . . MIKIO YAMAMOTO 768
Cosmic Rays in the Bering Sea . . . . . PAUL F. GAST AND D. H. LOUGHRIDGE 769
Magnetic Anisotropy of Gadolinium Sulphate Octahydrate . . K. S. KRISHNAN AND S. BANERJEE 770
Single Component for the Primary Cosmic Radiation . . . . . W. F. G. SWANN 770
Vibrational Structure of the $^4\Sigma_g^-(O_2^+) \leftarrow {}^3\Sigma_g^-$ Rydberg Series of O_2 . Y. TANAKA AND T. TAKAMINE 771
Variations in the Relative Abundance of the Carbon Isotopes . . . . . BYRON F. MURPHEY AND ALFRED O. NIER 771

Proceedings of the Metropolitan Section of the American Physical Society, March 28, 1941, Meeting 772

MAY 15, 1941

Recurrence Phenomena in Cosmic-Ray Intensity . . . . . JAMES W. BROXON 773
Scattering in the Pair Theory of Nuclear Forces . . . . . J. W. WEINBERG 776
Disintegration of Carbon by Deuterons . . . . . W. E. BENNETT, T. W. BONNER, E. HUDSPETH, H. T. RICHARDS AND B. E. WATT 781
Energy of the γ-Rays from the Disintegration of Fluorine by Protons and Deuterons . . . . . W. E. BENNETT, T. W. BONNER AND BOB E. WATT 793
Photographic Plate Spectrum of the Neutrons from the Disintegration of Lithium by Deuterons . . . . . H. T. RICHARDS 796
Deuteron Disintegration by Electrons . . . . . B. PETERS AND C. RICHMAN 804
Zeeman Effect of the Forbidden Lines of Pb I. I. Pure Quadrupole and Magnetic Dipole Lines . . . . . F. A. JENKINS AND S. MROZOWSKI 808
Dynamics of a Particle in General Relativity . . . . . C. LANCZOS 813
Electric Breakdown of Glasses and Crystals as a Function of Temperature . . . . . A. VON HIPPEL AND R. J. MAURER 820
Scattering, Trapping, and Release of Electrons in NaCl and in Mixed Crystals of NaCl and AgCl . . . . . A. VON HIPPEL AND G. M. LEE 824
Calculation of the Torque on a Ferromagnetic Single Crystal in a Magnetic Field . . . . . R. M. BOZORTH AND H. J. WILLIAMS 827

Letters to the Editor:

Effect of Neutron Energy on the Total Decay Curves of Fission Products . . . . . S. K. HAYNES 834
Lifetimes of Nuclear Levels with Respect to Electric Multipole Radiation . . . . IRVING S. LOWEN 835
Further Evidence for a Single Component in the Primary Cosmic Radiation . . . W. F. G. SWANN 836
Stable Isotopes of Nickel . . . . . G. E. VALLEY 836
Radiative Collision of Neutrons with Protons . . . . . TOSHINOSUKE MUTO 837
Comment on the Elastic Constants of Alpha-Quartz . . . . . A. W. LAWSON 838
Note on the Structure of Liquid Helium . . . . . L. I. SCHIFF 839
On the Production of Mesotrons . . . . . J. FRANKLIN CARLSON AND MARCEL SCHEIN 840
Proton-Induced Fission . . . . . G. DESSAUER AND E. M. HAFNER 840
Note on the Normalization of Dirac Functions . . . . . C. C. LIN 841
Note on the "Kepler Problem" in a Spherical Space, and the Factorization Method of Solving Eigenvalue Problems . . . . . A. F. STEVENSON 842
Distinction between Longitudinal and Transverse Mesons . . . . . M. KOBAYASI 843

JUNE 1, 1941

Rest Mass of the Mesotron . . . . . PAUL WEISZ 845
Investigation of the Properties of Proportional Counters. I. . . . M. E. ROSE AND S. A. KORFF 850
Temperature Diffuse Scattering of a Simple Cubic Lattice . . . . . W. H. ZACHARIASEN 860
Electron Emission of Metals in Electric Fields. II. Field Dependence of the Surface Photo-Effect . . . . . EUGENE GUTH AND CHARLES J. MULLIN 867
Species Classification and Rotational Energy Level Patterns of Non-Linear Triatomic Molecules . . . . . ROBERT S. MULLIKEN 873
On the Thermodynamic Interpretation of Certain Thermionic and Thermoelectric Phenomena . . . . . CONYERS HERRING 889
On the Measurement of Observables in Relativistic Quantum Mechanics . . . . . O. HALPERN AND M. H. JOHNSON 896

Letters to the Editor:

Radioactive Rb from Deuteron Bombardment of Sr . . . . . A. C. HELMHOLZ, CHARLES PECHER AND PERRY R. STOUT 902
Showers of Penetrating Particles . M. DAMY DE SOUZA SANTOS, P. A. POMPEIA AND G. WATAGHIN 902
Radioactivity Produced in Germanium . . . . . R. SAGANE, G. MIYAMOTO AND M. IKAWA 904
High Energy Gamma-Ray from Li + D . . . . . W. E. BENNETT, T. W. BONNER, H. T. RICHARDS AND B. E. WATT 904
High Magnetic Saturation Value for the Copper-Manganese-Tin Heusler Alloy, Cu_2MnSn . . . . . LOUIS A. CARAPELLA AND RALPH R. HULTGREN 905
On the Virial Theorem in the Theory of Metals . . . . . R. LANDSHOFF 906
Remarks on Energy Losses Attending Thermionic Emission of Electrons from Metals . . . . . W. B. NOTTINGHAM 906
On the Energy Losses Attending Thermionic and Field Emission . . . . . GERTRUDE M. FLEMING AND J. E. HENDERSON 907

On the Selection Rules in Beta-Decay . . . . . J. R. Oppenheimer 908
Non-Laue Diffraction Maxima from Rocksalt—Non-Equatorial Maxima . . . . . G. E. M. Jauncey, O. J. Baltzer and D. C. Miller 908
Temperature Diffuse Scattering Maxima for Rocksalt . . . . . W. H. Zachariasen 909
Geomagnetic Character and Cosmic-Ray Intensity Pulses . . . . . James W. Broxon 909

Proceedings of the American Physical Society:

Southeastern Section: Nashville, Tennessee, Meeting, April 4–5, 1941: Minutes and Abstracts 1–13 910
Washington, D. C., Meeting, May 1–3, 1941: Minutes and Abstracts 1–161; Author Index 913

June 15, 1941

Nuclear Particles in the Cosmic Radiation . . . . . S. A. Korff 949
Beta-Ray Energy of H^3 . . . . . Sanborn C. Brown 954
Production of Characteristic X-Rays by Deuteron Bombardment . . . . . J. M. Cork 957
On the Passage of Neutrons Through Ferromagnets . . . . . O. Halpern and T. Holstein 960
Passage of Neutrons Through Crystals and Polycrystals . . . . . O. Halpern, M. Hamermesh and M. H. Johnson 981
Studies of a Ring Discharge . . . . . Charles G. Smith 997
Magnetostriction, Young's Modulus and Damping of 68 Permalloy as Dependent on Magnetization and Heat Treatment . . . H. J. Williams, R. M. Bozorth and H. Christensen 1005
Theory of Liquid He II . . . . . Hsien-yü Hsü and William Band 1013
On the Theory of the Thermal Diffusion Coefficient for Isotopes. II . . . . . R. Clark Jones 1019
New Technique for Preparing Monocrystalline Metal Surfaces for Work Function Study. The Work Function of Ag(100) . . . . . Paul A. Anderson 1034

Letters to the Editor:

Mechanism of Deuteron-Induced Fission . . . . . N. Bohr 1042
Fission Cross Section in Uranium and Thorium for Deuteron Impact . . . . . J. C. Jacobsen and N. O. Lassen 1043
Resistivity of Interstellar Space . . . . . Fred L. Mohler 1043
Are There Spin One Mesotrons? . . . . . H. Snyder 1043
On Secondary Slow Mesotrons . . . . . V. I. Veksler and N. A. Dobrotin 1044
Time Lags in Geiger-Müller Counter Discharges . . C. G. Montgomery and D. D. Montgomery 1045
Süperconducting Films as Radiometric Receivers . . . . . D. H. Andrews, W. F. Brucksch, Jr., W. T. Ziegler and E. R. Blanchard 1045
Production of Radioactive Hydrogen by Neutron Bombardment of Boron and Nitrogen . . . . . R. Cornog and W. F. Libby 1046

Author Index to Volume 59 1047
Analytic Subject Index to Volume 59 1060
Volume Table of Contents iii

Physics Lib
JUN 30

THE PHYSICAL REVIEW

VOLUME 59 | *Second Series* | NUMBER 12

JUNE 15, 1941

Published for the

AMERICAN PHYSICAL SOCIETY

by the

AMERICAN INSTITUTE OF PHYSICS
Incorporated

LANCASTER, PA., AND NEW YORK, N. Y.

THE PHYSICAL REVIEW

A journal of experimental and theoretical physics established by E. L. Nichols in 1893

Published by the American Institute of Physics for the

American Physical Society

OFFICERS

President

G. B. PEGRAM
Columbia University
New York, New York

Vice President

G. W. STEWART
State University of Iowa
Iowa City, Iowa

Secretary

K. K. DARROW
Bell Telephone Laboratories
New York, New York

Treasurer

G. B. PEGRAM
Columbia University
New York, New York

Local Secretary for the Pacific Coast

PAUL KIRKPATRICK
Stanford University
California

Editor

JOHN T. TATE
University of Minnesota
Minneapolis, Minnesota

BOARD OF EDITORS

JOHN T. TATE, *Editor* J. W. BUCHTA, *Assistant Editor*

Associate Editors

W. BLEAKNEY
G. BREIT
D. M. DENNISON
S. K. ALLISON
P. M. MORSE
J. A. WHEELER
A. C. G. MITCHELL
I. I. RABI
G. E. UHLENBECK

Manuscripts for publication should be submitted to John T. Tate, University of Minnesota, Minneapolis, Minnesota.

Proof and all correspondence concerning papers in the process of publication, should be addressed to the Publications Manager, American Institute of Physics, 175 Fifth Avenue, New York, New York.

Subscription Price

United States and Canada $15.00
Elsewhere $16.50

Back Numbers

Complete set: Series 2,[1] Vol. 1, 1913–Vol. 58, 1940—$420.00
Yearly rate: $16.50
Single copies: $1.50 each prior to July, 1929; $.75 each after July, 1929.

Subscriptions and orders for back numbers should be addressed to Prince and Lemon Streets, Lancaster, Pennsylvania, or to the American Institute of Physics, 175 Fifth Avenue, New York, New York.

Advertising is not accepted for *The Physical Review* but attention is called to *The Review of Scientific Instruments* and the *Journal of Applied Physics*, companion publications of the Institute, and media through which the field of physics can be reached most effectively. Rates and other information will be furnished on request.

Changes of address in the case of members of the American Physical Society, should be addressed to the Treasurer; in the case of other subscribers, to the Publications Manager.

[1] For Series 1 inquire of Physics Department, Cornell University, Ithaca, N. Y.

The Physical Review is published semi-monthly at Prince and Lemon Streets, Lancaster, Pennsylvania.

Entered at the Post Office at Lancaster, Pennsylvania, as second class matter.

Acceptance for mailing at special rate of postage provided for in section 1103, Act of October 3, 1917, authorized September 6, 1926.

THE AMERICAN INSTITUTE OF PHYSICS

INCORPORATED

ADMINISTRATIVE STAFF

HENRY A. BARTON, *Director*

MADELINE M. MITCHELL, *Publications Manager*

JOHN T. TATE, *Adviser on Publications*

Office: 175 Fifth Avenue, New York, New York

JOURNALS

THE PHYSICAL REVIEW

REVIEWS OF MODERN PHYSICS

JOHN T. TATE, *Editor*

J. W. BUCHTA, *Assistant Editor*

JOURNAL OF THE OPTICAL SOCIETY OF AMERICA

GEORGE R. HARRISON, *Editor*

THE JOURNAL OF THE ACOUSTICAL SOCIETY OF AMERICA

FLOYD A. FIRESTONE, *Editor*

AMERICAN JOURNAL OF PHYSICS

(Formerly THE AMERICAN PHYSICS TEACHER)

DUANE ROLLER, *Editor*

THE REVIEW OF SCIENTIFIC INSTRUMENTS

GAYLORD P. HARNWELL, *Editor*

THE JOURNAL OF CHEMICAL PHYSICS

JOSEPH E. MAYER, *Editor*

JOURNAL OF APPLIED PHYSICS

ELMER HUTCHISSON, *Editor*

GOVERNING BOARD

PAUL E. KLOPSTEG, *Chairman*
Central Scientific Company

GEORGE B. PEGRAM, *Secretary*
Columbia University

For the American Physical Society:

KARL T. COMPTON
Massachusetts Institute of Technology

GEORGE B. PEGRAM
Columbia University

JOHN T. TATE
University of Minnesota

For the Optical Society:

R. C. GIBBS
Cornell University

A. C. HARDY
Massachusetts Institute of Technology

W. B. RAYTON
Bausch & Lomb Optical Company

For the Acoustical Society of America:

FLOYD A. FIRESTONE
University of Michigan

HARVEY FLETCHER
Bell Telephone Laboratories

WALLACE WATERFALL
The Celotex Corporation

For the Society of Rheology:

WHEELER P. DAVEY
Pennsylvania State College

A. STUART HUNTER
E. I. duPont de Nemours & Company

H. R. LILLIE
Corning Glass Works

For the American Association of Physics Teachers:

GEORGE R. HARRISON
Massachusetts Institute of Technology

PAUL E. KLOPSTEG
Central Scientific Company

A. G. WORTHING
University of Pittsburgh

The American Institute of Physics is a membership corporation of which five societies are the founding members. These five societies are the principal national societies devoted to pure and applied physics in America. Their names, and those of their representatives who form the Governing Board of the Institute, are given above. The principal work of the Institute is the publication of journals sponsored by the societies or by itself. The names and the editors of the journals are also listed above.

The broad purpose of the Institute is to represent, in all matters of wide or common interest, the five thousand or more members and subscribers associated with the Founder Societies and the journals. It aims to advance the science and profession of physics, and to promote cooperation between pure research, the applied sciences and the industries. To achieve these aims, it is greatly in need of an endowment and is empowered by law to administer grants and funds of any kind.

CONTENTS

PHYS. REV. 59 (1941) JUNE 15

Nuclear Particles in the Cosmic Radiation . . . . . S. A. KORFF 949

Beta-Ray Energy of H^3 . . . . . SANBORN C. BROWN 954

Production of Characteristic X-Rays by Deuteron Bombardment . . . . . J. M. CORK 957

On the Passage of Neutrons Through Ferromagnets . . . . . O. HALPERN AND T. HOLSTEIN 960

Passage of Neutrons Through Crystals and Polycrystals . . . . . O. HALPERN, M. HAMERMESH AND M. H. JOHNSON 981

Studies of a Ring Discharge . . . . . CHARLES G. SMITH 997

Magnetostriction, Young's Modulus and Damping of 68 Permalloy as Dependent on Magnetization and Heat Treatment . . . H. J. WILLIAMS, R. M. BOZORTH AND H. CHRISTENSEN 1005

Theory of Liquid He II . . . . . HSIEN-YÜ HSÜ AND WILLIAM BAND 1013

On the Theory of the Thermal Diffusion Coefficient for Isotopes. II . . . . . R. CLARK JONES 1019

New Technique for Preparing Monocrystalline Metal Surfaces for Work Function Study. The Work Function of Ag(100) . . . . . PAUL A. ANDERSON 1034

Letters to the Editor:

Mechanism of Deuteron-Induced Fission . . . . . N. BOHR 1042

Fission Cross Section in Uranium and Thorium for Deuteron Impact . . . . . J. C. JACOBSEN AND N. O. LASSEN 1043

Resistivity of Interstellar Space . . . . . FRED L. MOHLER 1043

Are There Spin One Mesotrons? . . . . . H. SNYDER 1043

On Secondary Slow Mesotrons . . . . . V. I. VEKSLER AND N. A. DOBROTIN 1044

Time Lags in Geiger-Müller Counter Discharges . . C. G. MONTGOMERY AND D. D. MONTGOMERY 1045

Superconducting Films as Radiometric Receivers . . . . . D. H. ANDREWS, W. F. BRUCKSCH, JR., W. T. ZIEGLER AND E. R. BLANCHARD 1045

Production of Radioactive Hydrogen by Neutron Bombardment of Boron and Nitrogen . . . . . R. CORNOG AND W. F. LIBBY 1046

Author Index to Volume 59 1047

Analytic Subject Index to Volume 59 1060

Volume Table of Contents iii

LANCASTER PRESS, INC., LANCASTER, PA.